MODELING DEEP GROUNDWATER FLOW THROUGH FRACTURED BEDROCK IN A MOUNTAINOUS HEADWATER CATCHMENT USING A COUPLED SURFACE WATER – GROUNDWATER MODEL, OKANAGAN BASIN, BRITISH COLUMBIA

by

Hendrik Maximilian Voeckler

M.Sc., Technical University of Berlin, 2004

A THESIS SUBMITTED IN PARTIAL FULFILLMENT OF
THE REQUIREMENTS FOR THE DEGREE OF

DOCTOR OF PHILOSOPHY

in

The Faculty of Graduate Studies

(Forestry)

THE UNIVERSITY OF BRITISH COLUMBIA

(Vancouver)

October, 2012

Abstract

Quantifying recharge to the mountain block from headwater catchments in snowmelt dominated upland mountainous regions is an important aspect of hydrologic studies. This study contributes to understanding of the interaction between surface water, soil water and deep groundwater flow in headwater catchments. A novel approach was developed for estimating the bedrock hydraulic conductivity of a regional-scale fractured bedrock aquifer using discrete fracture network (DFN) modeling. The methodology was tested in the mountainous Okanagan Basin, British Columbia, Canada. Discrete fractures were mapped in outcrops, and larger-scale fracture zones (corresponding to lineaments) were mapped from orthophotos and LANDSAT imagery. Outcrop fracture data were used to generate DFN models for estimating hydraulic conductivity for the fractured matrix (K_m). The mountain block hydraulic conductivity (K_{mb}) was estimated using larger-scale DFN models. Simulated K_m and K_{mb} values range from 10^{-8} to 10^{-7} m/s, are consistent with estimates from regional modeling studies, and are greatest in a N-S direction, coinciding with the main strike direction of Okanagan Valley Fault Zone. K_{mb} values also decrease away from the fault, consistent with the decrease in lineament density. Simulated hydraulic conductivity values also compare well with those estimated from pumping tests. The estimates of K_{mb} were then used to represent the deep bedrock in a coupled surface water - groundwater model using MIKE SHE for the Upper Penticton Creek 241 headwater catchment in the Okanagan Basin. Although highly uncertain due to parameter uncertainty and calibration error, recharge to deep groundwater was ~4% of the annual water budget. An specified outward flux from the catchment boundary, representing ~6%

of annual water budget, did not significantly impact streamflow calibration, indicating that such deep groundwater losses from the catchment can be accommodated in a model. This outflow may contribute to cross-catchment flow and, ultimately, to groundwater inflow to lower elevation catchments in the mountain block. The modeling exercise is one of the first in catchment hydrology modeling within steep mountainous terrain in which the lower boundary of the model is not treated as impermeable, and in which recharge to the deep bedrock and discharge to the surrounding mountain block were estimated.

Preface

This thesis contains one chapter (Chapter 4) that has been very recently published in a scientific journal. The co-author for the paper is Dr. Diana M. Allen (supervisory committee and primary supervisor for this portion of the research). All of the fracture data collection, fracture data analysis, and DFN modeling were conducted by myself, with guidance given by Dr. Allen. All of the figures and the majority of the text were also written by me; however, the text went through several rounds of editing by Dr. Allen.

- Voeckler, H. and Allen, D.M. (on line 2012). Estimating regional-scale fractured bedrock hydraulic conductivity using discrete fracture network (DFN) modeling. Hydrogeology Journal, DOI 10.1007/s10040-012-0858-y.

The integrated surface water – groundwater modeling exercise described in Chapter 5 will be submitted for publication to the Journal of Hydrology or Hydrological Processes soon.

Table of Contents

List of Tables

List of Figures

List of Abbreviations

AWSET	Automatic Weather Station Evapotranspiration
BC	British Columbia
BF	Boundary Flow
CWN	Canadian Water Network
DEM	Digital Elevation Model
DFN	Discrete Fracture Network
DHI	Danish Hydraulic Institute
DHSVM	Distributed Hydrology Soil Vegetation Model
ENSO	El Niño Southern Oscillation
ESRI	Environmental System Research Institute
ESSF	Engelmann Spruce Subalpine Fir
ET	Evapotranspiration
FRED	FracMan Reservoir Edition
GSC	Geological Survey of Canada
GMC	General Motors Company
GIS	Geographic Information System
GPS	Global Positioning System
GW	Groundwater
HD	Hydrodynamic
LAI	Leaf Area Index
LANDSAT	Land Remote-Sensing Satellite
MASL	Meters Above Sea Level
MBR	Mountain Block Recharge
MFR	Mountain Front Recharge
SHE	System Hydrologique European
MODFLOW	Modular Groundwater Flow Model
NRC	National Research Council
OL	Overland

OVFZ	Okanagan Valley Fault Zone
PDF	Probability Density Function
PDO	Pacific Decadal Oscillation
PET	Potential Evapotranspiration
PVC	Poly Vinyl Chloride
RD	Rooting Depth
REV	Representative Elementary Volume
SSSF	Subsurface Stormflow
SW	Surface Water
SWE	Snow Water Equivalent
SZ	Saturated Zone
TM	Thematic Mapper
TOC	Top of Casing
TRIM	Terrain Resource Information Management
UBC	University of British Columbia
U-L-S	Unlogged Scenario
UPC	Upper Penticton Creek
UZ	Unsaturated Zone
VDL	Variable Density Log
W-C-S	Warm Climate Scenario
WY	Water Year

List of Variables

K   Permeability / hydraulic conductivity [m/s]

P_{10} Fracture intensity - number of fractures per unit sample length [1/m]

P_{21} Fracture intensity - length per unit surface area [1/m]

P_{32} Fracture intensity - area per unit rock volume [1/m]

T_f Fracture transmissivity [m^2/s]

S   Storativity [dimensionless]

Ss   Specific storage [1/m]

r   Radius around well screen [m]

h   Groundwater head

q   Darcy flux [m/s]

I   Hydraulic gradient [dimensionless]

k_i Intrinsic permeability [m^2]

b   Fracture aperture [m]

C_f Fracture compressibility [m^2/N]

k   Fracture dispersion factor [dimensionless]

K_f Fracture permeability [m/s]

K_m Matrix permeability [m/s]

K_{eff} Effective lineament permeability [m/s]

b_{eff} Effective Lineament aperture b [m]

K_{mb} Mountain block permeability [m/s]

K_p Hydraulic conductivity from pumping test [m/s]

Ss_m Matrix specific storage [1/m]

Ss_{mb} Mountain Block specific storage [1/m]

T_{eff} Effective lineament transmissivity

C_{eff} Effective lineament compressibility [m^2/N]

Acknowledgements

University of Utah (UofU), who invited me to his research lab in Salt Lake City to learn the FRED software.

Sincerely, I wish to deeply thank my parents and family for their enduring support throughout my time as a student and life, both morally and financially. Most of my academic accomplishments would not have been possible without their encouragement and support.

Further grateful thanks I deeply owe to Tania Garcia Libreros and Dr. Sascha Müller for being two very special persons in my life, giving me support in whatsoever way.

Finally I want to mention Blanquita (my cat) and the "Orange House" with its occupants, my roommates and friends over the years, for providing a great environment and positive energy to live and study. It has been my home in Vancouver since I moved here about 7 years ago.

To my parents

1. Introduction

1.1. Groundwater recharge in mountain regions

Groundwater recharge is arguably the most difficult hydrologic parameter to quantify with confidence (NRC, 1996; Scanlon et al., 2002; Lerner et al., 1990). Of specific relevance to this PhD research is the potential for percolation into fractured bedrock in mountainous areas. In general, there is an absence of groundwater data in alpine environments worldwide. This is largely due to a lack of wells in alpine settings, which typically have sparse population and pose significant challenges for access and drilling. However, there is growing recognition that mountains play a critical role in the hydrologic cycle in many parts of the world, capturing precipitation by orographic effects, storing water in snowpack and in mountain aquifers, initiating transport of water from the surface to local and regional aquifers, and possibly even deeper to the upper crust of the Earth (Viviroli et al. 2007). In many cases, understanding regional aquifer systems requires an understanding of groundwater flow in adjacent mountains where most of the recharge occurs. Because mountains potentially serve as recharge zones and provide a gravitational driving force for deeply circulating waters, processes controlling groundwater movement into and through all levels of mountain masses deserve further study (Caine et al., 2006).

In mountainous watersheds, fractured rock often comprises the upland areas of the mountain block, while valley-bottom fill consists of unconsolidated sediment overlying bedrock (Figure 1.1).
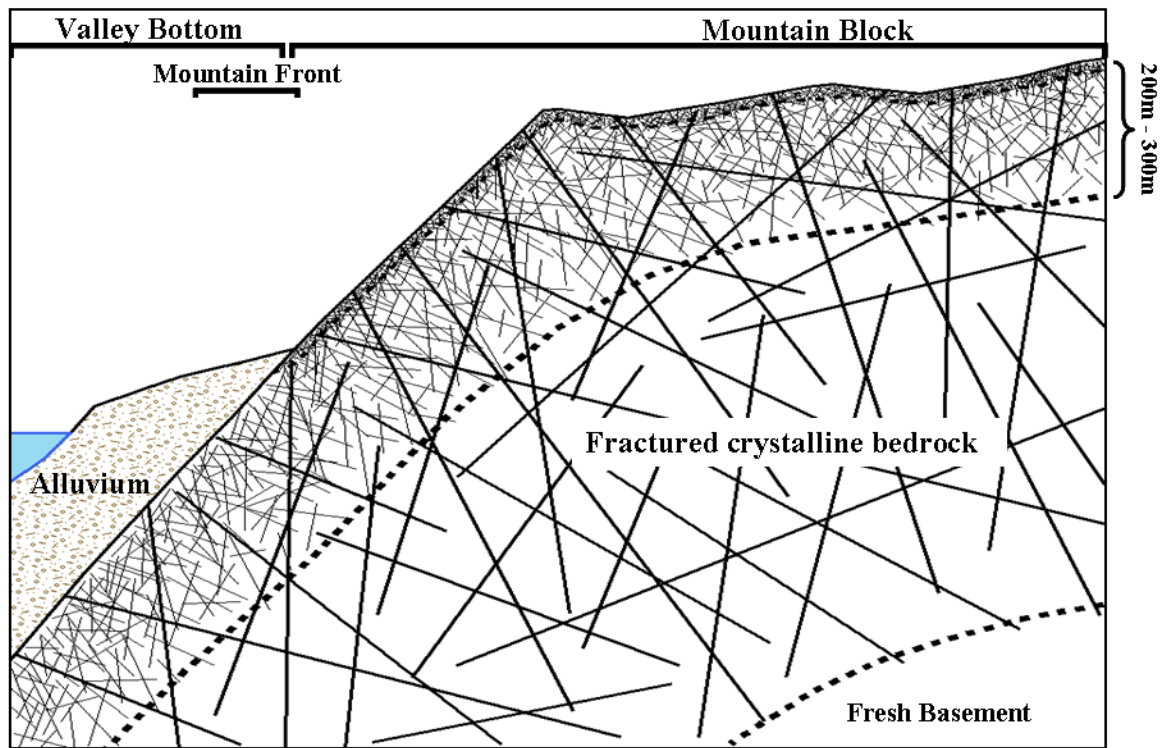
Figure 1.1. Geological model of a fractured crystalline mountain block bordering a valley bottom aquifer. The upper zone (~0-2 m thick) of the mountain block is weathered bedrock. Up to a depth of about 200-300 m the bedrock is highly fractured (fractured matrix). Extending from surface down to greater depths, large-scale fractures such as faults, are present. These may extend laterally across the mountain block over large distances.

In semi-arid and arid climates, a significant component of recharge to valley-bottom aquifers occurs along the mountain front, and is termed "mountain front recharge (MFR)" (Keith, 1980). Valley-bottom recharge is typically focused along stream channels and across the mountain front (diffuse recharge), and is the dominant source of replenishment (Maurer et al., 1999). Mountain block recharge (MBR) is the component of MFR derived from subsurface flow from adjacent mountains (Anderson et al., 1997; Manning and Solomon, 2003; Wilson and Guan, 2004). Diffuse recharge of valley-

bottom aquifers, through direct infiltration of precipitation, is limited or absent due to small precipitation volumes and deep vadose zones. In contrast, the mountains receive more precipitation, with a significant portion in the form of snow. Mountains also have thin soils that can store less water, thus reducing the potential for evapotranspiration (ET). Fast flow along bedrock fractures that underlie the thin soil cover may also limit water loss to ET.

Preliminary simulations by Wilson and Guan (2004) suggest that bedrock with sufficiently high bulk permeability (fracture and matrix) has the potential to allow for significant deep percolation (threshold intrinsic permeability of 10^{-16} m^2 or a hydraulic conductivity threshold of 10^{-9} m/s), leading to substantial MBR. Various studies have provided estimates in excess of this threshold value (e.g., Caine and Tomusiak, 2003; Surrette and Allen, 2008). For example, in the Salt Lake Valley of Utah, about 22% of the whole water budget for the valley aquifer enters through MBR from the adjacent Wasatch Mountain Range (Wilson and Guan, 2004). However, spatial variability in fracturing at the regional scale can result in significant differences in the amount of percolation, particularly in mountainous regions, where other factors, such as slope and vegetation differences come into play. Additional studies are needed to verify potential ranges of bedrock recharge in mountainous terrain, particularly in relation to structural character.

1.2. Purpose of research

The potential for percolation (recharge) into fractured bedrock requires estimates of bedrock permeability (or hydraulic conductivity, K). While pumping test data can

provide such estimates, typically few wells are available for testing. As well, often only a bulk (isotropic) estimate of hydraulic conductivity in vicinity of the wells is obtained. This is because the analysis of aquifer test data (e.g., pumping tests) rarely yields information on anisotropy ($Kx \neq Ky \neq Kz$) that can be related to fracture characteristics. To do so requires both a pumping well and several observation wells in a suitable test configuration. Thus, alternative approaches for estimating bedrock permeability have recently been tested. For example, Caine and Tomusiak (2003) characterized bedrock permeability at a local scale, where geometric characteristics were simulated through a discrete fracture network (DFN) approach on the basis of outcrop fracture data. Surrette and Allen (2008) used a DFN approach to derive estimates of potential permeability based on outcrop measurements of fractures in different hydrostructural domains observed throughout their study region, and related the range of estimates to hydraulic properties derived from pumping tests. They related regional trends in permeability to structural elements. Overall, there are few such studies reported in the literature.

Once the water has infiltrated, the capacity of a mountain block to transmit subsurface water to the basin depends on the hydrogeological architecture of the mountain block, particularly the properties controlled by geologic structural elements like regional lineaments/faults as well as small scale fractures, which can affect the amount of groundwater recharge to fractured rock aquifers (e.g., Caine et al., 1996; Olhmacher, 1999; Flint et al., 2001; Mayo et al., 2003; Haneberg, 1995; Mailloux et al., 1999). However, there are few studies that have explicitly examined the effect of scale in DFN approaches for estimating the bedrock permeability (e.g., fracture measurements in

outcrop versus regional lineaments detected through aerial photos and satellite images), and how measurements at one scale might be adjusted to give estimates at a different scale.

Hydrological processes in mountains have been studied for many decades at a variety of scales. Most of these studies have focused on streamflow generation or hillslope-runoff processes (e.g., Kirkby, 1988; Tani, 1997; McGlynn et al., 2002; Nippgen et al., 2011), hydroclimatology (e.g., Whitfield and Spence, 2011) and the effects of vegetation on evapotranspiration (e.g., Bosch and Hewlett, 1982). In recent years, however, there has been growing focus on groundwater-related processes (e.g., Mau and Winter, 1997; Constantz, 1998; Freer et al., 2002; Wenninger et al., 2004; Tromp-van Meerveld et al., 2008; Tague and Grant, 2009; Lowry et al., 2010; Kosugi et al., 2011; Haught and Meerveld, 2011; Penna et al., 2011).

Discharge to streams in mountain regions may be through alluvial cover materials and/or through fractured bedrock (Tromp-van Meerveld et al., 2007). In this context, hydrological research has documented subsurface stormflow (SSSF) and groundwater discharge as baseflow as important contributors to streamflow in mountainous areas (e.g., Anderson et al., 1997; Montgomery et al., 1997; Wohl, 2000; Tsujimura et al., 2001; Freer et al., 2002; Wenninger et al., 2004). Water recharged within the mountain catchments that does not "re-surface" as discharge to mountain streams (or stream valley sediments), forms deep groundwater flow systems within the bedrock mountain (Forster and Smith, 1988; Gleeson and Manning, 2008). This deep groundwater discharges to valley-bottom alluvial aquifers at the mountain front producing diffuse (through the

bedrock massive) or focused (through fault zones) mountain block recharge (Wilson and Guan, 2004). Thus, there is a partitioning of groundwater recharge whereby a portion is diverted back to the stream network and a portion contributes to deep groundwater flow in the mountain block.

Quantifying recharge to the mountain block from headwater catchments in snowmelt dominated upland mountainous regions is an important aspect of hydrologic studies, and modeling approaches involving coupling surface water (SW) processes and groundwater (GW) processes may provide a means for quantifying the various components of the water budget in mountainous areas. However, few have been conducted in arid and semi-arid regions, few have coupled surface water and groundwater processes in steep terrain, and most have considered only hydrologic processes in the thin soil layer above the bedrock surface (e.g., Merritt et al., 2006; Kuras et al., 2011; Kuras et al., 2012; Thyer et al., 2004; Sahoo et al., 2006; Whitaker et al., 2003; Schnorbus and Alila 2004). Thus, hydrologic science above the mountain front, incorporating a full view of the entire mountain block system, and not just the thin soil cover and its vegetation, is an area ripe for significant scientific advancement (Wilson and Guan, 2004). In general, a better understanding of groundwater processes in mountainous headwater catchments and how groundwater interacts with surface water is a major part of this PhD research.

This PhD project aims to test the following hypotheses:

1. Spatial variability in bedrock fracturing can be detected at the regional and local scales and this variability will result in different bedrock permeabilities at different scales.

2. DFN modeling can provide a reasonable estimate of fractured bedrock permeability for use in coupled surface water / groundwater models at the watershed scale.

3. Deep groundwater recharge occurs in high elevation catchments and this recharge moves beyond the catchment boundary and contributes to deeper groundwater flow systems.

1.3. Research objectives and scope

Two primary objectives of this research are addressed in two main studies:

1) Study 1: estimating bedrock permeability at the local outcrop scale and the regional mountain block scale to demonstrate spatial variability and scale dependence, and comparing these results with permeability estimates from pumping tests.

2) Study 2: using the bedrock permeability values from study 1 to construct, calibrate and validate a coupled SW-GW model (implemented in MIKE SHE/MIKE 11), and

estimate recharge to the saturated zone and recharge from a headwater catchment to the mountain block.

Figure 1.2 shows the hydrological and hydrogeological components in a mountain block / valley bottom aquifer system. Outlined in thick red is a headwater catchment at high elevation, illustrating conceptually the model area for study 2. The initial K values for the deep fractured aquifer, needed for simulation, are derived from study 1.
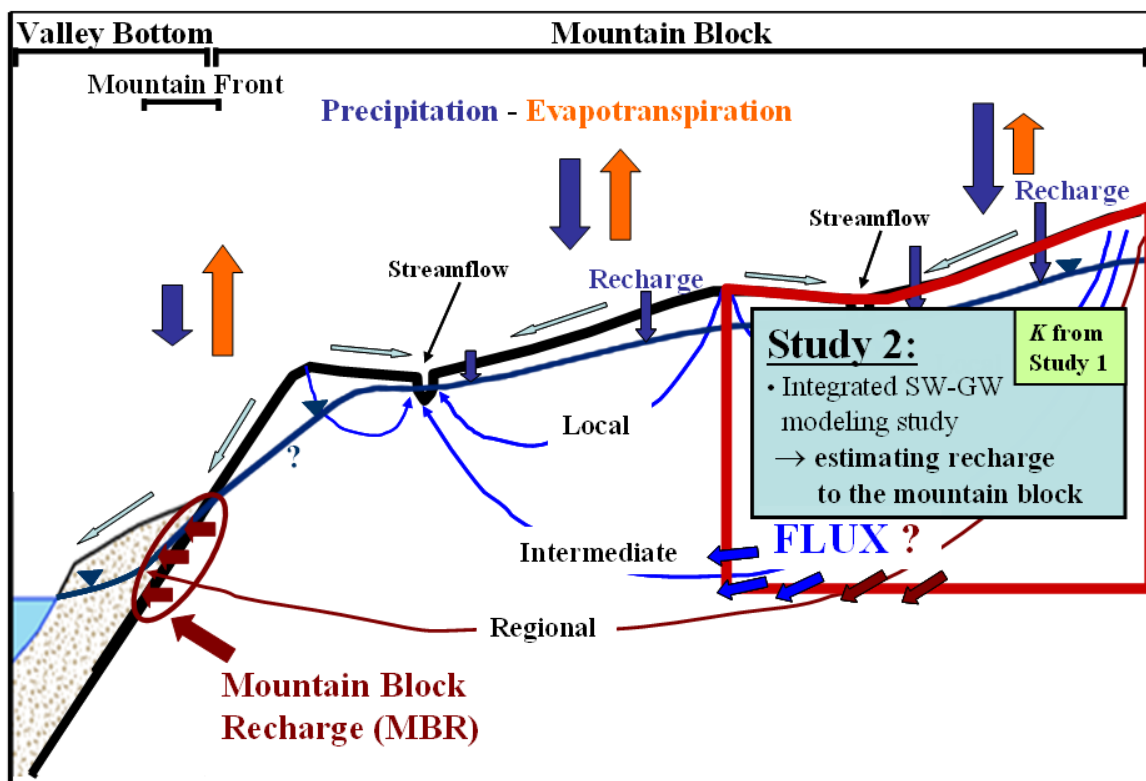
Figure 1.2. Hydrological and hydrogeological components of a mountain block / valley bottom aquifer system. A headwater catchment at high elevation within the mountain block is outlined in red to represent conceptually the model area for study 2.

A secondary objective of this research is to contribute to the Upper Penticton Creek Watershed Experiment by focusing on the deep groundwater component, in particular, the bedrock recharge.

Figure 1.3 shows a flow chart that gives an overview of the main steps involved in the research.
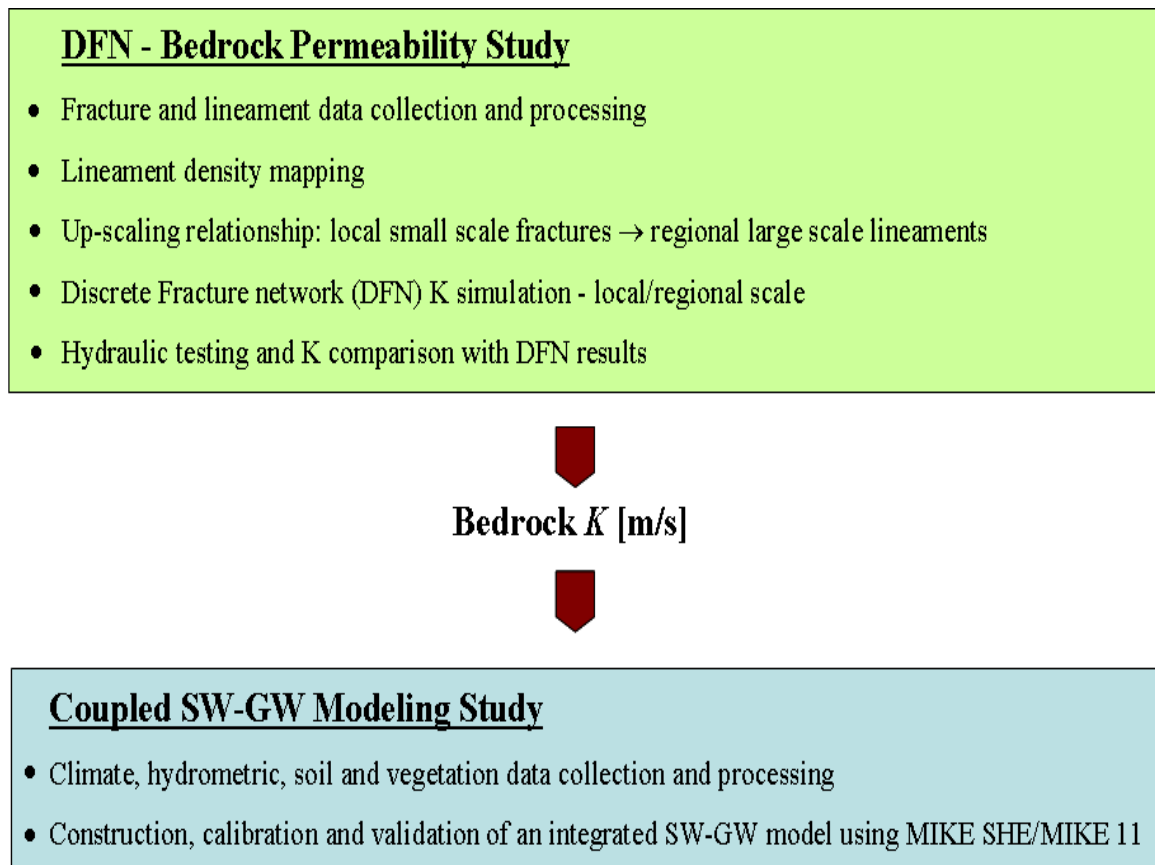
Figure 1.3.   Flow chart showing main components of the two studies

1.3.1.   Bedrock permeability study

The first part of the research involved deriving estimates of bedrock permeability throughout the study region at the local scale and the regional scale. Groundwater flow in

mountainous bedrock aquifers is expected to be predominantly in large scale fractures that might coincide with mappable lineaments. However, smaller scale fractures likely also play a role, particularly in recharge and groundwater storage (Caine and Tomusiak, 2003; Wilson and Guan, 2004).

Both DFN (Discrete Fracture Network) modeling and *in situ* aquifer testing approaches were used. The software FRED (Golder Associates, 2006, FRED software v. 6.54) was used to generate DFN models for estimating permeability. DFN modeling (Dershowitz et al., 1995) uses a stochastic approach to generate fracture/lineament distributions. Fracture data from outcrops throughout the study area and lineament data from aerial (ortho) photo analysis, DEMs and Landsat TM4 analysis were used. Possible scaling relations (e.g., persistence/length related to permeability) that correlate with fracture systems (Koike and Ichikawa, 2006) were investigated. The *in situ* aquifer testing included slug and bail tests as well as pumping tests, all carried out in the bedrock monitoring wells of the Upper Penticton Creek 241 watershed.

1.3.2. MIKE SHE/MIKE 11 SW-GW modeling study

The second main part of this research involved the construction and application of an integrated numerical SW-GW model for a small headwater catchment. The catchment is located in the snowmelt dominated alpine zone at high elevation below the ridges of the Okanagan Basin. The main goal of this numerical modeling study was to develop a better understanding of groundwater processes in headwater catchments and how groundwater interacts with surface water. In addition, recharge to the saturated zone and bedrock

recharge to the surrounding mountain block from the catchment was estimated through the modeling exercise. The permeability values for the bedrock aquifer were taken from the DFN modeling study the first part of this research (study 1).

The MIKE SHE/MIKE 11 code was developed by the Danish Hydraulic Institute (DHI). It is a physically distributed modeling system, which is able to simulate all the major physical processes of the hydrologic cycle. This code was selected because groundwater and surface water processes can be simulated in a coupled manner. MIKE SHE is horizontally discretized into an orthogonal network of grid squares to represent the spatial variability of catchment characteristics and input data. Within each grid square, a number of horizontal layers with variable depths are used to describe the vertical variations in soil and hydrogeological characteristics. The lateral flow between the grid squares is either overland flow or subsurface saturated zones flow (Thomson et al., 2004, Sultana and Coulibaly, 2010). The streams in the catchment are included in the model by the separate Mike 11 component, which solves the one-dimensional St. Venant equation based on the complete dynamic wave formulation for simulating channel hydraulics (Thompson et al., 2004).

1.4. Thesis organization

This thesis is organized into six chapters.

Chapter 1 provides background information on recharge in mountainous regions, defines the purpose of the research, the objectives and scope of work.

Chapter 2 provides an overview of the study area, Okanagan Basin. The general characteristics of the basin including physiography, climate, vegetation, water demand, geology and hydrogeology are discussed, followed by an overview of the Upper Penticton Creek Watershed Catchments – the modeling study site.

In Chapter 3, data collection, data processing and interpretation are discussed. This includes the outcrop scale fracture measurements, lineament mapping, an overview of the available hydrometeorological datasets, shallow soil piezometers and deep groundwater wells.

Chapter 4 discusses the results of study 1 on bedrock permeability estimation. This paper has been published in a scientific journal (Hydrogeology Journal).

Chapter 5 describes the modeling effort, including model setup, calibration and results. This chapter is intended for publication as a journal paper in the future.

Conclusions are provided in Chapter 6 along with recommendations for future research.

Three Appendices include the compiled datasets, the DFN modeling results and the MIKE SHE modeling results.

2. The Study Area

2.1. Regional and local scale areas

The study area is located within the Okanagan Basin in the southern interior of British Columbia (BC), Canada (Figure 2.1a). Field data were collected at two scales: a regional scale and a local scale (Figure 2.1b and 2.1c). The regional scale study area encompasses two first order watersheds, Penticton Creek and Naramata Creek, located east of the Okanagan Lake. Outcrop scanline mapping was carried out at 29 outcrop locations within these watersheds. Lineaments were also mapped across the watersheds using ortho photo and LANDSAT analysis. Discrete fracture network (DFN) models were constructed using both the outcrop and lineament data. More details on fracture and lineament data collection as well as DFN modeling for both scales are given in Chapter 3 and Chapter 4.

The local scale study area encompasses two small headwater catchments (Upper Penticton Creek watersheds 240/241), located about 20 km northeast of the Okanagan Lake (Figure 2.1c). The two catchments are part of the ongoing Upper Penticton Creek Watershed Experiment (described in detail later). Small scale fracture measurements and large scale lineament interpretation from ortho photos and LANDSAT images for DFN-K estimation were carried out in both catchments. Numerical modeling was only carried out in 241 given its extensive dataset. The Upper Penticton Creek (UPC) watersheds are situated within the alpine zone, beneath the local mountain crests. As part of this research, three bedrock monitoring wells were drilled within the UPC 241 watershed, and a series

of aquifer tests were carried out in each in order to estimate the hydraulic properties of the bedrock (Chapter 3). In addition, hydrological and meteorological data (e.g., streamflow, soil water table, precipitation, temperature, etc.) have been monitored over several years in the UPC watersheds. These data are used to develop a numerical coupled surface water-groundwater model of the 241 watershed using MIKE SHE/MIKE 11 software for estimating deep bedrock recharge from the catchment to the mountain block. More details on the data and modeling are provided in Chapter 3 and Chapter 5.

This chapter first describes the physiography, climate, land use, geology and hydrogeology of the Okanagan Basin as a whole, followed by a detailed description of the Upper Penticton Creek watersheds.
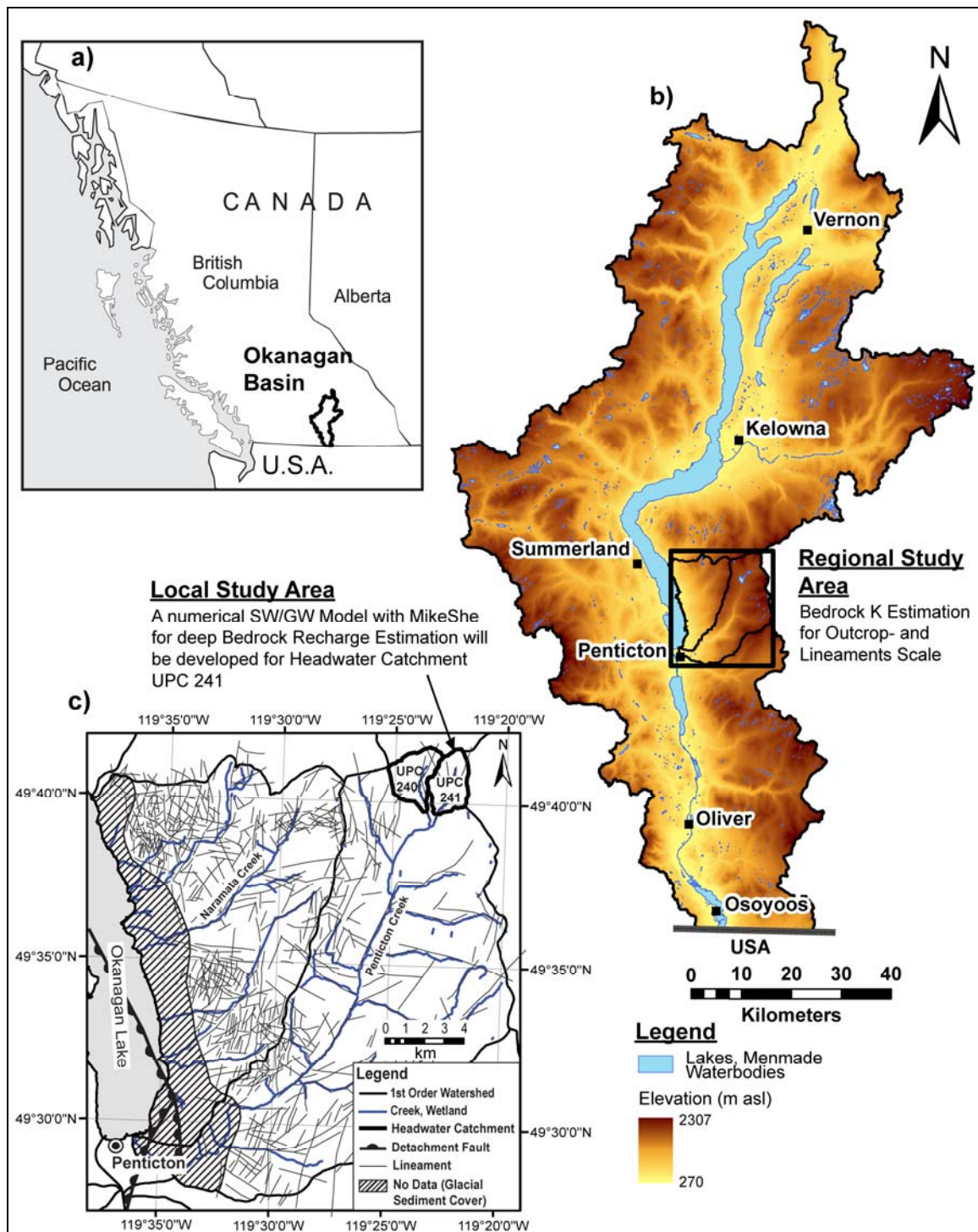
Figure 2.1. Maps showing (a) the location of the Okanagan Basin (black outline) in the interior of British Columbia, Canada; (b) a digital elevation model (DEM) of the Okanagan Basin including the regional study area (black square box) of

the two first order watersheds, Naramata Creek and Penticton Creek, located east of the Okanagan Lake; (c) inset map of the regional study area including the lineaments mapped through ortho photo and LANDSAT analysis and the larger streams. In the Upper right corner the outlines of the two headwater catchments UPC 240/241 (local study area) are shown.

2.2. Okanagan Basin

2.2.1. Physiography

The Okanagan Basin covers an area of about 8,200 km^2. It is a long, north-south trending, narrow (less than 7 km wide) basin stretching about 182 km from the Vernon area in the north to the Osoyoos area in the south (Figure 2.1a). The international border between Canada and the United States (Washington State) lies just to the south of Osoyoos. Okanagan Lake, with a surface area of 350 km^2, and five smaller main stem lakes of Okanagan River, with a combined surface area of approximately 87 km^2 are main features of the basin. The basins' hydrology is greatly impacted by these features through lake evaporation and interactions between surface water and groundwater systems. The valley is surrounded by upland plateaus and mountains. Surface elevations range from 270 to 2,300 metres above sea level (masl). Near the UPC watersheds, the mountain crests are at about 1,600 to 2,000 masl. The mean basin elevation is about 1,100 masl, although much of the populated valley-bottom area lies below 500 masl. Most of the hydrologically important runoff occurs at or above 1,200 masl elevation, with little or none below this level (Obedkoff, 1973).

2.2.2. Climate and vegetation

Due to a rain shadow effect, the mountain ranges to the west of the Okanagan Basin deliver the resulting dry air masses that originate over the Pacific Ocean. This is the reason for the basins' dry continental microclimate with dry mild winters and hot dry summers (Cohen et al., 2004). Very cold arctic air masses enter the region occasionally. These cold air masses are the main cause of severe vine and fruit tree damage in the valley (Okanagan Valley Tree Fruit Authority, 1995).

Okanagan Basin climate ranges from arid in the southern valley bottom around Osoyoos, to moist near the high elevation forested basin boundary. Semi-arid conditions characterize much of the valley bottom and the lower bench agricultural and municipal areas throughout the valley. In summer, weather conditions are among the hottest and driest in BC. Mean annual air temperature ranges from 7.4°C at Vernon to 10.1°C at Osoyoos (Environment Canada, 2006). The average annual precipitation at Vernon is 484 mm/yr, and at Osoyoos is 317.6 mm/yr (Environment Canada, 2006). In the uplands, at climate station P1 located in the 240 Upper Penticton Creek headwater catchment, the mean annual temperature is 2.0°C. Mean summer (June to August) and winter (November to March) air temperatures are 11°C and -5°C, respectively. The annual amount of precipitation in the uplands is about 750 mm/yr, approximately half of which falls as snow, and continuous snow cover generally lasts from late October until early June (Winkler et al., 2005). About 85% of precipitation in Okanagan Basin is lost through evapotranspiration (Cohen and Kulkarni, 2001).

Natural climatic variability occurs on many different time scales throughout the region. El Niño Southern Oscillation (ENSO) and Pacific Decadal Oscillation (PDO), occurring on inter-annual and inter-decadal time scales, respectively, are two predominant modes of natural variability affecting the climate of Western Canada including the Okanagan Valley. ENSO and PDO cycles are characterized by periods of anomalous warming and cooling of the Pacific Ocean accompanied by characteristic changes in atmospheric circulation. El Nino is distinguished by a warming of the tropical waters of the central Pacific with a corresponding decrease in the strength of the easterly trade winds. During La Niña, the opposite phase of ENSO, the central tropical Pacific cools and the trade winds become stronger (Wallace and Gutzler, 1981; Trenberth and Hurrell, 1994; Mantua et al., 1997).

The Basin's climate makes it a perfect location for agriculture, especially vineyards and orchards. The dry and reliable sunny summer Okanagan climate is the key reason that the tourism and agriculture industries are the mainstays of the valley economy (Cohen et al., 2004). The extensive range of microclimates is exploited by these rapidly modernizing industries. In the valley bottom and benchland areas, wine and tree fruit production are significant, while in higher elevation regions the land is covered by mostly pine forests. The forest industry exploits this land extensively (more details are given later in Section 2.3.3 of this Chapter).

2.2.3. Water demand

Agricultural and municipal development in many parts of the valley bottom is only possible because of the irrigation water supplied from about fifty high-elevation reservoirs throughout the valley. Okanagan Lake along the valley bottom is by far the largest reservoir. It supplies water for many of the municipalities and is exploited for its recreational and fish rearing potential. The two large communities of Kelowna (pop. 96,000) and Penticton (pop. 31,000) rely in part on the lake for their municipal water supplies, and the tourism industry depends on the lake for its recreational and aesthetic appeal (Statistics Canada, 2001).

Between 1971 and 2003 the population of Okanagan Basin more than doubled. This is the fastest growth rate among the 23 major river basins in Canada. The current population of the Okanagan-Similkameen basin is about 290,000. However, this region also has one of Canada's lowest renewable supplies of fresh water. The Okanagan-Similkameen basin has only 0.1% of the country's renewable supply of fresh water. In comparison, the Pacific Coastal basin has 15.8% of the renewable supply of fresh water. In 2001, the Okanagan-Similkameen basin ranked first in Canada in terms of the number of people for each square km of surface water, with nearly 439 people for every square km. For comparison, the Fraser River valley, which includes metropolitan Vancouver, has 224 people for every square km (Statistics Canada, 2003).

The rapidly expanding population of Okanagan Basin is increasingly placing demands on the available water supply. In fact, the Okanagan Basin has recently

completed a Water Supply and Demand Study in an attempt to quantify current and future trends in water availability and demand (Okanagan Basin Water Board, 2010).

2.2.4. Geologic and tectonic background of the Okanagan Basin

2.2.4.1. Bedrock geology

The bedrock in the study area consists primarily of metamorphic and intrusive igneous rocks (Figure 2.2a), ranging in age from Proterozoic to Lower Cretaceous (Massey et al., 2005). The bedrock is overlain in most of the valley bottom by unconsolidated Quaternary (including recent Holocene) sediments (as discussed below).

The Okanagan Valley follows a gently west dipping crustal shear zone (OVFZ – Okanagan Valley Fault Zone), across which the upper plate moved west above the lower plate during the middle Eocene. Matching the lower- and upper-plate rocks indicates about 90 km of offset and a southward strike. The shear zone is approximately 1 to 2 km wide, and is characterized by mylonite and microbreccia. Mylonitic gneiss at the top of the lower plate in the shear zone records the Eocene extensional strain, registering the zone's evolution through progressively shallower depths and cooler temperatures. Middle Eocene volcanics, normal faults and slide blocks demonstrate the upper-plate extension (Tempelman-Kluit and Parkinson, 1986).

Figure 2.2b shows a schematic view of a west-dipping, low angle detachment fault representing the Okanagan Eagle River Segment located just west of the study area under the Okanagan Lake (Johnson, 2006). The regional study area (red rectangle in Figure

2.2a) is partly located in the shear zone on top of the lower plate, east of the main trace of the Okanagan Eagle River Segment.
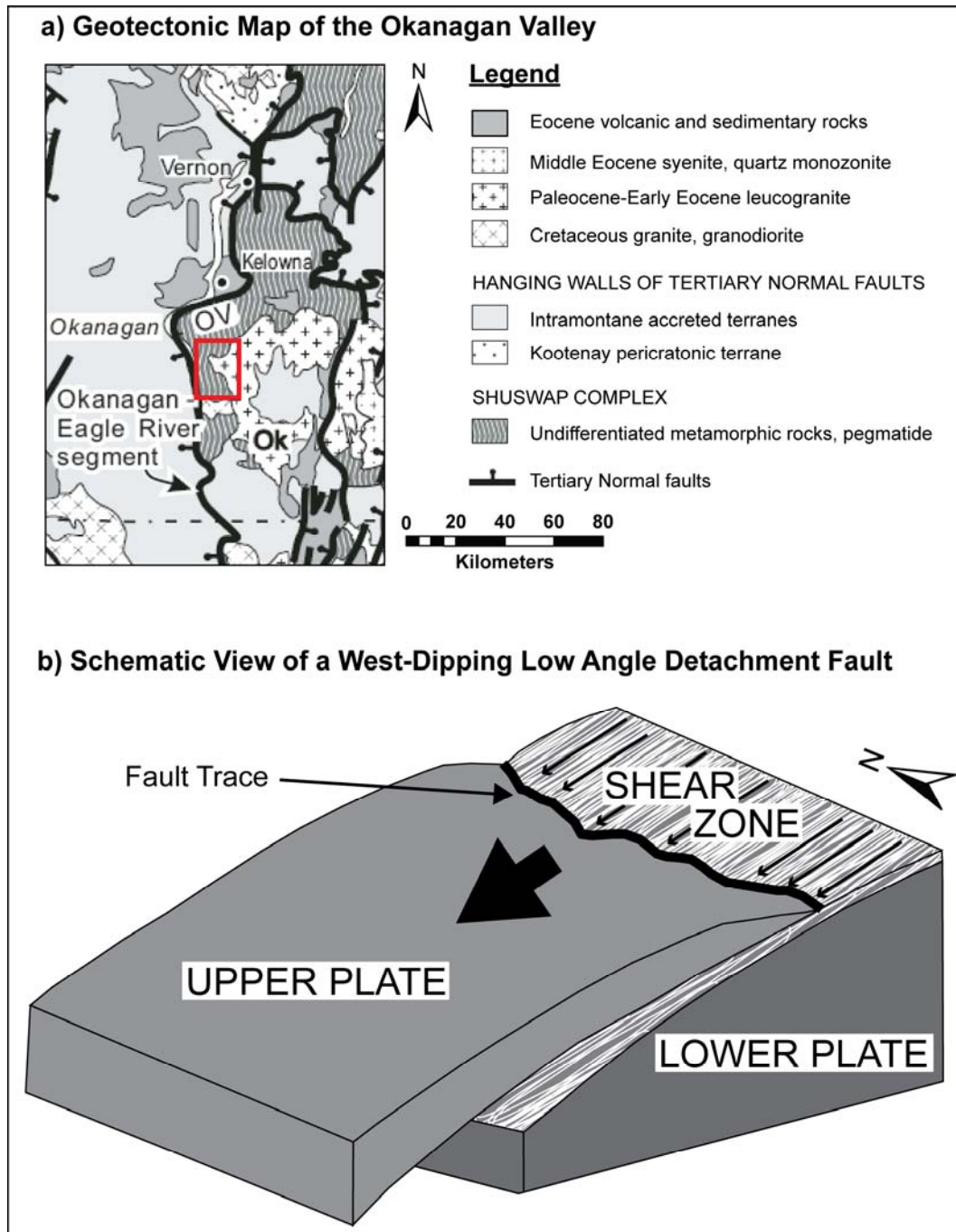
Figure 2.2. Geotectonic situation of the Okanagan valley and its surrounding mountains (geology from Johnson, 2006).

All bedrock encountered throughout the study area (including the regional and local study areas) belongs to the Omineca belt of the Canadian Cordillera (Monger and Price, 2002). As mapped by Massey et al. (2005), the northern and western part of the regional study area consist of undifferentiated metamorphic rocks of the Shuswap Assemblage, ranging in age from Proterozoic to Paleozoic (2500 to 245 millions of years). They are described as mostly undivided quarzofeldspathic gneisses, biotite-quarz schists, amphibolite and quartzite. Locally, pegmatites, muscovite granites and granodiorites are encountered. In the vicinity of the fault trace and in the shear zone, these rocks underwent extensional strain during the Eocene (as mentioned earlier) resulting in mylonitic gneisses. The rocks change their fabrics and textures upwards through the shear zone. Coarsely crystalline amphibole granodiorite gneiss at the bottom grades progressively through fine-grained mylonitic gneiss, augen gneiss, and mylonite to microbreccia at the top. Figure 2.3 shows a photograph of a fractured mylonitic gneiss of the upper shear zone found in areas close to the main fault trace of the Okanagan Valley Fault Zone (OVFZ).

Figure 2.3. Mylonitic gneiss of the Shuswap Assemblage. This crystalline rock type is often found in the upper areas of a shear zone close to the main Okanagan Valley Fault Zone trace.

Transitions are gradual over tens of metres. Low in the zone, recrystallization textures dominate, while ductile strain fabrics prevail at the top. Upward in the detachment zone, matrix grain size and the proportion and size of augen generally decrease. The shear zone's uppermost 10 to 100 m is occupied by chlorite-epidote-quartz microbreccias, probably the shattered and hydrothermally altered mylonite. Spaced, irregularly orientated extension faults cut the microbreccia and merge with the flaser

fabric downwards (Tempelman-Kluit and Parkinson, 1986; Johnson, 2006; Brown and Journeay, 1987).

The eastern part of the regional study area, including most of the area of the two headwater catchments UPC 240/241 in the northeastern corner, consists of undivided intrusive rocks of the Okanagan Batholith, ranging in age from Early to Late Cretaceous (145 to 65 Ma). These rocks are described as mostly leucogranites and granodiorites, including Tertiary "Ladybird" and "Valhalla" intrusions (Massey et al., 2005). Figure 2.4 shows a photograph of a fractured granodiorite found at higher elevations in the eastern part of the study area.

Figure 2.4. Granodiorite of the Okanagan Batholith.

In the southern part of the regional study area, intrusive rocks also of Early to Late Cretaceous age are encountered. These are mostly granites, granodiorites and monzonites (Massey et al., 2005).

2.2.4.2. Bedrock surface and erosion

The bedrock surface in the Okanagan Basin is highly irregular, with many cliff-like drops. This is confirmed from large differences in the elevation of bedrock-overburden contacts between closely-spaced boreholes in many regions of Okanagan Basin. While the depth to bedrock is generally shallow at high elevation, and covered only by a thin layer of sediments, the bedrock surface beneath the unconsolidated deposits within the valley bottom and benches is very deep and irregular. Interpreted from a seismic survey, MacAulay and Hobson (1972) mention the "extreme changes in bedrock slope". The deepest bedrock erosion is under Okanagan Lake at 650 m below sea level, which makes the Okanagan Valley possibly one of the deepest known erosional features within the North American continental landmass. The surrounding plateau into which the basin is cut has an average elevation of about 1500 masl, resulting in a total relief of over 2000 m. Compared to that, the relief of the Grand Canyon of Arizona is about 1600 m high (Eyles et al., 1990).

Erosion of the valley from rivers following deglaciation would have occurred early in the erosional history, and the extent of erosion would be limited to sea level elevation at that time (which would have been relatively higher than today); however, much of the bedrock valley is below present sea level (Fulton, 1972). Deep erosion has been attributed to glaciers, and the valley was termed a "fiord-lake" by Nasmith (1962) to

describe this phenomenon in the Okanagan Basin. However, the down-valley bedrock profile shows no sign of grading and is highly variable. Moreover, the cross-valley widths and profiles are extremely different along the valley. A map-view of the main side valleys reveals a braided pattern, whereby the main valleys diverge and converge from north to south. Those are signs that suggest that the classic valley glacier erosion was not only responsible for the over-deepening of the valley (Toews, 2007).

The suggestion that meltwater in subglacial drainage systems was actively flowing beneath the Cordilleran Ice Sheet was made by Eyles et al. (1991) and Vanderburgh and Roberts (1996). In addition, Shaw et al. (1999) and Lesemann et al. (2005) speculated that the subglacial meltwater drainage may have been periodically cataclysmic and responsible for the over-deepening of the valley. Subglacial fluvial systems have the ability to flow and potentially erode in any direction (including up and down). They can be considered as closed channel hydraulic systems. This erosional mechanism is supported by tunnel valleys along the sides of the main valley, some of which "flow uphill". The deep and irregular bedrock profile of the main valley is also supported by this mechanism.

2.2.4.3. Quaternary geology

Quaternary sediments in the Okanagan Valley can be simplified as mostly "white silt" (by volume), with sand and gravel along the sides and on top of the valley (Flint, 1935). Throughout the past one million years, British Columbia has been glaciated multiple times by the Cordilleran Ice Sheet. The most recent glaciation ended about 11,000 years ago (Clague, 1991). At the end of the last glaciation, an extensive Glacial

Lake Penticton (GLP) was formed and fine-grained material was rapidly deposited into it. The characteristic silt bluffs are part of those fine-grained deposits found in many valleys in the Interior of BC (Nasmith, 1962).

Flint (1935) first documented in detail the Quaternary stratigraphy of the Okanagan Basin. He described both the character and distribution of the silt deposits, and the gradation of sands and gravels along the valley margins. Geotectonic mapping and interpretation of the Quaternary deposits and landforms throughout the Okanagan was done by Nasmith (1962). He also identified several important depositional facies and landforms, including glaciofluvial deposits, kettled outwash, raised and present-day alluvial fans, and glaciolacustrine sediments. Multiple glaciations throughout the Cordilleran region, including in the valley bottom of Okanagan Basin, were interpreted by Fulton (1972) and Fulton and Smith (1978) through the construction of several stratigraphic sections across the BC Interior.

In the study area the characteristic silt bluff deposits (part of the glacial sediment cover) can only be found in the western part of the regional study area bordering the Okanagan Lake (see Figure 2.1c) The Quaternary deposits are not of particular interest in the regional scale study, apart from the fact that the deposits cover the bedrock, limiting exposure. Not only did the surficial cover result in difficulties finding exposed outcrop for scanline mapping of fractures, but it also made it difficult to map lineaments in the terrace areas bordering the Okanagan Lake. These issues are discussed further in Chapter 4. However, unconsolidated deposits are an important consideration in hydrogeological studies, in general, because their composition can strongly affect the amount of recharge

and stored soil moisture. For the local study area, the surficial deposits are discussed in more detail in Section 2.3.3 of this Chapter.

2.2.5. Hydrogeology

In the Okanagan Basin two groundwater systems are present: 1) a valley-bottom unconsolidated aquifer system and 2) a mountainous fractured bedrock aquifer system. These two systems interact at the interface between the mountainous bedrock and the valley-bottom sediments both at the surface and in the subsurface. The overall process is called mountain front recharge (MFR). Figure 2.5 shows a conceptual model of mountain catchment components, where regional-scale atmospheric, hydrological, and hydrogeological processes influence mountain front recharge (MFR).
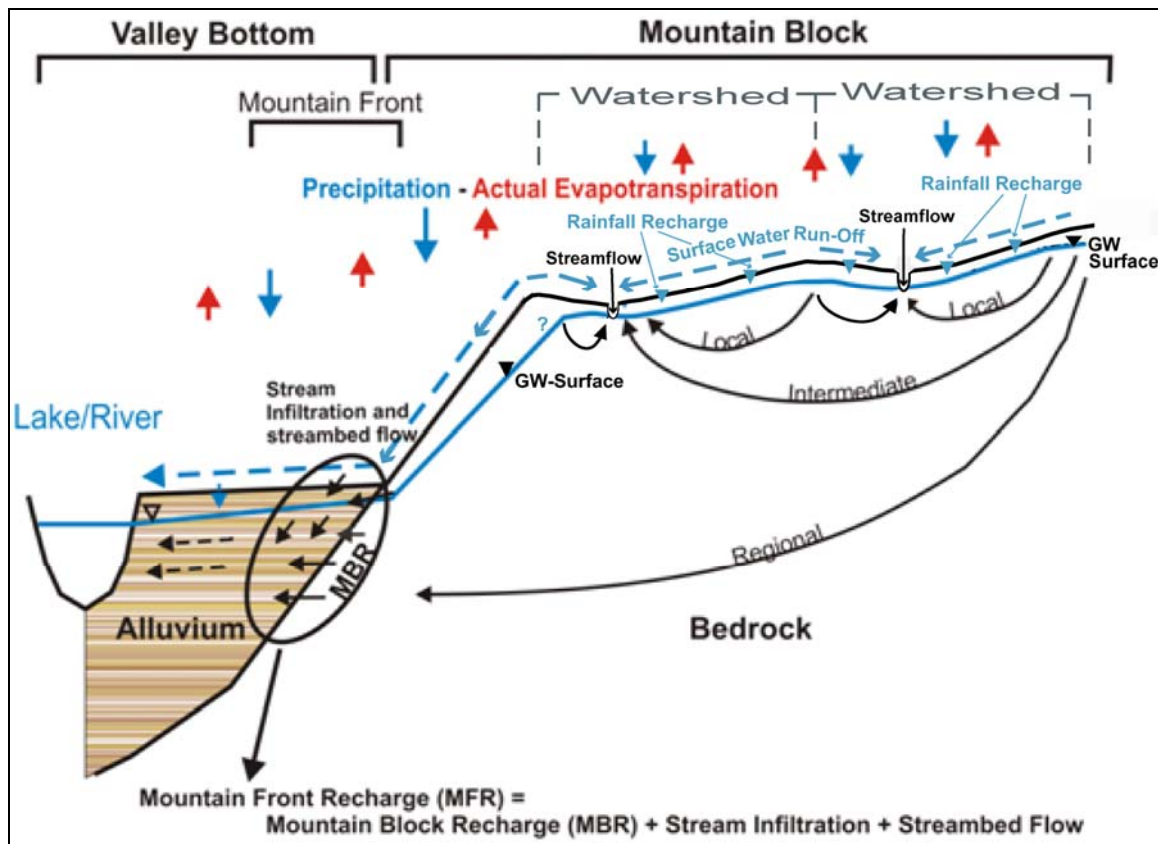
Figure 2.5. Conceptual model showing the mountain front recharge (MFR) process including the subsurface component called mountain block recharge (MBR), as it is present in the Okanagan Basin. It also shows two adjacent watersheds located in the mountain block with the main occurring hydrologic and hydrogeologic processes indicated (modified from L. Welch, SFU, personal communication, 2010).

Valley bottom aquifers in mountainous terrain form the principal groundwater resources for much of the western US and Canada. These aquifers are comprised of basin-fill sediments and are typically recharged by three mechanisms: (i) seepage from mountain streams and rivers (ephemeral and perennial); (ii) hidden groundwater flow from the adjacent mountain block; and (iii) direct, diffuse recharge to the valley bottom. Feth (1964) defined "hidden recharge" across the mountain front zone as "the subsurface

percolation of water from basin-margin mountains directly into aquifers in the valley basins". Feth (1964) further suggested that this mechanism of groundwater recharge may be important for valley-bottom aquifer replenishment; particularly in (semi) arid areas. This concept of "hidden recharge" across the mountain front zone has more recently been termed "Mountain Front Recharge" or "MFR" (Wilson and Guan, 2004).

Conceptual elements of regional-scale groundwater flow systems that generate MFR are well-established (Wilson and Guan, 2004) and are illustrated in Figure 2.5 (from L. Welch, SFU, personal communication, 2010). Specifically, within the mountain block (i.e., the bedrock mountains), local, intermediate, and regional groundwater flow systems develop as a result of recharge across variable topographic relief (Toth, 1963; Freeze and Witherspoon, 1967; Wilson and Guan, 2004; Gleeson and Manning, 2008). Discharge of groundwater to mountain streams from the shallow and intermediate flow systems occurs; generating streamflow (baseflow and stormflow). This process has been demonstrated through conceptual hydrogeological numerical modelling by Gleeson and Manning (2008) for systems representative of typical mountainous terrain. Hydrological research has also documented subsurface stormflow (SSSF) and groundwater discharge to streams in mountainous areas (e.g. Anderson et al., 1997; Montgomery et al., 1997; Wohl, 2000; Tsujimura et al., 2001). Stream discharge may be through alluvial cover materials and/or through fractured bedrock (Tromp-van Meerveld et al., 2007).

Streams generated within the mountain block (either perennial or ephemeral) typically lose water as they traverse the mountain front zone. This process is inferred to be the result of the hydraulic conductivity contrast at the mountain front between low

permeability bedrock materials and higher permeability alluvial sediments in the valley bottom (Wilson and Guan, 2004). Stream loss is one component of MFR and may occur as "focused recharge" for major tributaries, as well as "diffuse recharge" for small (e.g., disappearing or ephemeral) streams or surface runoff across the mountain front (Wilson and Guan, 2004). Longitudinal groundwater flow beneath dry ephemeral streams or perennial streams (i.e., through streambed materials overlying bedrock) has been identified as another potentially significant factor contributing to MFR, though research regarding the influence of such flow has not been completed (Wilson and Guan, 2004; Wolf et al., 2008).

Water recharged within the mountain block that does not "re-surface" as discharge to mountain streams (or stream valley sediments), forms deep groundwater flow systems within the bedrock mountain. This deep regional groundwater flow may be influenced by structural features of the bedrock (e.g., fault zones, fracturing, anisotropy) and/or geothermal influences (e.g., Forster and Smith 1988, Harte and Winter, 1995). In areas where valley-bottom unconsolidated deposits are minimal (e.g., at the edge of Okanagan Lake in some areas), MBR is inferred to discharge directly to the valley-bottom river/lake system.

One of the two main focuses of this PhD study is the development of a MIKE SHE/MIKE11 numerical surface water - groundwater model for simulating the deep groundwater flow/recharge contribution to the adjacent mountain block originating from the 241 headwater catchment. In addition, outcomes of this integrated modeling study are very important for a better understanding of groundwater processes in headwater

catchments and how groundwater interacts with surface water. Since small headwater catchments in the snowmelt dominated alpine zone can be considered as the main bedrock recharge areas for the Okanagan "mountain block", this information is highly important for possible future research on the MBR modeling and, in general, for the understanding the whole hydrogeological system in the Okanagan Basin. In the conceptual model (Figure 2.5), headwater catchments would be located in the high elevation areas of the mountain block, where small local groundwater flow systems interact through baseflow with the stream network of the catchment. Deep groundwater flow originating in the catchment contributes to intermediate and regional flow paths. The regional groundwater flow that discharges to valley-bottom alluvial aquifers at the mountain front, producing diffuse (through the bedrock massive) or focused (through fault zones) mountain block recharge (MBR) (Wilson and Guan, 2004), was once recharged in the mountain block system from smaller catchments such as UPC 241.

The rate at which water recharges the bedrock and moves through it depends on the bedrock permeability. However, few estimates of bedrock permeability are available, largely because there are few wells in these bedrock regions that can be tested hydraulically. As well, the permeability of fracture networks, their overall influence on the regional groundwater flow system, and their role in focused discharge of groundwater across the mountain front have not been fully explored. The first part of the research focuses on quantifying the permeability of the bedrock within the mountain areas using discrete fracture network modeling (DFN) based on fracture measurements made in outcrop and lineaments. The bedrock permeability values are compared with available

aquifer testing data from the wells at the UPC 241 watershed. The values will then be used in a coupled surface water-groundwater model aiming to quantify the proportion of deep bedrock loss relative to other components of the water balance in a headwater catchment as mentioned earlier.

2.3. Upper Penticton Creek headwater catchments

2.3.1.   Physiography

The Upper Penticton Creek watersheds UPC 240 and UPC 241 are two headwater tributaries to Penticton Creek. The watersheds are at high elevation, right below the local mountain crests. They are located in the Okanagan Highland alpine zone approximately 26 km northeast of the City of Penticton, BC (see Figure 2.1c). These two watersheds are part of the Upper Penticton Creek (UPC) Watershed Experiment (Winkler et al., 2008). More details on past work and available data for these two experimental watersheds are given in Chapter 3 and Chapter 5 and at the end of this Chapter. The 240 Creek and 241 Creek catchments each have a drainage area of about 5 km^2; they range in elevation from 1600 to 2100 m, and are plateau dominated, with 75% of the area having slopes less than 30% (Kuras et al., 2011; Thyer et al., 2004). Figure 2.6 shows the two headwater catchments including their respective stream networks, the meteorological and stream gauge stations, as well as bedrock monitoring wells and shallow soil piezometers for UPC 241. Details on the piezometers, the bedrock monitoring wells including aquifer testing and geophysical borehole logging are given in Chapter 3.
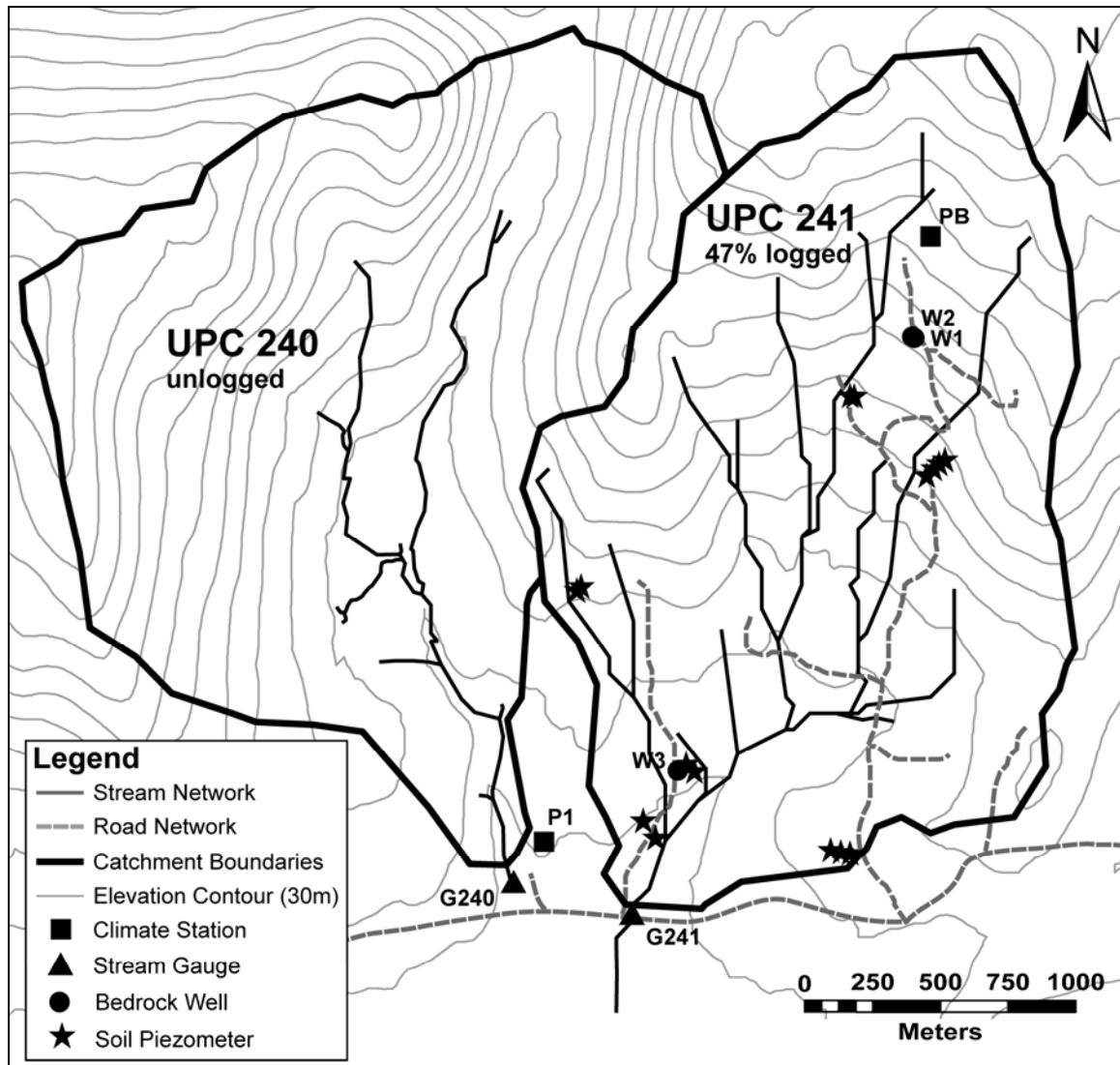
Figure 2.6.   The Upper Penticton Creek Watersheds 240/241 including locations of equipped measurement instrumentation.

2.3.2.   Climate

Mean annual precipitation at the two Upper Penticton Creek headwater catchments is approximately 750 mm, with 50-70% falling as snow. Mean summer (June–August) and winter (November–March) air temperatures are +11°C and -5°C, respectively. Permanent snow cover usually exists from late October until early June. The

late winter snowpack is normally 1 to 1.5 m deep, with April 1st Snow Water Equivalent (SWE) averaging 265 mm. The annual hydrograph is dominated by snowmelt, and the freshet peak typically occurs in late spring to early summer, with annual water yields ranging approximately 170-630 mm. More details on existing hydrological and meteorological time series data as they pertain to numerical modeling are given in Chapter 3 and Chapter 5.

2.3.3.   Vegetation, land use and soils

Both watersheds are situated within the dry Engelmann Spruce Subalpine Fir (ESSF) biogeoclimatic subzone. Forest cover is primarily mature lodgepole pine (Pinus contorta Douglas) with lesser amounts of Engelmann spruce (Picea Engelmannii Parry) and subalpine fir (Abies lasiocarpa). The trees at the study site are over 100 years old, reaching a maximum height of 20-26 m, with canopy densities ranging from 35-50%. The understory is composed of mosses, lichens, and shrubs less than 0.5 m tall.

Approximately 6% of the 241 Creek basin was clear-cut logged in Fall of 1992, and an additional 12% was clear-cut logged in 1997–1998, in total about 18% of the watershed at this time. In late winter of 2003, 28% of the watershed was logged. The final logging pass of about 47% was completed by late winter 2007. The 240 Creek control basin has been left undisturbed (Kuras et al., 2011; Thyer et al., 2004).

Soil textures in the study area are predominantly coarse sandy-loams and loamy-sands ranging in depth from 0.1-4 m, and are derived from glacial-tills and coarse-grained, granitic rock (Hope, 2001). Soils are low in clay content and high in coarse

fragment content, with forest floors generally less than 4 cm thick. Soils are generally well-drained and have a low water holding capacity, with late summer field observations verifying hydrophobicity in upper soil layers (Kuras et al., 2011; Thyer et al, 2004). The underlying geology consists of mostly fractured granite and gneisses of unknown permeability.

2.3.4. The Upper Penticton Creek watershed experiment

Due to the dry climate in the southern interior of BC and the increasing demand of limited fresh water, especially in regions like the Okanagan Basin, it is of high importance to secure the water supply and protect the aquatic habitat. These are issues of ongoing concern. In response, the Upper Penticton Creek (UPC) Watershed Experiment was established in 1984, with the aim of improving the understanding of hydrologic processes on the Okanagan Plateau and developing effective forest practices guidelines that help to sustain both timber and water resource values (Winkler et al., 2008).

The UPC Watershed Experiment was designed as a paired watershed study, where watershed scale measurements of hydrological and meteorological parameters have been conducted for pre- and post-treatment sampling periods in two logged (UPC 241, Dennis Creek) and unlogged (UPC 240) control watershed. Through stream channel and aquatic invertebrate monitoring, the effects of changing hydrologic processes on streams and aquatic habitat are being investigated and assessed. Thyer et al. (2004) undertook hydrologic modeling at the site with the distributed hydrological model (DHSVM - Distributed Hydrology Soil Vegetation Model) in order to simulate streamflow for the

logged (UPC 241) and unlogged (UPC 240) catchments. Also Kuras et al. (2011, 2012) studied the effects of forest roads and harvesting on the hydrology of the snow-dominated headwater catchment UPC 241 using DHSVM. His work combined a process-based study with physically-based, distributed hydrological modelling to contribute to improving the current understanding of snow-dominated catchment hydrology, with an examination of the impacts of forest management on such systems. The study specifically addressed the knowledge gap in forest hydrology regarding forest roads and harvesting in snowmelt-dominated regimes.

A network of six weather stations has been continuously monitoring meteorological data since 1962. Every two weeks from early March until the end of the snowmelt, detailed snow surveys were completed. All three watersheds remained undeveloped from 1984 to 1995. UPC 240 remains unlogged, whereas the current logging stage of the Dennis Creek catchment is 52% and for the UPC 241 it is about 47% (Winkler et al., 2008).

This research aims to contribute to the Upper Penticton Creek Watershed Experiment by focusing on the deep groundwater component, in particular, the bedrock recharge.

3. Data Collection, Processing and Interpretation

3.1. Outcrop scale fracture measurements – background

Two common sampling methods for estimating fracture parameters at the outcrop scale can be used: areal sampling and straight scanlines (Rohrbaugh Jr. et al., 2002) (Figure 3.1). The areal sampling method involves mapping the fracture trace pattern and recording the desired fracture characteristics at locations in the map area (Wu and Pollard, 1995). Straight scanlines map the fracture traces they intersect along a cross section of the outcrop. Each method has advantages and disadvantages.
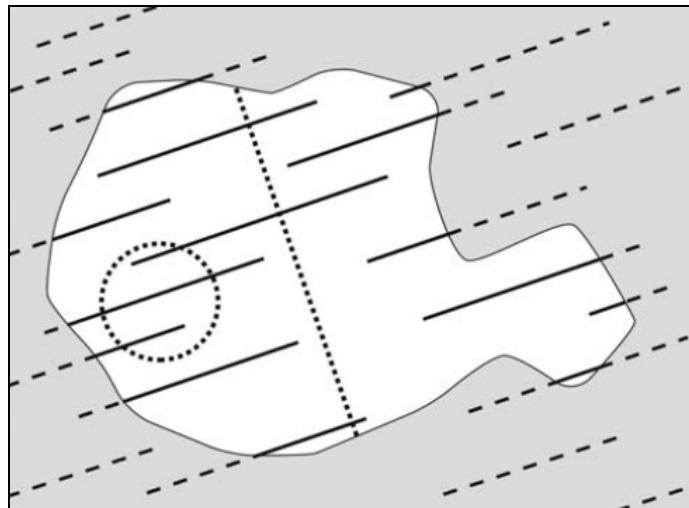
Figure 3.1. Areal (irregular white window), circular scanline/window (dotted circle), and straight scanline (dotted line) sampling of a fracture trace population. Solid lines represent visible fracture traces and dashed lines represent covered fracture traces (with permission, Rohrbaugh Jr. et al., 2002).

The straight scanline method provides rapid estimates of fracture intensity. One problem, however, is that unprocessed straight scanline data are often subject to sampling

biases, like length bias or orientation bias. If the scanline is not perpendicular to a fracture set, orientation bias occurs. If this is the case, the fracture intensity will be underestimated (Terzaghi, 1965). Longer fracture traces have a greater probability of being sampled than shorter traces, which results in the length bias (Baecher and Lanney, 1978). Mean trace-length estimates and trace-length distributions are biased toward longer fractures as a result (Rohrbaugh Jr. et al., 2002).

Areal sampling is more time consuming, but compared to scanline sampling, length bias is reduced. Rohrbaugh Jr. et al. (2002) indicates that areal sampling is subject to orientation bias in the plane for anything except a circular sampling area, and may hide pattern heterogeneities and introduce length bias for small sampling areas. Rohrbaugh Jr. et al. (2002) developed an estimator method for fracture density, intensity and mean trace length that corrects for sampling biases. The technique is used in combination with circular scanlines and windows. Despite its limitations, the scanline technique was used in this research. However, scanline measurements were made on two orthogonal faces of outcrops to reduce biases.

One important parameter that is measured is the fracture intensity. Fracture intensity is required for generation of the discrete fracture network (DFN), which later involves intensity up-scaling as defined by Dershowitz and Herda (1992). Intensity is defined as number of fractures per unit sample length (P_{10}), fracture length per unit surface area (P_{21}), or fracture area per unit rock volume (P_{32}), in one, two, or three dimensions, respectively. Whether the intensity is calculated linearly, areally, or volumetrically, the dimension of [1/m] is consequently the same for all three. Straight

scanlines are used in this study, which means the one dimensional linear intensity known as P_{10} intensity is recorded for each fracture set intersecting the scanline at an outcrop face. Through an up-scaling process done with the DFN-FRED modeling software (see Chapter 4), the P_{32} volumetric intensity, needed for the three-dimensional DFN-FRED models, is calculated.

3.2. Fieldwork - outcrop scale fracture data collection

Small scale fracture parameters needed for DFN model generation and, ultimately, simulations to determine the hydraulic properties, K and Ss, of the rock mass (see Chapter 4) were measured using the traditional scanline mapping technique (Rohrbaugh Jr. et al., 2002; Caine and Tomusiak, 2003) at selected outcrop locations throughout the study area during the summer of 2006. Prior to going to the field, geologic maps were examined to select natural outcrop locations that are representative of lithologically- and structurally-distinctive rock groups found in the study area. The final selection in the field was based on locating suitable outcrops for all rock types that are spatially distributed across the study area. Most of the outcrops selected are located in the lower elevation benchland areas of Okanagan Basin close to the Okanagan Lake, where accessibility was good; logging roads provided easy access. In general, the bedrock is well exposed closer to Okanagan Lake due to the semi-arid climate and resulting thinner vegetation cover. Further eastwards, up into the mountains, the terrain becomes steeper and the vegetation cover becomes thicker. In these upland areas, appropriate outcrops were difficult to locate and access. Figure 3.2 shows the locations of the 29 outcrops where the scanline mapping

was carried out in the Penticton and Naramata first order watersheds. Lineaments mapped through a combined LANDSAT and Orthophoto analysis are also displayed in the figure. More details on the lineament mapping are given later in this chapter.

At each of the 29 outcrop locations, measuring tapes (straight scanlines) were laid out on at least two near-orthogonal outcrop faces to capture all possible fracture set orientations and their fracture characteristics (Figure 3.3). Straight scanlines were orientated on the outcrop surface to intersect a fracture set orthogonally in order to minimize intensity bias. Besides measuring the P_{10} intensity, several fracture characteristics, such as the number, intersection position with scanline, orientation (measured with a geologic compass), trace length (strike/dip persistence), termination style, aperture, roughness (primary/secondary) and fracture fillings were recorded for each intersecting fracture.
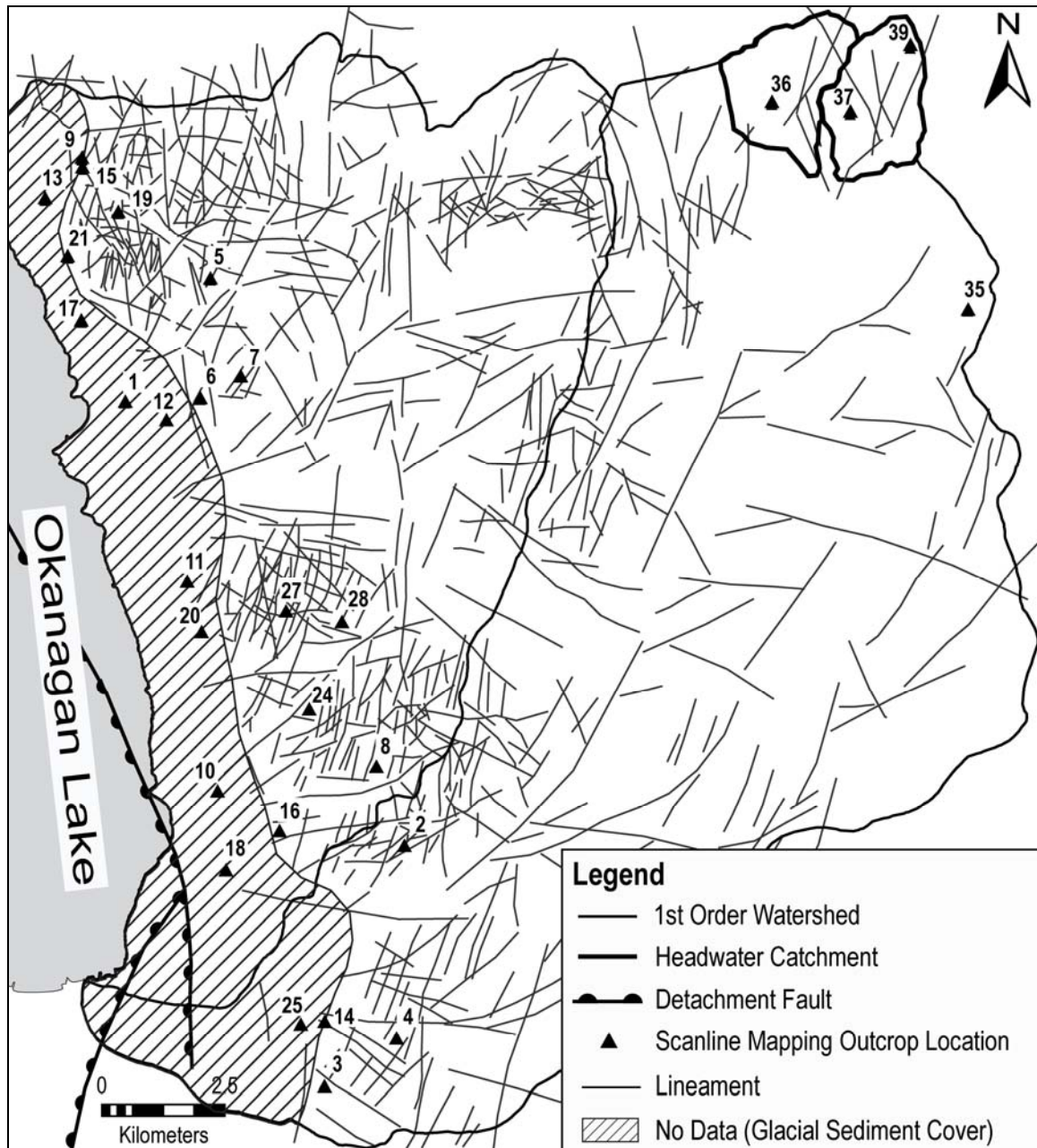
Figure 3.2. Map showing the outcrop scanline locations where small scale fracture parameters were measured. The lineaments mapped throughout the study area using LANDSAT imagery and orthophotos are also shown.

Figure 3.3. Scanlines on a vertical outcrop face (top image) and on the upper orthogonal surface of the outcrop (lower image) at outcrop location 1.

Fracture set information was systematically recorded in an Microsoft Excel table with a pocket PC in the field. Tables 3.1 to 3.3 give descriptions of the different fracture parameters (e.g. aperture, etc.) as well general characteristics of the outcrop, such as block size or degree of weathering of the outcrop. As an example, Tables 3.4 and 3.5 show the scanline and general data recorded at scanline (a) at outcrop location #1 (shown in Figure 3.3). All the other general information for each outcrop location and its fracture scanline data are listed in Appendix A.1.

Table 3.1. Fracture descriptions of aperture, discontinuity roughness and terminations noted during field measurements.

Descriptions 1				
Aperture			**Discontinuity roughness**	
Width	Description		Primary - [m] scale	Secondary - [cm] scale
<0.1 mm	very tight	"closed" features	planar (p)	rough (r)
0.1-0.25mm	tight		undulating (u)	smooth (sm)
0.25-0.5 mm	partly open		stepped (st)	slickensided (sl)
0.5-2.5 mm	open	"Gapped" features	**Terminations**	
2.5-10 mm	moderately wide		U = unknown - fracture trace is not observable	
> 10 mm	wide		T = terminates at high angle against another fracture	
			A = terminates at low angle or asymptotically against another	
1-10 cm	very wide	"Open" features	H = terminates by hooking into another fracture	
10-100 cm	extremely wide		B = fracture terminates in the rock matrix	
>1m	cavernous			

Table 3.2. Fracture descriptions of block shape and block size with reference to discontinuity roughness and terminations noted during field measurements.

Descriptions 2	
Block Shape	
Description	Shape
Few joints or very wide spacing	massive (m)
Approximately equidimensional	blocky (b)
One dimension considerably smaller than the other two	tabular (t)
One dimension considerably larger than the other two	columnar (co)
Wide variations of block size and shape	irregular (i)
Heavily jointed to "sugar cube"	crushed (cr)
Block size	
Description	joint/m^3
Very large (vl)	<1
Large (l)	1-3
Medium-size (ms)	3-10
Small (s)	10-30
Very small (vs)	>30

Table 3.3. Fracture descriptions of weathering stage of the rock material recorded during field measurements.

Descriptions 3		
Weathering of uniform material		
Grade	Classifier	Typical Characteristics
I	Fresh	Unchanged from original state perhaps slight discoloration on major discontinuity surfaces
II	Slightly weathered	Slight discolouration of rock and discontinuity surfaces, slight weakening
III	Moderately weathered	Considerably weakened, penetrative discolouration Large piece cannot be broken by hand
IV	Highly weathered	Large pieces can be broken by hand. Does not readily disaggragate (slake) why dry sample immersed in water
V	Completely weathered	Considerably weakened, Slakes, Original texture apparent
VI	Residual Soil	Soil derived by in situ weathering but retaining none of original texture or fabric

Table 3.4. General information noted during fracture field measurements as an example for outcrop location #1.

Outcrop #	1
General Data	
Outcrop Location #	1
Date	16-May-06
Name Surveyor	Hendrik Voeckler / Mary Ann Middleton
Character/dimension of outcrop	Wall-road cut (A,B-4mx11m), upper surface on top (C-20mx10m)
Near or away of fault zone?	500m E of lake
Lithology description	
Rock type	Quartzofeldspathic gneiss
Colour fresh/weathered	Fresh: light grey, banded with augen; Weathered: medium grey, abundant lichen
Homogeneous vs heterogeneous	heterogeneous
Sample taken?	no
Structures	
Foliation/bedding (Dip Dir./Dip)	274/38
Lineation (Trend/plunge)	nr
Folds (amplitude, wavelength, fold axis, fold plane)	
Fault (width, trace, gouge, orientation)	
Shear zone (width, trace)	
Rock mass description	
Block shape	irregular
Block size	ms
Weathering class	II
Seepage (presence/absence)	absent

Table 3.5. Excel table showing all the scanline and fracture parameters measured in the field as an example for scanline (a) at outcrop location #1 (see Figure 3.2 and 3.3).

Outcrop #: 1

One or more separate scanlines

			Dip Dir. [°]	Dip [°]
Photo #:	1	approximate surface orientation:	245	76

Outcrop Face Dimensions [m]:
y =11
z = 4

Scanline a)

Waypoint	E [m]	N [m]	Elev. [m]	SL length [m]	Trend [°]	Plunge [°]	Direction
1a	313039	5498096	445	8.5	321	-7	S-N

DATA

Fracture SL Intersection [m]	Dip Dir [°]	Dip [°]	Trace Length strike [m]	Trace Length dip [m]	Upper Termin.	Lower Termin.	Aperture [mm]	Primary roughness	Secondary roughness	Fillings	Movement	Comment
0.47	128	72		0.18	B	B	0	p	r	none	none	
0.64	135	78		0.21	B	T	0.73	p	r	none	none	
1.67	80	86		3.5	U	U	0	u	r	none	none	
1.85	240	86		0.28	B	B	0	p	s	none	none	
1.97	73	78		0.51	U	T	0	u	s	none	none	
2.69	254	76		0.84	B	T	0	p	r	none	none	
3.05	259	68		0.84	U	T	0	p	r	none	none	
3.19	261	74		0.96	B	T	0	p	r	none	none	
3.39	262	77		1.3	U	T	0	p	r	none	none	
3.52	265	80		0.89	T	T	0	p	r	none	none	
3.9	268	88		1.35	U	T	0	p	r	none	none	
4.11	270	85		1.54	U	T	0	p	r	none	none	
4.2	260	87		1.39	U	T	0	p	r	none	none	
4.39	253	89		nr	T	U	0	p	r	none	none	
5.08	74	79		1.95	B	T	0	p	r	none	none	

3.2.1. Processing of outcrop scale data for DFN modelling

A stereonet displays the poles of fracture planes in either a lower or upper hemisphere net. SpheriStat (SpheriStat v. 2.2, Pangea Scientific, 1998) was used to generate the stereonets and perform statistical analyses, like density distributions and cluster analysis. Figure 3.4 shows the poles of the fracture plane orientation data (trend [°] and plunge [°]) for all 29 outcrop locations (1199 fracture measurements). Also shown is the density distribution generated using a Gaussian counting model for contouring (SpheriStat v. 2.2, Pangea Scientific, 1998). The density contouring clearly identifies four outcrop fracture sets mapped at the regional scale for all outcrop locations. In many cases fracture set distributions can be described using a Fisher distribution (Fisher, 1953). A Fisher distribution is characterized by a uniform tight orientation cluster with limited dispersion k.
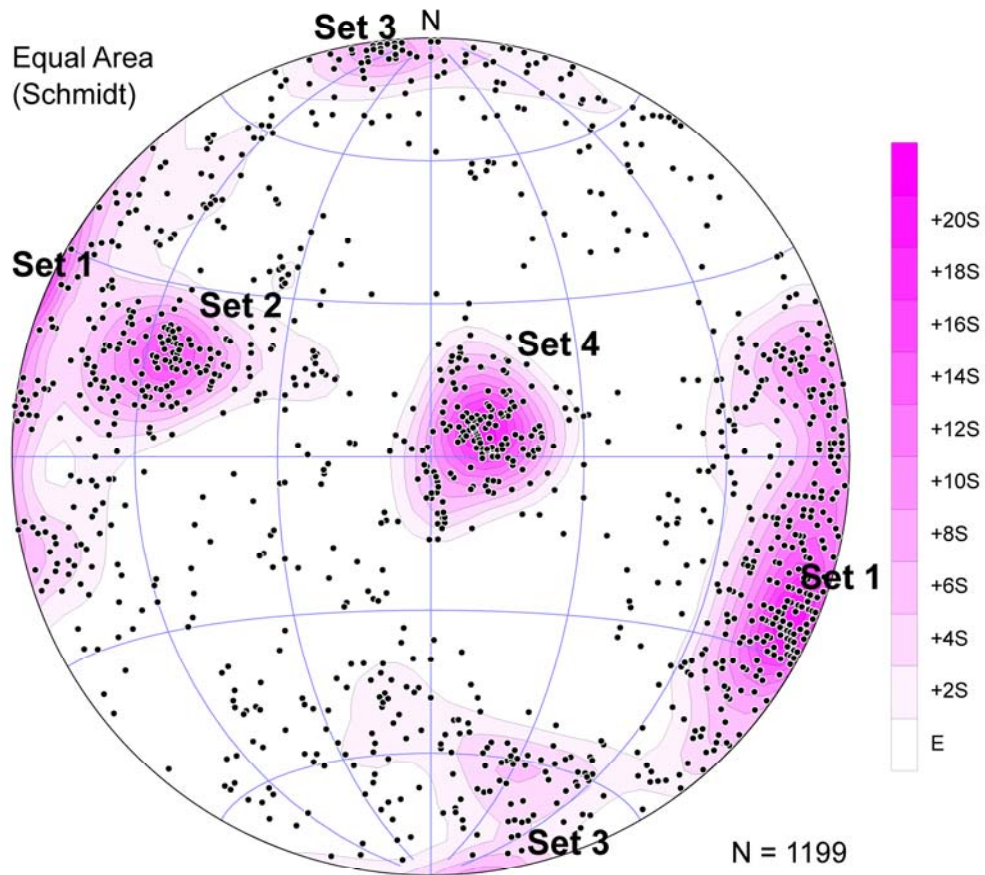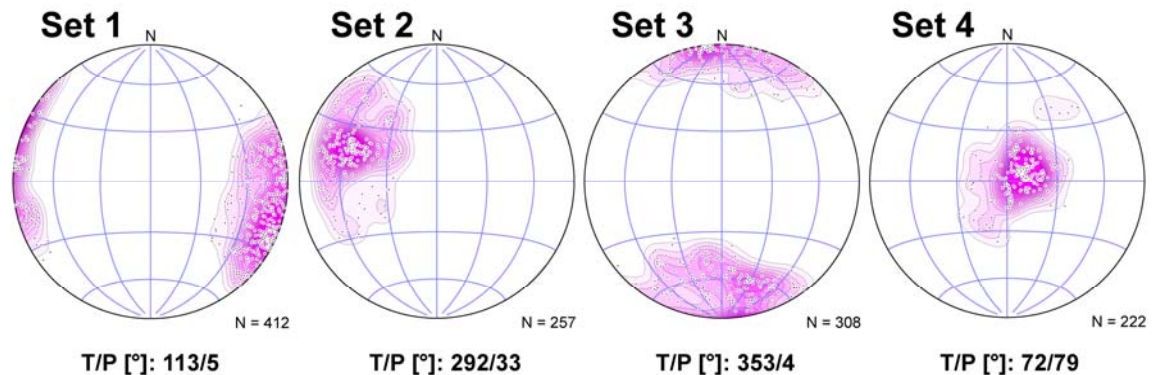
Figure 3.4. Stereonet showing the poles of all fractures measured at all outcrop locations throughout the study area and the four separated sets.

Figure 3.5 shows a stereonet of the fracture measurements at outcrop location #1. Only three sets of the four fracture sets can be identified. Through a cluster analysis, these three sets (set 1_1, set 1_2, set 1_4) were separated and displayed in single stereonets (lower portion of Figure 3.5). One clear and tightly clustered cloud (set 1_1) can be identified, which belongs to set 1. For the other two sets (set 1_2 and set 1_4) the clouds are not as well developed and tightly clustered as for set 1_1. The reason for that might be the low number of data points (fractures measured at that outcrop location) for those two sets. Poorly clustered clouds in a stereonet result in lower k-dispersion values, which are needed (see Chapter 4) for generating fracture sets with the DFN software. The generation of a fracture set also requires a distribution model. Similar to location #1, all separated sets of the other 28 outcrop locations (see Appendix A.2) were described using regular Fisher distributions. For most of the outcrop locations, set 4 as well as either set 1 or 2 are always present. Set 3 is missing at about one third of all outcrop locations.

It is also very interesting to notice that for the outcrop locations further away from the main Okanagan Valley Fault Zone (Loc. #35, #36, #37, #39, see Figure 4.7 in Chapter 4 and Appendix A.2.), the dip angles for fracture sets x_1 become shallower when moving further away from the main Okanagan Valley Fault Zone (OVFZ). Also at these four outcrop locations situated away from the fault zone, the dip directions for fracture sets x_4 change by about 180 degrees from nearly westward (locations closer to the fault) to nearly eastward (locations far away from the fault). Their dip angles remain similar.
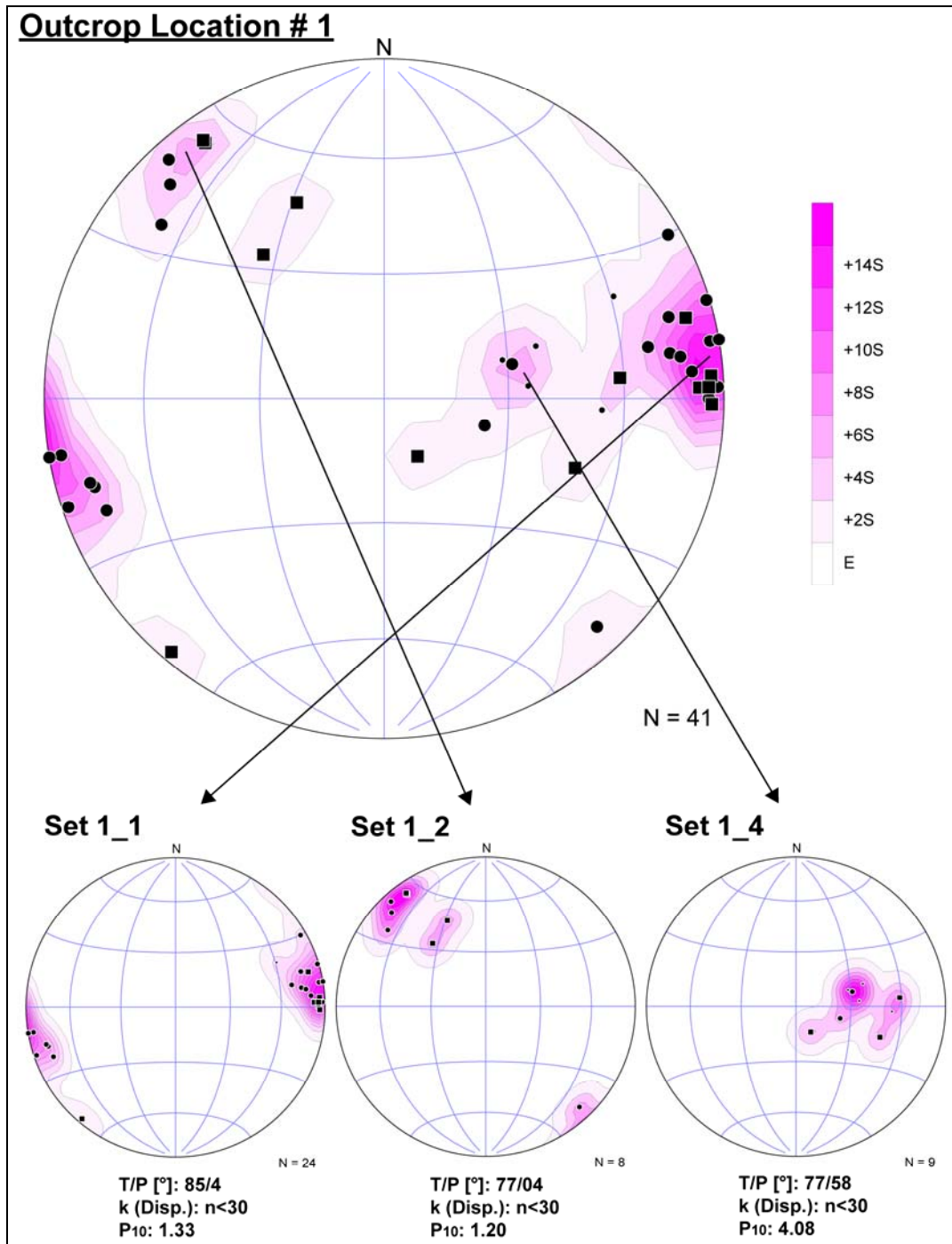
Figure 3.5. Stereonet of fractures measured at outcrop location # 1 and the stereonets of the separated fracture sets done through a cluster analysis (set 3 is missing at this site). Mean trend/plunge values and P_{10} intensity values for each set are also shown.

Also shown in Figure 3.5 beneath each separated stereonet are the mean trend and plunge values in [°] and the dispersion k [dimensionless] values calculated by SpheriStat for the contour cloud of each set. As mentioned earlier, the dispersion factor k is a measure of the clustering of each fracture data set. The higher the value of k, the more clustered are the data (Fisher et al., 1987). Dispersion values calculated from the individual outcrops are not considered representative, because for most of the outcrop locations, fewer than 30 fractures for each set were present. In general, for statistical analyses, the rule of thumb is that number of samples should be greater than 30. To account for the small sample size, the k values were adjusted for outcrop locations with fewer than 30 samples based on similar sets from nearby outcrop locations with greater than 30 samples. Figure 3.5 also shows the P_{10} values calculated for each set intersecting the scanline. Appendix A.2 shows a table above the stereonets for the separated sets for each outcrop location with the important parameters (Trend/Plunge [°], Dispersion, Mean Persistence [m], standard deviation (Std. Dev.), measured P_{10} intensity and upscaled P_{32} intensity) needed for DFN model generation. Concerning the persistence of fractures, only the mean values and standard deviations were calculated because typically fewer than 30 values were available for each set. In general, for those locations with a statistically representative number of data points (# of samples/fractures > 30) the most common fracture trace length distributions (e.g. Figure 3.6 for set 25_2) can be described as a log-normal distribution. Thus, all the fracture sets will be generated for the DFN models with a log-normal trace length distribution using the mean and standard deviation values calculated from the measured fractures.
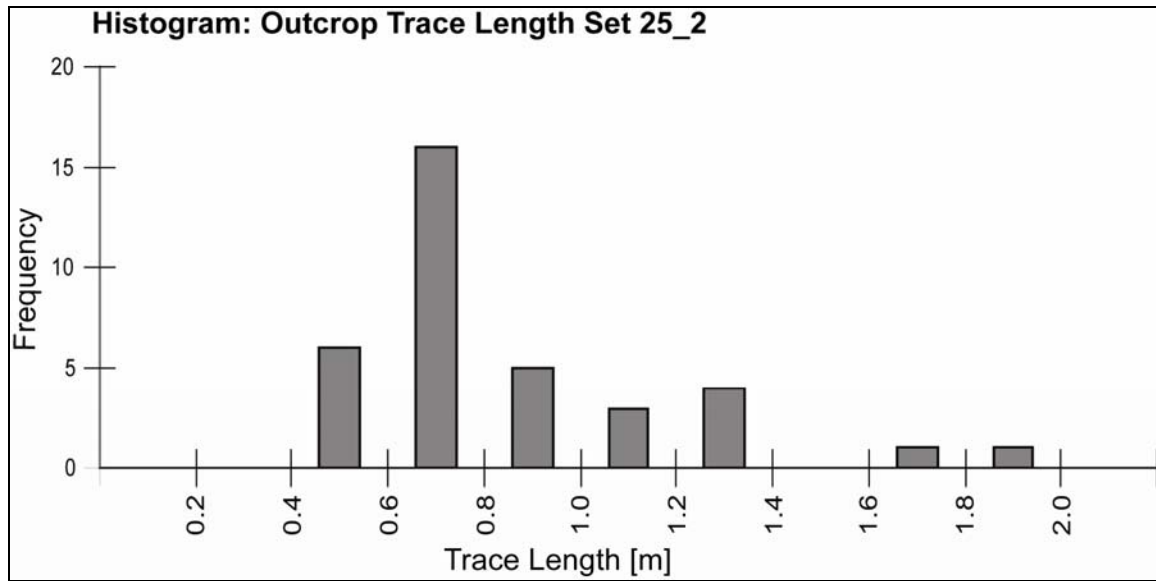
Figure 3.6. Histogram showing trace length distribution of outcrop fracture set 25_2 (36 data values). The histogram indicates a clear log-normal distribution.

3.3. Lineament scale fracture data collection

In geoscience, methods of remote sensing data collection permit the delineation of regional features and trends, provide representation for areas that may be inaccessible by field investigations, and save considerable time and resources when analyzing a large study (Singhal and Gupta, 1999).

The lineament analysis applied to the Naramata and Penticton Creek Watersheds in Okanagan Basin was undertaken by Natural Resources Canada. It incorporated a 25-m resolution digital elevation model (DEM) and 12.5 m LANDSAT 7 Thematic Mapper multispectral panchromatic imagery. Regional scale lineaments were mapped both using detailed aerial (ortho) photos and LANDSAT images from the near-infrared band 4. A hillshade was computed from the DEM to extract features of the landscape through the

use of shadowing and sun-angle illumination. By calibrating the hillshade to several different sun angles, different structural characteristics could be identified. Lineaments mapped using the LANDSAT image generally did not reveal one of the lineament sets that had been identified in both outcrop and using orthophotos, especially at higher elevations where the lineament density is lower. Therefore, for this study a composite lineament map was generated using the lineament data from both the orthophotos and LANDSAT imagery to ensure that all the lineaments were captured at the regional scale. The final lineament trace map is shown in Figure 3.2.

3.3.1. Lineament density mapping

Based on the lineaments shown in Figure 3.2, a lineament density map was constructed using the ArcGIS Kernel Density Tool for polylines. This method calculates a magnitude per unit area from the polyline features (length) using a Kernel function that fits a smoothly tapered surface to each polyline. Density was categorized into three zones (low, medium and high) (Figure 3.7). Two assumptions were made when constructing the map: 1) lineaments under the lake sediments are assumed to exist, but cannot be detected through the sediment cover. For this reason, the lineament density adjacent to the lake is assumed the same as that bordering the sediments to the east, and 2) patches where no lineaments were mapped are the result of either sediment cover or dense vegetation cover, making it impossible to detect them. In such areas, it was assumed that the lineament density is similar to that in neighbouring areas. Due to the above assumptions, some

corrections near the borders of the three zones and near big patches of no data had to be

made manually on the generated Kernel density map.
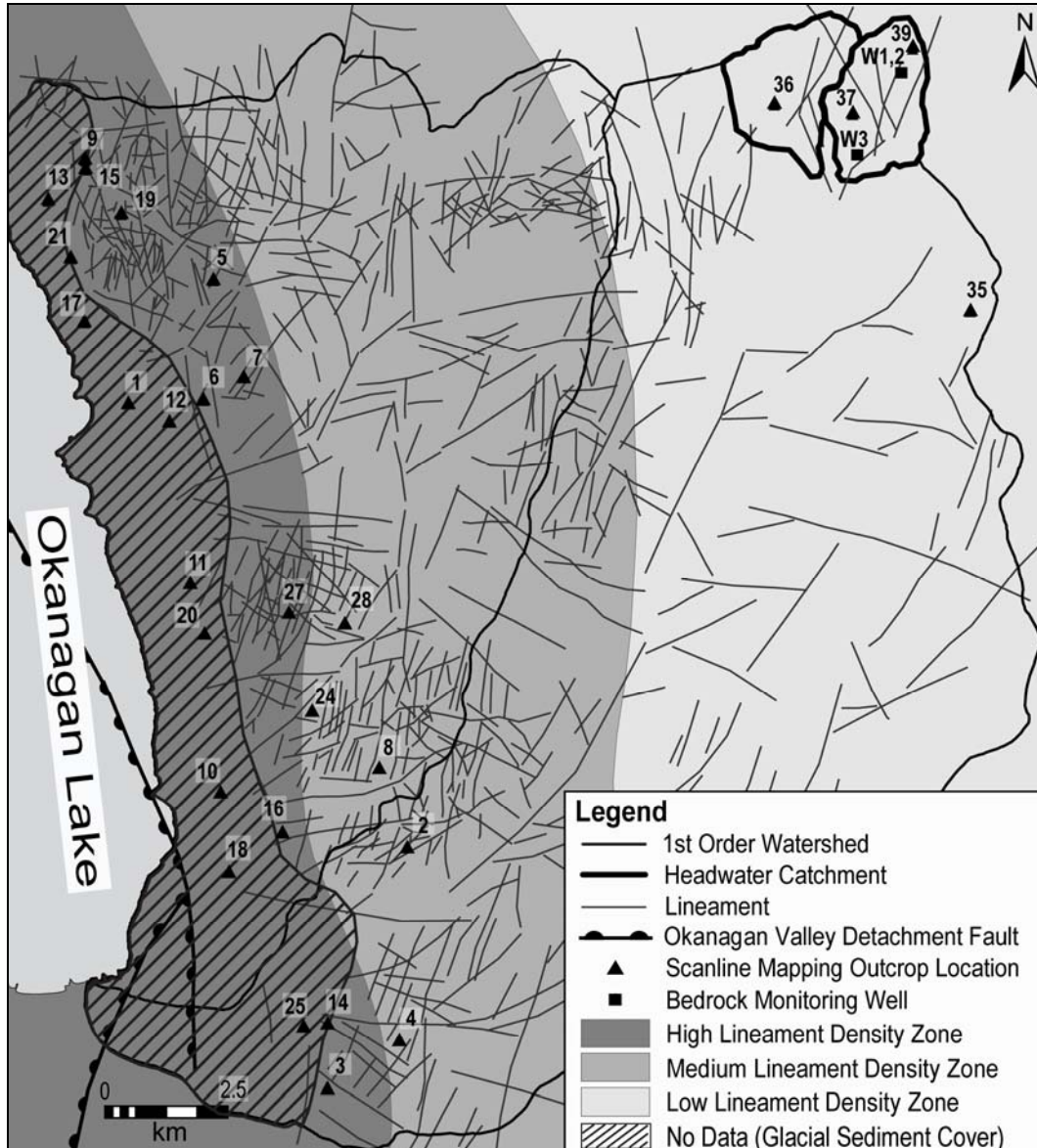
Figure 3.7. Map showing the three lineament density zones (high, medium and low) determined through an ArgGIS Kernel density analysis from lineament maps of orthophoto and LANDSAT imagery. Also shown on this map are the outcrop scanline mapping sites and the bedrock monitoring wells in the UPC 241 catchment (discussed in Section 3.6), located in the northeast portion of the map.

3.3.2. Processing of lineament scale data for DFN modelling

To generate the large scale DFN models for the lineaments, the trend/plunge values, dispersion factors, P_{32} values, and trace lengths distributions are needed for each density zone, similar to the outcrop scale models. Only the traces (strike orientation) on the Earth's surface can be analysed using these remote sensing methods. Therefore, information on the dip angles of lineaments cannot be obtained. For DFN modeling, further processing of the lineament data was undertaken. A technique was developed to estimate these missing parameters and is described in more detail in Chapter 4.

3.4. Hydrometeorology

Time series of all climate, streamflow and snow course data measured throughout the UPC 241 watershed are described in this section. Figure 3.8 shows the locations within the catchment where these measurements were made. Figure 3.8 also shows the locations of the soil piezometer transects (see Section 3.5), the bedrock monitoring wells (see Section 3.6) as well as the stream/road network, the elevation contours, and the most recent logging stage of about 47%.
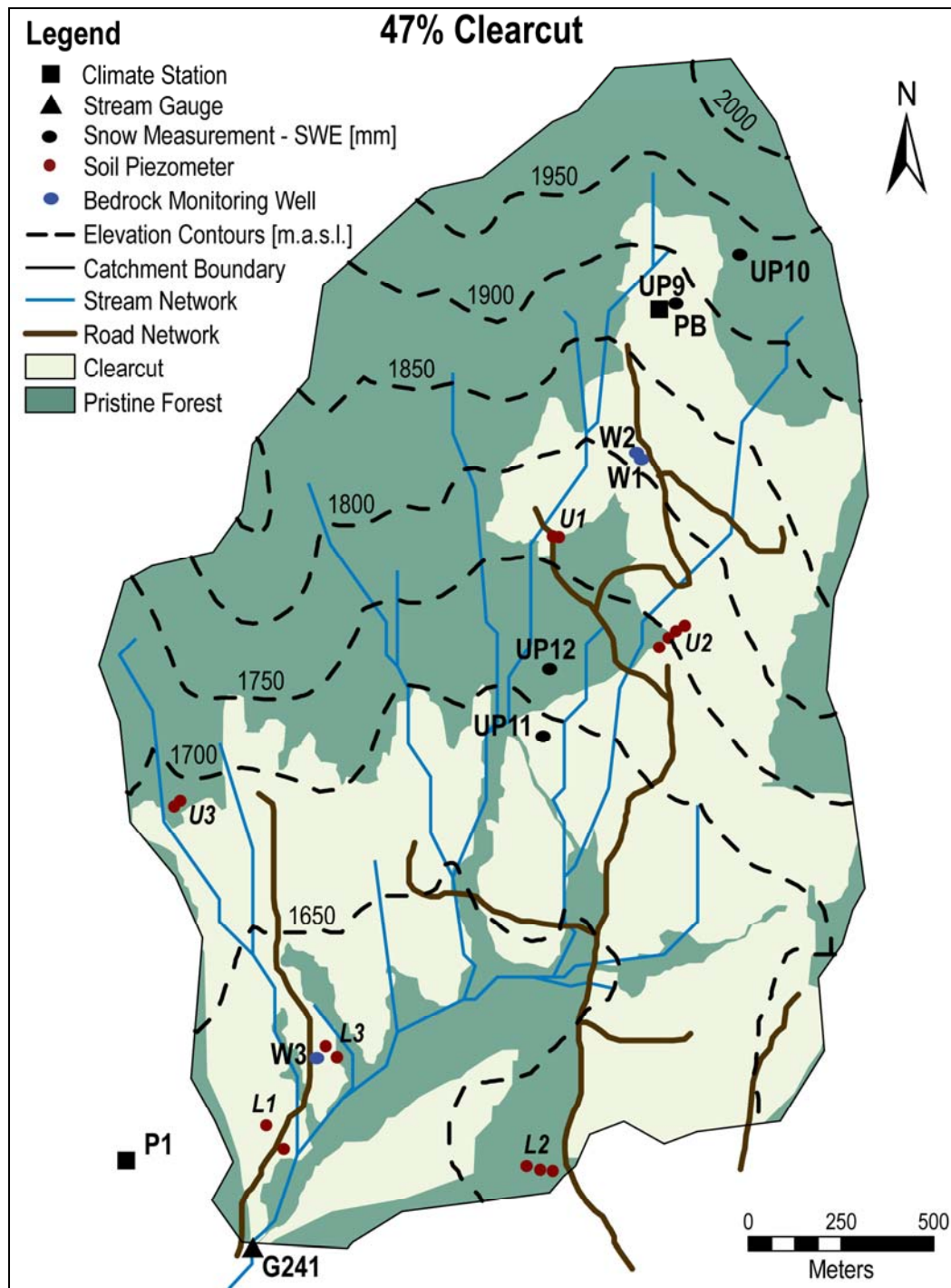
Figure 3.8. Location of the six soil water well transects in lower and upper elevations of UPC 241. The logged areas cover about 47% of the watershed. Also shown are the three bedrock monitoring wells, the piezometers, and the climate and hydrometric data measurement locations.

3.4.1. Climate data

Hourly climate data (air temperature, precipitation (rain and snow), relative humidity, shortwave solar radiation, and wind speed data) are available from the long term UPC watershed experiment database (BC Ministry of Forests and Range (BCMoFR EP956), and have been measured at a lower elevation P1 site (1620 m; Figure 3.8) in a large forest clearing since August 1997 as well as at an upper elevation PB clearcut site (1900 m; Figure 3.8) since September 1999. Both stations have their equipment mounted on a 10 ft (3.048 m) high, 10 inch (25.4 cm) triangular tower. The monitoring unit is a Campbell Scientific CR10X datalogger with a SM192 storage module in a waterproof housing. The sensors sample every 60 seconds and output data are provided as daily and hourly time series. The sensor for the air temperature and humidity is a Campbell Scientific HMP35C mounted at 2.5 m above the ground. The sensor for solar radiation is a LiCor LI200 pyranometer, mountetd at 3 m above the ground. The wind speed sensor for P1 is a RM Young 05103-10 Wind Monitor at 4 m above ground, and the one mounted at the PB station is a MetOne 013 anemometer at 3 m above ground. Snow depth is measured at the P1 station through a UDG01 sonic distance sensor mounted at 2 m above the ground. This sensor was replaced in 2008 with a SR50A sonic distance sensor. PB has a SR50 sensor at 2 m above the ground installed. Precipitation (rain and snow) is measured at both stations with a tipping bucket gauge Texas Electronic, Jarek 4000, or Sierra Misco 2502 at 0.5 m above the ground. Precipitation data as snow is measured through the sonic distance sensors just mentioned.

Figure 3.9 to 3.11 show the climate data from the two stations. These data are used as input to the MIKE SHE model used to simulate water flow in the watershed (see Chapter 5). The potential evapotranspiration (PET) (Figure 3.12), needed as input to MIKE SHE, was calculated with AWSET software (Cranfield University, 2002) from the climate data measured at the two stations. More details on the calculation are given later. Only the most recent data, spanning a period of nearly four years ranging from January 2007 to mid-September 2010, are displayed in the figures. Climate data from the earlier years (1998 to 2006 for P1 and PB) are included in the full dataset in Appendix A.3.

Figure 3.9 shows the hourly temperature variation over four years (2007 to 2010) from the two climate stations. The data from both climate stations look very similar. Due to the temperature gradient with elevation, temperatures measured at the higher elevation site (PB) are, in general, slightly lower (by ~2°C). The highest temperatures (up to 30°C) were measured in the summer months of July and August. The lowest temperatures (approx. -28°C) were measured during the winter months from December to March when temperatures rarely rise above zero degrees Celsius.
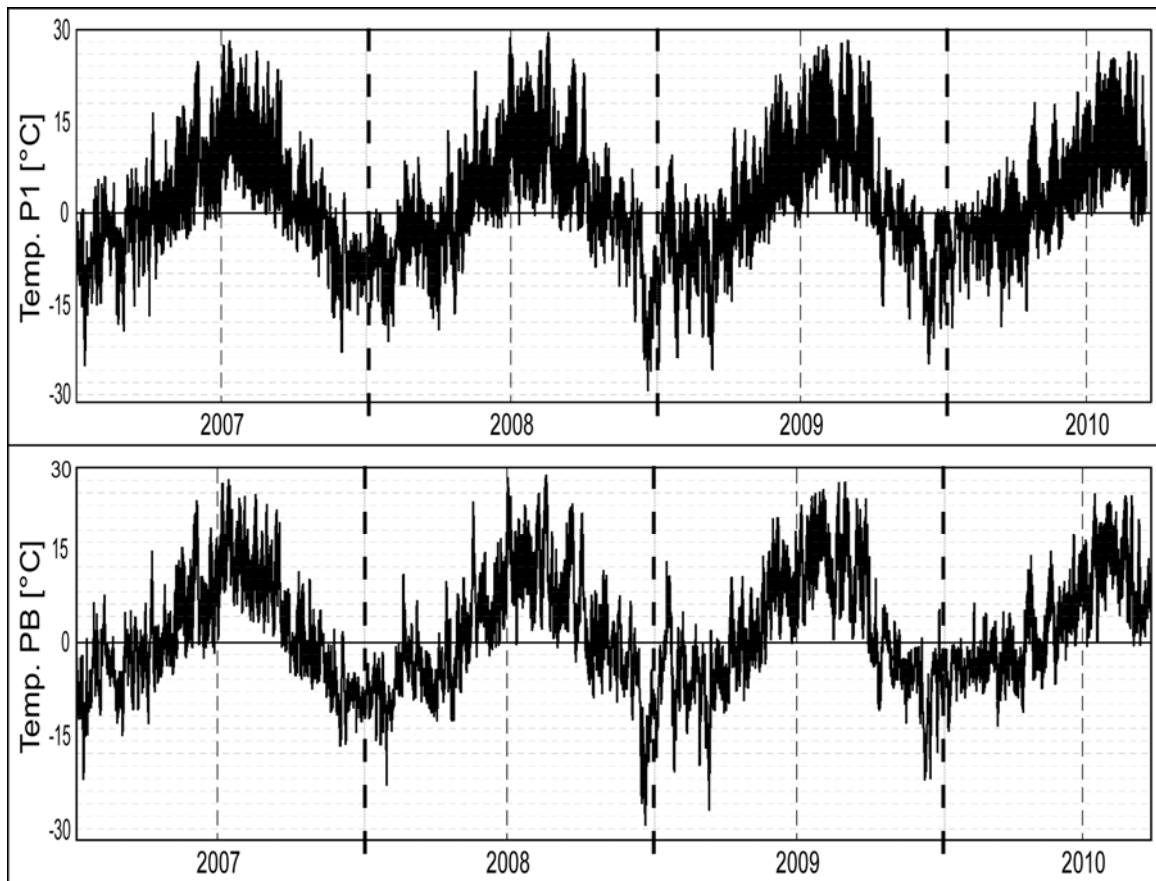
Figure 3.9. Four year variation of hourly air temperature data measured at the P1 (upper diagram) and the PB (lower diagram) climate stations within the UPC 241 catchment (2007-2011).

Figure 3.10 shows the hourly precipitation rate (rain and snow) for the same four year period from both stations P1 and PB. A maximum value of about 15 mm was measured at the higher elevation site PB in early June of 2007. The most intense precipitation events occur from April to the end of June. During the summer months of July and August, precipitation events decrease in number and intensity. In the fall (September to November) rain events increase again, but not as intensely as in spring. During the winter months (December to March) most of the precipitation falls as snow

(due to temperatures below zero) with events ranging from 0 mm to about 5 mm, similar to the intensity seen during the summer months. A precipitation gradient between the two stations due to elevation does not appear to exist.
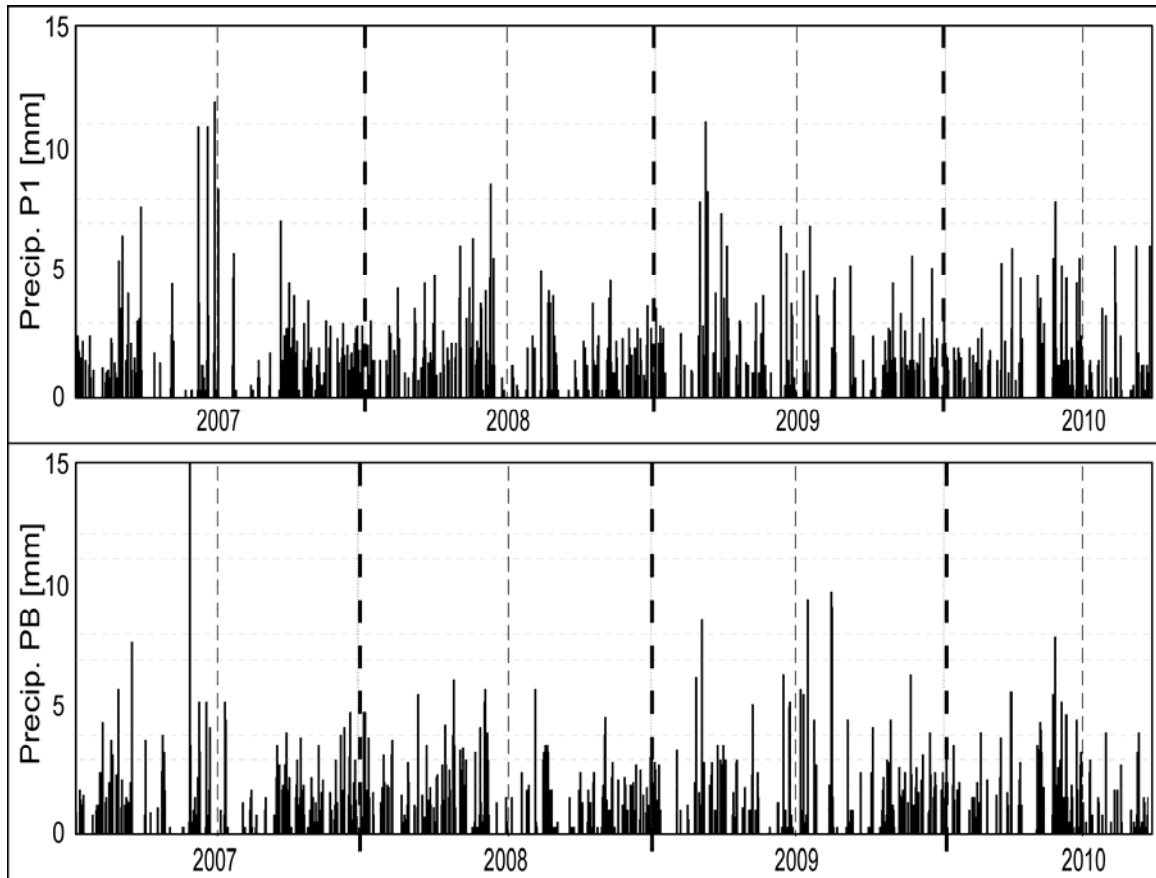
Figure 3.10. Four year variation of hourly precipitation data (rain and snow) measured at the P1 (upper diagram) and the PB (lower diagram) climate stations within the UPC 241 catchment (2007-2011).

Figure 3.11 shows the hourly short wave solar radiation measured at the two stations. Both patterns look very similar with highest values (~4000 KJ/m^2/h) during the summer months and lowest values (~500 KJ/m^2/h) during the winter months. At the

higher elevation PB site, values are in general slightly higher. Maximum values were measured at the PB site in July 2009 and June 2010.
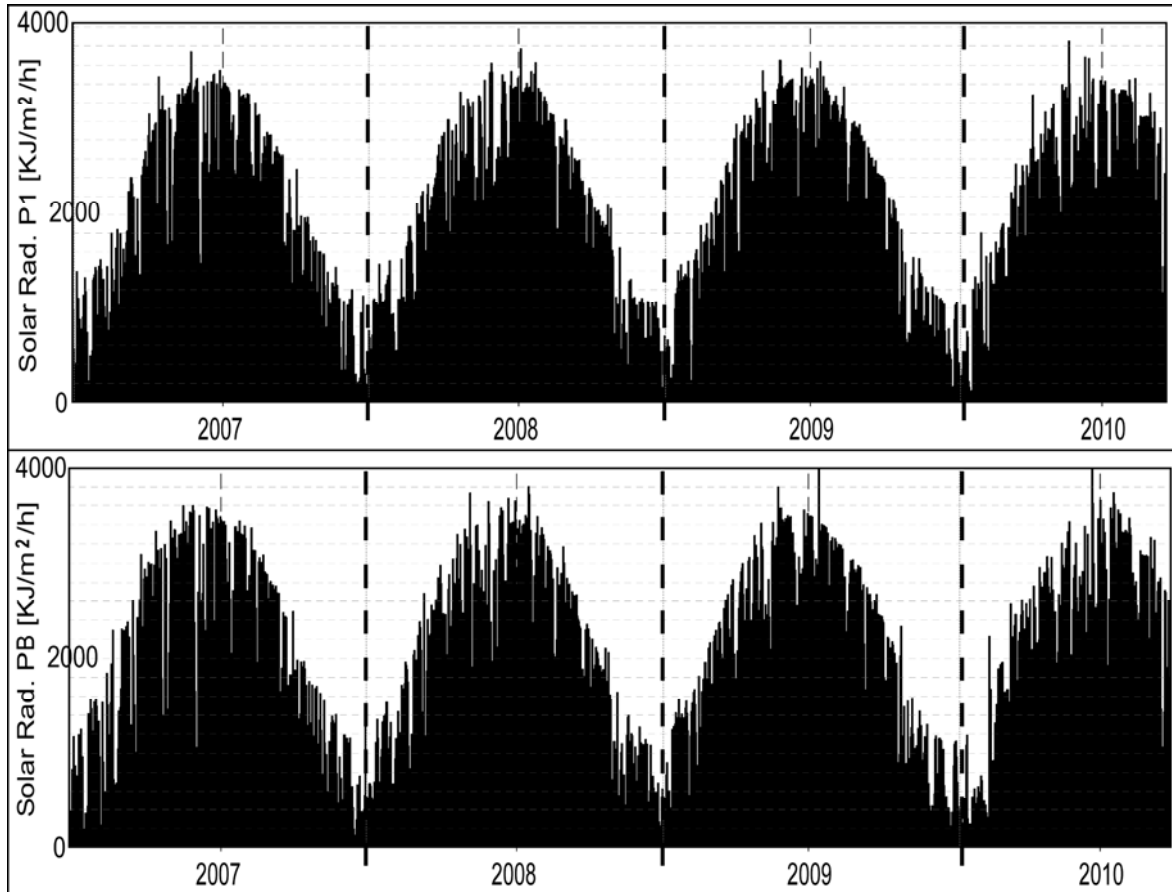
Figure 3.11. Four year variation of hourly short wave solar radiation data measured at the P1 (upper diagram) and the PB (lower diagram) climate stations within the UPC 241 catchment (2007-2011)**.**

Figure 3.12 shows the daily potential evapotranspiration (PET) calculated for both stations using AWSET (Cranfield University, 2002) software. The Penman-Monteith method was used to calculate PET (Allen et al., 1998). The minimum required input data are air temperature, humidity, solar radiation and wind speed, which were measured at the two climate stations P1 and PB at hourly time steps. The maximum PET is ~6 mm/d

during the summer months and the minimum PET is ~0.5 mm/d during the winter months.
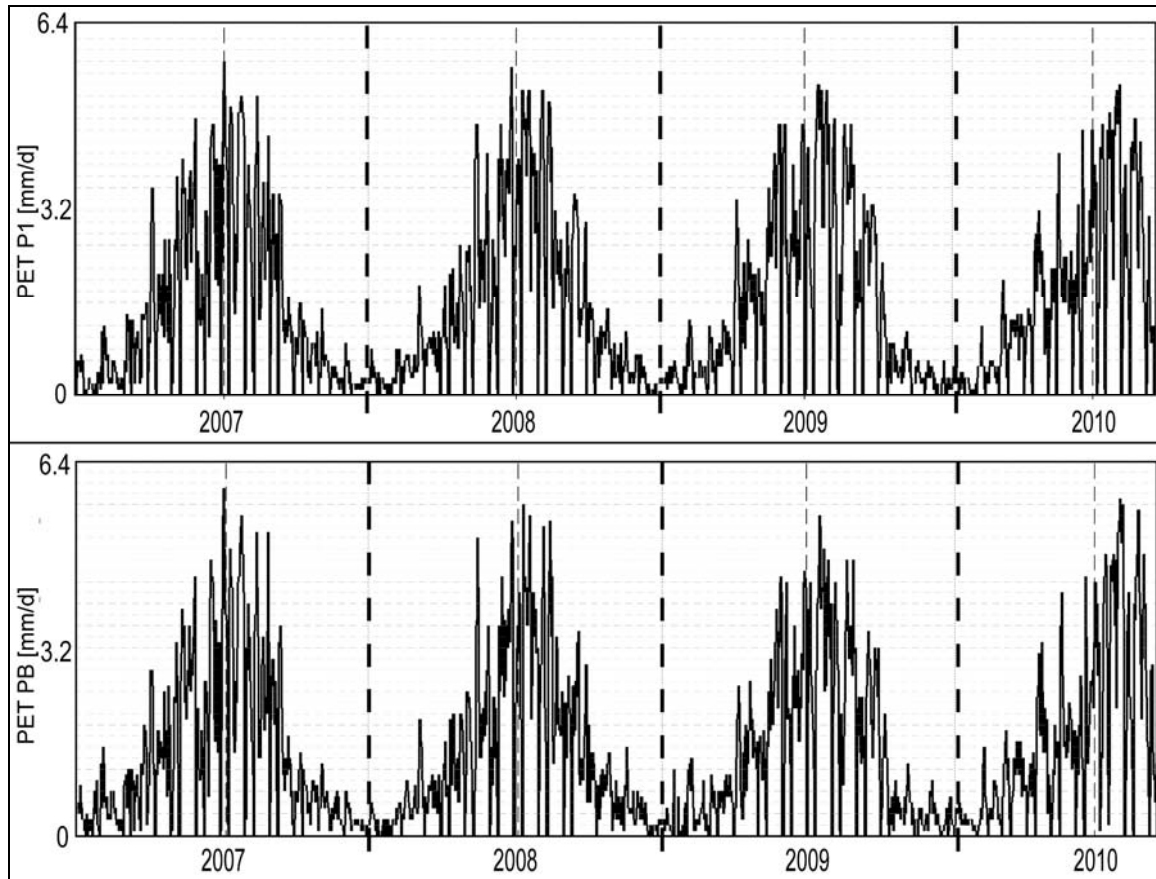
Figure 3.12. Four year variation of daily potential evapotranspiration (PET) calculated with AWSET software (Cranfield University, 2002) for the P1 (upper diagram) and the PB (lower diagram) climate stations within the UPC 241 catchment (2007-2011).

3.4.2. Stream flow data

The stream network for the watershed was originally derived by a DEM analysis with the ArcGIS Hydrology tool, which was modified using a GPS field survey to capture details of the stream network (Kuras, 2006). At the outlet of the watershed, the Water Survey of Canada (WSC) installed and maintains a hydrometric station (08NM241 –

renamed to G241 in this study), which has been measuring real time hydrometric data (river stage) since 1983. From the rating curve, which can be seen for the river gauging station G241 in Figure 3.13, streamflow discharge data in [m³/s] can be calculated from the measured raw river stage data for the same time step. The processed discharge data in hourly time steps was provided to us by the WSC.
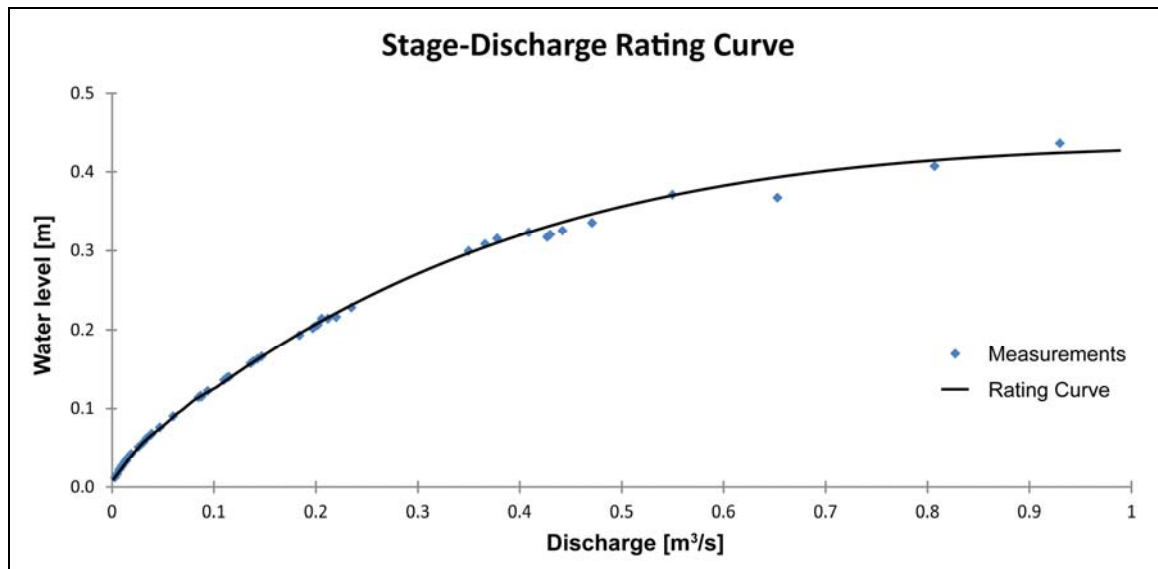
Figure 3.13. Rating curve developed from measurements taken at the gauging station G 241.

In general, a rating curve is established by making a number of concurrent observations of stage and discharge over a period of time covering the expected range of stages at the river gauging section. From that rating relationship, the observed stages can be transformed into corresponding discharges. At a hydrometric station, the river stage can be observed continuously or at regular short time intervals with comparative ease and economy. In its simplest form, a rating curve can be illustrated graphically, as shown in

Figure 3.13 above, by the average curve fitting the scatter plot between water level (as ordinate) and discharge (as abscissa) at any river section (Herschy, 1995).

With the provided hourly streamflow/discharge data, a hydrograph for the same time period as shown earlier for the climate data series (2007 to 2011) was developed (Figure 3.14). The additional years of streamflow (1998 to 2007 for each year) can be found in Appendix A.4.
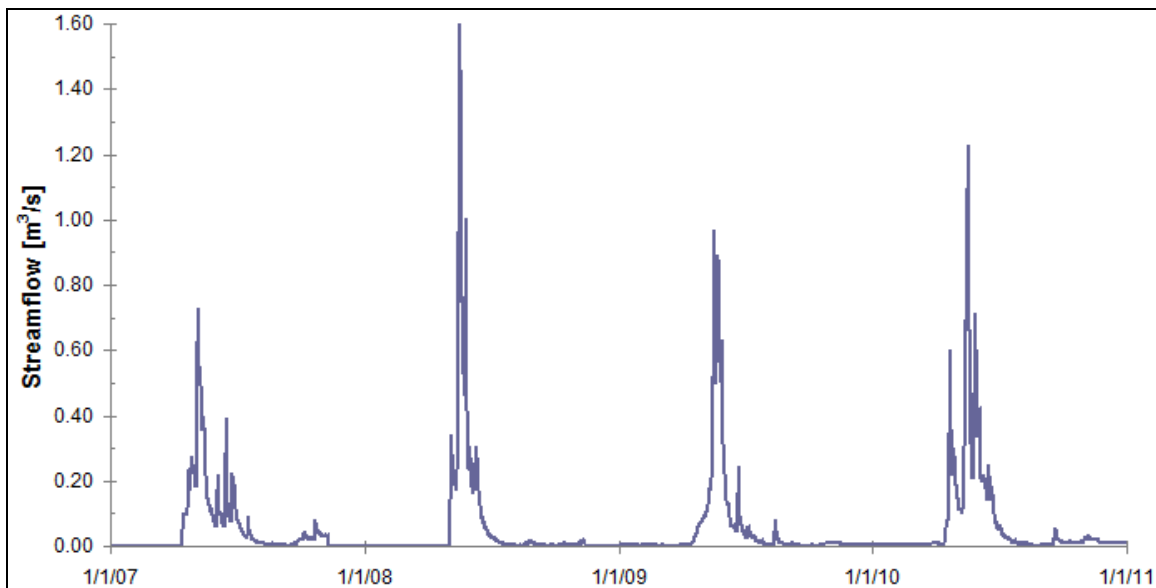
Figure 3.14. Four year hydrograph measured at a hydrometric station G241 at the outlet of the UPC 241 watershed (2007-2011).

The main peak flow responses (peak discharge) due to the spring snowmelt occur between late April and May. During the four years shown, the maximum peak flow was 1.60 m^3/s in 2008, while the lowest peak flow was 0.75 m^3/s in 2007. Peak flows in 2009 and 2010 are intermediate. The shapes of the annual responses differ due to different unique climatic events throughout the year. Smaller responses late in the year are due to rainfall events, while the early year high peak flow responses are a consequence of the

snowmelt in spring or rain on snow events. Rain on snow events result in very high peaks (McCabe et al., 2007). Baseflow at low discharge rates during the summer and winter months is generated through discharging groundwater from the fractured bedrock aquifer and possibly the soil zone.

3.4.3. Snow measurements

Snow water equivalent (SWE) was sampled during the 2004/2005 accumulation and melt periods at four permanent snow courses in early and mid-March, or near April 1, and then weekly throughout the melt period (Winkler et al., 2005). The four sites include each of a forest and clearcut location (UP12 and UP11, respectively) at mid elevation, and each of a forested and clearcut location (UP10 and UP9, respectively) in an upper elevation area of the catchment. The measurement locations consisted of 32 permanent sampling points, spaced equally on a 15 m by 15 m grid. At the forested sites, sample points were positioned in both gaps among trees and adjacent to trees in order to capture a range in conditions. Figures 3.15 to 3.18 show SWE at the four measurement sites for the 2004 and 2005 measurement periods.
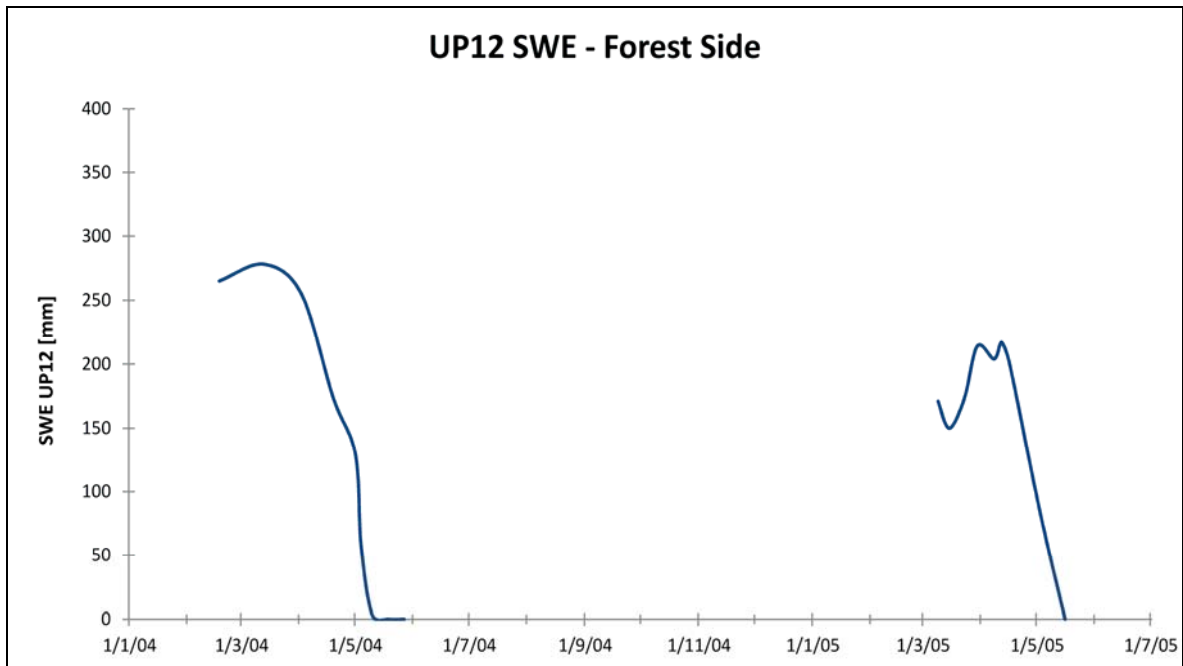
Figure 3.15. SWE for 2004 and 2005 at UP12 at mid-elevation situated in a forested area.
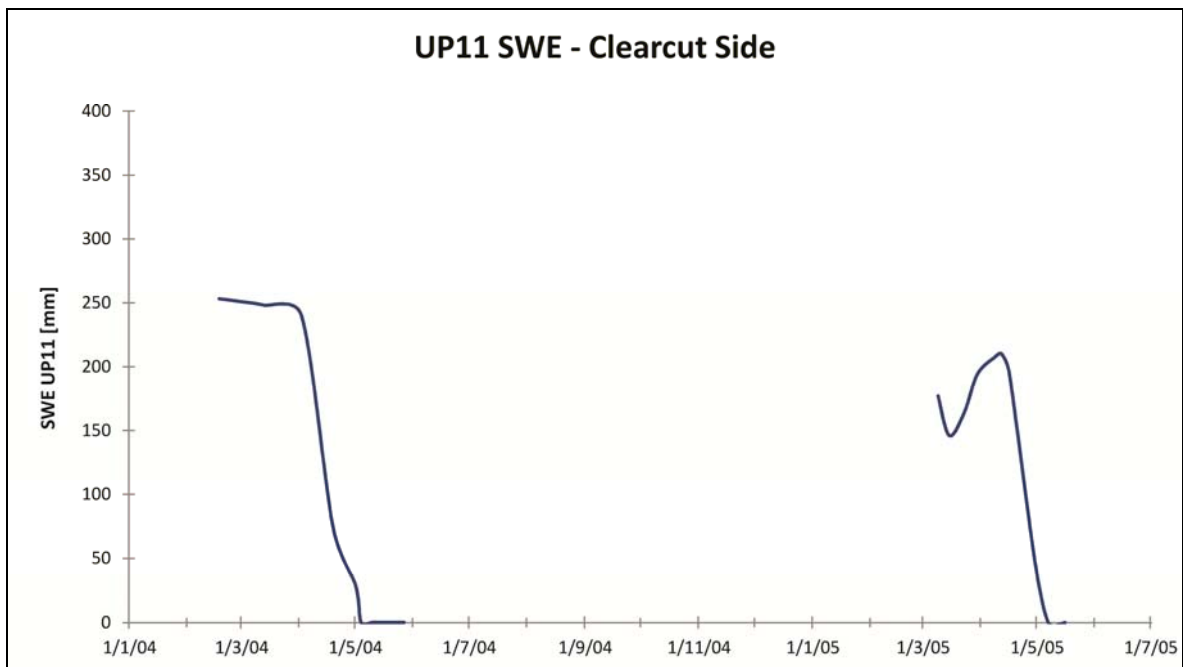
Figure 3.16. SWE for 2004 and 2005 at UP11 at mid-elevation situated in a clearcut area.
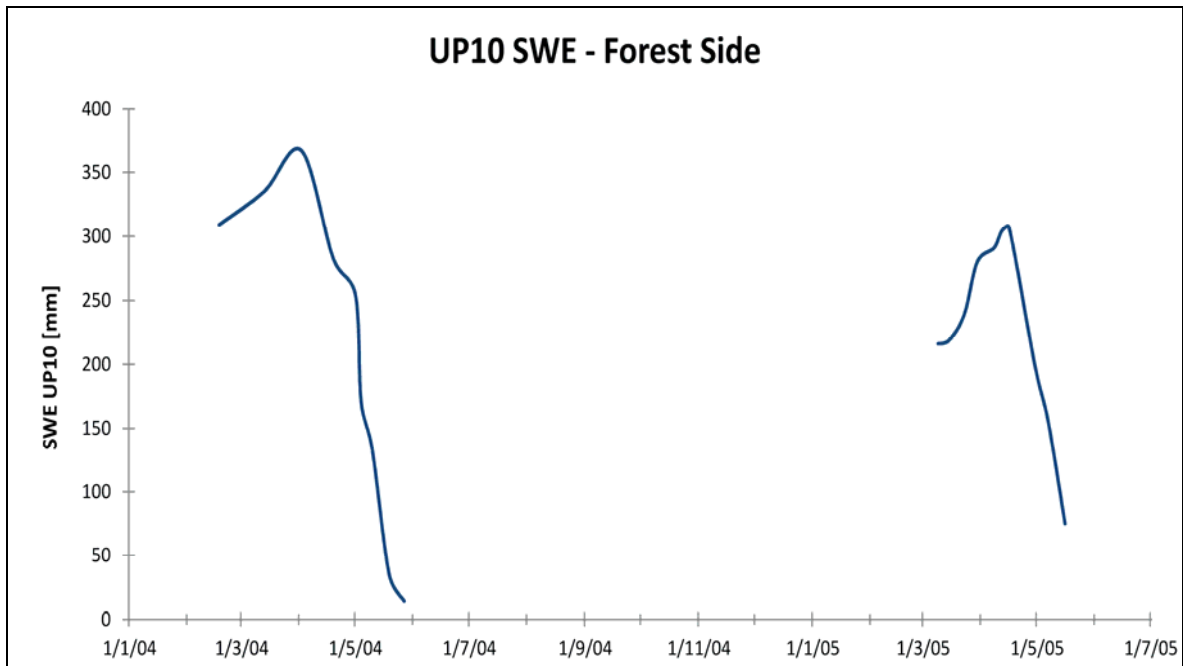
Figure 3.17. SWE for 2004 and 2005 at UP10 at high-elevation situated in a forested area.
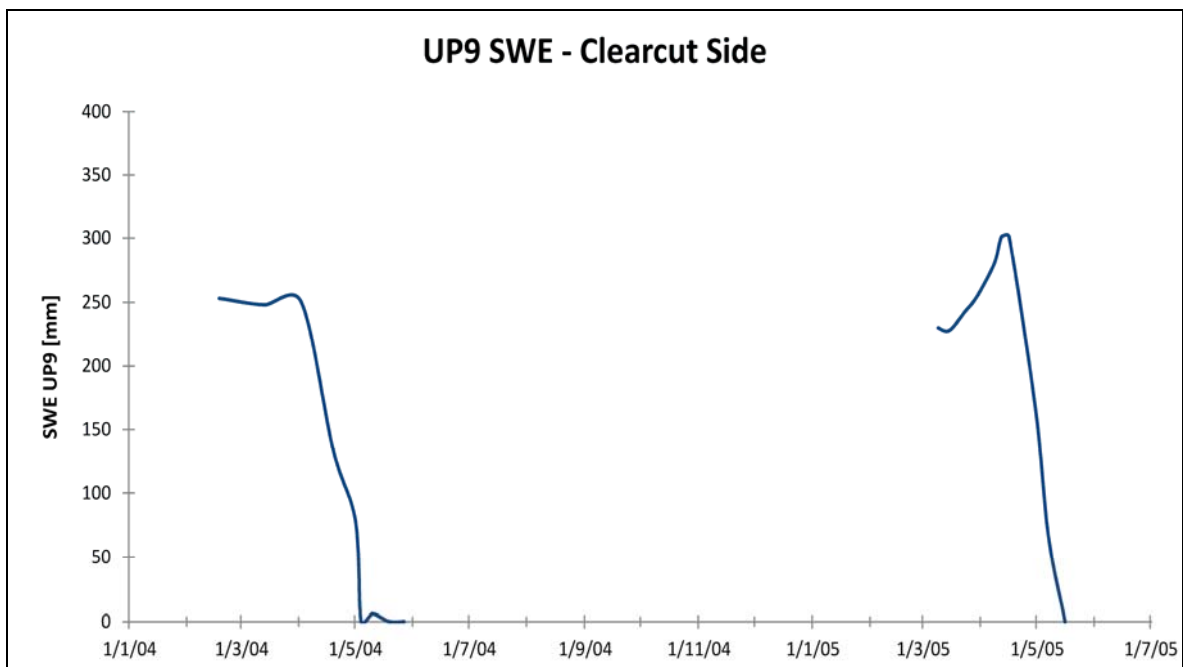
Figure 3.18. SWE for 2004 and 2005 at UP9 at high-elevation situated in a clearcut area.

3.5. Shallow soil water piezometers

As part of a Masters study carried out at UPC 241 by Piotr Kuras from 2004 to 2006, soil water levels were observed in shallow piezometers throughout the study area. The soil water dynamics has been described as shallow, perched saturated flows above the bedrock joints and fractures (Kuras, 2006). Before the spring snowmelt season of 2005, Kuras installed soil water monitoring transects (9 piezometers) strategically throughout the watershed to give an overall representation of soil water fluctuations from the hillslopes towards the riparian zones in upper and lower elevations, as well as in clearcuts, clearcut edges and forested areas. Six additional soil water piezometers were installed as part of this study in July and December 2007 at locations not covered by the nine piezometers previously installed by Kuras. The piezometer transects were positioned to follow the downslope routing of flows along hillslopes (approximated by surface topography). The piezometers were installed insuring that there were no topographic disconnections (rises or depressions) between the piezometers. At the riparian zones, in order to avoid influx of subsurface water influenced by local stream levels, the piezometers were installed with the base level set a small height above the water surface of proximal streams. The change in elevation between each piezometer in a transect was large enough to prevent overlap, and ranged approximately 3-6 m. Figure 3.8 (above) shows the locations of six soil water well transects (15 piezometers in total) in upper (U1 and U2 transects) and lower elevations (L1, L2 and L3 transects) throughout the UPC 241 watershed.

Each soil water piezometer is an open-ended PVC pipe (Ø32 mm). To allow for soil water infiltration, holes (Ø6.35 mm) were drilled around the circumference up to a length of 30 cm from the bottom end. This lower portion of the pipe was fitted with fine-meshed tube gauze to avoid sediment influx. Boreholes were augered beyond the depth of the pre-melt season water table, and the void interface between the soil and pipe was filled with fine gravel to a level 10-15 cm below the surface to create sufficient hydraulic conductivity around the pipe. The upper portion of the interface was filled with bentonite clay to seal the hole from surface runoff. This ensures that standpipe water levels are only representative of subsurface flows. Each piezometer was equipped with an Odyssey Capacitance Water Level Probe (Data Flow Systems Pty Ltd., Christchurch, New Zealand). Data were recorded automatically with the datalogger set to a sampling interval of 30 minutes. Table 3.6 gives an overview of the main details of all the soil water piezometers.

Table 3.6.   Soil water well/piezometer details.

Location	Well	Elevation [m]	Cover Type	Hillslope Position	Depth [cm]
U1	P6	1740	clearcut edge	hillslope	55
	P5	1736	clearcut edge	riparian	119.5
U2	P1	1740	clearcut	hillslope	70.5
	P3	1728	clearcut	hillslope	91.5
	P2	1721	clearcut	hillslope/riparian	69.5
	P4	1716	clearcut	riparian	105
U3	P15	1697	forest	hillslope	69
	P14	1678	forest	hillslope/riparian	89
L1	P7	1595	clearcut	lower depression	77
	P8	1590	young regen	riparian	80
L2	P9	1644	forest	hillslope	76.5
	P10	1638	forest	hillslope	70
	P11	1635	forest	hillslope	94
L3	P13	1628	clearcut	hillslope/riparian	97
	P12	1619	clearcut edge	riperian	95

3.5.1.   Soil water dynamics - data collection and interpretation

For the same four years (2007 to 2011) the soil water level fluctuations of four selected piezometers (P2, P8, P11, and P14; shaded grey in Table 3.6) are discussed in this section. The dataset for the full monitoring period (2005 to 2011) of all piezometers can be found in Appendix A.5. P2 and P14 are located at high elevation in a hillslope/riparian interface zone; P8 is closest to the outlet of the watershed and is located in the riparian zone of a newly regenerated forest; P11 is located on the hillslope of a forested area.

Figure 3.19 shows the soil water fluctuations in piezometers P2 (upper) and P14 (lower). Water levels are shown in units of head elevation in the unsaturated zone in metres above sea level. As mentioned, both piezometers are located in the hillslope/riparian interface zone at high elevation of the watershed; P2 in a clearcut area and P14 is in a forested unlogged area. P14 was installed later than P2, at the end of 2007. Peak responses of the soil water fluctuations in both piezometers occur around the same time of the year; between late April and May due to the spring snowmelt and rain on snow events. However, the overall response is different between the two. For the piezometer located in an unlogged area (P14), the rising and recession limbs go up and down smoothly in comparison to the response in the clearcut piezometer (P2), where the soil water table rises up abruptly and recedes very quickly, with a very small time lag. The reason for this fast response is the high disturbance of the soils due to logging, resulting in a low retention ability of those soils; this low retention also possibly causes flooding in the lower parts of the watershed (Kuras, 2006). The maximum fluctuation in soil water level at P2 throughout the four years is about 60 cm. P14 fluctuates within a range of about 40 cm. It is also very interesting that peak responses measured in P14 due to late fall rain events (see November of 2009 and 2010) barely appear in P2. The response to the same events in the clearcut area is very low.
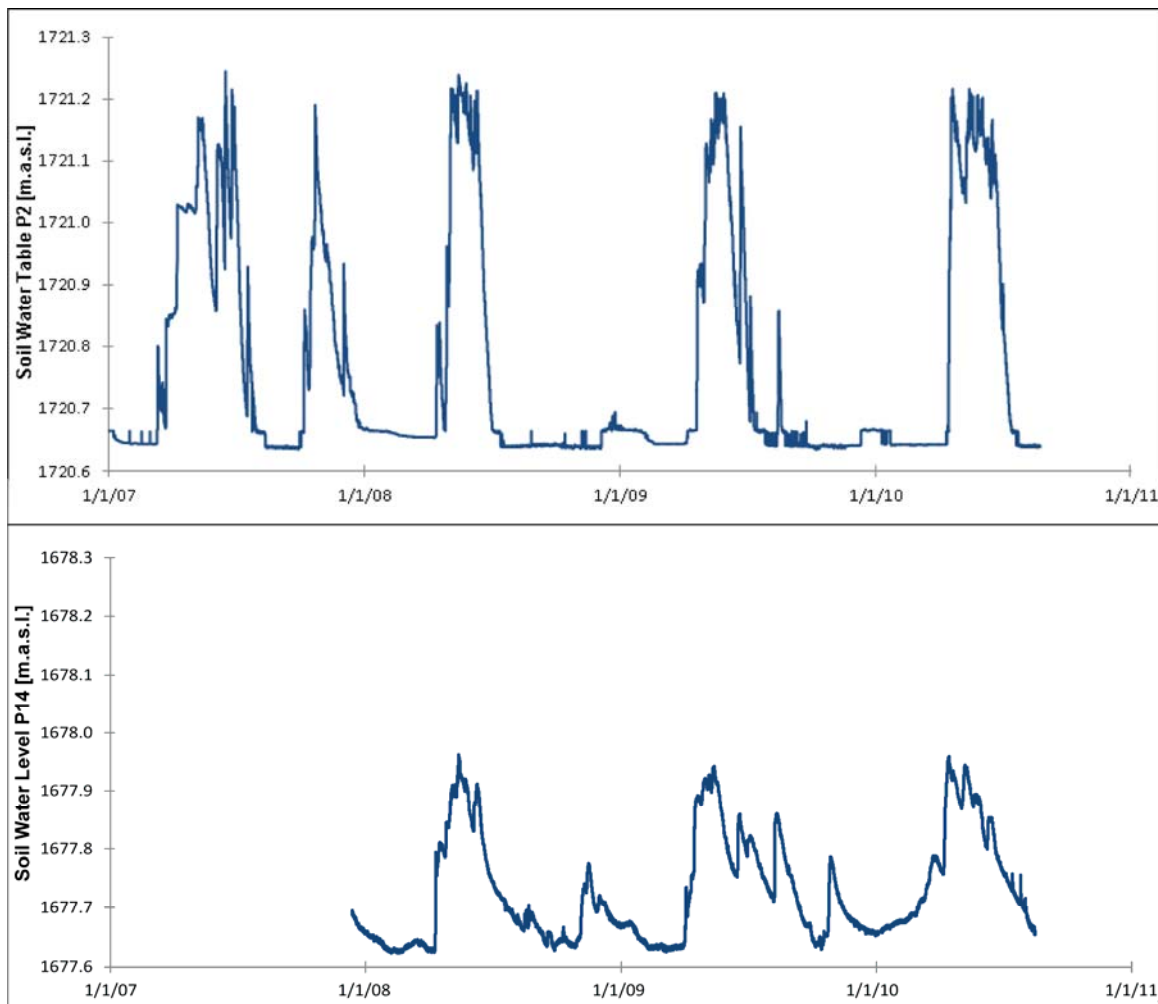
Figure 3.19. Soil water fluctuations measured in two piezometers (P2: clearcut, P14: unlogged) situated in a hillslope/riparian interface.

Figure 3.20 shows the soil water fluctuations over the four year period for a piezometer located in a newly regenerated forest area located in a riparian zone (P8) and for a hillslope zone in an unlogged area (P11). The responses of the soil water fluctuations in P8 are very similar to those seen in the clearcut area (P2; Figure 3.14). This indicates that the soils in a newly regenerated forest area respond very quickly and do not retain water like an undisturbed soil. Despite early re-growth, retention capability

still seems to be poor. The responses to the snowmelt in P8 are smoother and slower especially for the recession limbs. Similar to the fluctuations seen at P2, the responses to late fall rain events are also absent in the newly regenerated forest area, whereas distinctive wide peaks are evident in late fall/winter for piezometer P11 in an undisturbed forested area. Fluctuations between minimum and maximum water levels are about 60 cm in P8 and about 1 m in P11. Piezometers located on hillslopes appear to always have a higher overall change from highest to lowest water levels throughout the year compared to piezometers located in the riparian zones of the catchment.
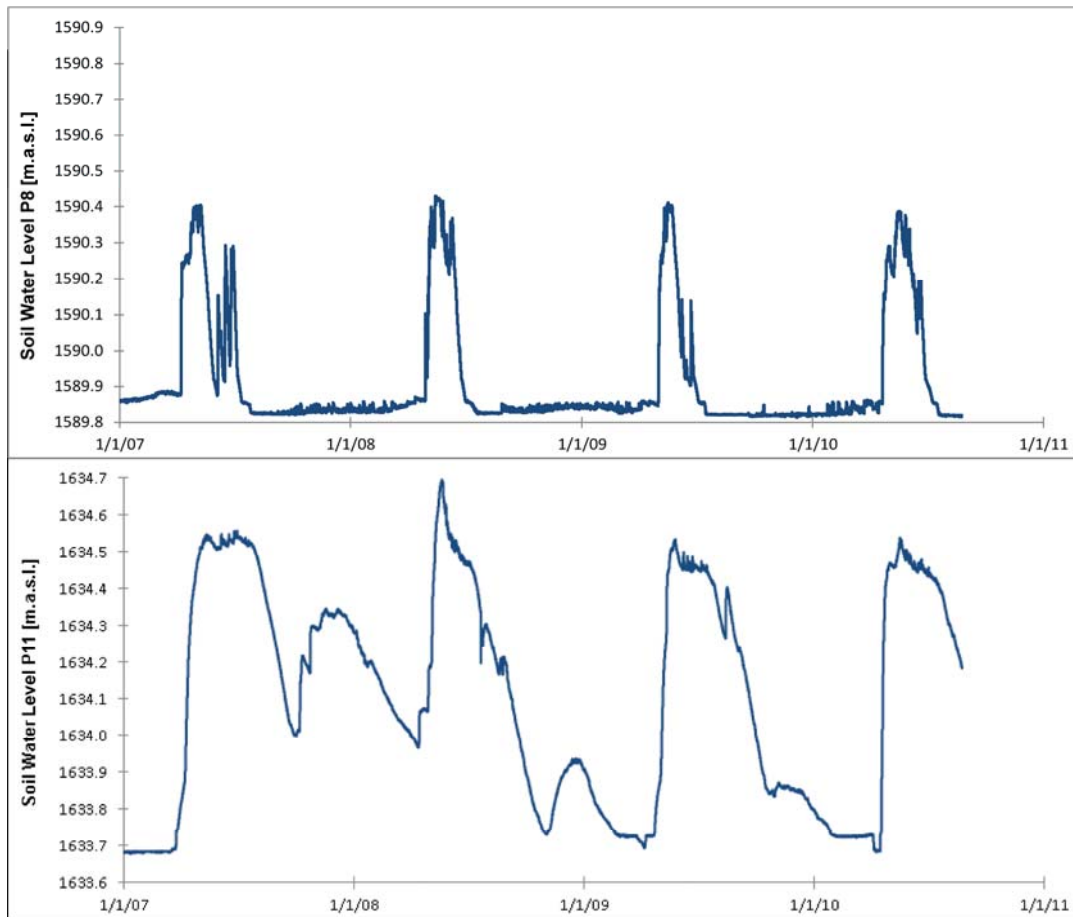
Figure 3.20. Soil water fluctuations measured in two piezometers (P8: riparian zone in a newly regenerated forest; P11: hillslope in a forested area).

3.6. Deep groundwater wells

Three deep bedrock wells were drilled by Cascade Drilling Ltd. (based in Kelowna, BC) at the UPC 241 watershed in July 2007. The drill rig was a 1988 Ingersoll-Rand Cyclone T-H 60 Air Rotary Drill rig mounted on a GMC general Tandem axle chassis. Two nested (~3 m apart) bedrock monitoring wells (W1 and W2) were drilled in the upper part of the headwater catchment at the end of July 2007. Well 1 is 46 m deep (150 ft) and well 2 is 30 m deep (100 ft). A third well (W3) (30 m deep – 100 ft) was drilled at lower elevation in the catchment, down gradient of wells 1 and 2 by about 1,800 m (see Figure 3.8).

At wells 1 and 2, the overburden was very thin (less than 0.2 m (0.5 ft)); well 3 had about 5 m (18 ft) of overburden (well report summaries with depths in feet in Tables 3.7-3.9). Steel casing was grouted in place to a depth of about 2.5 m (8 ft) for well 1 and 2 and to about 6.4 m (21 ft) for well 3. The boreholes are uncased for the remainder of the depth. Water injection was used with air lift to remove cuttings, which were examined and recorded on the well report forms submitted to the BC Ministry of Environment. The bedrock is described as granodiorite of the Ladybird and Vallhala intrusions, possibly slightly metamorphosed (note green colouration recorded at some depths in Well 3 (Table 3.9). Water production and estimated yield from water bearing fractures were also recorded. Water bearing fractures appear to correlate well with fracture zones identified from the geophysical borehole logs (see Section 3.6.2). Well plate tags were attached to each well as per government regulation.

Table 3.7. Well construction details for Well #1 – Well Plate Number 15849.

Well location:
This well is located near the top of the 241 Penticton Creek watershed. The well is at the south side of a small landing near the top of the highest accessible logging road.

GPS coordinates:
Zone 11 N
UTMs – 328254, 5504627
Elevation of top of casing – 1805.47 masl
Estimated ground elevation – 1805 masl (error ± 6.0m)
Type of Well – Class: Monitoring Well, Sub-Class: Permanent

Lithologic Description:

From (ft. bgl)	To (ft. bgl)	Relative hardness	Colour	Material Description	Water-bearing (est. flow)	Comments
0	0.5	Loose	Brown	Soil	Dry	Shallow overburden, only a few inches
0.5	17	Medium	Grey	Crystalline	Dry	Described as granodiorite of the Ladybird and Vallhala intrusions, possibly slightly metamorphosed
18	20	Medium	Grey	Crystalline	1 USgpm	Small fracture
20	40	Medium	Grey	Crystalline		No change in flow
40	60	Soft	Grey	Crystalline	Dry	Water loss, cuttings were like powder
60	65	Medium	Grey	Crystalline	Wet	Small fractured zone, cuttings were wet
65	80	Soft	Grey	Crystalline	Dry	water loss, cuttings again like powder
80	80	Medium	Grey	Crystalline	Wet	fracture, some water gain
80	100	Medium	Grey	Crystalline	3 USgpm	slightly fractured interval, gained some additional water
100	150	Medium	Grey	Crystalline		no major increase in water flow

Casing Details: Casing stickup – approximate 1.5 ft. - 10 ft. of casing total

From (ft. bgl)	To (ft. bgl)	Diameter	Casing Material/Open hole	Wall thickness	Drive Shoe
0	8	6	steel		

Estimated yield at the end of drilling – 3 USgpm.
Static water depth (measured from top of casing) - 4.76m.
Estimated static water table elevation (1805m- 4.76m = ~1800.824 m above mean sea level).

Table 3.8. Well construction details for Well #2 – Well Plate Number 15850.

Well location:
This well is situated approximately 3.30m to the right (north) of Well#1.

GPS coordinates:
Zone 11 N
UTMs – 328259, 5504625.
Elevation of top of casing = 1805.81 masl
Estimated ground elevation – 1805.20 masl (error ± 6m)
Type of Well – Class: Monitoring Well, Sub-Class: Permanent

Lithologic Description:

From (ft. bgl)	To (ft. bgl)	Relative hardness	Colour	Material Description	Water-bearing (est. flow)	Comments
0	0.5	Loose	Brown	soil	Dry	Shallow overburden, only a few inches
0.5	10	Medium	Grey	Crystalline	Dry	Described as granodiorite of the Ladybird and Vallhala intrusions, possibly slightly metamorphosed
10	20	Medium	Grey	Crystalline	1 USgpm	Small fracture, a bit of water when the drill rods were changed.
20	40	Medium	Grey	Crystalline	Wet	Gradual reduction in the amount of water
40	60	Soft	Grey	Crystalline	Dry	Complete water loss, cuttings were like powder.
60	85	Soft	Grey	Crystalline	Dry	Still no water, cuttings like powder.
85	85	Medium	Grey	Crystalline	1 USgpm	Small fracture, a bit of water
85	92	Medium	Grey	Crystalline		
92	92	Medium	Grey	Crystalline	2 USgpm	Small fracture, gain in water
92	100	Medium	Grey	Crystalline		

Casing Details: Casing stickup – approx. 2 ft. - 10 ft. of casing total

From (ft. bgl)	To (ft. bgl)	Diameter	Casing Material/Open hole	Wall thickness	Drive Shoe
0	8.5	6"	steel		

Estimated yield at the end of drilling – 2 USgpm
Static water depth (measured from top of casing) - 5.10 m (and continuing to rise).
Estimated static water table elevation (1806m-5.10m = ~1800.9 m above mean sea level)

Table 3.9. Well construction details for Well #3 – Well Plate Number 15851.

Well location:
Well is located near the base of 241 watershed directly down gradient of wells #1 and #2.
GPS coordinates:
Zone 11 N
UTMs – 327379, 5503001.
Elevation of top of casing = 1624.47 masl
Estimated ground elevation – 1624 masl (error ± 7m)
Type of Well – Class: Monitoring Well, Sub-Class: Permanent
Lithologic Description:

From (ft. bgl)	To (ft. bgl)	Relative hardness	Colour	Material Description	Water-bearing (est. flow)	Comments
0	18	Loose	Brown	soil	Dry	Overburden relatively deep; bedrock depth deeper than anticipated.
18	18	Medium	Grey	Crystalline	Wet	Described as granodiorite of the Ladybird and Vallhala intrusions, possibly slightly metamorphosed. A bit of water at the bedrock interface;
18	38	Medium	Grey	Crystalline	Wet	Loss of water during drilling
38	40	Medium	Green	Crystalline		Slight greenish colour
40	64	Soft	Grey	Crystalline	Dry	No water, powder drill cuttings
64	64	Medium	Grey	Crystalline	5 USgpm	fracture
64	80	Soft	Green	Crystalline	12 USgpm	Possible fracture zone, granular cuttings, look like coarse sand
84	84	Medium	Green	Crystalline		Fracture
84	100	Medium	Green	Crystalline		

Casing Details: C. stickup - approx. 1.5 ft. - 10 ft. of c. total - not full 3ft. into bedrock					
From (ft. bgl)	To (ft. bgl)	Diameter	Casing Material/Open hole	Wall thickness	Drive Shoe
0	20.5	6"	steel		

Estimated yield at the end of drilling – 12 USgpm
Static water depth (measured from top of casing) - 6.56m (and rising).
Estimated static water table elevation (1624m-6.56m = 1617.44 m above mean sea level)

When drilling was completed, each well was equipped with a pressure transducer and data logger to monitor the deep groundwater dynamics (Section 3.6.1). Borehole geophysical logging was undertaken in July 2009 (Section 3.6.2). A series of aquifer tests were carried out (pumping tests: Section 3.6.3; and slug tests: Section 3.6.4). For the nested upper two wells, the vertical flux was estimated at different times of the year (Section 3.6.5).

3.6.1.   Groundwater dynamics - data collection and interpretation

As mentioned, immediately following drilling, at the end of July 2007, all three wells were equipped with a PT2X submersible pressure/temperature Smart Sensor data logging device (range: 30 psi) made by Instrumentation Northwest Inc. The loggers were installed at a depth of about 15 m below the top of the casing (TOC). The logging interval was set to twice daily; 6 a.m. in the morning and 6 p.m. in the evening. The first logger readout was intended for the end of July 2008. Unfortunately, it was discovered that all three logging devices had not been work properly. The loggers were removed and sent for repair and possible data recovery. Fortunately, all data for well 1 for the first year were recovered. Data for the first year from the loggers in wells 2 and 3 could not be recovered. It was discovered that the loggers had been exposed to extreme temperatures, indicating that the loggers were not submerged sufficiently in the water column. As a result, three new loggers made by Onset Computer Corp. were installed (range: 58 psi). The logging interval of the new loggers was set to every hour. The loggers were installed to a depth of 20 m below TOC in each well at the beginning of November 2008. As a

result, there is a gap in the data July 2008 to November 2008 for well 1 and there is a range of missing data from July 2007 to November 2008 for wells 2 and 3.

Figures 3.21 and 3.22 show the water table fluctuations for wells 1 and 3, respectively. The data for well 2 are not shown (see Appendix A.6.), because the response is essentially the same as for well 1, with just a few centimetres difference in water table elevation due to their difference in depth (W1: 50 m; W2: 30 m).

Figure 3.21 shows the groundwater fluctuation in well 1 from the end of July 2007 to the most recent date of data readout (end of September 2010), with the data gap in Fall 2008. On an annual basis, the water table fluctuations are similar with minor differences in the shape of the response due to climate variations. Examining the 2009 data, the late Fall (mid- to late October) is characterized by the lowest water levels (1798 m). After that, due to intense fall rain events the water level rises to about 1801 m and then drops again during the frost period in the winter months. The beginning of April sees an abrupt rise in water level (by about 7 m), which corresponds to the spring snowmelt and rain on snow events. At the end of May the highest peak is reached (1805 m). A long recession follows from May to September.
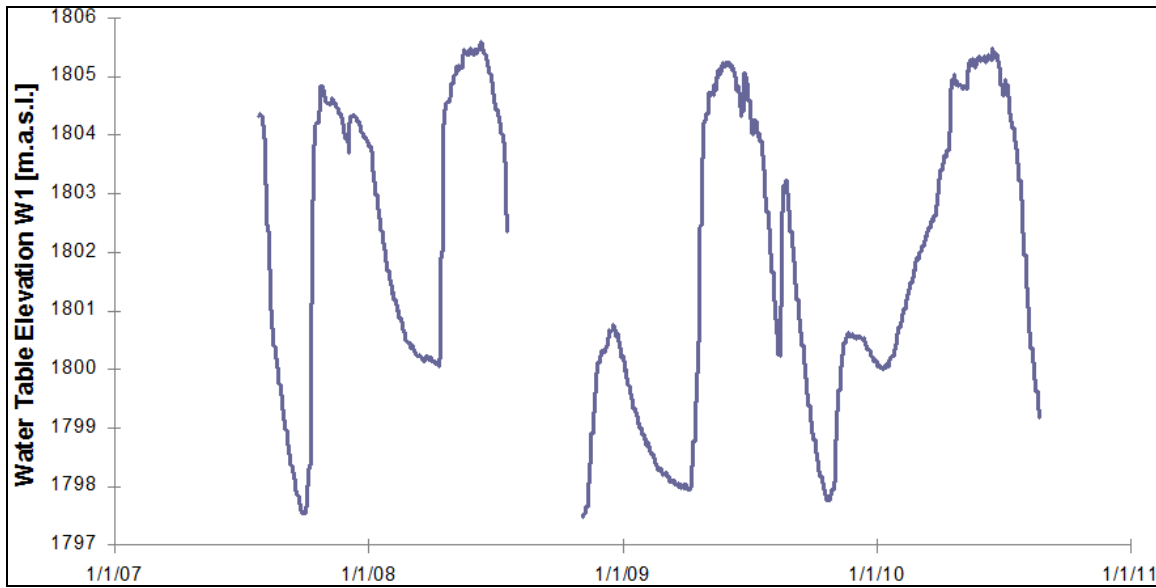
Figure 3.21. Time series of the deep groundwater fluctuation in the bedrock aquifer measured at well 1 (July 2007-July 2008 and November 2008-September 2010).
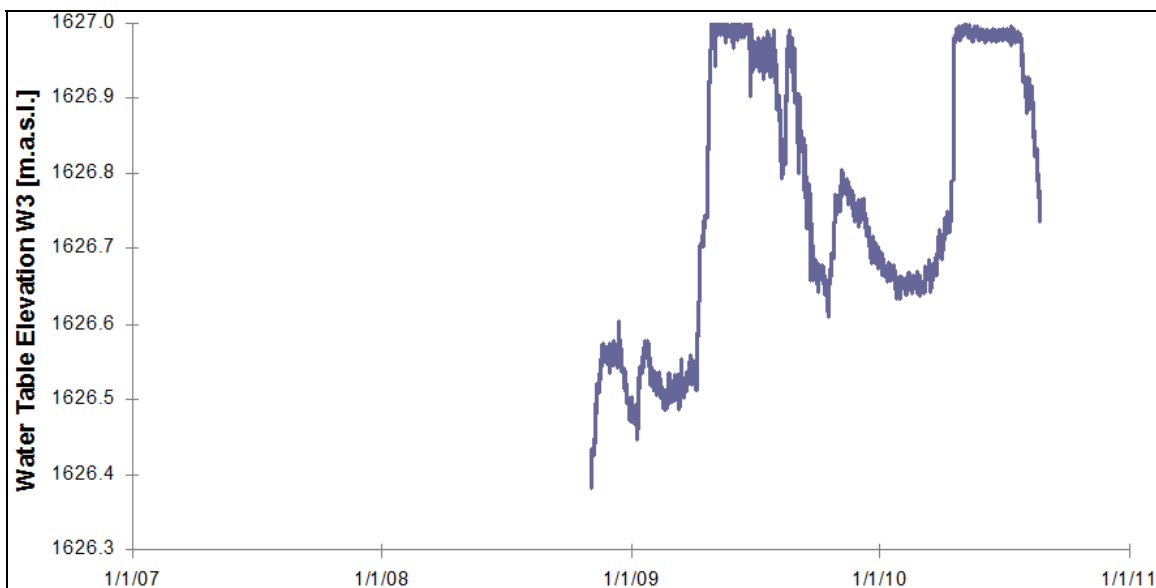
Figure 3.22. Time series of the deep groundwater fluctuation in the bedrock aquifer measured at well 3 (November 2008-August 2010).

Figure 3.22 shows the groundwater fluctuation in well 3. The main responses, i.e. the peaks following spring snowmelt or fall rain events, and lows during summer and winter are very similar to well 1, but there are higher frequency fluctuations (up to 5 cm). The maximum change in water level elevation from the winter low flow period to the snowmelt high flow season is about 50 cm in comparison to well 1 which was about 7 m for the same period. Well 3 appears to be more sensitive to climatic factors. It is also worth noting that during the high flow season well 3 is a flowing well (the water level graph "flatlines" because the water in the well cascades over the top of casing). This well is located in the discharge area of the watershed, whereas wells 1 and 2 are located in the recharge zone of the upper area of the watershed.

3.6.2. Geophysical borehole logging and interpretation

Geophysical borehole logging techniques are commonly used to map fractures and assess fractured aquifers. Common logging tools include resistivity, sonic, density and temperature.

In July 2009 geophysical borehole logging was carried out in each well using a newly developed Geological Survey of Canada (GSC) Triple Parameter probe (J. Mwenifumbo, GSC, personal communication, 2010). Three parameters were acquired in each of the wells; magnetic susceptibility, resistivity and temperature. Two logging runs were acquired; a down run (logging while the probe is going down the drillhole) and an up run (logging while the probe is coming up the drillhole). This procedure provides a means of evaluating the data quality, repeatability, and also acts as a check on any drift

characteristics of the sensor. The measurements are acquired as frequencies and are converted into their respective quantitative units during subsequent processing. Several other probes were run in the wells including: (1) the IFG multiparameter probe which measures natural gamma, galvanic resistivity, single point resistance, magnetic susceptibility, and temperature; (2) the Russian capacitive resistivity probe; (3) full wave form sonic probe, and (4) the newly developed GSC fluid conductivity probe. Only selected logs are shown in this thesis.

Figures 3.23-3.25 show the selected geophysical logs: magnetic susceptibility, capacitive resistivity, tube wave amplitude and full waveform log presented as variable density log (VDL). The magnetic susceptibility log is primarily used for lithology identification, but it can also be used to map alteration zones where magnetic minerals have been altered to non-magnetic minerals. If fluid flow occurs in porous or fractured rocks, it offers an oxidizing environment which may alter magnetic minerals to non-magnetic minerals and, therefore, show as lower magnetic susceptibility zones. Lower resistivity within a rock formation is often an indicator of a fracture zone, since they are more porous and hence exhibit low resistivity. Variations in resistivity in crystalline rocks are primarily a function of pore water content and salinity. Low tube wave amplitudes are often exhibited by porous fractured rocks given their low density compared to unfractured rock.

In well 1, the zones of low resistivity especially the ones below 30 m correlate well with the tube wave amplitude log and are indicated as low amplitude, blue color zones in the VDL on the right of Figure 3.23. The horizontal purple lines (fracture zone

column) indicate the fracture zones whose characteristics are depicted in the resistivity, susceptibility and tube wave amplitude logs. At around 28 m the resistivity is very low, but it is not indicated on the tube wave amplitude. The decrease of the tube wave amplitude in crystalline rocks has been correlated to permeable fractures, which suggests that the fracture zone around 28 m is not permeable.
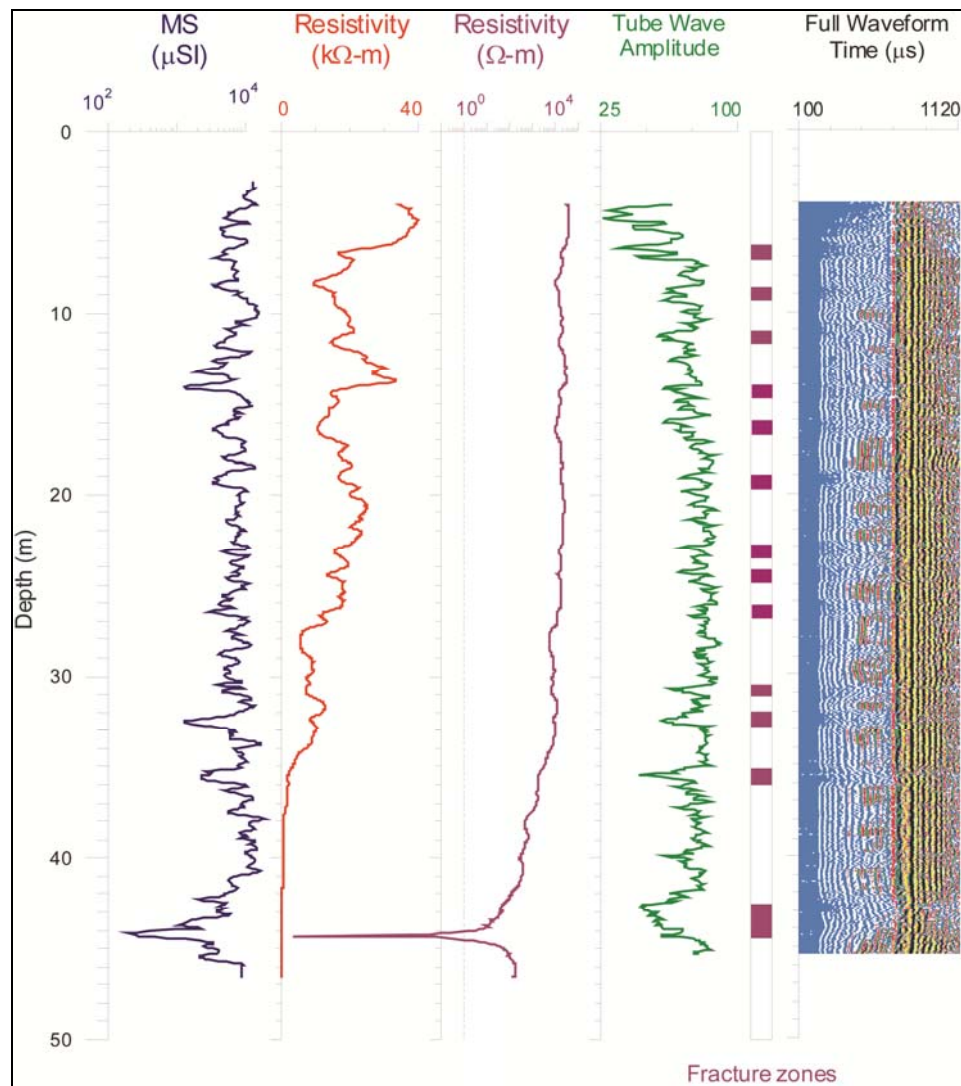
Figure 3.23. Magnetic susceptibility, capacitive resistivity, tube wave amplitude and full waveform log presented as a variable density log for Well #1 – BC Well Plate Number 15849.

At well 2 (Figure 3.24), there is a similar correlation between the tube wave amplitudes and several lower resistivity zones. A similar number of fractures was interpreted for well 1 down to a depth of 30 m (see fracture zone column). Between 25-28 m, the lower resistivity zone does not show an expression in the tube wave amplitude, similar to what was observed in well 1. If this lower resistivity zone is a consequence of a fracture zone, then those fractures are probably not open. Around 25.5 m there is a very interesting low magnetic susceptibility zone which needs further investigation.
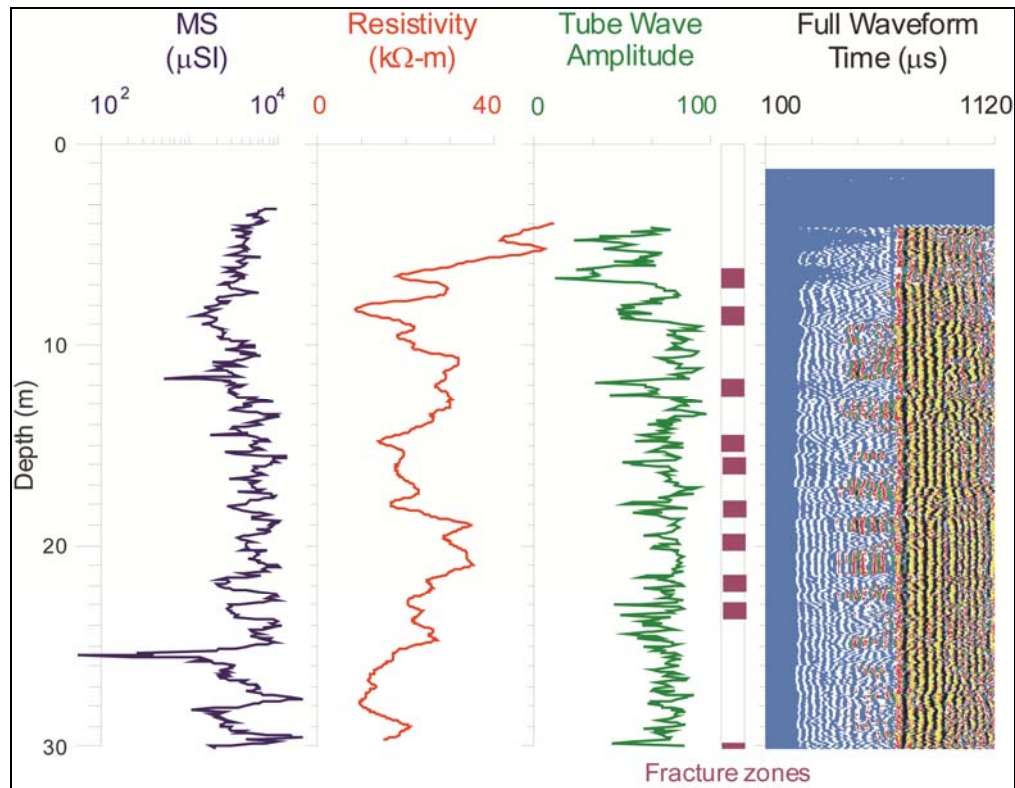
Figure 3.24. Magnetic susceptibility, capacitive resistivity, tube wave amplitude and full waveform log presented as a variable density log for Well #2 – BC Well Plate number 15850.

In well 3, most of all the lower resistivity zones (Figure 3.25) correlate very well with the tube wave amplitude log and are indicated as low amplitude, blue color zones in the VDL. Several fractures are identified (see fracture zone column). At shallow depth around 6 m below the TOC, there is a large fracture zone about 4 m wide.
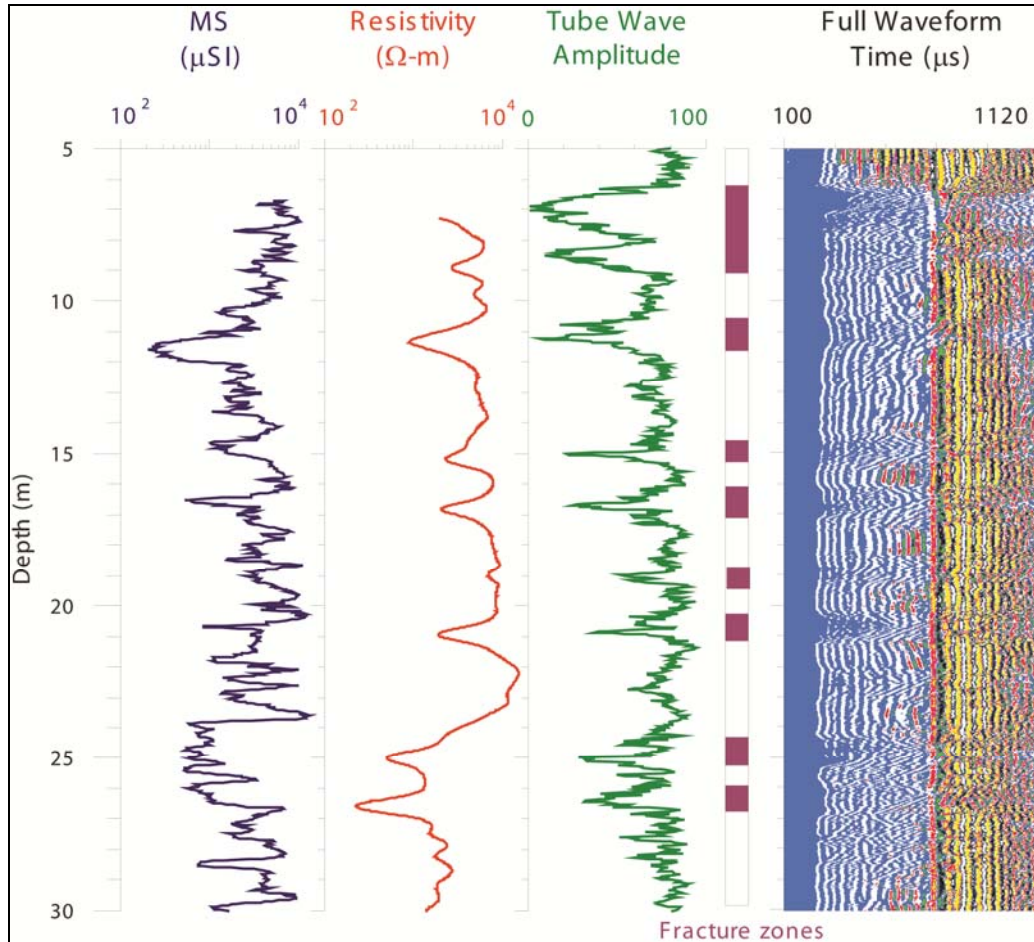
Figure 3.25. Magnetic susceptibility, capacitive resistivity, tube wave amplitude and full waveform log presented as a variable density log for Well #3 – BC Well Plate number 15851.

In general, the fracture zones in well 3 seem to have lower tube wave amplitudes than those in wells 1 and 2, suggesting that the bedrock around well 3 is more permeable.

The differences in fracturing between the wells likely account for the variations in well yield. Well 3 has a relatively high yield at 0.761 l/s compared to wells 1 and 2 (0.13 and 0.19 l/s, respectively).

Based on the fracture mapping, it is likely that most or all the intersecting fracture zones consist of low dipping fractures (~between 25-30° towards the east), similar to the small scale factures of set 4 measured at outcrop location 39 within the low density zone (Appendix A.2). The likelihood that near vertical fracture would intersect the borehole is low given that they are nearly parallel to the borehole. However, there is clearly a difference in fracture intensity in well 3 compared to wells 1 and 2, which suggests that this well is situated closer to an area of more intense brittle deformation. As such, it is surmised that this well is situated near a larger scale fracture zone.

3.6.3. Aquifer tests and analyses

In summer 2008, step tests and constant discharge pumping tests were carried out in wells 1 and 3. Well 2, which is about 3 m away from well 1, was used as an observation well for the tests in well 1. The optimum pumping rate for the constant discharge tests were estimated by first conducting step tests in wells 1 and 3 (data not shown). Well 1 was pumped at a constant discharge rate of 0.06 l/s for 480 minutes (8 hours). Then, the pump was turned off and the recovery response was monitored for 30 minutes. Well 3 was pumped at a slightly higher pumping rate of 0.08 l/s, also for 480 minutes (8 hours), with a 30 minute recovery period. Drawdown was measured using a pressure transducer and datalogger as well as manually with a water level tape.

The pumping test data were analyzed using different analytical methods (Theis, Cooper-Jacob, and more specialized methods as discussed below) in order to calculate the hydraulic properties of the surrounding aquifer, transmissivity T [m^2/s] and storativity S [ ] (note storativity could only be calculated using the observation well data for well 2). The software AquiferTest Pro version 4.2. (Schlumberger Water Services, 2010) was used for analysis. Figures 3.26 to 3.28) show the log-log graphs of the head drawdown versus time and first derivative of drawdown with time. The derivative curve is commonly referred to as a diagnostic plot and can be helpful for identifying whether a response is radial (most common; flow is horizontal and radial toward the well), linear (flow is one dimensional and linear in a vertical plane toward the well) or spherical (where flow is three dimensional) (Renard et al., 2009). Recovery graphs are not shown in this thesis, but the results from the analyses using the Theis Recovery method can be found in Table 3.10.

Figure 3.26 shows the drawdown curve for well 1. For the first minute after turning on the pump borehole storage occurs. During this time water is removed solely from the borehole and not from the formation. Up to about ten minutes the flow appears to be linear. From 10 minutes to the end of the test, the response is almost radial (horizontal line in the derivative plot. It is during this radial flow period that a radial flow model, Theis (1935) or Cooper-Jacob (1946), can be used to analyze the data. Both methods were used; the time interval 10 to 167 minutes was used. Results are given in Table 3.10.
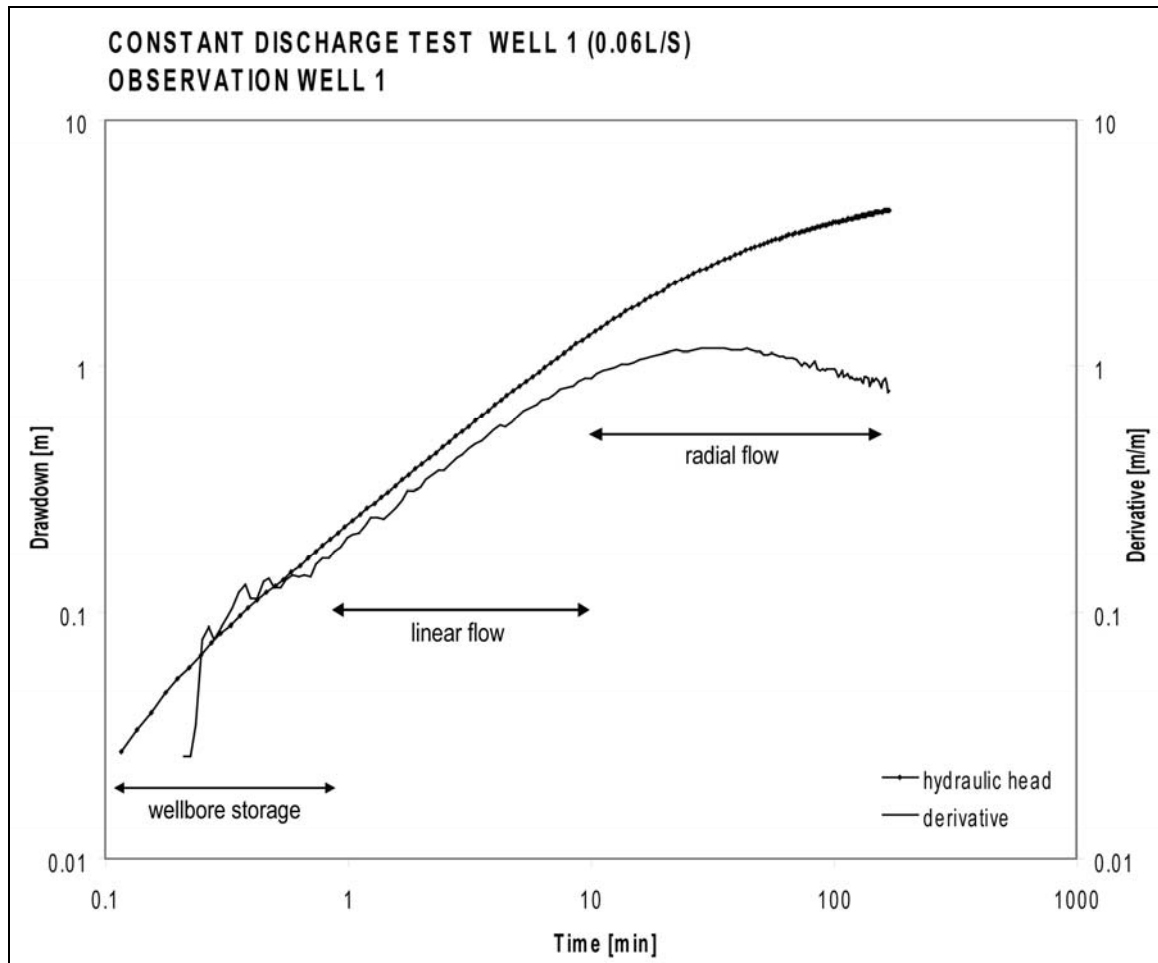
Figure 3.26. Log-log graph showing the head drawdown curve and its first derivative for the pumping test carried out in well 1.

Figure 3.27 shows the head drawdown curve and the derivative curve for the observation well 2 during the pumping test carried out in well 1. Since well 2 was not pumped, borehole storage is not evident. As these wells are very close to each other, the shapes of the curves are similar, with a brief period of linear flow lasting about 9 minutes (from 1 to 10 minutes). In well 2, however, the radial flow period is much better defined; the derivative curve is nearly horizontal. The pumping test data for well 2 were analyzed

using both the Theis and Cooper-Jacob methods over the period 20 to 270 minutes. Results are given in Table 3.10.
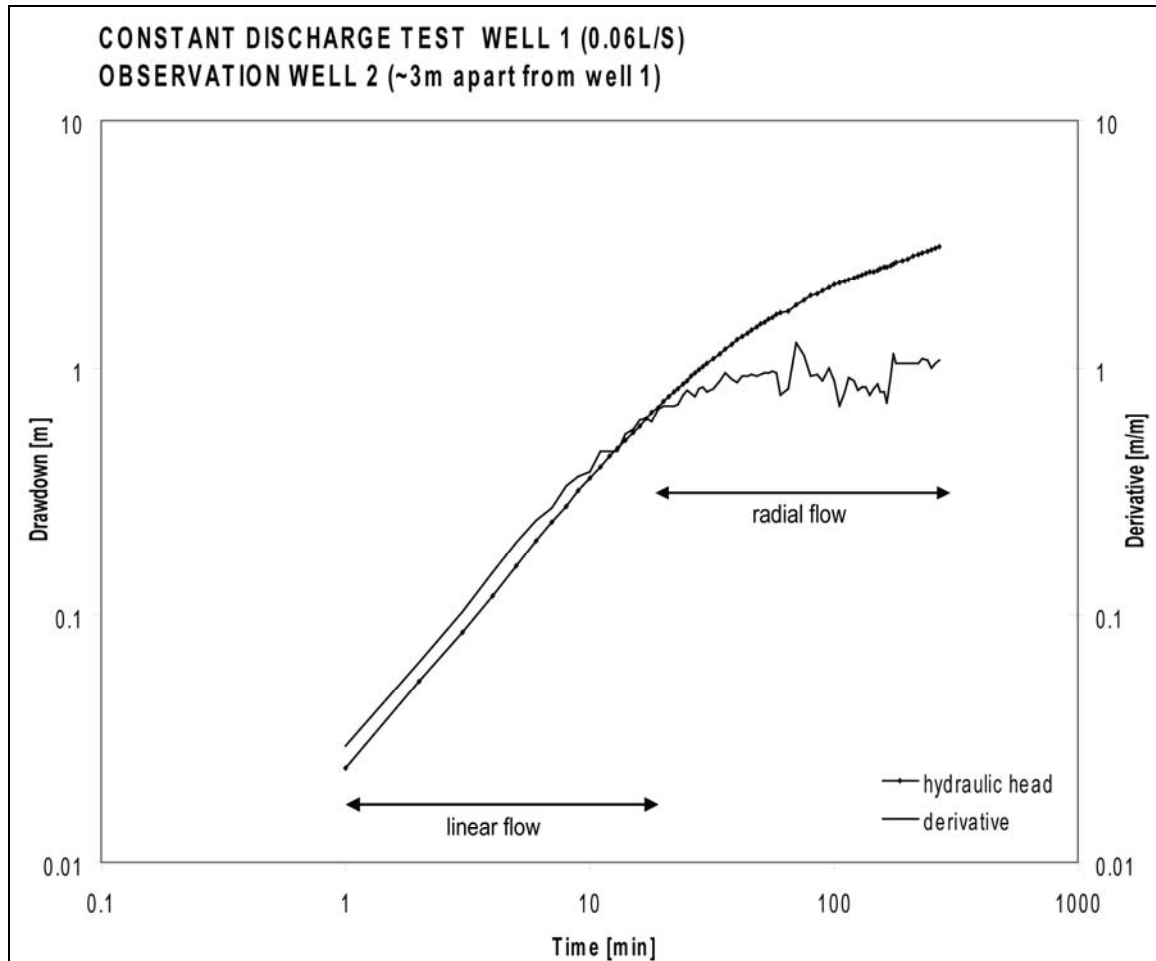
Figure 3.27. Log-log graph showing the head drawdown curve and its first derivative for well 2 from the pumping test carried out in well 1.

Compared to the response at wells 1 and 2, the drawdown curve and its derivative from the pumping test conducted in well 3 (Figure 3.28) shows radial flow at the beginning of the test up to about one minute. After that, linear flow dominates until the end of the test. This linear response is indicated by the near straight curves for the drawdown and its derivative. This dominant linear response indicates that this well is

highly influenced by some vertical feature, such as a vertical fracture zone in close proximity to the well. The feature does not appear to intersect the well because radial flow is first observed. The high fracture intensity observed in this well is consistent with its proximity to a major fracture zone. Due to its linear response, a linear flow model (Gringarten and Witherspoon, 1971) was also used to analyze the pumping test data for well 3. The entire curve is used in this analysis, rather than just the radial flow data.
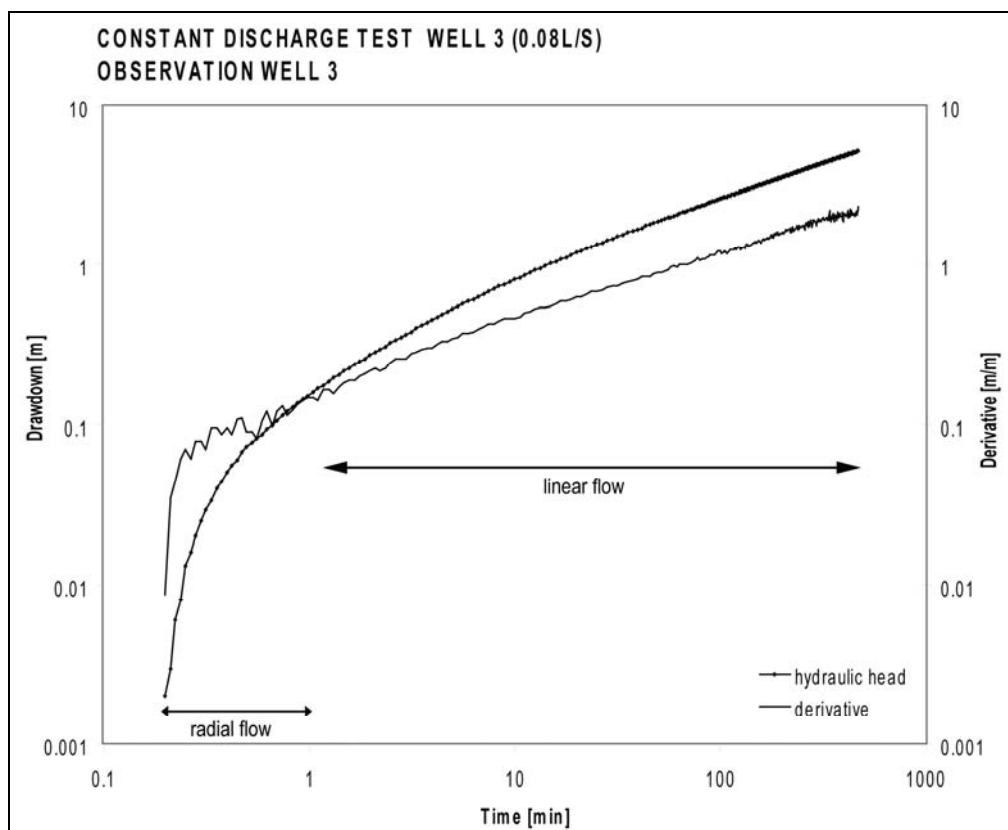
Figure 3.28. Log-log graph showing the head drawdown curve and its first derivative for the pumping test carried out in well 3.

Table 3.10 gives an overview of the hydraulic properties estimated from the different methods in AquiferTest. All analysis graphs (Theis recovery and Cooper-Jacob

method) can be found in Appendix A.6. The analytical methods derive estimates of transmissivity T and storativity S for the aquifer surrounding the well. Hydraulic conductivity K is estimated by dividing T by the representative aquifer thickness b. Commonly, the open hole interval is used in a bedrock well (i.e. from the base of the well casing to the bottom of the borehole) even though the water-bearing fractures are separated down the borehole. In unconsolidated materials, the screened interval is used. In this study, the open borehole length was used to represent the aquifer thickness.

The hydraulic properties from the pumping test results are very similar for wells 1 and 2, regardless of method. K values range from 1.1×10^{-7} to 1.4×10^{-7} m/s. This makes sense, because these wells are very close to each other and it is very likely that the same fractures or fracture zones intersect both wells. The K values calculated for well 3 using the radial flow models (early pumping test data only) range from 2.2×10^{-6} to 9.8×10^{-7} m/s (one order of magnitude higher than wells 1 and 2). The linear flow model applied to the pumping test data in well 3 gave a value for K of 1.1×10^{-6} m/s. The results for the recovery tests were generally consistent, although very slightly higher in wells 1 and 2, and intermediate in well 3.

Table 3.10. Overview of T, K and S results from the different methods used to analyze the pumping tests in the three bedrock wells.

Pumping Test in Well 1	T [m²/s]	K [m/s]	S (Storativity) [-]
Well 1 – Cooper & Jacob – radial flow	4.44E-06	1.17E-07	2.89E-01*
Well 1 – Theis – radial flow	4.25E-06	1.12E-07	3.04E-01*
Well 1 – Theis Recovery – radial flow	4.68E-06	1.23E-07	NA
Well 2 – Cooper & Jacob – radial flow	5.50E-06	1.44E-07	6.24E-04
Well 2 – Theis – radial flow	4.70E-06	1.23E-07	7.78E-04
Well 2 – Theis Recovery – radial flow	7.26E-06	1.91E-07	NA
Pumping Test in Well 3	**T [m²/s]**	**K [m/s]**	**S (Storativity) [-]**
Well 3 – Cooper & Jacob – radial flow	6.66E-05	2.20E-06	3.05E-01*
Well 3 – Theis – radial flow	2.96E-05	9.77E-07	4.20E-01*
Well 3 – Theis Recovery – radial flow	1.16E-05	3.83E-07	NA
Well 3 – Ramey & Gringarten – lin. fl.	3.39E-05	1.13E-06	NA

* Storativity values are not representative of the aquifer in the pumping well. Only observation well data can be used to obtain S.
NA – storativity values cannot be calculated using these methods.

3.6.4. Slug and bail testing and analyses

At the end of July 2008, slug and bail testing was conducted in all three bedrock wells. In a slug test, a solid "slug" is lowered into the well, instantaneously raising the water level. The reverse process is a bail test, whereby a "slug" or volume of water is removed instantaneously resulting in a decline in water level. Repeated tests are normally conducted. With slug and bail testing, the region of the aquifer "tested" for hydraulic conductivity is small compared to a pumping test, and is limited to a cylindrical area of small radius (*r*) immediately around the well screen (Schlumberger Water Services, 2010). Therefore, the resulting K values can be different compared to those determined from pumping tests. In this study, all slug and bail tests were analysed with the software Aquifer Test Pro version 4.2 using two analytical methods: Bouwer-Rice (1976) and Hvorslev (1951).

The Bouwer-Rice solution is appropriate for either a fully penetrating or partially penetrating well completed in an unconfined or leaky confined aquifer. The Hvorslev solution assumes the aquifer is non-leaky and confined, and the well must fully penetrate the aquifer. In a fractured bedrock aquifer, none of these conditions are truly met. Nevertheless, both methods were applied and the results compared.

Figures 3.29 and 3.30 show the normalized head curves (h/h_0) on logarithmic scale versus time, where h_0 is the initial head displacement in the well and h is the head at different times. The results are for well 1; both for a slug test (top graph) and a bail test (bottom graphs). Figure 3.29 shows the results using the Hvorslev method and Figure 3.30 shows the results using the Bouwer & Rice method. The other eight diagrams for each one slug and bail test using both methods for well 2 and 3 can be found in Appendix A.8.
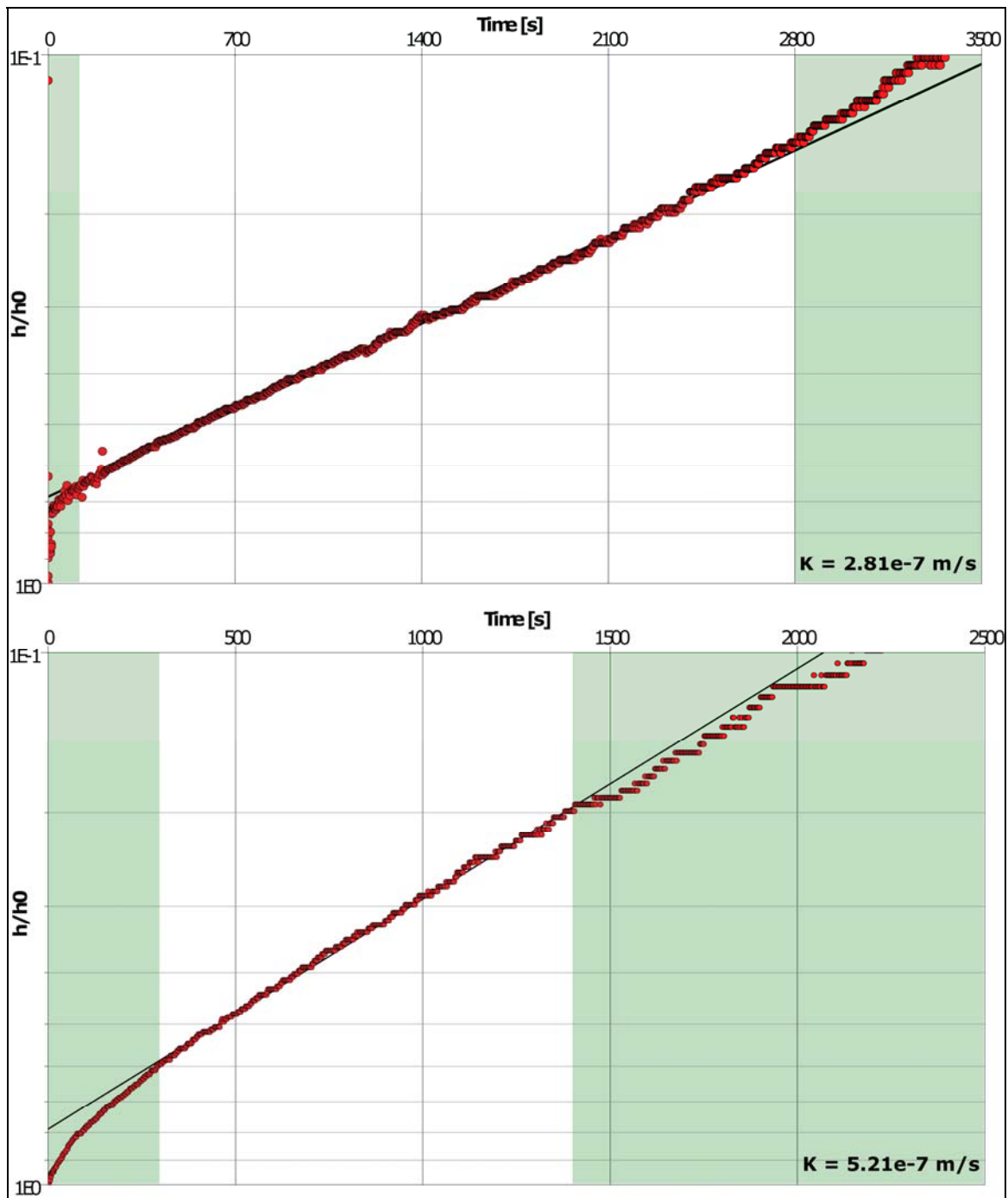
Figure 3.29. Two graphs (upper: slug; lower: bail) showing the automatically fitted curves using the Hvorslev method for well 1.
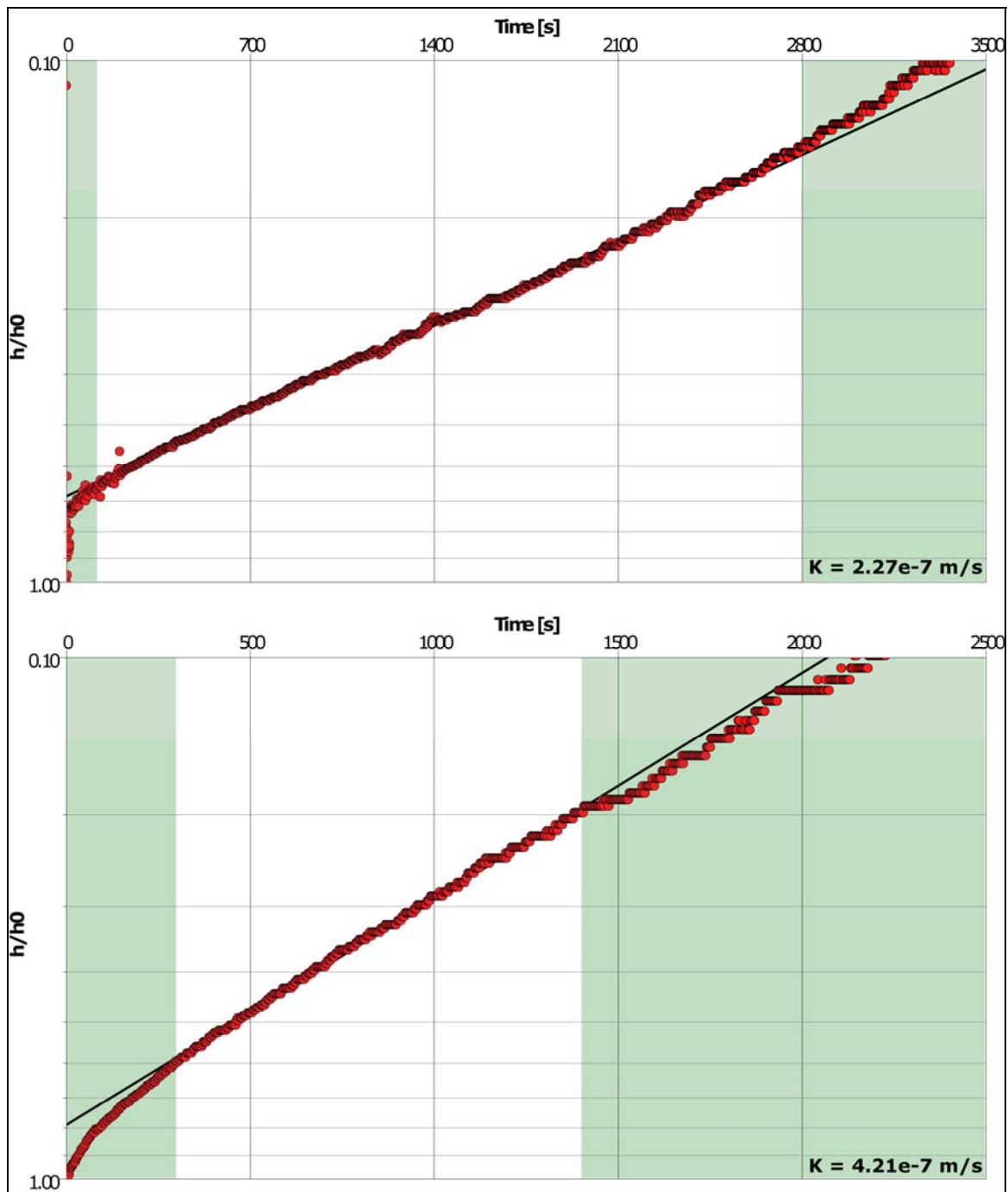
Figure 3.30. Two graphs (upper: slug; lower: bail) showing the automatically fitted curves using the Bouwer & Rice method for well 1.

Table 3.11 gives an overview of the K results from the slug and bail tests carried out in all three wells analysed using the Hvorslev and Bouwer & Rice methods. A geometric mean K value was calculated for each well. Both methods give similar values for each well, although the Hvorslev method results in slightly higher K value compared to the Bouwer & Rice method. The good fit observed in the graphs suggests that either one of these methods is appropriate for analyzing the data. It is also worth noting that the K values are slightly higher in all well compared to the results of the pumping tests. This suggests that the fractures close to the wells tend to influence, very slightly, the bail and slug tests.

Table 3.11. Overview of K results for all three wells using the Hvorslev and Bouwer & Rice methods for slug and bail testing.

Slug & Bail Testing in Wells	K [m/s] - Hvorslev	K [m/s] - Bouwer-Rice
Well 1 Slug	2.81E-07	2.27E-07
Well 1 Bail	5.21E-07	4.21E-07
Geometric Mean W1	**3.83E-07**	**3.09E-07**
Well 2 Slug	4.02E-07	2.96E-07
Well 2 Bail	3.44E-07	2.54E-07
Geometric Mean W2	**3.72E-07**	**2.74E-07**
Well 3 Bail 1	3.49E-06	2.79E-06
Well 3 Bail 2	8.25E-06	6.60E-06
Geometric Mean W3	**5.37E-06**	**4.29E-06**

3.6.5. Darcy flux (q) estimation for nested wells 1 and 2

In this section, the Darcy flux q (or net vertical flux) was calculated as a time series for the nested wells W1 and W2. The Darcy flux is defined by the following equation:

$$q = K * I \qquad\qquad (3.1)$$

where q is the Darcy flux [L/T], K is the hydraulic conductivity in [L/T], and I is the vertical hydraulic gradient [ ]. For K, the geometric mean value estimated from all the pumping tests was used. The head time series in wells 1 and 2 (from November 2008 to the end of July 2010) were used to obtain the head values at different times. The head in well 1 (deeper well) is always slightly lower than the head in well 2, suggesting a downward flux. The separation between the wells (dl) was 15 m, which is the difference in well depth.

Figure 3.31 shows the resulting flux as a time series between wells 1 and 2. All q values are negative between -1.60 x 10^{-9} and -3.00 x 10^{-9} m/s. A negative value of q means that the flux is downward and suggests recharge conditions. At the beginning of November 2008, the flux is about -2.20 x 10^{-9} m/s. After a small reduction to about -2.00 x 10^{-9} m/s around the beginning of January 2009 the flux increases, reaching its highest value during the spring snowmelt by the end of May of about -2.50 x 10^{-9} m/s. Following this, the flux decreases to about -1.70 x 10^{-9} m/s during the summer with some higher fluxes in between likely due to summer rain events. Around the beginning of October, the flux again increases to about -2.20 x 10^{-9} m/s. It remains at that value until the beginning of February 2010. From February 2010 to mid-May 2010 (peak of the spring snowmelt),

there are two periods in between where the flux decreases to a minimum value of -3.10 x 10^{-9} m/s, unlike the year before. The reason for that might be some very unusually low temperature drops during late winter/early spring of that year, which result in minimal snowmelt. Those temperature drops did occur during that period and can clearly be seen in Figure 3.9.
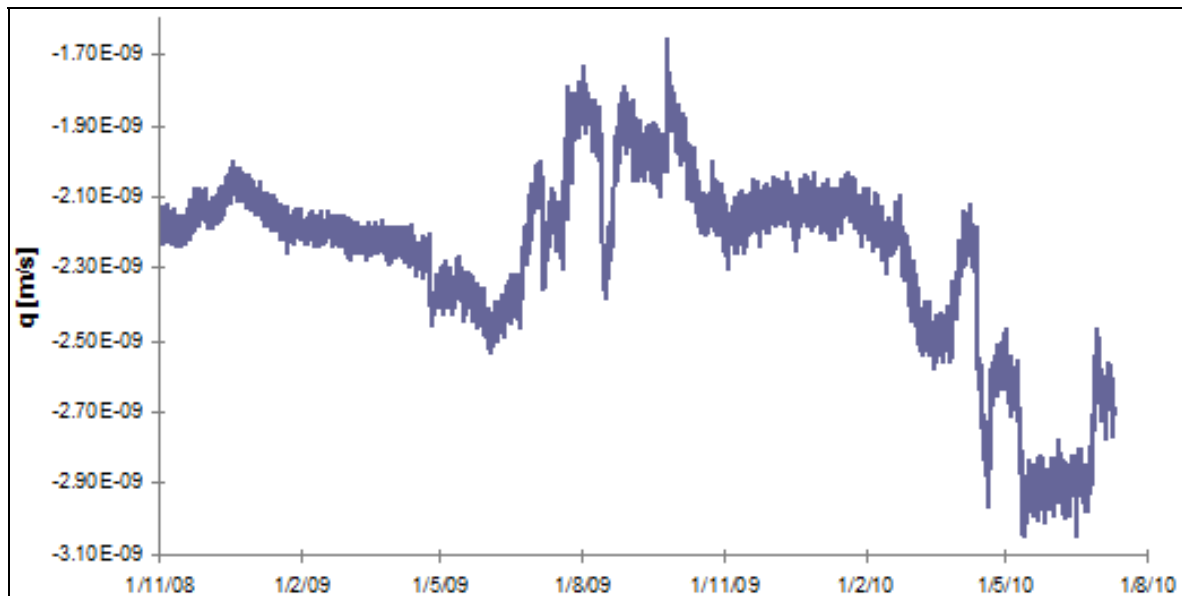
Figure 3.31. Time series showing the vertical flux between wells 1 and 2.

3.7. Comparison of climate, streamflow and water table data

Figure 3.32 shows the climate data (temperature, precipitation), the streamflow data at the outlet of UPC 241, the fluctuations of the deep groundwater level at wells 1 and 3, and the soil water level fluctuation at piezometer P2. The responses of the different components of the watershed to the snowmelt and rain events and their response times can be briefly compared. The integrated surface water-groundwater model developed in Chapter 5 will attempt to simulate these responses.

During the winter months, from December to March the air temperature is mostly below zero, which means that all of the precipitation falls as snow. The baseflow in the stream at the outlet during this time is assumed to derive only from discharging groundwater from the bedrock aquifer, because the soil zone is likely frozen. When the temperatures increase to above zero, around April, the spring snowmelt starts. Almost immediately, the stream at the outlet responds, and the discharge increases, reaching its peak around the end of May. The soil water levels peak at the same time as streamflow. The deep bedrock wells respond to snowmelt almost at the same time as the streamflow. The highest water table is reached a little later (order of days) than the highest peak flow. This suggests that the groundwater system responds very quickly to the climate.
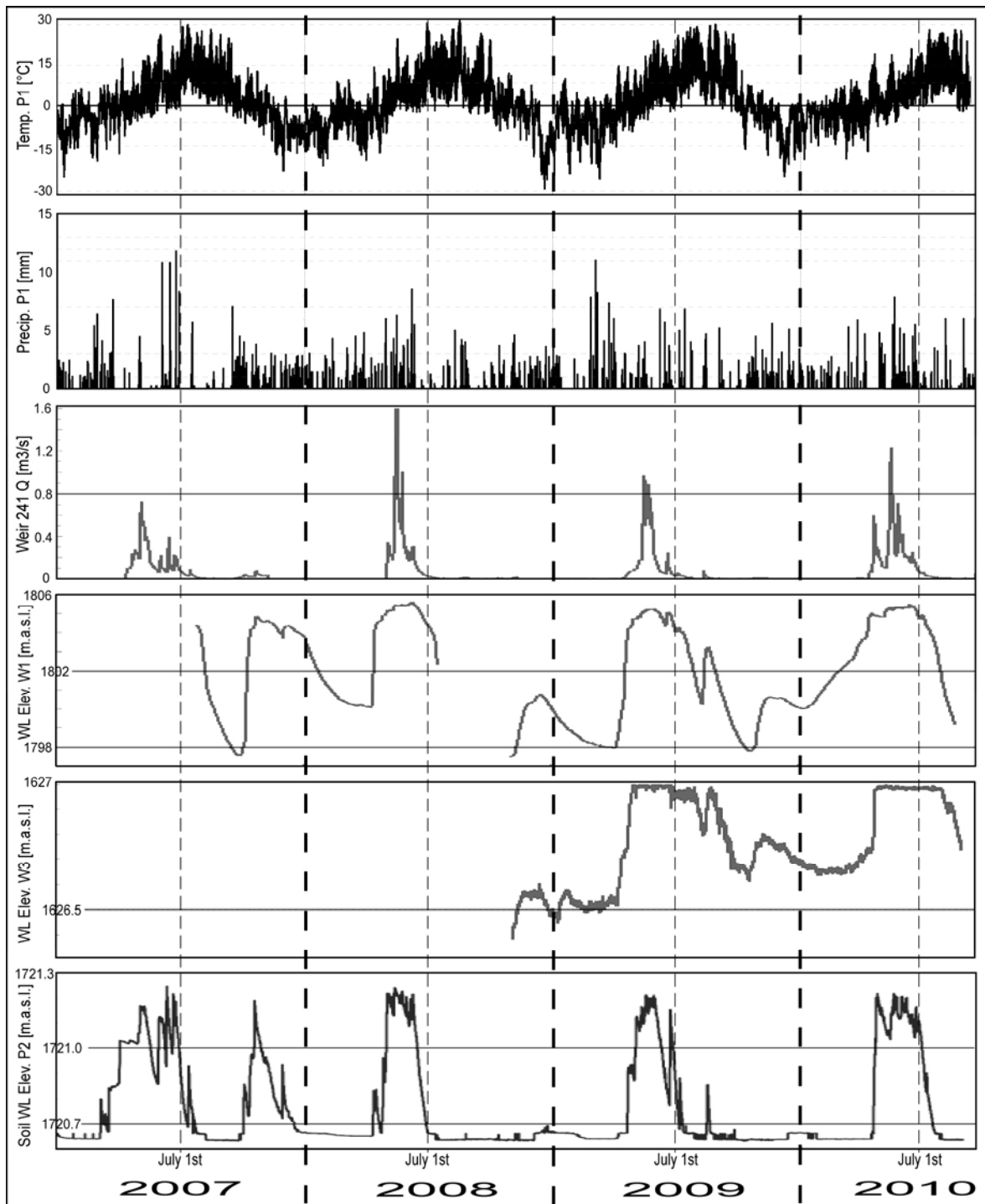
Figure 3.32. Comparison of climate, streamflow, and water level fluctuation data (2007 to 2010).

4. Estimating Regional-Scale Fractured Bedrock Hydraulic Conductivity Using Discrete Fracture Network (DFN) Modeling

This chapter has been published in a scientific journal (Hydrogeology Journal, online 2012)

4.1. Introduction

In mountainous watersheds, fractured bedrock comprises the upland areas, while valley-bottom fill typically consists of unconsolidated sediments overlying bedrock. In general, there is a paucity of groundwater data in mountainous environments worldwide due to a lack of wells in these high elevation settings, which typically have sparse human population and terrain that poses significant challenges for access and drilling. However, there is growing recognition that mountains play a critical role in the hydrologic cycle, capturing precipitation by orographic effects, storing water in snowpack and mountain aquifers, and initiating transport of water from the surface to local and regional aquifers and possibly even deeper to the upper crust of the Earth (Viviroli et al., 2007). Water management in such regional aquifer systems requires an understanding of groundwater flow in adjacent mountains where most of the recharge occurs. Because mountains serve as recharge zones and provide a gravitational driving force for deeply circulating waters,

processes controlling groundwater movement into and through all levels of mountain masses deserve further study (Caine et al., 2006).

Because the hydraulic gradient from the mountain top to valley bottom can be high in high relief areas, even where the bedrock hydraulic conductivity is limited, the sheer volume of bedrock can allow for significant flow into the valley bottom. This deep bedrock flow that enters the valley bottom has been termed mountain block recharge (MBR) (Wilson and Guan, 2004), and in regions where direct valley-bottom recharge is limited due to arid conditions, mountain block recharge can represent a significant component of the overall water budget (e.g. Manning and Solomon, 2003; 2005; Gleeson and Manning, 2008; Smerdon et al., 2009).

In these mountain bedrock aquifers, and indeed in fractured bedrock aquifers more widely (e.g. Canadian Shield, Scandinavian Shield), the hydraulic conductivity is often controlled by a network of discrete fractures, because the host rock has been either metamorphosed, deformed through tectonism, and/or is comprised of igneous intrusions (i.e. primary porosity is typically low). If fracturing is fairly uniform, then the bedrock can be considered as having a "fractured matrix" hydraulic conductivity that can be considered homogeneous, but is more commonly heterogeneous due to differences in the degree of fracturing present. Mackie (2002) and Surrette and Allen (2008) used the term "hydrostructural domain" to refer to an area that has the same overall structural character that imparts unique hydrogeological properties to the rock in that area. Thus, in regions with complex tectonic history, there can be several hydrostructural domains.

In addition to the "fractured matrix" hydraulic conductivity, there is often a series of larger scale structural elements, such as fracture zones, that impart additional permeability to the bedrock. These features are typically larger in scale (comprised of numerous side-by-side fractures) and often can be mapped as lineaments on air photos. At the scale of the mountain block, those fracture zones have the potential to act as conduits for groundwater flow over significant distances. Lineaments, however, have also been associated with hydraulic barriers (e.g. Gleeson and Novakowski, 2009). Thus, the capacity of a mountain block to transmit subsurface water depends on the hydrogeological characteristics of both the fractured matrix and larger scale structural elements (Caine et al., 1996; Ohlmacher, 1999; Flint et al., 2001; Mayo et al., 2003; Haneburg, 1995; Mailloux et al., 1999).

Simulations by Wilson and Guan (2004) suggest that bedrock with sufficiently high bulk hydraulic conductivity has the potential to allow for significant deep percolation. They estimate a threshold intrinsic permeability of 10^{-16} m^2 or a hydraulic conductivity threshold of 10^{-9} m/s. Various studies have K values in excess of this threshold value (e.g. Caine and Tomusiak, 2003; Gleeson and Novakowski, 2009; Surrette and Allen, 2008). Henceforth in this paper, hydraulic conductivity is referred to simply as K (measured in m/s), but this is not to be confused with intrinsic permeability k_i (measured in m^2).

To estimate the volume of groundwater flowing through the bedrock, or to estimate mountain block recharge, an estimate of the bedrock K of the mountain block is needed. While pumping test data can provide such estimates, typically there are few wells

available for testing in these remote areas. Pumping test results are also site-specific, or even well-specific, due to the heterogeneous nature of fracturing over a range of scales. It is often not possible to obtain estimates of K for the larger scale structural features because most analytical methods provide only an estimate of the fractured matrix K (Kruseman and de Ridder, 1990). Furthermore, such well or aquifer tests often yield a bulk isotropic estimate for K with little information on anisotropy, which can significantly influence flow directions within fractured rock. To obtain information on anisotropy from a pumping test, both a pumping well and several observation wells in a suitable test configuration are required (e.g. Kruseman and de Ridder, 1990).

Because of these challenges, alternative approaches for estimating bedrock K have recently been tested. For example, Caine and Tomusiak (2003) characterized bedrock potential K at a local scale, where geometric fracture characteristics were simulated using a discrete fracture network (DFN) modeling approach on the basis of outcrop fracture data. Surrette et al. (2008) used a DFN approach to derive estimates of potential K based on outcrop measurements of fractures in different hydrostructural domains observed throughout their study region, and related the range of estimates to K values derived from pumping tests. They also related regional trends in K to structural elements (e.g. folds).

Neither of these studies, however, specifically addressed the issue of upscaling, whereby fracture measurements and modeling carried out at the outcrop scale could potentially be used to derive estimates of K at a larger scale that would be relevant for regional scale groundwater flow problems, such as that represented by mountain block recharge. As discussed above, matrix K estimates derived either by fracture modeling

from outcrop data or through pumping tests may not be adequate for representing a network of larger scale features. Furthermore, few studies have examined fracture K distribution over a range of different scales. Koike and Ichikawa (2006) investigated scale dependency on K using fracture data from LANDSAT satellite images, boreholes, and thin sections. However, the analysis was only carried out for two dimensions (x-y direction).

The purpose of this research was to develop and test a method for estimating bedrock K for a mountain block at the outcrop scale (fractured matrix) and regional scale (lineament scale) using a discrete fracture network (DFN) modeling approach. DFN modeling uses a stochastic approach to generate fracture distributions and compares these to observed data (Dershowitz et al., 1995). In this study, the FRED software was used (Golder Associates, 2006, FRED software v. 6.54). The generated fracture data are then input into a flow model to derive estimates of the bedrock K at the two scales. Fractures are assumed permeable as supported by well testing data and regional well yields. Details concerning DFN modeling can be found in Dershowitz et al. (1995) and in case study examples by Caine and Tomusiak (2003) and Surrette et al. (2008).

The premise for the study is that the hydraulic properties of larger scale structural features, such as fracture zones associated with lineaments, can be derived through lineament and outcrop mapping in combination with inverse DFN modeling. The approach constitutes an informal upscaling process from small scale outcrop fracture DFN models, where all important statistical DFN fracture generation parameters are

known, to the larger scale lineament DFN model. The methodology is tested in the mountainous region of Okanagan Basin, British Columbia, Canada (Figure 4.1).

4.2. The study area

The study area is located to the east of Okanagan Lake (main stem lake) in Okanagan Basin (Figure 4.1). Specifically, field and modeling work were carried out in two first order watersheds, Penticton Creek Watershed (184 km^2) and Naramata Creek Watershed (141 km^2), which flank the Okanagan Valley (Figure 4.1). The elevations of the two watersheds range from about 340 metres above sea level (masl) (Okanagan Lake level) to 2100 masl in the Okanagan Highlands.

The study site is located in a gently west dipping (plunging) crustal shear zone referred to as the Okanagan Valley Fault System. There is ~90 km of offset due to the upper plate (~1-2 km thick) moving westwards above the lower plate east of the main trace of the fault (Tempelman-Kluit and Parkinson 1986). The complexity of fracturing observed over a range of scales (outcrop to lineaments) is largely attributed to the Okanagan Valley Fault Zone (OVFZ). The trace of the OVFZ (identified as the detachment fault in Figure 4.1b) is located under the Okanagan Lake and Okanagan Valley. Chlorite-epidote-quartz microbreccias occupy the shear zone's uppermost 10-100 m. Spaced, irregularly orientated extension faults cut the microbreccia and merge with the flaser fabric downwards (Johnson, 2006; Tempelmann-Kluit and Parkinson, 1986; Brown and Journeay, 1987).
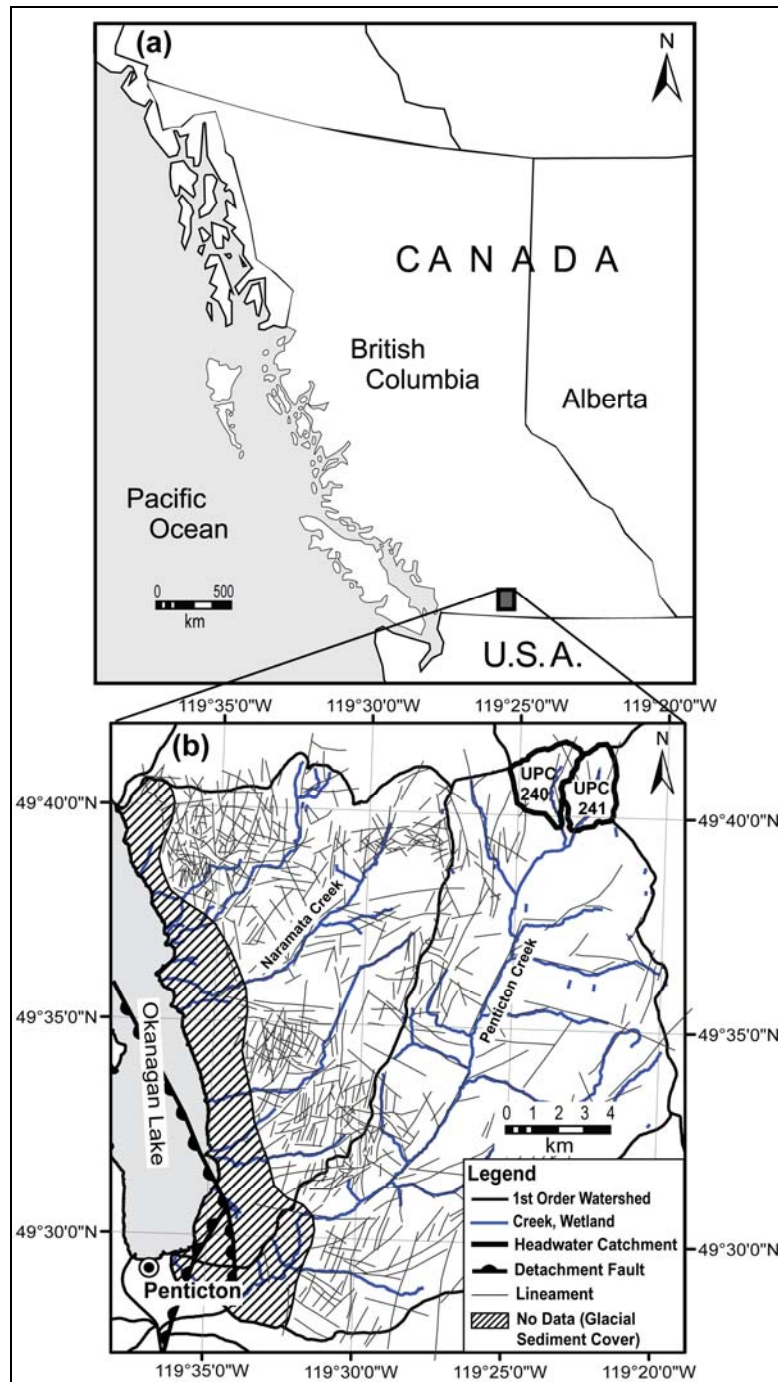
Figure 4.1. Maps showing (a) the location of the study area in the Okanagan region of British Columbia, and (b) Naramata Creek and Penticton Creek Watersheds to the east of Okanagan Lake within the Okanagan Highlands. The UPC 241 catchment is situated at the northeast corner of the Penticton Creek Watershed.

Most of the rocks in the region belong to the Monashee Group, a mylonitic gneiss of Eocene age. The bedrock in the northeastern part of the study area is granite/granodiorite of Eocene age, belonging to the Okanagan Batholite Group. The bedrock is mostly exposed at lower elevations close to Okanagan Lake as well as at higher elevation above the tree line. Bedrock exposure at low elevation coincides with an area that receives little precipitation and, therefore, has less vegetation cover.

The Upper Penticton Creek 241 (UPC 241) catchment, situated at the northeastern corner of the Penticton watershed (see Figure 4.1b), is a headwater tributary to the Penticton Creek first order watershed; it drains an area of 4.74 km^2. In July 2007, three deep wells (two 30 m wells and one 50 m well) were drilled at the UPC 241 watershed. Two of these wells are situated at high elevation and are ~3 m apart (wells W1 and W2), and one is at lower elevation (well W3) close to the outlet of the catchment about ~2 km away from the upper ones (Figure 4.2). The wells are open boreholes with the exception of a cased interval that extends from surface to ~1 m into the bedrock. No core is available; however, the drilling was overseen as part of this project, with observations noted on the well drilling record related possible fracture locations based on drilling resistance and changes in flow. Granodiorite was encountered within 0.5 m of the surface in W1 and W2. There was no change in rock type with depth. Several small fractures were intersected in both wells between approximately 6 m and 24 m depth. The deepest fracture provided the majority of water during drilling, although flow accumulated gradually down the boreholes; the estimated yield of both wells is approximately 0.13 - 0.19 L/s (litres per second). A suite of borehole geophysical logs was acquired in June

2009. Logging tools included capacitive resistivity and normal resistivity, single point resistance, magnetic susceptibility, temperature, and full wave form sonic (tube wave amplitude and variable density). The logs consistently point to a series of small fractures at roughly the same depths in W1 and W2 (~8 fractures over 50 m in W1). The low flow rates and the few fractures in these wells suggest that neither is close to any major lineament.
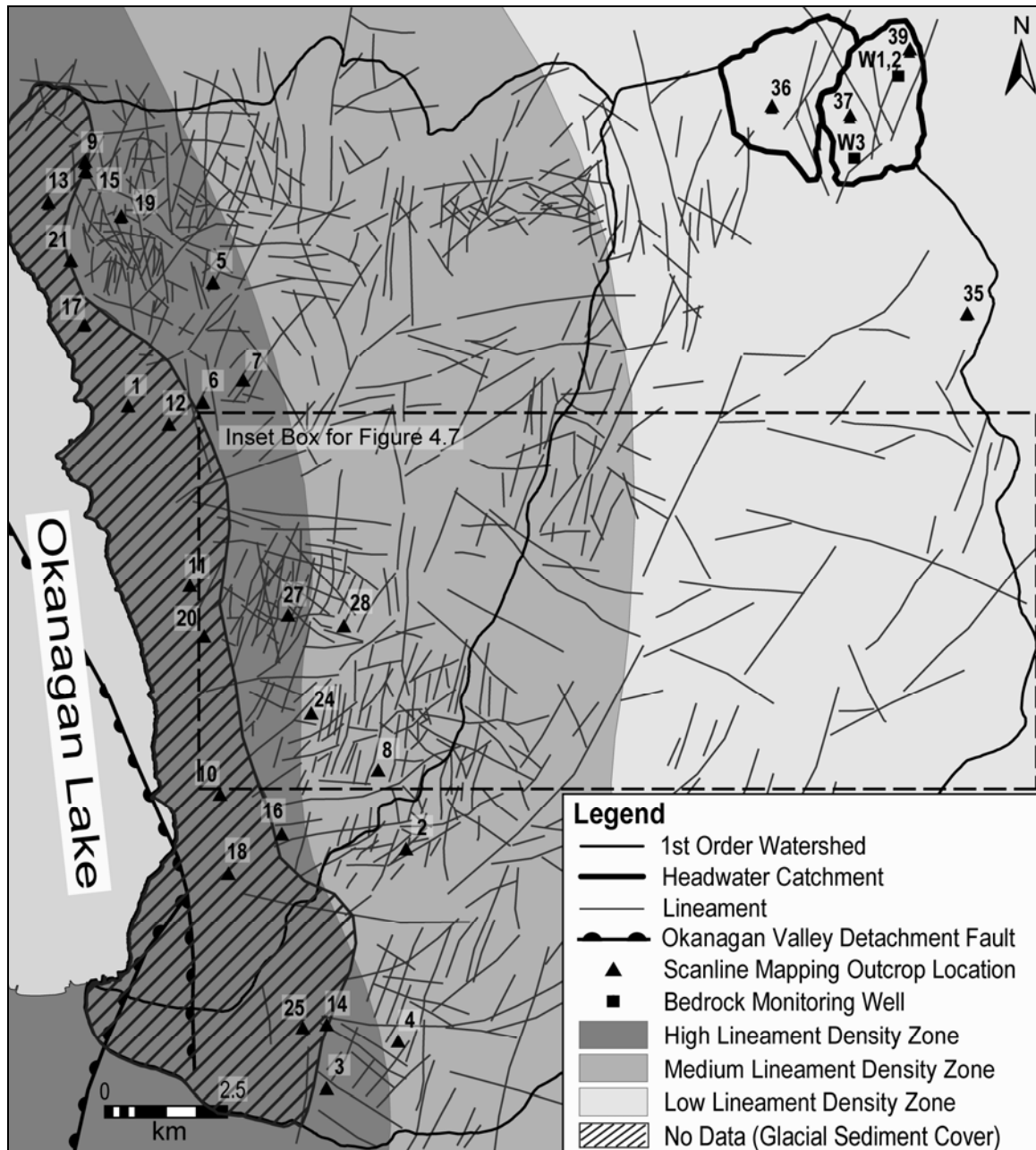
Figure 4.2. Map showing the three lineament density zones (high, medium and low) determined from lineament mapping from orthophoto and LANDSAT imagery. Lineaments are also shown in this figure as well as an inset box for Figure 4.7. Also shown on this map are the outcrop scanline mapping sites and the bedrock monitoring wells (W1, W2 and W3) in the UPC 241 catchment.

The depth to bedrock in W3 (also granodiorite over the full well depth) was considerably deeper (4.5 m). The well is situated in a topographic low and is roughly 200 m from the main stream that drains the catchment. Here the bedrock presumably has been eroded, leading to the lower topography. While some water was produced from several fractures (similar to W1 and W2), a major water-bearing fracture zone was encountered between 20 and 25 m. Cuttings at this depth were granular as opposed to competent chips, suggesting less competent rock. The yield of this well was higher at 0.76 l/s. The geophysical logging confirmed that W3 intersects a series of more substantive fractures (not as narrow as in W1 and W2), which are more closely spaced along the length of the well; the density of fracturing is higher than that seen in W1 and W2 (~7 wide fracture zones over 30 m). Of significance is a highly resistive zone between 25 and 28 m). At the time of drilling, it was thought that the well may be situated near a major fracture zone that resulted in the valley topography. The lineament analysis later confirmed that a large scale NE-SW striking fracture zone is situated nearby (within 200 m of W3).

In August 2008, step tests and constant discharge pumping tests were conducted at W1 and W3. Water levels were recorded using pressure transducers. The step tests were done to determine an optimum pumping rate for the constant discharge test. W1 was pumped at a rate of 0.06 l/s for a total of 8 hours. Water levels were measured both in the pumping well, W1, and in the adjacent well observation well, W2. W3 was pumped at a constant rate of 0.08 l/s for ~ 8 hours. As there is no other well close to W3, it was not possible to obtain data from an observation well for this test. Data collected during these

tests were analyzed using a variety of analytical methods appropriate to the characteristics of the tests (see Chapter 3).

Radial flow dominates the test at W1 (Figure 3), while linear flow dominates at W3. Radial flow follows the classic Theis type curve for homogeneous and isotopic media, while linear flow is characterized by a straight line on a log-log graph of drawdown versus time. Linear flow typically occurs in the presence of a large scale, vertical to sub-vertical discrete fracture or fracture zone (Allen and Michel, 1998) that intersects, or is in close proximity to, the well. The pumping test results suggest that the bedrock near W1 and W2 can likely be approximated by an equivalent porous medium with properties that reflect a reasonably uniform distribution of fractures. In W3, however, the linear flow suggests that there is a significant vertical to sub-vertical fracture zone close to the well influencing the pumping response.
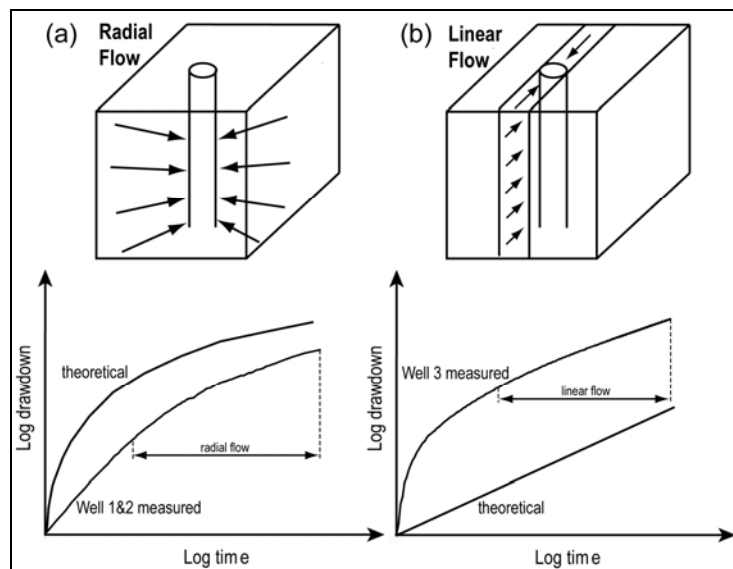
Figure 4.3. Schematic diagram showing the pumping test curves (log drawdown versus log time) and related conceptual models for (a) W1 and W2 (radial) and (b) W3 (linear).

4.3. Material and methods

4.3.1. Overview of methodology

Figure 4.4 shows a schematic diagram of the overall modeling approach. The details are described in the following sections. Outcrop scale fractures are mapped using a scanline technique and fracture sets determined using a statistical analysis. The fracture properties for the sets are used to generate small scale discrete fracture network (DFN) models for the different outcrops. The resulting hydraulic conductivity value, K_m, represents the fractured rock matrix at the outcrop scale.

Lineaments mapped from orthophotos and LANDSAT imagery are used to identify fracture sets at the regional scale. The effective K, aperture and compressibility of larger scale fracture zones associated with lineaments, are estimated using an inverse modeling approach whereby a pumping test in a well near a lineament is simulated and the best fit model parameters identified. DFN models representing the mountain block are then generated to estimate the mountain block hydraulic conductivity, K_{mb}.

Fracture aperture is known to decrease with depth (e.g. Boutt et al., 2010). As well, depending on current stress regime, fractures in some orientations may be closed. Both of these factors would serve to reduce the K of the fracture network. In this study, the estimates of K are assumed to represent a uniformly fractured zone, 200-300 m thick. The network of fractures is assumed to be open and conductive.
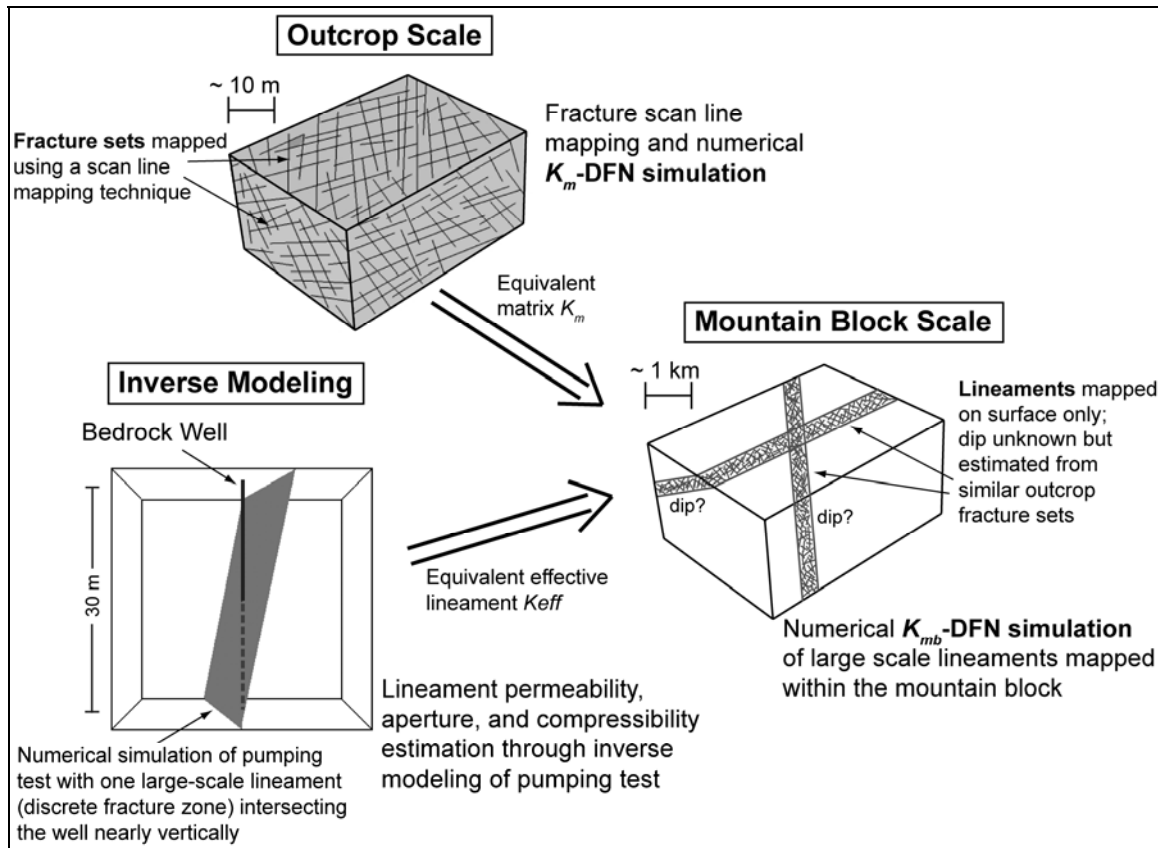
Figure 4.4. Schematic diagram showing the overall approach for estimating mountain block permeability.

4.3.2. Fracture/lineament data collection

Fracture data for DFN model generation and subsequent K and specific storage determination were collected at two scales: the local outcrop scale and the regional or lineament scale.

For outcrop scale measurements, geologic maps were examined prior to going into the field to help select natural outcrop locations that were representative of lithologically- and structurally-distinctive rock groups in the study area. Fracture mapping was undertaken in summer 2006 at 29 outcrop locations throughout the Penticton and

Naramata watersheds using traditional scanline mapping techniques (Caine and Tomusiak, 2003). Measuring tapes were laid out on at least two near-orthogonal outcrop faces to capture all possible fracture set orientations (Figure 5.5). Position, orientation (measured with a geologic compass), trace length, termination style, aperture, roughness (primary/secondary) and fracture fillings were recorded for each fracture intersecting each scanline.
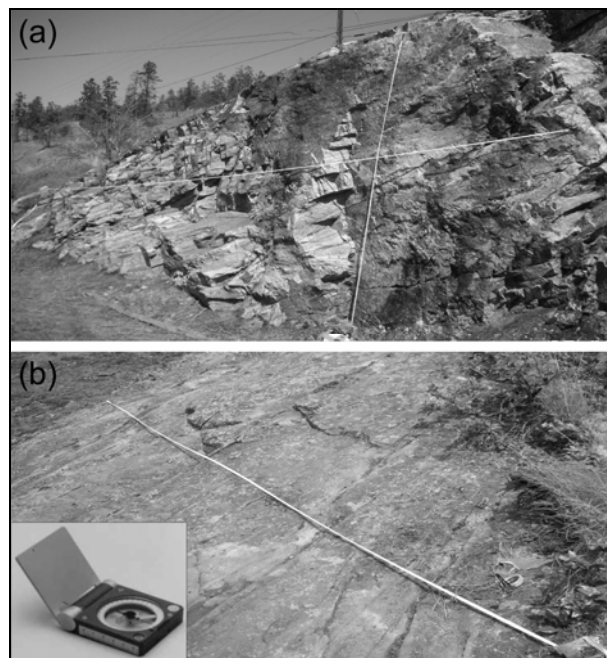
Figure 4.5. Schematic diagram showing the overall approach for estimating mountain block permeability.

Regional scale lineaments were mapped both using detailed aerial (ortho) photos and LANDSAT images. Lineament data were provided by Natural Resources Canada, and were projected onto the study area map using a geographic information system (ArcGIS v. 9.3, ESRI, 2008). The lineament analysis incorporated a 25 m resolution digital elevation model (DEM) and 12.5 m LANDSAT 7 Thematic Mapper multispectral

116

panchromatic imagery (near-infrared band 4). A hillshade was computed from the DEM to extract features of the landscape through the use of shadowing and sun-angle illumination. By calibrating the hillshade to several different sun angles, different structural characteristics could be identified. Lineaments mapped using the LANDSAT image generally did not reveal one of the lineament sets that had been identified in outcrop and on the orthophotos, especially at higher elevations where the lineament density is lower. Therefore, for this study a composite lineament map was generated using the lineament data from both the orthophotos and LANDSAT imagery to ensure that all the lineaments were captured at the regional scale (see Figure 4.2). Lineament data collection can be highly subjective (Mabee et al., 1994) and use of such data requires careful scrutiny. In this study, the overlap of lineaments mapped using the two methods provided some confidence in the results.

4.3.3. Lineament density mapping

Lineament density was visually observed to vary across the study area. Proximal to Okanagan Valley Fault, lineament density appears high, decreasing with distance away from the fault (Figure 4.2). Because fracture intensity is an important control on K (see Section 4.3.4), it was thought that there might be spatial differences in K related to fault proximity. To explore this issue, the study area was divided into different zones on the basis of lineament density. A lineament density map was generated using the ArcGIS Kernel Density Tool for polylines. This method calculates a magnitude per unit area from polyline features (length) using a Kernel function that fits a smoothly tapered surface to

each polyline. For the purpose of this study, density was categorized into three zones (low, medium and high) (Figure 4.2). Two assumptions were made when constructing the map: 1) lineaments under the lake sediments are assumed to exist, but cannot be detected through the sediment cover. For this reason, the lineament density adjacent to the lake is assumed the same as that bordering the sediments to the east (see the extent of surficial cover in Figure 4.2), and 2) small patches where no lineaments were mapped are the result of either sediment cover or dense vegetation cover, making it impossible to detect them. In such areas, it was assumed that the lineament density is similar to that in neighboring areas. Due to the above assumptions, some corrections near the borders of the three zones and near big patches of no data had to be made manually on the generated Kernel density map.

4.3.4. Discrete fracture network (DFN) modeling - background

Discrete fracture network (DFN) modeling uses a stochastic approach to generate fracture distributions and compares these to observed data. In this study, modeling was carried out using the FRED software, which implements FRACMAN (Golder Associates, 2006, FRED software v. 6.54,). Details concerning DFN modeling using FRED can be found elsewhere (e.g. Geiger et al., 2006; Zahm and Hennings, 2009).

In a stochastic fracture network, most characteristic variables are represented as probability distribution functions. Fracture network properties are approximated by the best-fit theoretical statistical distributions that are based on the field data (e.g. fracture mapping on rock exposures). Each generated fracture is a product of one Monte Carlo

sampling from a number of statistical distributions, each representing a certain fracture property. The combination of all fractures generated in such a manner results in a three-dimensional discrete fracture field (Starzec and Andersson, 2002).

For generating a DFN model, the mean trend and plunge (or dip) of the poles to fracture planes and dispersion (or variability about the mean) are needed for each fracture set. Dispersion values closer to 100 describe well clustered data, while values closer to 0 describe a poorly clustered fracture data set. Standard deviation and the probability density function (PDF) of the trace-length (persistence) from the field data are also needed (Caine and Tomusiak, 2003). As well, fractures in the DFN model must be assigned an aperture in order to provide a fracture transmissivity. Each element in the mesh of a DFN model is assigned a fracture transmissivity, T_f, that can be directly related to fracture aperture using the cubic law (Snow, 1968):

$$T_f = \frac{b^3}{12} \frac{\rho g}{\mu} \qquad (4.1)$$

where T_f is fracture transmissivity [m^2/s], b is aperture [m], ρ is the density of water equal to 999.70 kg/m^3 at 10ºC, g is the acceleration due to gravity [m/s^2], and μ is the dynamic fluid viscosity of water equal to 1.307 x 10^{-3} Ns/m^2 at 10ºC. This fracture transmissivity model assumes flow through parallel plates of aperture b. Finally, the fracture compressibility, C_f, is needed for fracture generation within the DFN model. A value of 3 x 10^{-4} m^2/N was used based on lab experiments for granite (Fisher and Tester, 1980).

Estimates of fracture transmissivity derived using Equation (4.1) were input into FRED for generating the fractured matrix models from outcrop data. In this case, the

fractured matrix is assumed to be comprised of a network of discrete fractures that can be represented as parallel plates. For the larger scale lineament models, an inverse modeling approach was used to estimate the "effective" lineament aperture, and the corresponding effective lineament K and compressibility, as described later.

Before DFN flow simulations can be performed to derive estimates of K, it is necessary to upscale from a scanline "P_{10}" intensity (number of fractures per scanline length) to the "P_{32}" intensity (number of fractures per volume) (Caine and Tomusiak, 2003; Oehman and Niemi, 2003) and to estimate a representative elementary volume (REV) size. This is a threshold volume of a DFN model for which there are no further changes in the hydraulic properties with increased model volume, which means K becomes constant. For the upscaling process, simulated fracture intensities are fit to observed scanline intensities for each fracture set by using multiple realizations of simulated scanlines for determination of a best-fit, single DFN model. The relative error of the simulated P_{10} intensity should not be higher than 20%. Once a best single DFN model for each set is found, the P_{32} intensity for that model is noted. Using the upscaled P_{32} intensities assigned for each fracture set, DFN models are generated for final K estimation with an appropriate model domain volume equal to or bigger than the REV. More details on the final model domain sizes/REV estimation for both scales in this study are given later.

Flow through the cubes is simulated in each of east-west (x), north-south (y), and top-bottom (z) directions, and corresponding potential K values are computed for each of these directions. Potential K values are calculated by simulating water flow at standard

temperature and pressure in the best-fit DFN model using the three-dimensional finite-element code MAFIC (Miller et al., 1995), which is incorporated into FRED. The term potential K is used because the orientation of the flow field is in the primary compass directions, and K values in these directions are estimated. These potential K values may not coincide with the true principal directions of anisotropy. The maximum principal direction of anisotropy will likely be in the same direction as the dominant strike direction, while the minimum principal direction of anisotropy will be perpendicular to this fracture set. To estimate the true principal directions of anisotropy would require an infinite number of flow simulations in all possible geographic coordinate directions (Surrette and Allen, 2008). In this study region, the dominant fracture sets are roughly oriented N-S and E-W, so the generated potential K values will likely reasonably approximate the principal directions of anisotropy.

The one-dimensional, directional equivalent bulk potential intrinsic permeability, k_i, for each full model domain face is calculated based on Darcy's law:

$$k_i = \frac{\mu}{\rho g} \frac{Q}{IA}$$

(4.2)

where k_i is the calculated potential intrinsic permeability [L^2], μ is the fluid dynamic viscosity [M/LT], ρ is the fluid density [M/L^3], g is the acceleration due to gravity [L/T^2], Q is the simulated volumetric flow rate [L^3/T], I is the specified hydraulic gradient [dimensionless], and A is the specified cross-sectional area across which the discharge flows [L^2] (Caine and Tomusiak, 2003).

Potential hydraulic conductivity, K [m/s], is then calculated by FRED from the intrinsic permeability values according to:

$$K = k_i \frac{\rho g}{\mu}$$

(4.3)

DFN modeling is a stochastic approach and generated fracture models of each model generation are always a little different. Because of this, the calculated K values vary over some narrow range. For this reason, more than one DFN model should be simulated for the same domain, and the arithmetic mean of the K value computed. In this study, five simulations were run for each DFN model.

FRED also calculates a "storage" value for the cube using the Oda analysis (Oda 1985). The Oda analysis transforms the hydraulic properties of the discrete fracture network to equivalent properties in a geocellular grid. Each cell in the grid is characterized by a K tensor and a specific storage according to:

$$Ss = \frac{SA}{V} = \frac{C_f b A \rho g}{V}$$

(4.4)

where Ss is the specific storage [1/m], S is the storativity [dimensionless], A is the area [L^2], V is the cell volume [L^3], C_f is the facture compressibility [m^2/N], b is the fracture aperture [L], ρ is the fluid density [M/L^3], and g is the acceleration due to gravity [L/T^2] (Golder Associates 2006, FRED manual v. 6.54). Total storage is determined by summing up the Ss values for each cell. Note that the Oda analysis yields the hydraulic properties for each cell in a geocellular grid that can be imported into an equivalent porous media code, such as MODFLOW. In this study, however, the code MAFIC was used to generate the hydraulic conductivity tensor directly from the discrete fracture network. The code is

a module within FRED. Only the equivalent specific storage value for the cube was determined using the Oda approach.

4.3.5. Outcrop scale DFN modeling

4.3.5.1. Statistical characterization of the outcrop fracture sets

For the purpose of illustrating the statistical methods used to characterize the fracture sets measured at each outcrop location, which are used subsequently for DFN model generation, fracture data from one outcrop location in the low density zone (Site #39 – and closest to W1 and W2) are considered (Figure 4.6). The same procedure is applied to all other outcrop locations. For the DFN model, different fracture apertures and their corresponding K values, calculated using the cubic law (see Equation 4.1), were tested. For these outcrop-based models, the K_m, as well as the specific storage for the fractured matrix, Ss_m, are simulated. The K_m results for the different apertures are then compared to the values of K derived from pumping tests, K_p, conducted in W1 and observed in W2. The best estimate of fracture aperture is then assumed to be representative of other outcrops and is used for all further DFN models for the outcrop locations in the low, medium and high density zones. The assumption is made that even though fracture density varies, the fracture aperture remains the same.

Fractures mapped in outcrop were displayed in a lower hemisphere stereonets. A density distribution was performed using a Gaussian counting model for contouring. Statistical fracture data analyses were performed using the software SpheriStat (SpheriStat v. 2.2,

Pangea Scientific, 1998). Most of the fracture set distributions can be modeled using a Fisher distribution (Fisher, 1953), which is characterized by a uniform tight orientation cluster (with limited dispersion). A cluster analysis was performed to separate each set and to obtain the individual statistical parameters (mean trend/plunge, dispersion factor k, and mean persistence) that are needed for the discrete fracture network model generation (see Table 4.1). The dispersion factor k is a measure of the clustering of each fracture data set. The higher the value of k, the more clustered are the data (Fisher et al., 1987). Stereonets for all outcrop measurements are provided in Appendix A.2.
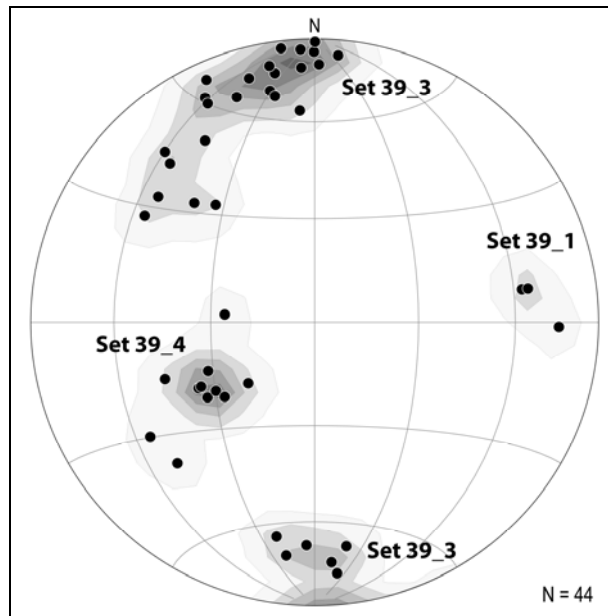
Figure 4.6. Stereonet showing all poles to the fractures from four outcrop locations in the low density zone at outcrop location 39 (see Figure 4.2 for outcrop location). Contours for each set were generated following a cluster analysis.

Figure 4.7a shows the outcrop stereonets for the three lineament density zones. Outcrop fracture data and lineaments within an arbitrary lineament window (Figure 4.7b panel) are used to illustrate results. Four outcrop fracture sets are identified.
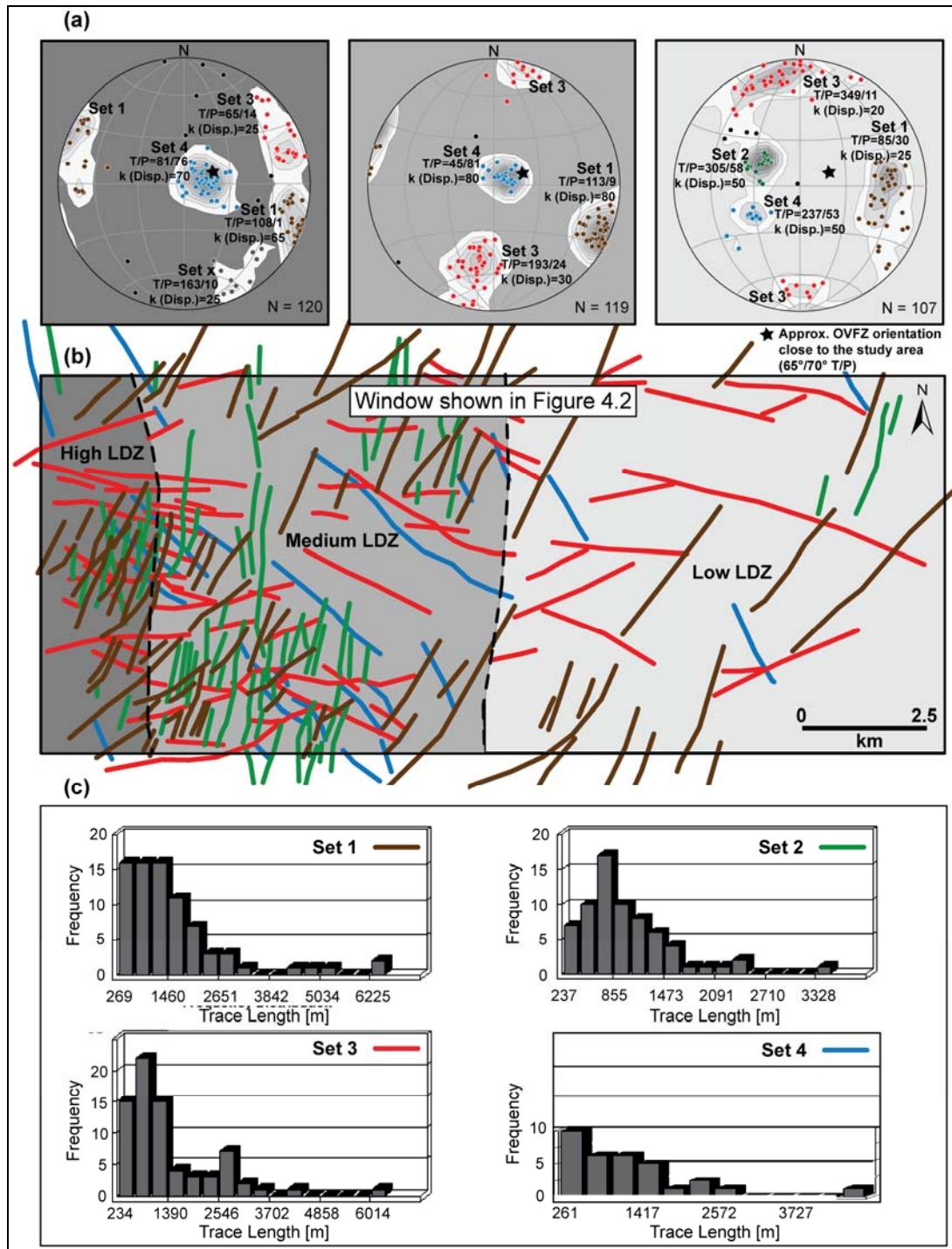
Figure 4.7. (a) Stereonets of outcrop locations within the three lineament density zones (LDZs) shown in the lineament window in (b). Four lineament sets are identified (color coded). (c) Lineament trace length distributions for each set. The location of the lineament window is shown in Figure 4.2.

125

4.3.5.2. Fracture properties

As mentioned above, a range of aperture values was considered. The chosen range was based on values from the literature. For example, Folger (1995) used the cubic law to calculate apertures from transmissivity values obtained from single-well, short-term aquifer tests in the Silver Plume crystalline rock (quartz monzonite) in the vicinity of Conifer, Colorado (USA). For ~20 tests, the calculated aperture estimates ranged between 60 and 570 μm. Caine and Tomusiak (2003) and Surrette and Allen (2008) used a value of 100 μm. In this study, a range from 10 μm to 1000 μm was considered, because aperture data were not available for un-weathered (exposed) fractures. Table 4.1 shows the range of aperture values considered in a sensitivity analysis, together with the other DFN generation and simulation parameters for outcrop location 39. Based on the results of the comparison with the pumping test data, a fracture aperture of 50 μm and its corresponding potential fracture K value were selected (values identified with an * in Table 1). Fracture hydraulic conductivity K_f [m/s] was calculated by dividing the fracture transmissivity T_f [m^2/s] by the aperture b. As mentioned earlier, T_f (not shown in Table 1) was estimated using the cubic law of transmissivity for the different aperture values (see Equation 4.1). T_f for a corresponding aperture of 10 μm would be 5 x 10^{-10} m^2/s.

Table 4.1. Overview of DFN generation and simulation parameters for the outcrop scale model at outcrop location 39. The different tested aperture range and corresponding K values are also shown. Values identified with an * correspond to the selected parameters used for DFN models at the outcrop scale.

Parameter	Set 39_1	Set 39_3	Set 39_4
Trend/Plunge [°]; Dispersion k	85/22, k= 35	346/10, k= 25	238/51, k= 38
Mean persistence [m]; Standard deviation	1.90; 0.36	1.28; 0.68	1.25; 0.45
Fracture aperture b [μm]	10 50 * 100 150 1000	10 50 * 100 150 1000	10 50 * 100 150 1000
Fracture hydraulic conductivity K_f [m/s]	5.4×10^{-5} 1.3×10^{-3} * 5.4×10^{-3} 1.2×10^{-2} 5.4×10^{-1}	5.4×10^{-5} 1.3×10^{-3} * 5.4×10^{-3} 1.2×10^{-2} 5.4×10^{-1}	5.4×10^{-5} 1.3×10^{-3} * 5.4×10^{-3} 1.2×10^{-2} 5.4×10^{-1}
Fracture compressibility C_f [m^2/N]	3.3×10^{-4}	3.3×10^{-4}	3.3×10^{-4}
P_{10} Intensity	0.7	3.14	1.43
P_{32} Intensity	0.27	0.68	0.82

4.3.5.3. Domain size for simulations and upscaling

To calculate the threshold REV for the small scale outcrop simulations, multiple realizations of the fracture sets at location 39 were generated within cube domains of different sizes. A series of test simulations were first run using different DFN cube sizes ranging from 5m x 5m x 5m to 100m x 100m x 100m. The results showed little difference in the K_m results above a volume threshold of 20m x 20m x 20m. Therefore, this volume was selected as the REV for the simulations. It is noted that this sensitivity analysis was only conducted at outcrop location 39; however, the results revealed that the length of a rectangular cube side in a DFN model always needs to be greater than the maximum mean trace length value of any fracture set at the same location. Thus, as a general rule,

longer fracture lengths require larger cubes. None of the fracture sets at the other locations had mean trace length values greater than 20 m. Therefore, it was determined that a 20m x 20m x 20m cube would be adequate for all the outcrop scale simulations. For the lineament scale simulations, the same general rule was applied to select an REV size for the longer lineaments. This is described in the next section.

The P_{10} intensity from trace length distributions and upscaled P_{32} intensity values are shown in Table 4.1. Trace length distributions for outcrops (not shown) are generally log-normally distributed.

Five different stochastic fracture generations using the same domain at each outcrop location in each density zone were simulated, and a geometric mean K_m value estimated for each flow direction. Individual K_m values in x,y,z-direction for every outcrop location as well as the results for specific storage Ss_m were computed. In the low density zone there were four outcrop locations; in the medium density zone there were five outcrop locations; and in the high density zone there were 20 outcrop locations, for a total of 29 outcrop locations.

4.3.6. Lineament scale DFN modeling

4.3.6.1. Determining statistical lineament sets

To generate the large scale DFN models for the lineaments, the trend/plunge values, dispersion factors, P_{32} values, and trace lengths distributions are needed for each density zone, similar to the outcrop scale models. As these lineaments are surface traces

of fracture zones, dip (or plunge) cannot be measured directly. Therefore, dips for each lineament set had to be approximated from outcrop data. An assumption was made and verified that the small scale fracture sets have the same general orientations as the large scale lineaments. Within this study region, the main tectonic feature is the extensional Okanagan Valley Fault Zone (OVFZ), a low angle detachment fault. Therefore, it is reasonable to assume that fractures might be correlated at different scales in relation to this extensional tectonic event (e.g. Rahiman and Pettinga, 2008). Multiple deformation events, strike-slip faulting, etc. may lead to differences in fracturing at different scales, thus the approach may not be widely suitable for areas affected by other deformation types.

To test for correlation, a buffer analysis (Degnan and Clark, 2002) or domain overlap analysis (Mabee et al., 1994) was undertaken. Those lineaments whose buffers (305 m around each lineament) contain at least one steeply dipping fracture (at least 45°) and have a trend within ±5° of the strike of the lineament are considered correlated. In the low density zone, the four outcrops had an average correlation of 46% (but as high as 77% at one outcrop). Stronger correlations were observed in the high and medium density zones (high – ave. 64%; medium – ave. 81%). Figure 4.8 shows rose diagrams of outcrop and lineament data for the low density zone. Note that stereonets for lineaments could not be generated because dip data are not available. Rose diagrams show the frequency distribution of the strike directions of fractures/lineaments. As seen in the top two rose diagrams (all fractures combined), the strike directions are similar regardless of scale. The four extracted lineament sets (right column in Figure 4.8) show similar principal

directions as the outcrop scale fractures (left column in Figure 4.8). All four fracture sets are present in all three zones, but their frequencies and dispersion factors differ slightly. Similar results were found for the medium and high density zones (results not shown). Figure 4.7 shows the mapped lineaments within a window (Fig. 4.7b) that are color-coded according to outcrop fracture sets (Fig. 4.7a). Four sets are evident at both scales, although there are slight deviations. Also shown (in Fig. 4.7c) are the trace length distributions for the lineament sets in each zone. Sets 1, 3, and 4 are clearly log-normally distributed, similar to most of the outcrop data.

Overall, these statistical and visual measures of comparison suggest that there is reasonable correlation between outcrop fractures and lineaments. Based on the four separated small outcrop scale fracture sets and their defined strike ranges (in the low density zone Set 1: 20ºW-20ºE; Set 2: 20º-60º; Set 3: 60º-130º; Set 4: 130º-160º), all lineaments from the combined orthophoto and LANDSAT analysis were assigned to one of the four sets through a SQL query in ArcGIS. Each lineament set was then assigned the same average plunge value as the corresponding outcrop fracture set. The same process was repeated for the medium and low density zones.
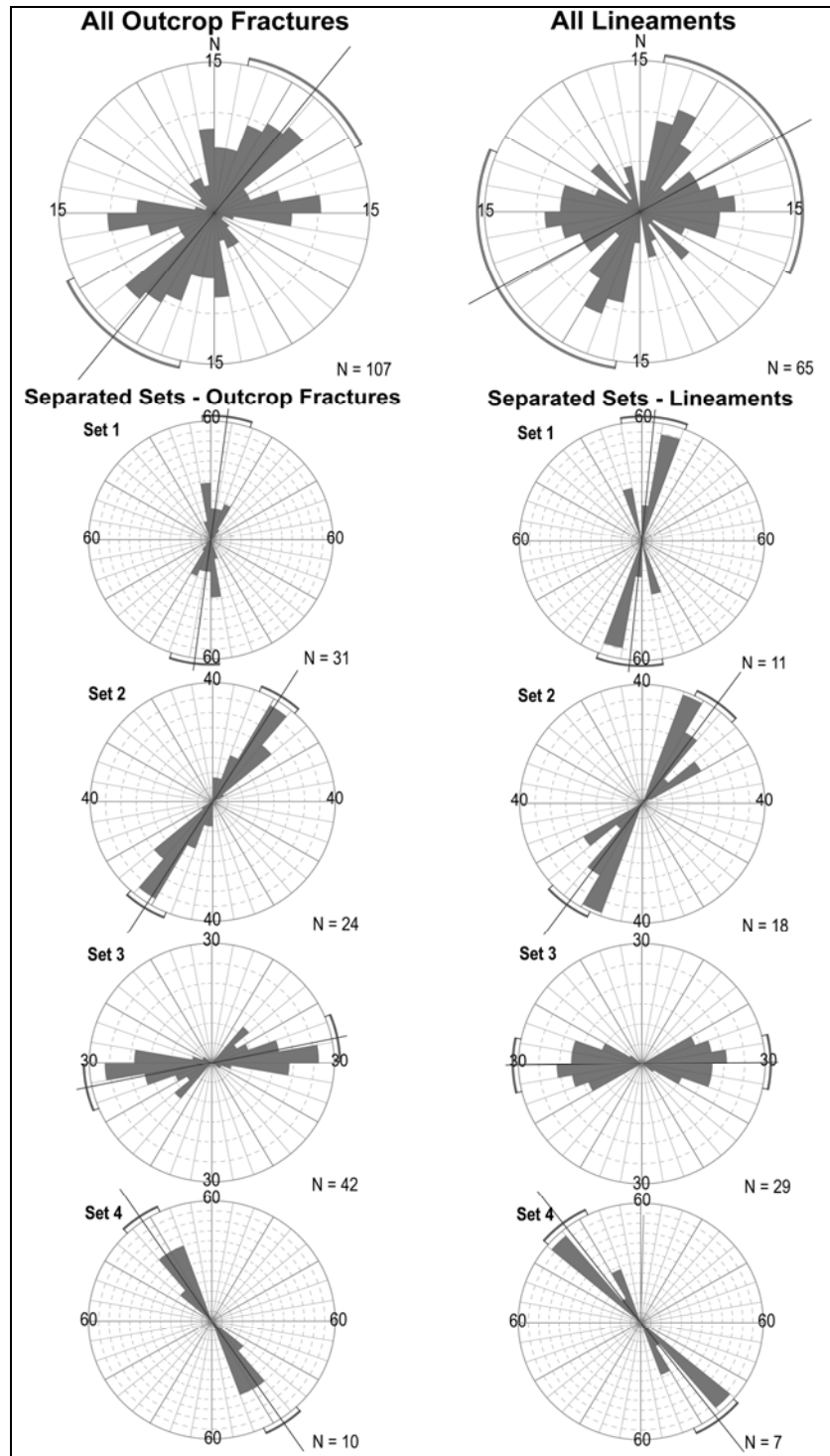
Figure 4.8. Rose diagrams for outcrop fractures (left column) and lineaments (right column) within the low density zone. The top row shows all fractures; four separated sets are shown below.

4.3.6.2. Determining lineament properties through inverse modeling

The purpose of the inverse modeling is to identify plausible parameter combinations that can be used to represent the lineaments in the DFN modeling of the larger scale model domains. Lineament K cannot be calculated using the cubic law as was done for the outcrop scale models, because the effective aperture (or width) of the lineament is unknown. In fact, the lineament itself is a surface expression of series of fractures, likely parallel to each other, which have some equivalent bulk hydraulic conductivity. The challenge is estimating this bulk K value. Due to the phenomenon of equifinality in numerical modeling, parameter combinations are non-unique for model calibration. Therefore, it is important to consider plausible combinations of model parameters that can reproduce the observed behavior.

In order to estimate plausible parameter combinations of potential effective lineament aperture, potential lineament K, and potential lineament compressibility, the constant discharge test in W3 was simulated in a DFN model. These parameter combinations were then used to generate DFN models of the lineaments. W3 was used for the simulation because it is thought to be in close proximity to a fracture zone as evidenced by the shape of the drawdown curve from the constant discharge test (see Figure 4.3). Of course, the test may have been influenced by a different fracture zone that is not visible as a lineament, but for the purpose of demonstrating this approach it is assumed that the fracture zone corresponds to the mapped lineament and that this lineament intersects the well

Figure 4.9 shows a model domain built with the FRED software used for the inverse modeling process. In the DFN model, a large discrete fracture is assumed to intersect the well at a depth of 20 m. Note that fractures must intersect the well in FRED in order to run the simulation. The only estimate of the hydraulic conductivity in the model is that derived from the effective K of a single fracture, representing the large lineament intersecting W3. The matrix K setting for the pumping test option in FRED was assumed to be zero (note that non-zero values did not appear to change the simulation results). Information on the plunge angle of the fracture zone is not available, but different simulations showed that changing the angle of the intersecting feature had no effect on the shape of the simulated drawdown curve. Thus, the fracture was given a nearly vertical plunge and fully penetrated the model domain. The dimension of the cubic model domain was set at 30m x 30m x 30m, corresponding to the depth of W3 of 30 m. Test runs with different cube sizes showed that a 30 m cube size length was sufficiently large to prevent the pressure drawdown from reaching the model boundaries. All boundaries of the model were set as impermeable boundaries and the domain was considered fully saturated.
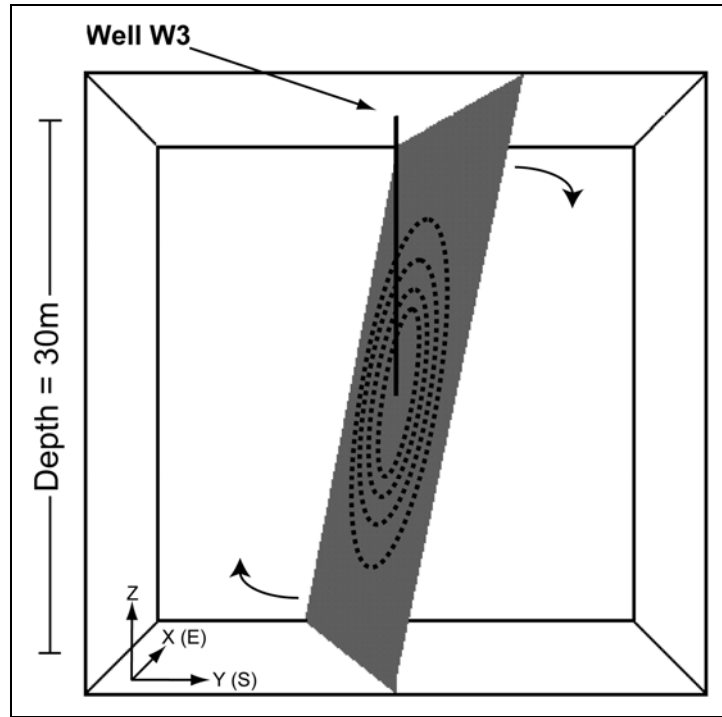
Figure 4.9. DFN model for simulating the constant discharge test in W3. A near-vertical fracture was inserted in the model, intersecting the well at 20 m depth. Fracture orientation did not appear to influence the results as indicated by the arrow.

Numerous parameter combinations were considered. The model domain was the same for all three combinations. The individual parameters included: 1) effective lineament (fracture) aperture, 2) effective lineament K, and 3) effective lineament compressibility. Four effective lineament apertures were considered: 1 m, 5 m (estimated from drilling), 7 m and 10 m. The preliminary estimate of effective lineament K was 10^{-5} m/s, taken to represent a fractured granitic rock. The preliminary estimate of effective lineament compressibility, C_f, was set to $\sim 10^{-11}$ m^2/N since no values for effective compressibility of a fracture zone in a granitic aquifer were available.

The modeling process was very time-consuming for simulation runs with these different parameter combinations. Each model, with its initial parameter combination of the fixed aperture value and the preliminary estimates of effective lineament K and compressibility, was stressed by pumping to generate a pressure response that could be compared with the observed drawdown data. The K and compressibility of the intersecting fracture in each of the simulation runs were adjusted manually until a reasonable match between the measured drawdown curve and the simulated drawdown curve was obtained. The overall tendency was that as the aperture was increased, the effective K and compressibility had to be lowered to maintain the model fit. The parameter combinations that gave the most favourable results are shown in Table 4.2.

Table 4.2. Range of effective lineament parameters that resulted in a reasonable match between measured and simulated drawdown.

Combination	Effective lineament aperture [m]	Effective lineament hydraulic conductivity K_{eff} [m/s]	Effective lineament compressibility [m^2/N] C_{eff}
1	5	1.1×10^{-6}	4.4×10^{-6}
2	1	5.0×10^{-6}	2.2×10^{-5}
3	10	5.0×10^{-7}	2.9×10^{-6}

The best match between the simulated drawdown and the measured drawdown was achieved with the parameter combination where the effective aperture was set to 5 m, the effective lineament hydraulic conductivity, K_{eff}, was 1.1×10^{-6} m/s, and the effective lineament compressibility was 4.4×10^{-6} m^2/N (combination 1 in Figure 4.10). The drawdown at the beginning and at the end of the pumping test was matched very well using this combination, although the shape of the drawdown curve could not be matched

perfectly, despite many calibration attempts. The most likely reason for the mismatch between the measured and observed data is well inefficiency, which cannot be simulated. The model simulates the theoretical drawdown, based on the input parameters, but the actual well test may be affected by the pump. Nevertheless, the overall range of values for each parameter was generally small (Table 4.2).

Figure 4.10 also shows the results from two sets of parameter combinations that achieved a reasonable fit with the observed pumping response (combinations 2 and 3). Notably, K_{eff} and effective aperture play off against each other, whereby a similar fit can be achieved by increasing effective aperture and lowering K_{eff} in such a way as to maintain the effective fracture transmissivity ($T_{eff} = K_{eff}$ x *effective aperture*). As such, the model results are non-unique. However, the fracture transmissivity appears to be important because selecting different combinations (for example, combinations 4 and 5) leads to poor results.

Finally, the parameter combination of effective lineament aperture, K_{eff} and compressibility corresponding to those of combination 1 were used to generate the large-scale DFN models for each zone. It is important to note that it was assumed that the same properties characterize the lineaments in all three lineament density zones despite the fact that the chosen parameters were derived through calibration of the DFN model using pumping test data acquired in the low lineament density zone. A very basic sensitivity analysis was conducted to investigate how changing K_{eff} impacts the results. The results are discussed later.
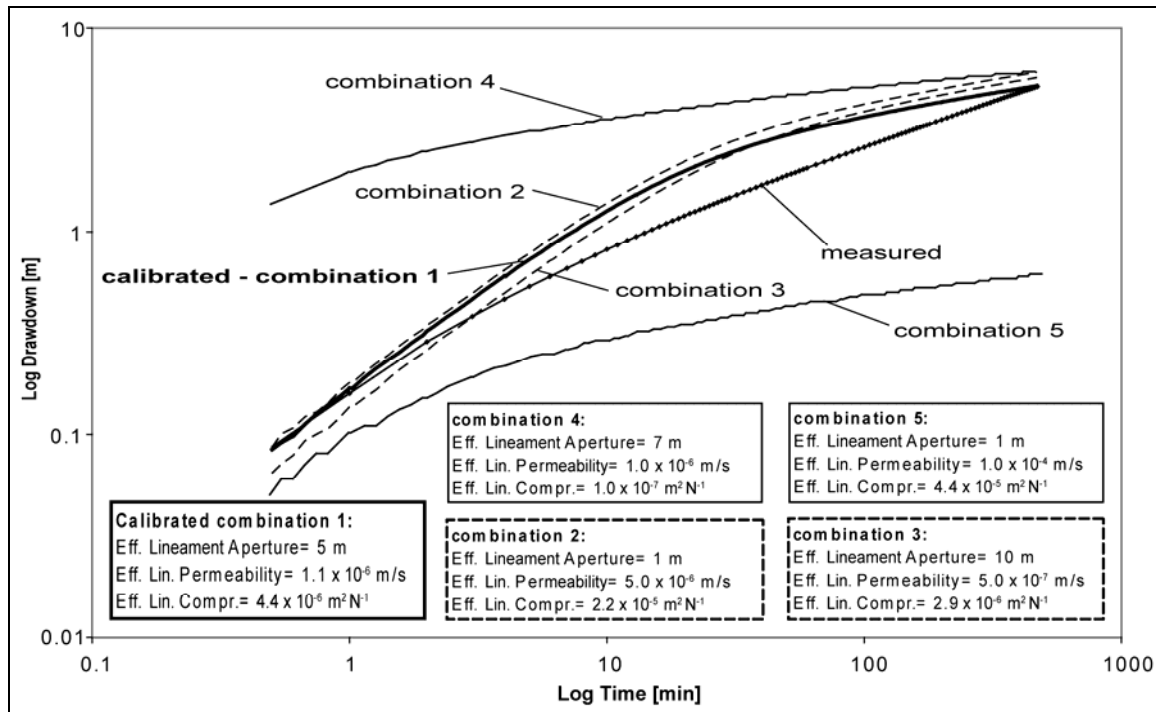
Figure 4.10. Measured drawdown data from the constant discharge pumping test in W3 (470 minutes). Also shown are the DFN simulation results of the pumping test at W3 for five different parameter combinations. The best match was achieved with combination 1. Combinations 4 and 5 lead to poor results.

4.3.6.3. Domain size for simulations and upscaling

Appropriate model domain sizes for the large scale DFN models were determined based on the findings of REV estimation for the small scale DFN models, whereby K results are not influenced by truncating lineaments. Effectively, the shortest cube side length of the rectangular DFN domain should always be greater than the mean trace length of its distribution. With this in mind, appropriate domain sizes for modeling (A – low density, B – medium density, C – high density) were chosen as shown in Table 4.3.

The P_{10} to P_{32} upscaling process for the large scale lineaments is illustrated in the low density zone for the set 3 lineaments (Figure 4.11). The procedure is the same as that

used for the small scale models. Figure 4.11 (right panel) shows an imaginary scanline (dashed black line) laid over the set 3 lineaments (for illustration purposes, the scanline is restricted to the rectangular window, but all fractures within the zone were analyzed). Using ArcGIS, the P_{10} intensity for set 3 was estimated by calculating the number of lineaments per scanline length. This value was then upscaled in a DFN model generation to estimate the P_{32}. The same procedure was carried out for all other sets in the low, medium and high density zone modeling windows A, B, and C.
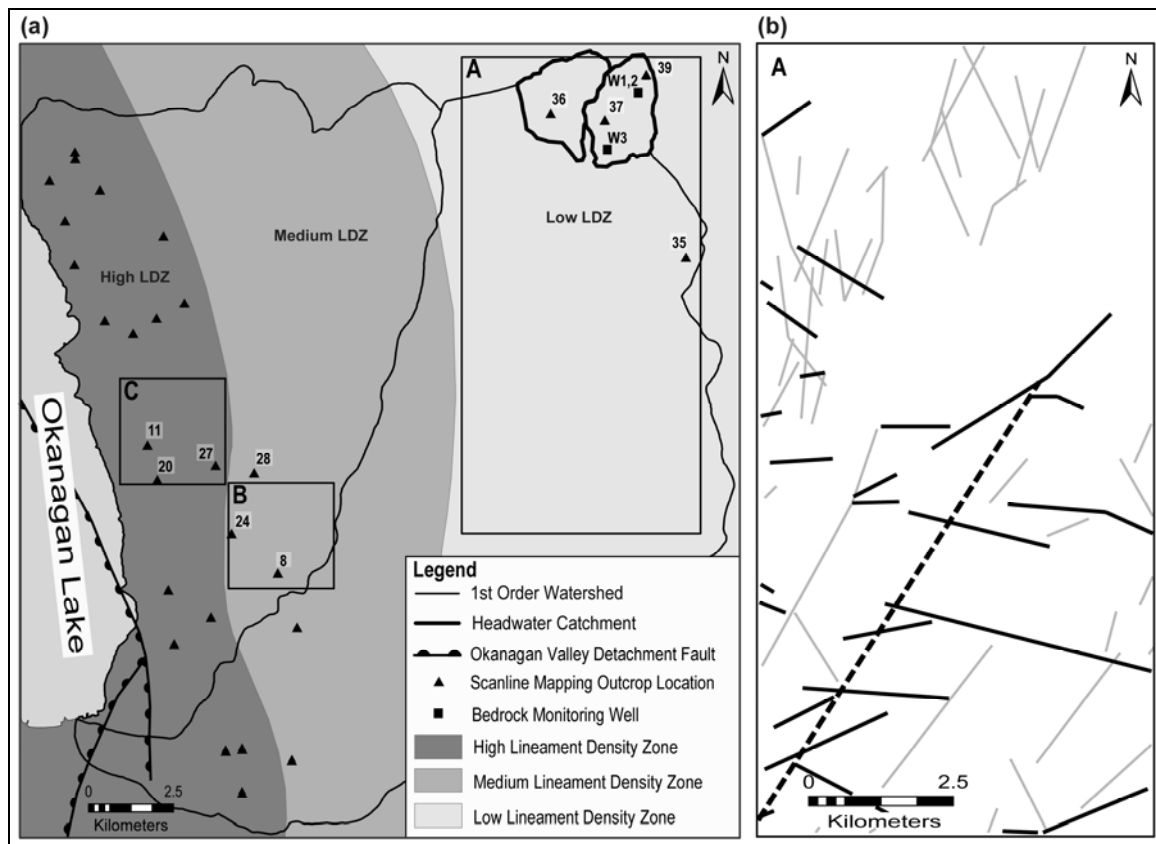
Figure 4.11. (a) The three lineament density zones (LDZ) and the model domains (labelled A, B and C for the low, medium and high density zones, respectively). (b) The lineament trace map for domain A, where set 3 is highlighted as bold black lines. The dashed line is an imaginary scanline laid over the lineaments in order to calculate the P_{10} intensity needed for upscaling to P_{32} intensity.

Table 4.3 gives an overview of the final DFN generation and simulation parameters for all three large scale model domains A, B, C. Parameters include the orientation and dispersion parameters of the small scale fracture sets in or close to the same domain from which the large scale lineament sets were derived, and the unmapped plunge and dispersion values that were estimated from outcrop data. Table 4.3 also includes the effective fracture aperture, effective fracture K and compressibility, and the P_{10} and P_{32} values for the lineaments. As shown in Table 4.3, set 4 for the high density zone is missing a P_{10} value, because only one lineament of this set could be detected. The P_{32} value for set 4 in the high density zone was estimated based on the P_{32} value from set 4 in the medium density zone. The value was increased slightly to take its closer proximity to the main fault trace into account, where fracture intensity appears to be higher based on the other sets. Set 2 is missing for the medium and high density zone for the outcrop scale, but not for the lineament scale (see Figure 4.8). For generating lineaments of set 2 for the medium and high density zone, DFN generation parameters were taken from set 2 in the low density zone (Table 4.3).

Table 4.3. Overview of final simulation parameters for DFN modeling at the lineament (mountain block) scale. Also shown are the dimensions of the domains and the orientation data (Trend/Plunge) of the small scale (outcrop) fracture sets from each zone. Minor adjustments to the outcrop scale mean trend and dispersion factors were made for representing these properties for the lineament sets.

DFN model	Parameter	Set 1	Set 2	Set 3	Set 4
Low density zone					
Outcrop scale (locations35,36,37,39)	Trend/Plunge [°], Dispersion _k_	85/30, k= 25	305/58, k= 50	349/11, k= 20	237/53, k= 50
Lineament scale (6.8km x 13.6km x 5km)	Trend/Plunge [°], Dispersion _k_	80/30, k= 50	295/58, k= 45	359/11, k= 40	237/53, k= 55
	Mean persistence [m]; Std. dev.	1383, 596	1577, 1153	1509, 1513	1843, 992
	Effective lineament aperture [m]	5	5	5	5
	Effective lineament hydraulic conductivity K_{eff} [m/s]	1.1×10^{-6}	1.1×10^{-6}	1.1×10^{-6}	1.1×10^{-6}
	Effective lineament compressibility [1/psi]	3.0×10^{-2}	3.0×10^{-2}	3.0×10^{-2}	3.0×10^{-2}
	P_{10} intensity from trace map	1.4×10^{-3}	7.0×10^{-4}	1.2×10^{-3}	9.6×10^{-4}
	Upscaled P_{32} intensity	5.7×10^{-3}	3.6×10^{-3}	6.7×10^{-3}	5.0×10^{-3}
Medium density zone					
Outcrop scale (locations 8,24,28)	Trend/Plunge [°], Dispersion _k_	113/9, k= 80	Not present	193/24, k= 30	45/81, k= 80
Lineament scale (3km x 3km x 3km)	Trend/Plunge [°], Dispersion _k_	103/9, k=80	295/58, k= 45	153/24, k= 60	35/81, k= 80
	Mean persistence [m]; Std. dev.	810, 427	1277, 1030	741, 595	353, 262
	Effective lineament aperture [m]	5	5	5	5
	Effective lineament hydraulic conductivity K_{eff} [m/s]	1.1×10^{-6}	1.1×10^{-6}	1.1×10^{-6}	1.1×10^{-6}
	Effective lineament compressibility [1/psi]	3.0×10^{-2}	3.0×10^{-2}	3.0×10^{-2}	3.0×10^{-2}
	P_{10} intensity from trace map	4.2×10^{-3}	7.0×10^{-4}	7.0×10^{-3}	3.6×10^{-3}
	Upscaled P_{32} intensity	8.2×10^{-3}	3.6×10^{-3}	1.0×10^{-2}	8.9×10^{-3}

DFN model	Parameter	Set 1	Set 2	Set 3	Set 4
High density zone					
Outcrop scale (locations 11,20,27)	Trend/Plunge [°], Dispersion k	108/1, k= 65	Not present	65/14, k= 25	81/76, k= 70
Lineament scale (3km x 3km x 3km)	Trend/Plunge [°], Dispersion k	108/1, k= 65	295/58, k= 45	5/14, k=50	81/76, k= 70
	Mean persistence [m]; Std. dev.	972; 352	903, 598	628; 356	2000, 800
	Effective lineament aperture [m]	5	5	5	5
	Effective lineament hydraulic conductivity K_{eff} [m/s]	1.1×10^{-6}	1.1×10^{-6}	1.1×10^{-6}	1.1×10^{-6}
	Effective lineament compressibility [1/psi]	3.0×10^{-2}	3.0×10^{-2}	3.0×10^{-2}	3.0×10^{-2}
	P_{10} intensity from trace map	9.2×10^{-3}	7.0×10^{-4}	5.4×10^{-3}	N=1
	Upscaled P_{32} intensity	2.8×10^{-2}	3.6×10^{-3}	5.0×10^{-2}	4.0×10^{-2} Est.

4.4. Results

4.4.1. DFN small scale outcrop K_m estimation

The K_m results as well as the FRED specific storage values (Ss_m) for the small scale DFN models in the low density zone (for outcrop location 39) and for different fracture apertures are shown in Table 4.4. The main observation is that if the fracture aperture is increased by one order of magnitude, the K_m values in x,y,z-direction increase by three orders of magnitude. The storage values only increase by one order of magnitude. The DFN K_m results with fracture apertures of 50 μm (Table 4.4) are very similar to the result from the pumping test in W1 with a K_p value of 1.1 x 10^{-7} m/s (see Chapter 3). This suggests that 50 μm for the small scale fracture apertures is a plausible value for simulation of outcrop fractures through DFN modeling in the medium and high density zone. The Ss_m value of 2.0 x 10^{-4} m^{-1} at 50 μm is one order of magnitude higher than the one estimated from the pumping test in W2, which is 2.0 x 10^{-5} m^{-1}. This indicates that DFN specific storage modeling through the Oda analysis results in a close value to that estimated from a pumping test.

Table 4.4. Overview of K_m and Ss_m values from the DFN small scale fracture outcrop model (location 39) in the low density zone closest to W1 and W2 for the different fracture apertures.

Outcrop scale fracture aperture [μm]	K_mx [m/s] E-W	K_my[m/s] N-S	K_mz[m/s] T-B	Ss_m [m^{-1}]
10	8.7 x 10^{-10}	8.0 x 10^{-10}	9.9 x 10^{-10}	4.0 x 10^{-5}
50 *	1.0 x 10^{-7}	1.0 x 10^{-7}	1.2 x 10^{-7}	2.0 x 10^{-4}
100	8.7 x 10^{-7}	8.0 x 10^{-7}	9.9 x 10^{-7}	4.0 x 10^{-4}
150	2.9 x 10^{-6}	2.7 x 10^{-6}	3.2 x 10^{-6}	6.0 x 10^{-4}
1000	8.7 x 10^{-4}	8.0 x 10^{-4}	9.9 x 10^{-4}	4.0 x 10^{-3}

* parameters used for outcrop scale DFN models

Table 4.5 shows the results for the DFN outcrop scale models with 50 μm fracture aperture for the low, medium and high lineament density zones. The geometric mean values for the directional hydraulic conductivity (K_m x,y,z) and specific storage (Ss_m) are shown. The full table of DFN K results for all outcrop locations is provided in Appendix B.1. Overall, the values in each zone are of similar magnitude, although the values in the low density zone are perhaps slightly lower than those in the medium and high density zones, which themselves are very similar. The same applies for the specific storage values. Directional potential K is also highest in N-S direction compared to the E-W direction, and both are higher than the T-B (top-to-bottom) direction. The K_m values are fairly close to a fractured matrix value of 2.0 x 10^{-8} m/s for a crystalline rock estimated through numerical modeling by Gleeson and Novakowski (2009).

Table 4.5. Geometric mean values for K_m and Ss_m from DFN small scale outcrop fracture modeling locations in the low, medium and high lineament density zones throughout the mountain block.

Small scale outcrop model	$K_m x$ [m/s] E-W	$K_m y$ [m/s] N-S	$K_m z$ [m/s] T-B	Ss_m [m^{-1}]
Low density zone – 50μm aperture	8.6 x 10^{-8}	9.5 x 10^{-8}	7.0 x 10^{-8}	2.2 x 10^{-4}
Medium density zone – 50μm aperture	1.0 x 10^{-7}	1.5 x 10^{-7}	1.1 x 10^{-7}	3.4 x 10^{-4}
High density zone – 50μm aperture	9.2 x 10^{-8}	1.4 x 10^{-7}	1.1 x 10^{-7}	3.0 x 10^{-4}

4.4.2. DFN large scale mountain block K_{mb} estimation

The DFN simulation results for the low, medium and high lineament density zones using the parameters from combination 1 (see Table 4.2) are shown in Table 4.6. As expected, the directional potential K values (K_{mb} x,y,z) for the three zones of the

generated models increase from the low to the high density zone. They differ by about one half an order of magnitude, ranging from about 8×10^{-8} m/s in the low density zone to about 3×10^{-7} m/s in the high density zone. The potential K of the medium density zone is on the order of 1×10^{-7} m/s. The specific storage values for the same models follow a similar pattern, with lowest values simulated for the low density zone.

When comparing the potential K values in the different directions (N-S, E-W, T-B) for all three large scale generated models, the highest values are in N-S direction, while the lowest are in T-B direction. The values in E-W direction are very close to the ones in N-S direction for all models. This pattern is similar to the outcrop scale models. These results are discussed later.

Table 4.6. Overview of K_{mb} and Ss_{mb} values from large scale DFN generated models

Mountain block model	$K_{mb}x$ [m/s] E-W	$K_{mb}y$ [m/s] N-S	$K_{mb}z$ [m/s] T-B	Ss_{mb} [m^{-1}]
Low density zone – Combination 1	8.0×10^{-8}	8.2×10^{-8}	7.3×10^{-8}	3.2×10^{-3}
Medium density zone – Combination 1	9.6×10^{-8}	1.1×10^{-7}	9.2×10^{-8}	4.1×10^{-3}
High density zone – Combination 1	3.3×10^{-7}	3.7×10^{-7}	2.8×10^{-7}	1.3×10^{-2}

4.4.3. Sensitivity analysis

Three sensitivity analyses were conducted. As part of the first sensitivity analysis, K_{eff} was increased for the medium and high density zones relative to the low density zone. Recall that K_{eff} had been estimated from the inverse modeling in the low density zone. The sensitivity analysis was done to determine what the effect might be if the fractures in the medium and high density zones were sequentially made more permeable in closer

proximity to OVFZ. The other two parameters (effective lineament aperture and effective lineament compressibility) remained the same. K_{eff} was increased one half order of magnitude from low to medium to high density zones, that is from 1.1 x 10^{-6} m/s (combination 1) to 6.1 x 10^{-6} m/s (sensitivity 1 for medium density zone) and to 1.1 x 10^{-5} m/s (sensitivity 2 for high density zone). The results are shown in Table 4.7.

Table 4.7. Sensitivity analysis results for K_{mb} and Ss_{mb} values resulting from increasing the effective lineament K_{eff} in the medium and high density zones. Values can be compared to those given in Table 4.6

Mountain block model	$K_{mb}x$ [m/s] E-W	$K_{mb}y$ [m/s] N-S	$K_{mb}z$ [m/s] T-B	Ss_{mb} [m^{-1}]
Medium density zone – Sensitivity 1	5.4 x 10^{-7}	6.2 x 10^{-7}	5.0 x 10^{-7}	4.1 x10^{-3}
High density zone – Sensitivity 2	3.3 x 10^{-6}	3.7 x 10^{-6}	2.8 x 10^{-6}	1.3 x 10^{-2}

It is noticed that when increasing the K_{eff} for the medium density zone by half an order of magnitude, the overall K_{mb} results in each direction increase by a half an order of magnitude as well. For the high density zone, the K_{mb} results increase by one order of magnitude higher. The specific storage values do not increase. Thus, K_{mb} is sensitive to K_{eff} as would be expected, and if the lineaments do become more permeable in proximity to the OVFZ, then the overall K_{mb} values would also be higher.

A second sensitivity analysis was conducted to test changes in the mean plunge and dispersion factors for the lineaments. Mean plunge values were varied by ±30° and dispersion factors k were varied by up to ±60 for the lineament sets. Also mean trend was varied by up to ±50°. None of these changes resulted in any significant impacts on K values; less than one quarter of an order of magnitude. Consequently, it appears that the

'upscaling' process to obtain plunge and k values from similar sets from outcrop scale measurements is reasonable.

A third sensitivity analysis for trace length was also conducted. For some lineament sets, there were fewer than 30 values. A number of 30 data points is considered a threshold for statistical analysis (SpheriStat v. 2.2, Pangea Scientific, 1998). Nonetheless, trace length distributions for data sets less than 30 were used, because changing mean trace length values of lineament sets up to ±1000 m resulted in very small changes in K_{mb}. The P_{32} value upscaled from the scanline intensity P_{10} is the most sensitive parameter concerning K_{mb}. Changing this value by one order of magnitude results in a K_{mb} change of about half an order of magnitude.

4.5. Discussion

In general, the simulated K values for both scales are on the order of 10^{-8} m/s to 10^{-7} m/s and coincide very well with the values from the literature (Gleeson et al., 2011; Gleeson and Novakowski, 2009; Wilson and Guan, 2004) for crystalline granitic fractured rocks. Gleeson et al. (2011) report a geometric mean permeability of roughly 8 x 10^{-15} m^2 (K = 6 x 10^{-8} m/s) for crystalline rock based on a compilation of permeability estimates from regional scale models. The results of this study seem to lend additional support to their estimate of K for regional scale crystalline bedrock.

The fact that there is little overall difference at the two scales is an interesting result, and suggests that the large scale fracture zones, despite their higher K_{eff} (estimated at 1.1 x 10^{-6} m/s), does not result in a higher K_{mb}. Gleeson et al. (2011) also noted a lack

of scale dependence for crystalline rock. This is likely due to the lower density of larger scale features at the regional scale, which results in an overall lower connectivity. Of course, at a local scale, these fracture zones can significantly impact groundwater flow as evidenced by the pumping test results in W3. Looking more closely at the results, the K_m and K_{mb} values are very similar in the low and medium density zones at both scales. This may have implications for regional scale modeling, in that outcrop scale DFN modeling (and perhaps pumping tests) may provide reasonable estimates of regional scale K (i.e. no apparent scale effect). However, K_{mb} is consistently higher by a factor of roughly 3 compared to K_m in the high density zone, which may reflect a more important role of larger scale fractures if P_{32} is sufficiently high.

K_{mb} is most sensitive to K_{eff} and P_{32}. K_{mb} appears to scale nearly directly with an increase in these parameters. Fracture zone connectivity appears to be sufficiently high throughout the site such that the actual controlling parameter is the effective fracture zone transmissivity, T_{eff}, which increases as both K_{eff} increases (see Table 4.7) and the number of fractures zones per unit volume (P_{32}) increases. If fracture zones were very poorly connected, increasing P_{32} may increase K_{mb} by greater than a 1:1 ratio because increasing P_{32} also improves fracture zone connectivity (creating more flow paths) as well as fracture zone transmissivity.

From a directional perspective, the highest K values for both scales (outcrop and lineament) were encountered in N-S direction. This result is consistent with outcrop fracture data, which show a dominant N-S strike direction, parallel to the main trace of the Okanagan Valley Fault Zone (OVFZ). The results of this study also suggest that K_{mb}

values increase from the low density zone towards the high density zone (see Table 4.6). The higher P_{32} values in the medium and high density zones are mostly responsible for this increase because the lineament aperture and K_{eff} were the same for all three zones (see Table 4.2). These results suggest that the area can be divided into hydrostructural domains based on variations in K as suggested by previous authors (e.g. Surrette and Allen, 2008).

To evaluate whether lineament aperture may be greater near the OVFZ, well yields were examined throughout the region. Only one well in the low density zone (W3 at UPC) was available for comparison. In general, mean well yields of all wells in the medium zone (24 wells) are about half an order of magnitude higher than the yield in W3, and about one order of magnitude higher in the high density zone (189 wells). Thus, it is possible that lineament K values (K_{eff}) in the medium and high density zones were underestimated in this study (see Table 4.7). Future work could include inverse modeling for wells located in the medium and high density zones, thereby providing possibly better estimates of the lineament properties closer to the main fault.

The fact that well yields, and possibly lineament K, become higher closer to the main OVFZ Fault trace is not surprising. Gibson (HD), Simon Fraser University, (personal communication, 2010) indicated that greater fracture apertures nearest the surficial trace of the fault are a natural consequence of the decrease in confining pressure with the fault's proximity to the Earth's surface.

Specific storage values for all outcrop (or fractured matrix) scale models (Ss_m) in the low, medium and high density zones are about one order of magnitude lower than

those of the lineament (or mountain block) scale models (Ss_{mb}) within the same zones (see Tables 4.5 and 4.6). This is a direct consequence of the greater aperture value in the large scale model and consequent larger storage volume.

As mentioned earlier the K_p results from the pumping test analyses for W1 and W2 (see Chapter 3) were compared to the results of the DFN small scale model (for outcrop location 39) using different fracture apertures. An aperture of 50 μm was used in the DFN K_m simulations for all small scale outcrop fractures throughout the three density zones. As seen in Table 4.5, for the low density zone, the geometric mean values (K_m x,y,z) range from 7.0-9.5 x 10^{-8} m/s. Those values are very close to the K_p values of the pumping tests (K_p = roughly 1.1-1.2 x 10^{-7} m/s) in W1 and W2 of the same low density zone. This close agreement of these two estimates of K, as well as the similarity of the specific storage values, is encouraging in respect of comparing DFN results to observed pumping test data.

For the pumping test at W3, the drawdown curve was nearly linear on a log-log scale. As discussed earlier, this is related to linear flow due to the proximity of a large fracture. The pumping test data were analyzed using the Ramey and Gringarten method (Gringarten and Witherspoon, 1972), which gives a value for the aquifer surrounding the lineament; the resulting K_p value was 1.13 x 10^{-6} m/s (see Chapter 3). This value is slightly higher than the range of K_{mb}-xyz (7.3-8.8 x 10^{-8} m/s) for the low density zone. The proximity of W3 to the lineament may be the cause for the higher value from the pumping test, which itself may reflect localized enhanced fracturing. The overall similarity of K_p and K_{mb}, however, lend support to the proposed methodology.

One final point of discussion concerns the selection of only two scales for modeling. This two-scale approach ignores the presence of mid-scale fractures that are undoubtedly present. There are no distinct scales of fractures, but rather a continuum of fracture sizes. Whether these intermediate scale fractures are more numerous and better connected than the larger scale lineaments, and whether their effective K values are also high enough to influence the overall K is uncertain, but is an interesting avenue to pursue. However, given the consistency between K_m and K_{mb} at both scales in this study, it would seem reasonable that intermediate scale fractures would have similar values.

5. Modeling Coupled Surface Water – Groundwater Processes in a Small Mountainous Headwater Catchment

5.1. Introduction

Hydrological processes in mountains have been studied for many decades at a variety of scales. Most of these studies have focused on streamflow generation or hillslope-runoff processes (e.g., Kirkby, 1988; Tani, 1997; McGlynn et al., 2002; Nippgen et al., 2011), hydroclimatology (e.g., Whitfield and Spence, 2011) and the effects of vegetation on evapotranspiration (e.g., Bosch and Hewlett, 1982). In recent years, however, there has been growing focus on groundwater-related processes (e.g., Mau and Winter, 1997; Constantz, 1998; Freer et al., 2002; Wenninger et al., 2004; Tromp-van Meerveld et al., 2008; Tague and Grant, 2009; Lowry et al., 2010; Kosugi et al., 2011; Haught and Meerveld, 2011; Penna et al., 2011).

Discharge to streams in mountain regions may be through alluvial cover materials and/or through fractured bedrock (Tromp-van Meerveld et al., 2007). In this context, hydrological research has documented subsurface stormflow (SSSF) and groundwater discharge as baseflow as important contributors to streamflow in mountainous areas (e.g., Anderson et al., 1997; Montgomery et al., 1997; Wohl, 2000; Tsujimura et al., 2001; Freer et al., 2002; Wenninger et al., 2004). Water recharged within the mountain catchments that does not "re-surface" as discharge to mountain streams (or stream valley sediments), forms deep groundwater flow systems within the bedrock mountain (Forster

and Smith, 1988; Gleeson and Manning, 2008). This deep groundwater discharges to valley-bottom alluvial aquifers at the mountain front producing diffuse (through the bedrock massive) or focused (through fault zones) mountain block recharge (Wilson and Guan, 2004). Thus, there is a partitioning of groundwater recharge whereby a portion is diverted back to the stream network and a portion contributes to deep groundwater flow in the mountain block. Estimating this deep groundwater flux is part of this modeling study.

Quantifying recharge to the mountain block from headwater catchments in snowmelt dominated upland alpine zones is an important aspect of hydrologic studies, and modeling approaches involving coupling surface water (SW) processes and groundwater (GW) processes may provide a means for quantifying the various components of the water budget in mountainous areas. However, few have been conducted in arid and semi-arid regions, few have coupled surface water and groundwater processes in steep terrain, and most have considered only hydrologic processes in the thin soil layer above the bedrock surface (e.g., Merritt et al., 2006; Kuras et al., 2011; Kuras et al., 2012; Thyer et al., 2004; Sahoo et al., 2006; Whitaker et al., 2003; Schnorbus and Alila 2004). Thus, hydrologic science above the mountain front, incorporating a full view of the entire mountain block system, and not just the thin soil cover and its vegetation, is an area ripe for significant scientific advancement (Wilson and Guan, 2004).

One of the challenges in understanding and quantifying the relative contribution of groundwater to mountain streamflow and deep groundwater flow is estimating the bedrock permeability. The rate at which water recharges the bedrock and moves through

it depends on the bedrock permeability; however, few direct estimates of bedrock permeability are available, largely because there are few wells in these mountainous regions that can be tested hydraulically. As well, the permeability of fracture networks and its overall influence on the regional groundwater flow system are difficult to characterize. Modeling approaches involving coupling surface water (SW) processes and groundwater (GW) processes may provide a means for understanding groundwater processes and interactions between groundwater and surface water, and quantifying recharge and the various components of the water balance in mountainous areas.

In this study, a coupled surface water - groundwater model is developed for a small headwater catchment (Upper Penticton Creek 241 – UPC 241 catchment) in a mountainous, semi-arid region of British Columbia, Canada. The UPC 241 catchment (elevation 1,600 to 2,025 masl) is ideally suited to this type of study because the watershed has been studied as part of a paired watershed study (Winkler et al., 2005) and has been highly instrumented to this end. The code selected for this modeling study is MIKE SHE/MIKE 11, because groundwater and surface water processes can be simulated in a coupled manner. However, MIKE SHE modeling performance has rarely been tested in steep mountainous headwater catchments, simultaneously modeling streamflow, unsaturated soil water levels, and saturated deep bedrock groundwater dynamics within the mountain block. Therefore, one of the objectives of this study is to investigate the performance of MIKE SHE and MIKE 11 (DHI, 2007) for simulating coupled hydrological processes at the catchment scale. This will be accomplished by comparing time series for the various monitoring datasets and examining the partitioning of

groundwater recharge to both the stream network and deep groundwater flow. The modeling results will also be compared to the results of a previous modeling effort (Thyer et al., 2004; Kuras et al., 2011) using the surface water model DHSVM (Wigmosta et al., 1994) for the same catchment. More generally, the model performance will be compared to other recently published modeling studies using MIKE SHE (e.g., Hammersmark et al., 2008; Sultana and Coulibaly, 2010; Rahim et al., 2012; Sahoo et al., 2005). All of these studies, besides Sahoo et al. (2005), simulated watersheds that were relatively flat (i.e., with little change in elevation within the catchment) and demonstrated acceptable modeling performances concerning the components simulated.

5.2. The study area

The study area is the Upper Penticton Creek watershed (UPC 241), which is a headwater tributary catchment to the regional Penticton Creek 1st order watershed (Figure 5.1). It is located in the Okanagan Highland alpine zone approximately 26 km northeast of the City of Penticton, British Columbia (BC), Canada. UPC 241 is at a high elevation, right below the local mountain crest, which has an elevation of about 2,100 metres above sea level (masl).
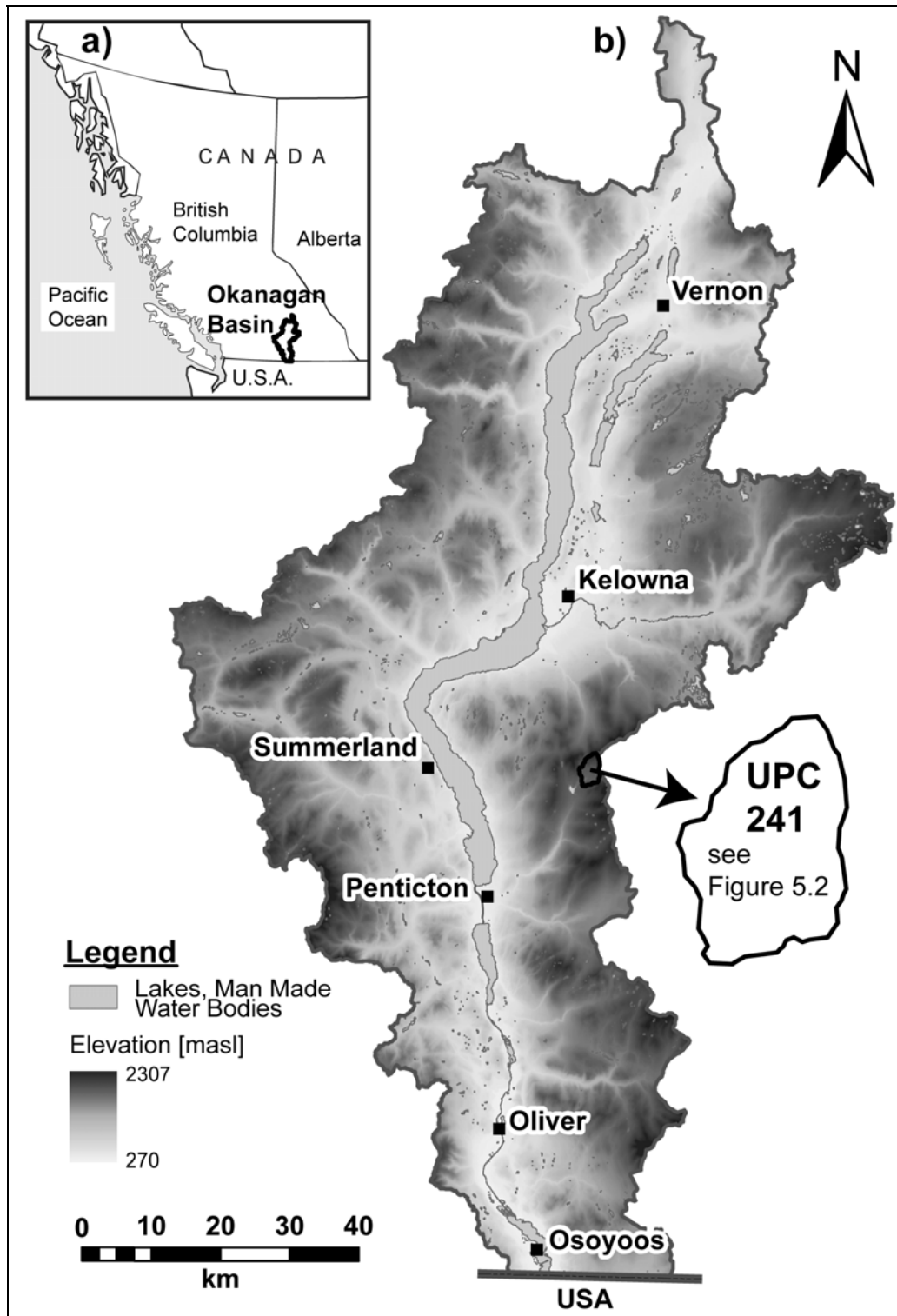
Figure 5.1. a) Okanagan Basin, British Columbia, Canada. b) Location map of the UPC 241 headwater catchment in Okanagan Basin.

The watershed is part of the Upper Penticton Creek (UPC) Watershed Experiment (Winkler et al., 2005), which was designed as a paired watershed study. Watershed scale measurements of hydrological and meteorological parameters have been conducted for pre- and post-treatment sampling periods in two logged (UPC 241, Dennis Creek) and one unlogged (UPC 240) control watershed. UPC 241, the focus of the current study, was logged in stages for comparison with the pristine adjacent watersheds. A total of about 20% of the watershed area had been clearcut logged at the time of reporting by Thyer et al. (2004). The most recent logging stage is at about 47%. This most recent (and final) treatment was done prior to the spring freshet of 2007 when the current study was initiated.

Thyer et al. (2004) undertook hydrologic modeling at the site using the distributed hydrological model (DHSVM - Distributed Hydrology Soil Vegetation Model) (Wigmosta et al., 1994) in order to simulate streamflow for the logged (UPC 241) and unlogged (UPC 240) catchments. Kuras et al. (2011) and Kuras et al. (2012) studied the effects of forest roads and harvesting on the hydrology of the snow-dominated headwater catchment UPC 241 also using DHSVM. Their work combined a process-based study with physically-based, distributed hydrological modeling to contribute to improving the current understanding of snow-dominated catchment hydrology, with an examination of the impacts of forest management on such systems. The studies specifically addressed the knowledge gap in forest hydrology regarding forest roads and harvesting in snowmelt-dominated regimes.

The 241 Creek catchment has a drainage area of about 4.7 km^2 and ranges in elevation from ~1,600 to 2,025 masl. It is plateau dominated, with 75% of the area having slopes less than 30%. The lower 1.5 km^2 of the watershed is relatively flat (<7% slope). The remaining upper area is substantially steeper and accounts for 45% of the catchment's relief (Kuras, 2006; Thyer et al., 2004). Figure 5.2 shows the topography of the headwater catchment including its stream network, the climate and stream gauge stations, as well as bedrock monitoring wells, shallow soil piezometers and snow measurement locations.
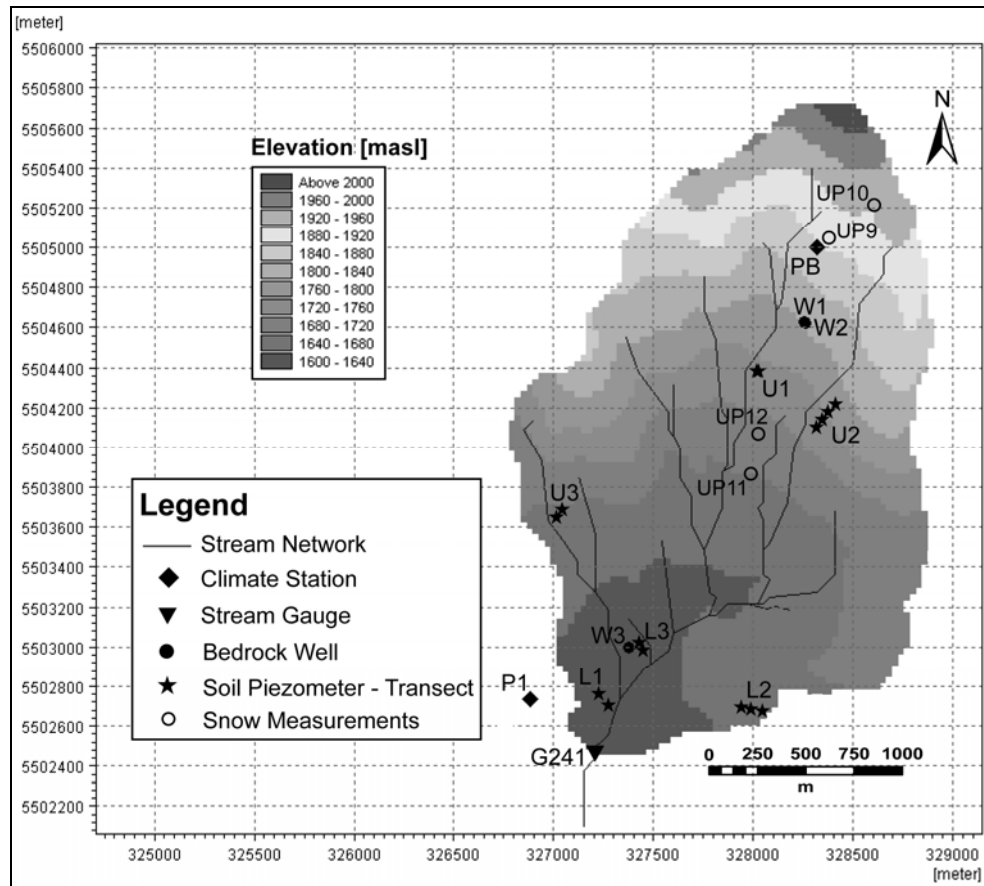
Figure 5.2. Upper Penticton Creek watershed showing elevation, the stream network, and the various monitoring sites (climate stations, stream gauging stations, bedrock monitoring wells, soil piezometers and snow measurement sites).

5.3. Methodology

5.3.1. The MIKE SHE / MIKE 11 modeling interface

MIKE SHE is a physically distributed modeling system developed by the Danish Hydraulic Institute (DHI) (DHI Software, 2007). The software is able to simulate all the major physical processes of the hydrologic cycle through six process-oriented components: evapotranspiration (ET), overland/channel flow, unsaturated and saturated subsurface flows, snow melt, and exchange between aquifers and rivers (Thomson et al., 2004; Sultana and Coulibaly, 2010). Within MIKE SHE, the model domain is discretized horizontally into an orthogonal network of grid squares (finite difference cells) to represent the spatial variability of catchment characteristics and input data. A number of horizontal layers with variable thicknesses are used to describe vertical variations in the soil and their respective hydrogeological characteristics within each grid square. Lateral flow between the grid squares is either as overland flow or subsurface flow within the saturated zone (Thomson et al., 2004; Sultana and Coulibaly, 2010).

Actual/potential evapotranspiration (PET) is estimated using the Kristensen and Jensen model (Kristensen and Jensen, 1975). Vertical unsaturated flow in the soil zone is modeled in this study using Richards' equation. The Richard's equation is solved numerically using the finite difference implicit approximation method (Gauss-Seidal iteration). The Boussinesq equation (Boussinesq, 1872) represents subsurface flow in the saturated zone. This equation is solved implicitly (iteratively) using a 3D-finite difference technique. The unsaturated zone (UZ) and saturated zone (SZ), however, are explicitly coupled. The coupling is limited to the entire unsaturated zone and the uppermost

calculation layer of the saturated zone. If the water table is below the bottom of the first SZ calculation layer, the UZ module treats the bottom of SZ calculation layer one as a free drainage boundary or a zero-flux boundary (Richard's equation).

MIKE SHE uses MIKE 11 to route channel flow. MIKE 11 has an integrated modular structure with various add-on modules, such as the hydrodynamic (HD) module, the advection-dispersion module, the sediment transport module, etc. The basis for most modules is the HD module, which can be applied for flood forecasting, simulation of flood control measures, channel system design, tidal and storm surge studies in rivers and estuaries, etc. The HD module comprises four components: the river network, river cross sections, boundary data and HD parameters (DHI, 2005). MIKE 11 includes the streams in the catchment and solves the one-dimensional St. Venant equation based on the complete dynamic wave formulation for simulating channel hydraulics (Thompson et al., 2004). The modified Gauss Seidel method is used for the numerical solution.

MIKE 11 can be dynamically coupled to the MIKE-SHE modeling system. The exchange of saturated zone flow and overland flow is calculated implicitly using the Darcy equation, continuously updating of the overland water depth. Dynamic coupling of MIKE-SHE and MIKE 11 is done through river links, which are line segments between adjacent MIKE SHE grid squares. In MIKE 11 water levels are calculated at H-points within the coupled reaches. During simulation these points are transferred to adjacent MIKE SHE river links. Then MIKE SHE calculates the overland flow to each river link from adjacent grid squares, as well as the river-aquifer exchange, which are later used as

lateral inflows or outflows to the corresponding MIKE 11 H-points for the next computational time step (DHI, 2007).

5.3.2. Model setup

Separate MIKE SHE / MIKE 11 models were developed for UPC 241. For this application, the MIKE SHE model components were set to simulate the two-dimensional (horizontal) overland flow, unsaturated flow using the Richards' equation, and saturated flow through a 3D finite difference method. The stream network was simulated using MIKE 11. MIKE SHE and MIKE 11 output time steps were set to one day (24 hours).

5.3.3. Model domain

The topographic information (Digital Elevation Model, DEM) of the watershed UPC 241 was obtained from a 1:20,000 digital map series developed by the Terrain Resource Information Management (TRIM) program for the province of BC (available from Base Mapping and Geomatic Services, Integrated Land Management Bureau, Ministry of Agriculture and Lands). The DEM resolution (and model cell discretization) is 30 m with a total of 5270 pixels (Figure 5.2). The watershed's topography is a key variable that defines the drainage surface for overland flow and for the uppermost surface of both unsaturated and saturated columns (Sahoo et al., 2005).

The horizontal extents of the model domain for the surface and subsurface components are the same – that is, at the edges of the model domain the boundaries extend vertically downward. The model domain was delineated by the 241 watershed

boundary derived from the DEM (Figure 5.2). The vertical extent of the model was 200 m based on the depth to which the bedrock is assumed to be highly permeable (see Section 5.3.7). A total of 20 layers were included in the model, vertically discretized into 5 m, 10 m and 20 m layer thicknesses as discussed later in Section 5.3.7.

5.3.4. Meteorological data

Meteorological data were available from the long term UPC watershed experiment database maintained by the BC Ministry of Forests and Range (BCMoFR EP956) and have been measured at the lower elevation P1 site (1620 m; Figure 5.2) in a large forest clearing since August 1997, as well as at an upper elevation PB clearcut site (1900 m; Figure 5.2) since September 1999. Three types of meteorological input data are available: precipitation, air temperature and short wave solar radiation. Each has been measured at both climate stations at hourly intervals. In addition, snow data from four stations (one forest location and one clearcut location, in each of an upper and mid elevation of the watershed - see Figure 5.2), were collected three times per month during late winter and spring snowmelt of 2004 and 2005 (Winkler et al., 2005).

To apply the meteorological data to the model, the model domain was divided into two parts (Figure 5.3), the upper part covered by the climate data derived from station PB and the lower part with climate data from station P1. The border between the climate zones was placed at roughly mid elevation within the watershed. In the upper zone, the topography is much steeper than in the lower zone. No precipitation gradient was applied to the site based on the similarity of precipitation records at the two climate stations as

discussed in Chapter 3. However, due to the temperature gradient with elevation, temperatures measured at the higher elevation site (PB) are, in general, slightly lower (by ~2°C). The highest temperatures (up to 30°C) were measured in the summer months of July and August. The lowest temperatures (approx. -28°C) were measured during the winter months from December to March when temperatures rarely rise above zero degrees Celsius. Figure 5.4 shows the hourly temperature variation over four years (2007 to 2010) for site P1. Therefore, the air temperature within each elevation/climate zone was corrected for elevation by including a temperature lapse rate of -0.24°C/100 m according to Thyer et al. (2004).
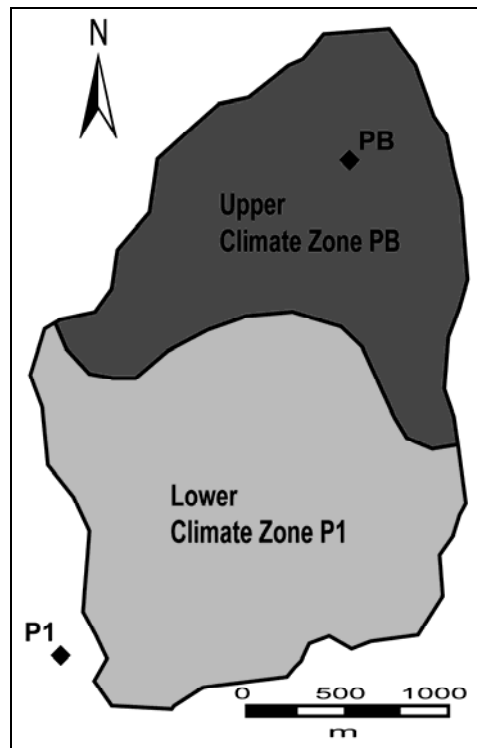
Figure 5.3. Upper and lower climate zones within the UPC 241 watershed. The upper zone uses the climate data measured at station PB and the lower one uses climate data measured at station P1.
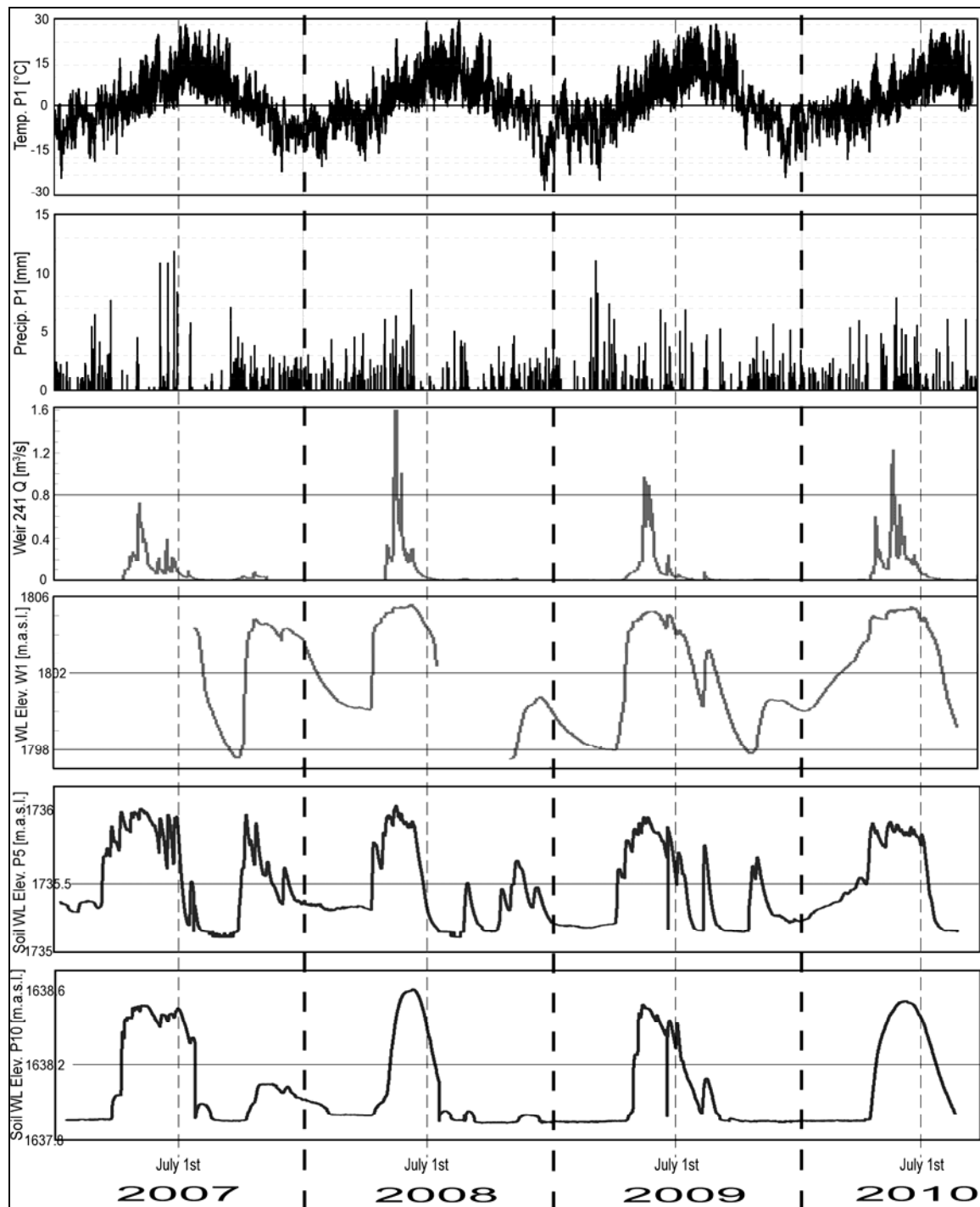
Figure 5.4. Time series data for hourly temperature and precipitation at site P1, discharge at the 241 weir, water level elevation in observation well W1, and soil water level in piezometers P5 and P10. The locations of all sites are shown in Figure 5.2.

Figure 5.4 also shows the precipitation data for the period 2007 to 2010 for site P1. The most intense precipitation events occur from April to the end of June. During the summer months of July and August, precipitation events decrease in number and intensity. In the fall (September to November), rain events increase again, but not as intensely as in spring. During the winter months (November to April) most of the precipitation falls as snow (due to temperatures below zero). The mean annual precipitation is 750 mm, approximately half of which falls as snow; a continuous snow cover usually lasts from late October to early June. April 1st snow water equivalent (SWE) averages about 265 mm and the late winter snowpack is normally 1 to 1.5 m (Kuras et al., 2011). As discussed later, the degree day method (DHI, 2007) was used to simulate snowmelt, and the snowmelt parameters were calibrated to reproduce the snow water equivalent during the first phase of model calibration (see Section 5.3.9.).

Short wave solar radiation is similar at both sites (data not shown). The highest values (~4000 $KJ/m^2/h$) are measured during the summer months and lowest values (~500 $KJ/m^2/h$) are measured during the winter months

Potential evapotranspiration (PET) is also needed as an input data time series file. PET was calculated using AWSET (Cranfield University, 2002) at daily time steps from the three meteorological data time series plus two additional time series data (hourly wind speed and humidity). AWSET uses the Penman-Monteith method for calculating PET (Allen et al., 1998). The maximum PET is ~6 mm/d during the summer months and the minimum PET is ~0.5 mm/d during the winter months (data not shown).

5.3.5. Land surface data

The catchment is located within dry Engelmann Spruce Subalpine Fir (ESSF) biogeoclimatic sub-zone. In the remaining unlogged 52% of the watershed, mature logdepole pine (*Pinus contorta* Dougl.) with small amounts of Englemann spruce (*Picea engelmanni* Parry) and sub-alpine fir (Abies *lasiocarpa*) are present (Figure 5.5). The trees at the study site are over 100 years old and reach maximum heights of 20-26 m. The canopy densities range from 35 to 50%. The understory is composed of lichens, mosses, and shrubs (<0.5 m in height) (Kuras et al., 2011).
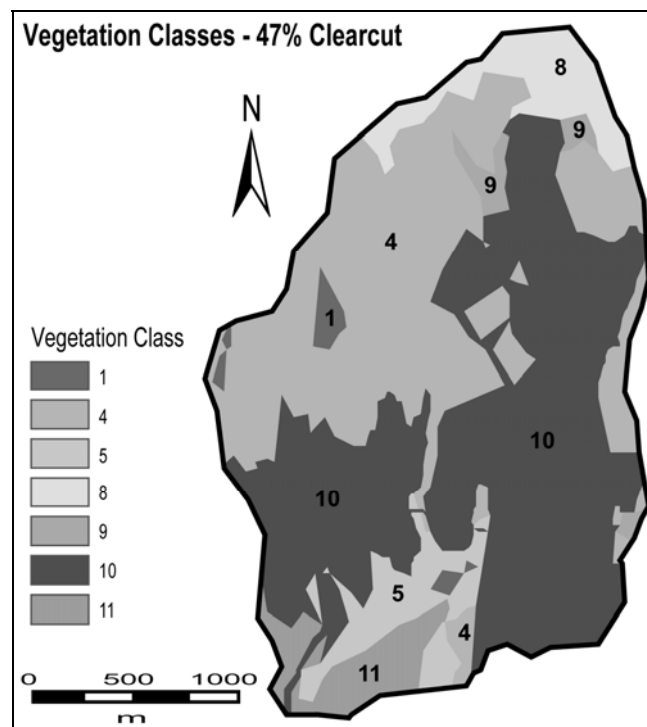
Figure 5.5. Vegetation classes at 47% logging stage. Parameters for each vegetation class are shown in Table 5.1.

Figure 5.5 shows seven different vegetation classes identified for the catchment (after Kuras et al., 2011). Vegetation class was mapped in ArcGIS and imported to MIKE

SHE. Each vegetation class is assigned a representative leaf area index (LAI) and rooting depth. Table 5.1 gives a description of the overstory, dominant height, LAI and rooting depth for each vegetation class. LAI and rooting depth values were not subject to calibration and were kept constant.

Table 5.1. Physical characteristics of vegetation classes (MIKE SHE input data) (data after Kuras et al., 2011).

Class	Overstory Description	Dominant Height [m]	LAI [m^2/m^2]	Rooting Depth [mm]
1	bedrock	N/A	N/A	50
4	Lodgepole pine	20	4.0	300
5	Lodgepole pine	25	4.0	300
8	Englemann spruce	23	2.4	300
9	Englemann spruce	26	3.8	300
10	clearcut	N/A	N/A	50
11	regenerated clearcut	0.6	0.5	50

LAI values for Lodgepole pines are higher than those for Engelmann spruces. No leaf area index exists for bedrock areas, and therefore, a value of zero was assigned. A very low value of 0.5 was assigned to regenerated clearcut areas. A rooting depth (RD) value of 300 mm was assigned to all the tree classes, whereas bedrock areas and regenerated clearcut areas have lower values of 50 mm.

The land surface data setting (vegetation dialogue) in MIKE SHE requires evapotranspiration parameters in order to calculate the actual evapotranspiration. The evapotranspiration parameters in this dialogue do not vary in time and are global for the model. These parameters are the canopy interception C_{int} [mm], the gravity flow and Richards' ET parameters C1, C2, C3 [mm/d], and the root mass distribution parameter Aroot [1/m]. The MIKE users' manual indicates that the interception process is modeled

as an interception storage, which must be filled before stem flow to the ground surface takes place. C_{int} defines the interception storage capacity of the vegetation per unit of LAI. A typical value is about 0.05 mm. The Kristensen and Jensen equations are used by MIKE SHE to calculate actual transpiration and soil evaporation. They contain three empirical coefficients, C1, C2, and C3. The coefficients C1 and C2 are used in the transpiration function. C3 is also part of that equation, but is the only variable found in the soil moisture function. A typical value for C1 is 0.3 mm/d, for C2 is 0.2 mm/d and for C3 is 20 mm/d. In the Kristensen and Jensen model, water extraction by the roots for transpiration varies over the growing season. In MIKE SHE, Aroot is the parameter responsible for how much water will be extracted with depth. The default value used in this study is 0.25 1/m. All the evapotranspiration parameters are not subject to calibration and the default values were used (DHI, 2007).

5.3.6. Unsaturated zone data

Soil classes and soil depths were determined from field mapping by Hope (2001) as shown in Figure 5.6. In general, soils are mostly coarse sandy loams and loamy sands ranging in depth from 0.1-4 m. They are derived from glacial tills and coarse-grained, granitic rock (Hope, 2001). The soils' clay content is low, whereas the content of coarse fragments is high. Each soil class always consists of an upper surface rooting depth soil layer (Layer 1) with a depth of 0.3 m and a lower subsurface soil layer (Layer 2) of varying depths.
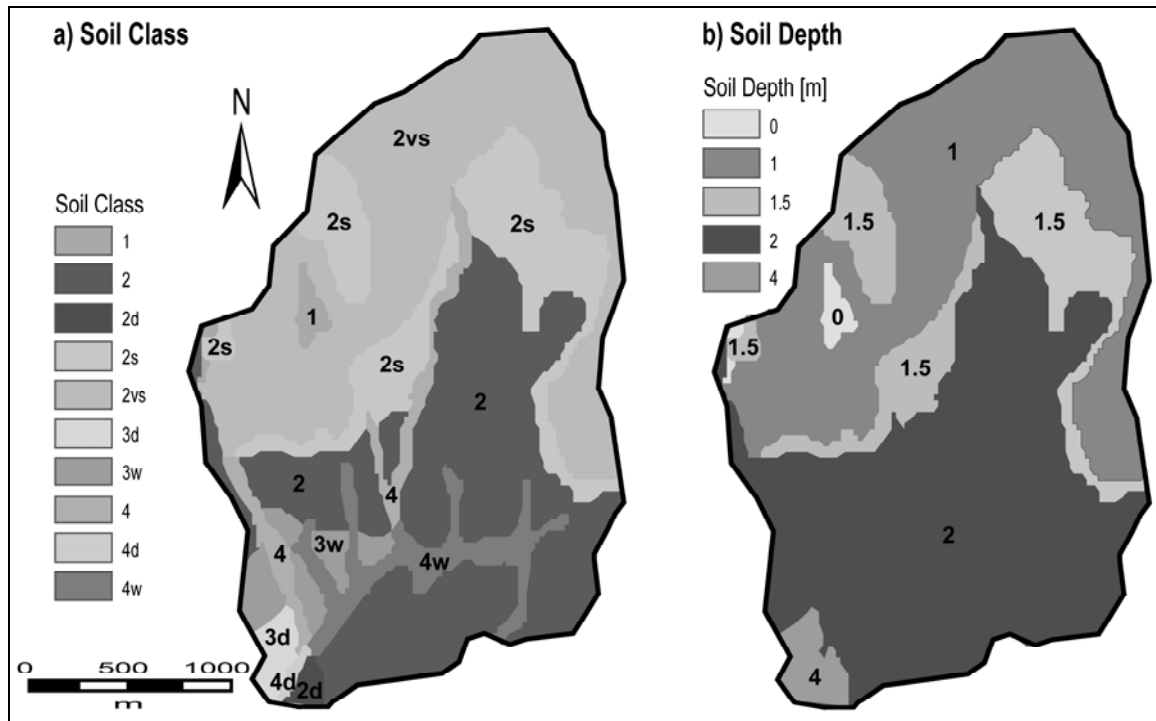
Figure 5.6. Maps showing (a) soil class and (b) soil depth in the UPC 241 catchment. Table 5.2 gives a description of each soil class.

The deepest soils of up to 4 m are found in the riparian zones at the lowest elevations of the watershed close to the stream outlet. At higher and steeper elevations in the hillslopes of watershed, the soils become thinner. Surface soil layers are in general coarse sandy loam, although areas with fine sandy loam or silty loam occur as well. Subsurface soils are generally loamy sand in texture and slightly compacted at depths below 0.6 m. The water holding capacity is low, which means that the soils are generally well drained. Parameter values for the van Genuchten model for unsaturated flow (saturated water content, residual water content, empirical constant alpha $[cm^{-1}]$ and empirical constant n) for the different soil texture classes of each layer were assigned according to van Genuchten (1996) and kept constant during calibration (Table 5.2). The

van Genuchten values for the fractured bedrock were taken from Smerdon et al. (2009). The vertical hydraulic conductivity Kz [m/s] of each soil class and layer was derived based on textural analyses using published empirical relationships (Rawls et al., 1993), but these values were adjusted during model calibration. Vertical hydraulic conductivities of Layer 1 are always slightly lower than those of Layer 2. Soil class 1 refers to those areas where in situ bedrock with no soil cover was encountered (Table 5.2). Porosity, and the van Genuchten parameters for bedrock, however, are highly uncertain and are based on different values for different soil types from van Genuchten (1996). Values for pF_{fc} (suction pressure of the soil when it is at field capacity) and pF_w (suction pressure of the soil when it is at the wilting point) were also taken from van Genuchten (1996). The same values of $pF_w = 4.2$ and $pF_{fc} = 2.0$ were assigned to all soil classes for both layers including the bedrock. The vertical saturated Kz used to represent the bedrock was the same as that used for the saturated zone as discussed below and was subject to calibration. The calibrated value is shown in Table 5.2.

Table 5.2. Soil parameters for each soil class and soil layer (data from Hope, 2001 and van Genuchten, 1996). The bulk density values were taken from Kuras (2006). Soil classes and depths are mapped in Figure 5.6.

Soil Class	Soil Layer	Depth [m]	Texture[1]	[2]Vertical saturated K_z [m/s]	Porosity	Saturated Water Content[3]	Residual Water Content[3]	Constant alpha[3] [cm^{-1}]	Constant[3] n	[4]Bulk Density [kg/m^3]
1	1	200	N/A (bedrock)	2.9×10^{-7}	0.10	0.1	0.05	0.0036	2.75	1200
2	1	0.3	SL	8.2×10^{-4}	0.32	0.41	0.065	0.075	1.89	1000
	2	2	LS/SL	1.5×10^{-3}	0.24	0.41	0.057	0.124	2.28	1450
2vs	1	0.3	cSL	1.1×10^{-3}	0.30	0.41	0.065	0.075	1.89	1100
	2	1	LS/SL	1.5×10^{-3}	0.23	0.41	0.057	0.124	2.28	1490
2s	1	0.3	SL	9.7×10^{-4}	0.32	0.41	0.065	0.075	1.89	1000
	2	1.5	LS/SL	1.9×10^{-3}	0.23	0.41	0.057	0.124	2.28	1500
2d	1	0.3	SL	8.2×10^{-4}	0.32	0.41	0.065	0.075	1.89	1000
	2	4	LS/SL	1.2×10^{-3}	0.24	0.41	0.057	0.124	2.28	1470
3w	1	0.3	SL	7.0×10^{-4}	0.33	0.41	0.065	0.075	1.89	970
	2	2	LS	1.5×10^{-3}	0.24	0.41	0.057	0.124	2.28	1450
3d	1	0.3	SL	8.8×10^{-4}	0.32	0.41	0.065	0.075	1.89	1000
	2	4	LS	1.5×10^{-3}	0.24	0.41	0.057	0.124	2.28	1450
4	1	0.3	SiL	8.8×10^{-4}	0.35	0.45	0.067	0.02	1.41	850
	2	2	SL/LS	6.3×10^{-4}	0.27	0.41	0.065	0.075	1.89	1280
4d	1	0.3	SiL	8.8×10^{-4}	0.35	0.45	0.067	0.02	1.41	850
	2	4	SL/LS	6.3×10^{-4}	0.27	0.41	0.065	0.075	1.89	1280
4w	1	0.3	SiL	8.8×10^{-4}	0.29	0.45	0.067	0.02	1.41	735
	2	2	SL/LS	7.7×10^{-4}	0.27	0.41	0.065	0.075	1.89	1280

[1] S: sand(y), Si: silt(y), L: loam, c: coarse; [2] Calculated using empirical relationships from Rawls et al. (1993); [3] values taken from van Genuchten (1996); [4] values taken from Kuras (2006)

Soil water levels have been measured with soil piezometers positioned along transects since the freshet of 2005 (see Figure 5.2 for piezometer transect locations). The soil water levels are shallow and reflect perched saturated flows above the bedrock for piezometers in higher and steeper elevation of the watershed (e.g., U2). The remaining piezometers, which are located in the lower and flatter riparian zones of the watershed close to the streams, are most likely connected to the saturated zone, where deep bedrock groundwater discharges to the streams and to the soils of the bordering riparian areas from smaller scale fractures and large scale lineaments. The actual deep water table that reflects the deep groundwater flow in the fractured bedrock in higher and steeper areas of the watershed seems to be connected with the riparian zones in the shallower areas of the watershed. However, previous modeling attempts (e.g., Kuras et al., 2011; Kuras et al., 2012; Thyer et al., 2004; Whitaker et al., 2003; Schnorbus and Alila 2004) using DHSVM (Wigmosta et al., 1994) could not test this hypothesis because the DHSVM code used for those studies included only a soil zone bounded below by an impermeable boundary and assumed a tight water balance. A tight water balance (Thyer et al., 2004) means that underlying bedrock is impermeable. This is a common assumption made in most hydrologic models when simulating catchments. That is, that the interaction between the soil zone and the fractured deep bedrock aquifer is not simulated. Findings from the current study strongly indicate this interaction, because the response time of the bedrock well W1 to precipitation lags minimally behind the responses of streamflow and soil piezometers to precipitation as seen in Figure 5.4. In addition, the large changes in water levels measured throughout the year in W1 and W2 indicate a strong connection between

the bedrock and the overlying soil zone. The use of MIKE SHE in this study, which is able to simultaneously simulate the unsaturated and saturated zone, might shed more light on this topic of a tight water balance.

Table 5.3 shows the details of all piezometer transects located in upper (U) and lower elevation (L) of the watershed.

Table 5.3. Soil piezometer details for each transect.

Transect	Well	Elevation [m]	Cover Type	Hillslope Position	Depth [cm]
U1	P6	1740	clearcut edge	hillslope	55
	P5	1736	clearcut edge	riparian	119.5
U2	P1	1740	clearcut	hillslope	70.5
	P3	1728	clearcut	hillslope	91.5
	P2	1721	clearcut	hillslope/riparian	69.5
	P4	1716	clearcut	riparian	105
U3	P15	1697	forest	hillslope	69
	P14	1678	forest	hillslope/riparian	89
L1	P7	1595	clearcut	lower depression	77
	P8	1590	young regen	riparian	80
L2	P9	1644	forest	hillslope	76.5
	P10	1638	forest	hillslope	70
	P11	1635	forest	hillslope	94
L3	P13	1628	clearcut	hillslope/riparian	97
	P12	1619	clearcut edge	riperian	95

Piezometer transects were situated strategically throughout the watershed in order to give an overall representation of perched soil water fluctuations. Transects were positioned to follow the downslope routing of flows along hillslopes (approximated by

surface topography). In the design of the transects, it was important that no topographic disconnections (rises or depressions) exist between the piezometers. The change in elevation between each piezometer along a transect was large to prevent overlap, ranging from about 3-6 m. Piezometers were drilled using a hand auger to a depth beyond that of the pre-melt season perched water table. To reduce the influence of local stream stages on subsurface soil water levels, the bottoms of piezometers located in riparian zones were set approximately 15 cm above the water surface (at full bank stage) of proximal streams. All piezometers are completed in the lower, compacted soil layer L2. The installation of the piezometer transects was done during summer low flow season to assure that the depths of the piezometers was sufficient to capture perched water level fluctuations throughout the monitoring period.

Odyssey capacitance water level probes were installed in each piezometer; soil water levels are continuously monitored every 30 minutes. Figure 5.4 shows the soil water level fluctuations measured in two piezometers (P5, P10) over the period 2007 to 2010 in comparison with climate data, streamflow data and deep bedrock water table fluctuations from well W1 for the same period.

Figure 5.7 shows how the unsaturated zone is represented in MIKE SHE. As discussed above, the actual water table lies within the bedrock at some depth below the soil zone in the higher and steeper areas of the catchment, where the bedrock groundwater table can be very deep and the soils are very shallow and mostly dry. Surface water infiltrates either directly into the fractures in the bedrock or runs off as overland flow across the steep hillslopes. As noted above, in the lower, flatter riparian areas of the

watersheds, the actual water table lies within the soil zone, where groundwater discharges from the deep bedrock below into the soils and streams. The initial model setup assigned soils only to the unsaturated zone and the bedrock to the saturated zone; however, an error message occurred during simulation indicating that the water table was below the depth of the unsaturated zone in the higher and steeper areas of the catchment. To overcome this problem, bedrock was also assigned to the unsaturated zone to a depth of 200 m, the same depth as for saturated zone domain to (Figure 5.7). Thus, the unsaturated zone had three layers representing layers 1 and 2 of the soil (L1 and L2, respectively), and the bedrock. The thickness of L1 was set to 0.3 m, and the thickness of layer 2 was variable as indicated in Table 5.2.
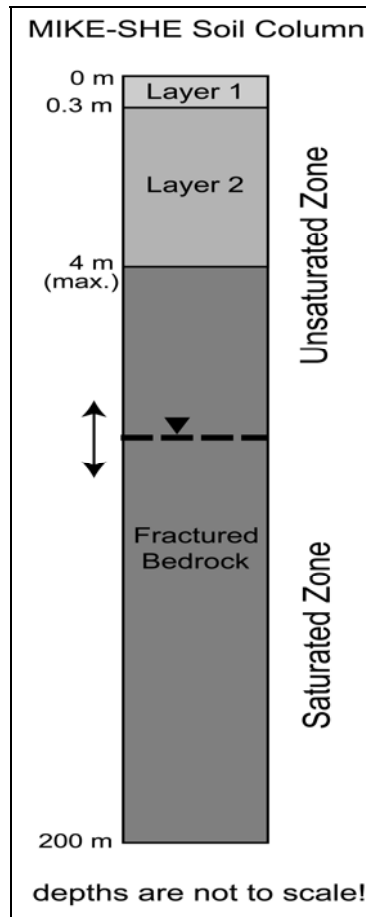
Figure 5.7. Example of the MIKE SHE soil column setting for this study.

5.3.7. Saturated zone data

The saturated zone of the model is based on a conceptual model of a fractured bedrock aquifer. In the study area, the bedrock is crystalline, consisting of mostly fractured granite and gneiss. In Chapter 4, a discrete fracture network modeling approach was used to estimate the regional scale bedrock permeability using a combination of outcrop scale and lineament scale fracture data collected in this study area. The estimates of K were assumed to represent the top 200-300 m of the bedrock for a network of fractures that is open and conductive. The K values were found to be relatively consistent

regardless of scale (ranging from $\sim 10^{-8}$ to 10^{-7} m/s) and generally agree with other published estimates of K for fractured crystalline rock (Gleeson et al., 2011).

Given the estimated depth considered to be an active groundwater flow zone, the vertical depth of the model was set to 200 m, with a vertical discretization of 5 m assigned to the upper ten layers, followed by five 10 m layers and five 20 m layers. This lower boundary was assigned as a no flow (zero flux) boundary. Thus, groundwater cannot leave the model via the bottom. However, to allow for some component of the deep groundwater flow to exit the catchment (i.e., not contribute to streamflow within the catchment), water was permitted to leave the model domain along the southern lateral edge (Figure 5.2) in lieu of through the base of the model. .These southern edge model boundaries were assigned specified flux (non-zero) values. Of course, this flux value is not known, but if the groundwater system is to be calibrated along with the surface water system, then presumably there will be some constraint on the value of this exiting flux. The initial flux estimate across each 5 m layer was -5 x 10^{-3} m/s (negative to indicate outflow), but the flux was adjusted during calibration. To allow for the same outward flux across the thicker layers, this 5 m flux value was multiplied by 2 for the 10 m layers and multiplied by 4 for the 20 m layers. If the outward flux is set too low, then the water levels in the bedrock may be too high or the streamflow too high, whereas if the outward flux is too high, then there will be insufficient streamflow and lower than observed groundwater levels. The problem is highly non-unique, however, as will be discussed later. This flux was also considered to be invariant with time, but in reality the flux would likely be greater during the snowmelt period. Finally, the northern, eastern and western

boundaries were assigned no flow boundaries. The upper boundary of the saturated zone is a flux boundary as well, as represented by the recharge from the unsaturated zone. This flux varies in time and is computed at the interface of the unsaturated and saturated zones.

Initial hydraulic conductivities for the bedrock of 10^{-7} m/s were assigned (see Chapter 4). The aquifer type was set to strictly confined, and an initial specific storage value of as 10^{-4} was assigned (see Chapter 4). Both parameters were subject to calibration. Figure 5.8 shows a conceptual three dimensional model of the headwater catchment, including the main components: boundary conditions, discretization, unsaturated zone, saturated zone, etc..

Groundwater levels were monitored in three deep monitoring wells (W1, W2 and W3; see Figure 5.2). All wells are completed in the bedrock and cased through the surficial sediments. W1 and W2 are within 3 m of each other at high elevation in the catchment (W1 is 50 m deep and W2 is 30 m deep), and W3 (30 m deep) is situated at low elevation. Figure 5.4 shows the groundwater level variation in W1 (the response for W2 is nearly identical). W3 is a flowing artesian well and the water level rises above the top of the casing during the freshet period.
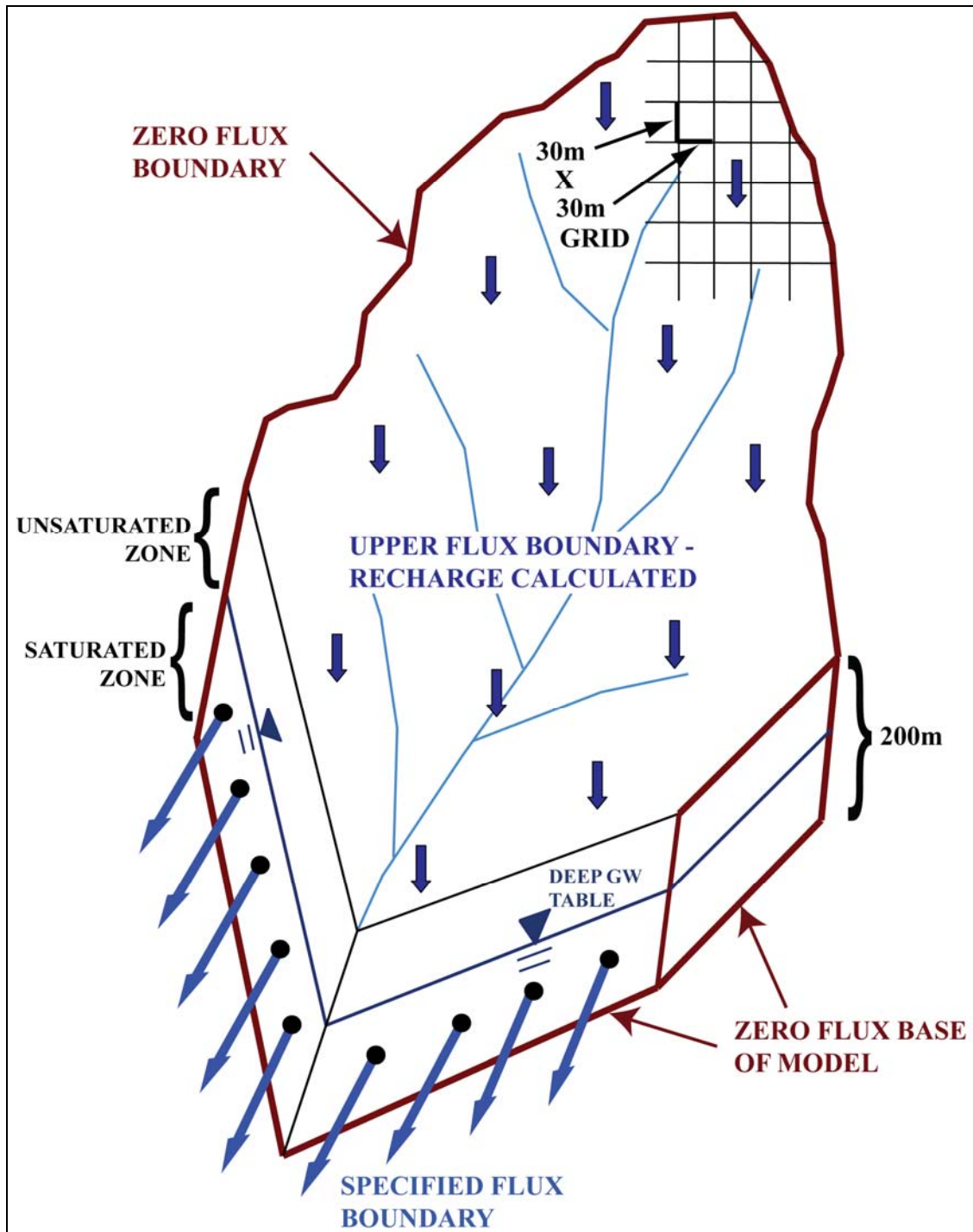
Figure 5.8. Conceptual model of the UPC241 catchment, showing boundary conditions, horizontal discretization, vertical domain depth and other important information such as the unsaturated and saturated zone.

5.3.8. MIKE 11 stream network and streamflow data

The stream network for the watershed was originally derived by a DEM analysis with the ArcGIS Hydrology tool, which was modified using a GPS field survey to capture details of the stream network (Kuras, 2006). Figure 5.2 (shown previously) shows the stream network. At the outlet of the watershed, the Water Survey of Canada (WSC) installed and maintains a hydrometric station (08NM241 – renamed to G241 in this study). Hydrometric data have been measured since 1983, with data taken roughly bi-monthly throughout the flow seasons of the simulation years. Stream stage is recorded hourly in real time. Stream discharge [m^3/s] was calculated using an existing rating curve. Daily stream discharge data (m^3/s) for the period 2007 to 2010 are shown in Figure 5.4 along with precipitation, air temperature, soil water elevation at two piezometers (P5 and P10), and groundwater fluctuation of one bedrock monitoring well W1. Snowmelt dominates the annual hydrograph and the freshet peak typically occurs in late spring with 170-630 mm of water flowing from the watershed annually. The WSC considers streamflow measurement accuracy to be about 10% (steam flow error estimate).

As input data for the MIKE 11 stream network component and part of the hydrodynamic model settings in MIKE 11, boundary conditions were assigned to each end of all the streams. Closed boundaries were set to all the upstream ends of each branch, whereas a water level boundary was assigned to the downstream end at the main outlet of the watershed where the stream gauge is located. This water level boundary was assigned a time series of water level (stage). The hydrodynamic model settings in MIKE 11 also require a global value of Mannings' n for the stream bed resistance. An initial

value of 0.032 m$^{1/3}$/s (Soultana and Coulibaly, 2010), was assigned. This value was subject to calibration and adjusted later. Additional input parameters for MIKE 11 included the leakage coefficient, which governs river-aquifer exchange. An initial value of 1 x 10^{-5} m/s (Thompson et al., 2004) was assigned and later adjusted during calibration. River cross sections had to be assigned along each stream. Those data derive from the stream survey undertaken by Kuras (2006).

5.3.9. Model calibration and validation

For calibration, including the so called warm up period, the simulation time of the coupled MIKE SHE/MIKE 11 model was set to run for about 14 years, starting on August 1st 1994 until September 30th 2008. Even though climate data only exist for both stations from August 1997, three more years of real data were added to the beginning to allow for the model to start in 1994; the data series from 1997 to 2000 was used. Thus, the first three years of the simulation used a repeated data sequence. This was necessary, because the deep bedrock aquifer response needed about 10 years before a stable condition was reached (Figure 5.9). During this warm up period of about 10 years (1994 to 2004) the saturated zone water level dropped down continuously, since the initial water table elevation of the saturated zone was set to zero metres, meaning the model is completely filled with water from the ground surface, when starting a simulation. From the year 2004 onward, the aquifer response appeared to reach a stable state (no longer consistently declining). Thus, the calibration period extended from 2005-2008. Because snow data were only available for 2004-2005, this period was used for calibrating snowmelt. Data of

just one snow season (2004/2005) for calibration is very short, but that was all the data

available. The validation period for the model included the years 2009 to 2010.
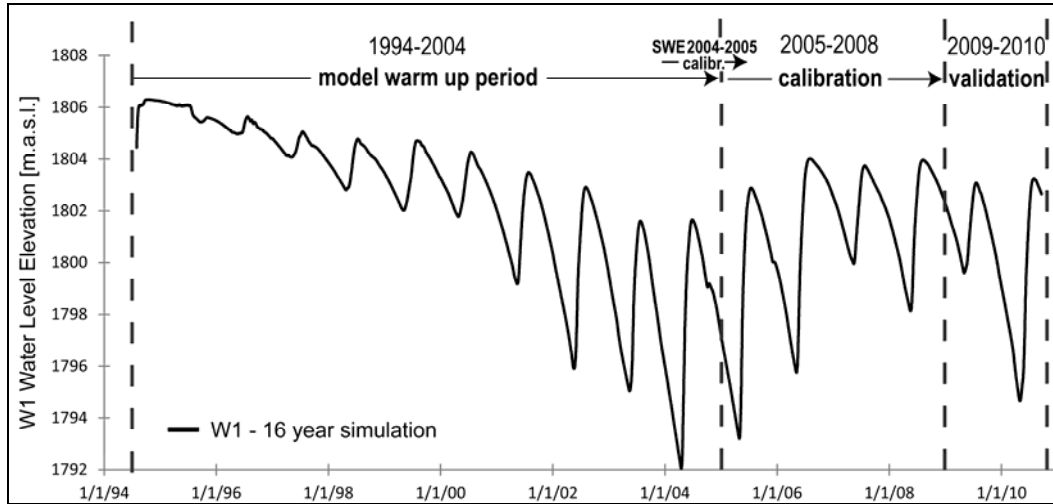
Figure 5.9. Deep bedrock aquifer response of W1 for a 16 year simulation, showing the identified model warm up period and the years used for calibration and validation.

The water years 2004 to 2008 (i.e. October 1st 2003 to September 30th 2008) were

used for model calibration, which was done in two main steps. First the model was

calibrated against the measured snow water equivalents (SWE) for each of a forest and

clearcut location (UP12, UP11) at mid elevation, and for each of a forested and clearcut

location (UP9, UP10) in an upper elevation area of the catchment (see Figure 5.2). In

general, the model needs to be capable of first simulating a reasonable snow distribution

of the water year, before streamflow and other responses can be calibrated.

Systematically, each of the snowmelt parameters (degree-day coefficient, the radiation

melting coefficient and the minimum snow storage) were changed separately in order to

match the observed graphs of snow accumulation and melt with the simulated ones for the

water years 2004 and 2005 for which snow data are available (i.e. October 1st 2003 to

September 30th 2005) (Figures 5.10 to 5.13). It is important to mention that the snowmelt

parameters also affect the shape and timing of the streamflow hydrograph, since melting

snow mostly generates the streamflow during the high flow season. During this snowmelt

calibration step, the simulated streamflow hydrograph time series from 2004 onward were

also evaluated in order to identify possible parameter combinations that generated a

reasonable streamflow response. After about 45 simulation runs, a reasonable

combination was found. This combination of snowmelt parameters was kept fixed for all

further calibration runs. Table 5.4 shows the initial snowmelt calibration parameters

based on the literature and the final calibrated values. The degree-day coefficient

[mm/°C/d] describes the amount of snow that melts per day for every degree the air

temperature is above the threshold temperature (which is normally zero). It is a time

varying coefficient, because the rate of melting varies as the snow pack changes over the

winter. It is often used as a calibration parameter to calibrate the volume of snowmelt to

observed runoff (DHI, 2007). In this study, the degree-day coefficient had hardly any

effect on the shape of the SWE curves and the streamflow hydrographs, but it changed the

volumes of snow water equivalent and the discharge peaks in the stream. In comparison,

the radiation melting coefficient [mm/KJ/m^2] is responsible for shifting the SWE graph

and the streamflow graph in time. In principle, this coefficient is a time varying parameter

that varies as the snow darkens with age. This coefficient had hardly any effect on the

snowmelt peaks simulated in this study. Thus, the degree day coefficient is the primary

calibration parameter for calibrating runoff (DHI, 2007). Three additional snowmelt

parameters, the maximum, wet snow fraction, initial total snow storage, and the initial total wet snow fraction were not included in the calibration process and set to zero and kept constant. This is justifiable, because the start time of the model for calibration was August 1994, when no precipitation in the form of snow was present. Measured and simulated graphs of SWE can be seen in the Results Section 5.4.1.

The second step of the calibration, which was non-trivial, was to adjust the overland flow (Manning number and detention storage) and MIKE 11 channel flow parameters (Manning number for streamflow and leakage coefficient for stream-aquifer exchange) in tandem with the hydraulic conductivities of the unsaturated and saturated zones, the groundwater flux exiting the domain, and the specific storage of the bedrock aquifer. Calibration of the model to observed streamflow, soil water elevation, and bedrock groundwater elevation for the water years 2005 to 2008 (i.e. October 1st 2004 to September 30th 2008) required simultaneous adjustment of each parameter in MIKE SHE and MIKE 11. Modifications of a calibration parameter in one model can influence results in the other (Sultana and Coulibaly, 2010). The Manning number for overland and streamflow [$m^{1/3}$/s] is a coefficient describing the roughness of a surface and a stream, respectively. A higher value of Manning's n for overland flow decreases the total amount of water flowing as surface runoff and results in higher streamflow peaks. The value of Manning's n for streams/channels is typically in the range of 0.01 (smooth channels) to 0.10 (thickly vegetated channels). Detention storage [mm] is used to limit the amount of water that can flow over the ground surface. The depth of ponded water must exceed the detention storage before water will flow as sheet flow to the adjacent cell. If detention

storage is low, more water can flow over the surface resulting in higher streamflow peaks. The leakage coefficient for stream-aquifer exchange [m/s] defines a loss of water from the river to the groundwater (DHI, 2007). Peak flows of the hydrograph were calibrated by adjusting the detention storage and Manning's n for both overland and channel flow. The degree day coefficient snowmelt parameter also affects the peak flow, but this parameter was not changed further during the second step of the calibration, since it was already adjusted during the first step of the SWE calibration with good results for the streamflow peaks.

Initial values of all these parameters were either taken from the literature (Sultana and Coulibaly, 2010; Hammersmark et al., 2010; Thompson et al., 2004) or the default values in MIKE SHE were used. The initial calibration values for the saturated K values of the bedrock and the specific storage were from the DFN modeling result for the mountain block of the low density zone (see Chapter 4). All values were adjusted during calibration. In total, some 300 simulation runs were completed. Parameters were adjusted one by one and comparisons made for each of stream discharge measured at G241, soil water level at P5 and P10, and groundwater level in W1. The overall shape of the response at each monitoring site, as well as the model fit, was recorded. The final results are shown in Table 5.4.

Table 5.4. Initial and final calibration parameter values of the coupled MIKE-SHE MIKE 11 flow model. Ranges are reported for soil K_z as there is more than one soil type in each layer.

Model	Parameter	Initial calibration value	Final calibration value
MIKE-SHE	*Snowmelt parameters:*		
	Degree day coefficient [mm/°C/d]	5	3
	Radiation melt. coeff. [mm/KJ/m^2]	0 (default)	5.0×10^{-7}
	Minimum snow storage [mm]	5.5	5
	Overland flow parameters:		
	Manning's n [m$^{1/3}$/s]	0.07	0.02
	Detention storage [mm]	2	1
	Unsaturated soil zone K_z (vertical):		
	K_z Layer 1 [m/s]	5.8×10^{-4} -1.1×10^{-3}	5.8×10^{-8} -1.1×10^{-7}
	K_z Layer 2 [m/s]	6.3×10^{-4} -1.9×10^{-3}	6.3×10^{-5} -1.9×10^{-4}
	Saturated bedrock K's and storage:		
	$K_x=K_y$ (horizontal) [m/s]	8.1×10^{-8}	3.8×10^{-7}
	K_z (vertical) [m/s]	7.3×10^{-8}	2.9×10^{-7}
	Specific storage [m^{-1}]	3.2×10^{-3}	1.0×10^{-5}
	Outflux from saturated zone [m/s]	-5×10^{-3}	-5.0×10^{-5}
MIKE 11	Manning's n for channel flow [m$^{1/3}$/s]	0.03	0.05
	Leakage coeff. (river-aquifer) [m/s]	1.0×10^{-5}	1.0×10^{-5}

5.4. Results

5.4.1. Model calibration and validation

5.4.1.1. Snowmelt

Figures 5.10 to 5.13 show the snow measurements (as SWE) at the four sites (grey triangles), together with the simulated graphs for the snowmelt calibration period. Table 5.5 gives the modeling performance results for the calibration period of the snow seasons 2004 and 2005.
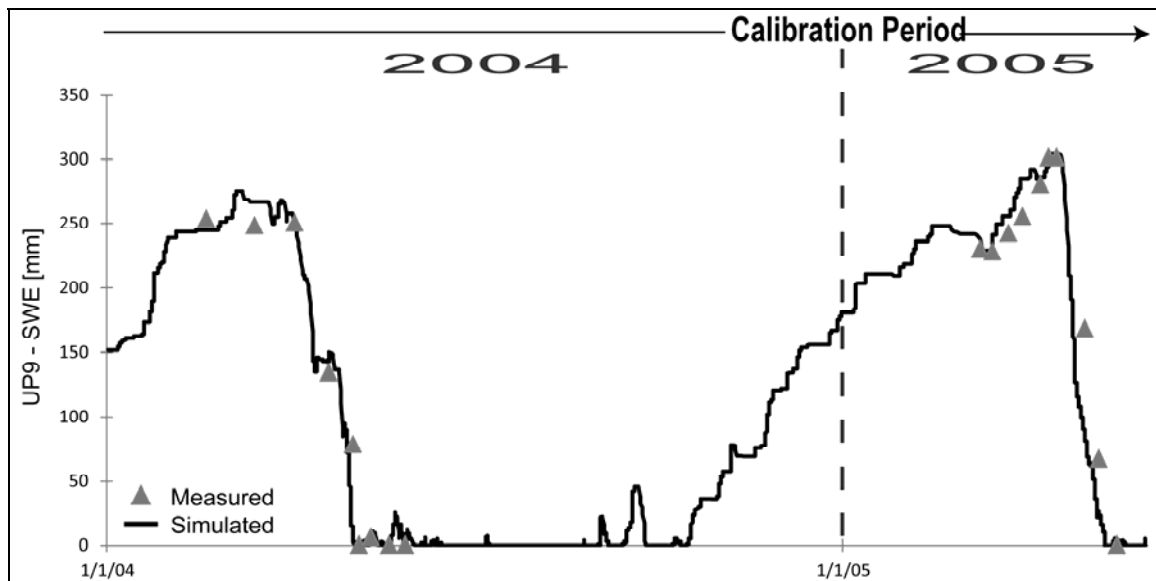
Figure 5.10. Measured and simulated SWE graphs at site P9 in an upper elevation clearcut area of the watershed.
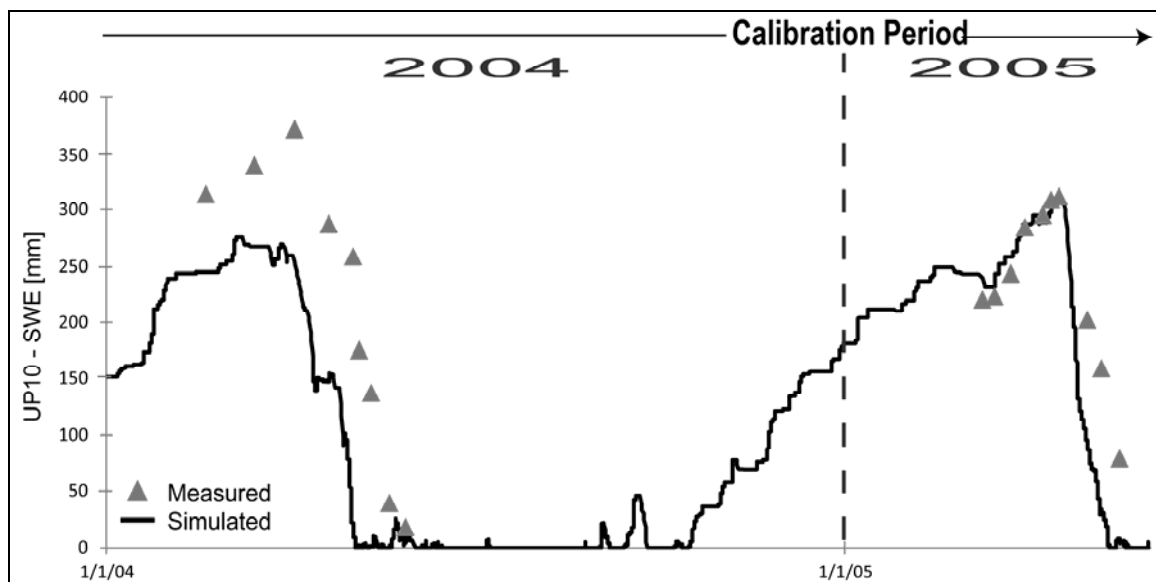
Figure 5.11. Measured and simulated SWE graphs at site UP10 in an upper elevation forested area of the watershed.
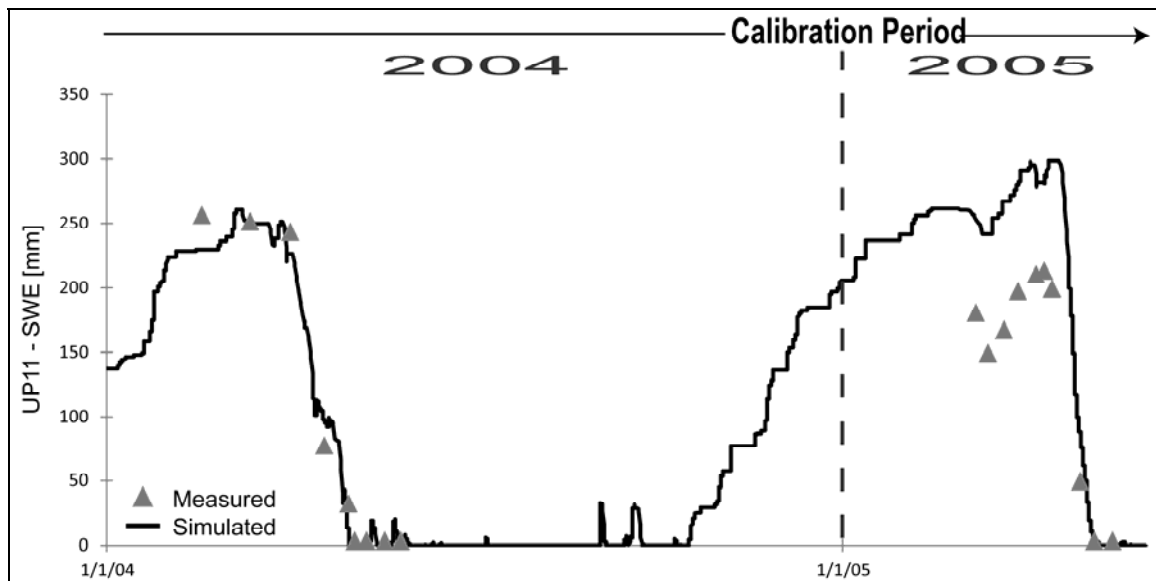
Figure 5.12. Measured and simulated SWE graphs at site UP11 in a mid-elevation clearcut area of the watershed.
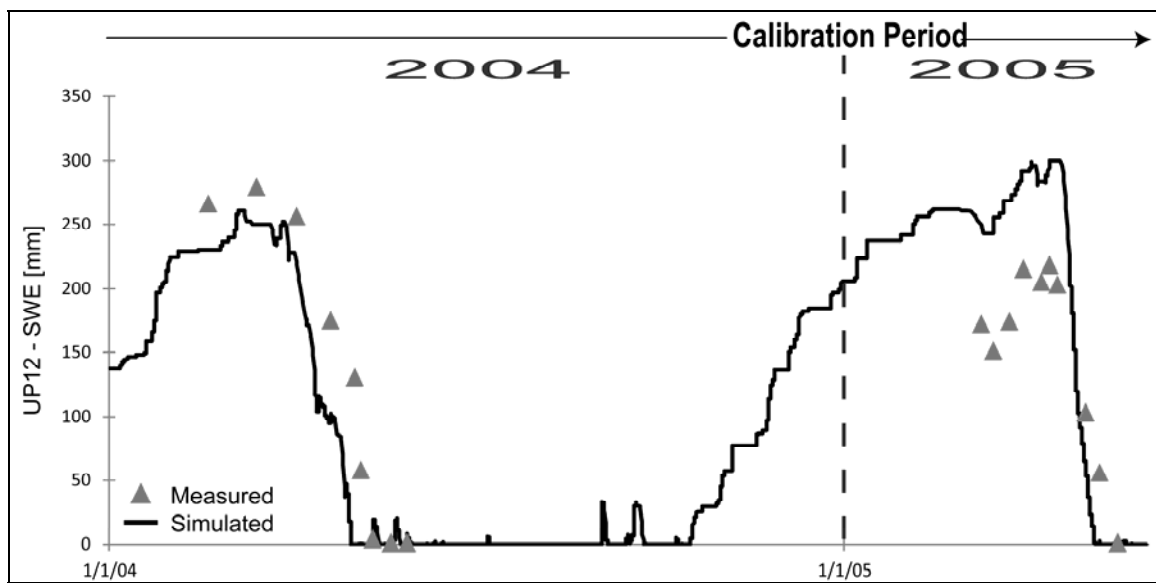
Figure 5.13. Measured and simulated SWE graphs at site UP12 in a mid-elevation forested area of the watershed

The calibration results are better for the clearcut sites, with an R (correlation) value of 0.98 achieved at site UP9 at upper elevation (Figure 5.10). An R value of 0.95 was achieved at the clearcut site UP11 at mid elevation (Figure 5.11). At the forested locations, R (correlation) values are in general a little lower than those from the clearcut sites, with an R value of 0.82 at UP10 at high elevation (Figure 5.12) and 0.86 at UP12 at mid elevation (Figure 5.13). In general, R correlation results are good, with values between 82% to 98%. The correlation coefficient (R) is a measure of the linear dependency between simulated and measured values. The closer the value is to 1.0, the better the match (DHI, 2007). Also shown in Table 5.5 is the Nash Sutcliffe (R^2) correlation coefficient, which is commonly used for model performance analysis in hydrology. The Nash-Sutcliffe R^2 value will also be 1.0 if there is a perfect match between simulated and observed data. Comparison of data is related to both volume and shape (Nash and Sutcliffe, 1970). For comparison, Sultana and Coulibaly (2010) obtained R correlation values for SWE between 50% and 81% for a MIKE SHE modeling study in southern Ontario.

Table 5.5. Model performance statistics for the SWE calibration period of 2004-2005 at the four snow measurement locations.

Snow Stations	R (correlation)	Nash-Sutcliffe
UP9	0.98	0.96
UP10	0.82	0.12
UP11	0.95	0.68
UP12	0.86	0.49

5.4.1.2. Streamflow

Figure 5.14 shows the results for the measured (grey) and the simulated (black) streamflow at the outlet G241 for the calibration period of 2005 to 2008. Simulated discharge values during the snowmelt high flow seasons are, in general, lower than the measured ones, meaning that less volume of water is routed out of the watershed through the main river than is observed. The simulated years 2006 and 2008 seem to reproduce the shape of the hydrograph better than the years 2005 and 2007.

For the first and main peak flow response of 2005, its rising limb is well simulated, but the following recession limb is poorly simulated. Two additional peaks during the recession from the main peak could not be simulated at all and flow almost declines to baseflow level. The timing of the following three peaks, which occur in late June, were adequately simulated, but had much less discharge than measured. In late Fall of 2005, during the baseflow period, the simulated hydrograph shows a response that was not measured.

For the following flow season of 2006, the timing of the three small peaks before the main rising limb of the peak flow were simulated well, but simulated discharge was lower than observed. The simulated main peak flow is shifted by a few days (a delayed response) and discharge is lower than observed. During the recession, smaller peaks in the measured hydrograph were poorly simulated. Similar to 2005, during the late fall/early winter baseflow period, responses were simulated, but were not actually measured.

For the year 2007, the main simulated peak flow response also occurs later in time and with less discharge. Smaller responses within the rising limb are poorly simulated. The simulated hydrograph also shows two early peaks, which were not measured. Similar to 2005, three peaks occurring in late June of the snowmelt season hardly rise above baseflow level in the simulated hydrograph and do not show the three separated peaks, but the timing is reasonable. Responses during the baseflow period of late fall/early winter are very well simulated in comparison to the two years before.

The simulated year 2008 also shows one early response event, which was not measured. Responses during the rise and recession of the main peak flow were simulated with reasonable timing, but similar to all other calibration years, the discharge was too low. The discharge and timing of the main peak itself was well simulated for this calibration year. Late fall/early winter baseflow responses were simulated but not measured.

In general, it seems that simulated discharge during baseflow seasons of the calibration years 2006-2008 are always high relative to measured discharge, whereas the simulated discharge during the spring snowmelt periods of all years are always lower than observed. This corresponds to a smaller volume of water being transported out of the watershed during the snowmelt peak flow seasons and more during baseflow periods in the simulation. A possible reason for this mismatch in discharge could relate to the presence of logging roads, which exist throughout the watershed, but which cannot be represented in the MIKE SHE/MIKE 11 model. The MIKE SHE code is not able to simulate the routing of water through a road ditch and culvert system of logging roads in

a watershed. More details on the influence of the logging roads on the streamflow hydrograph will be discussed later.
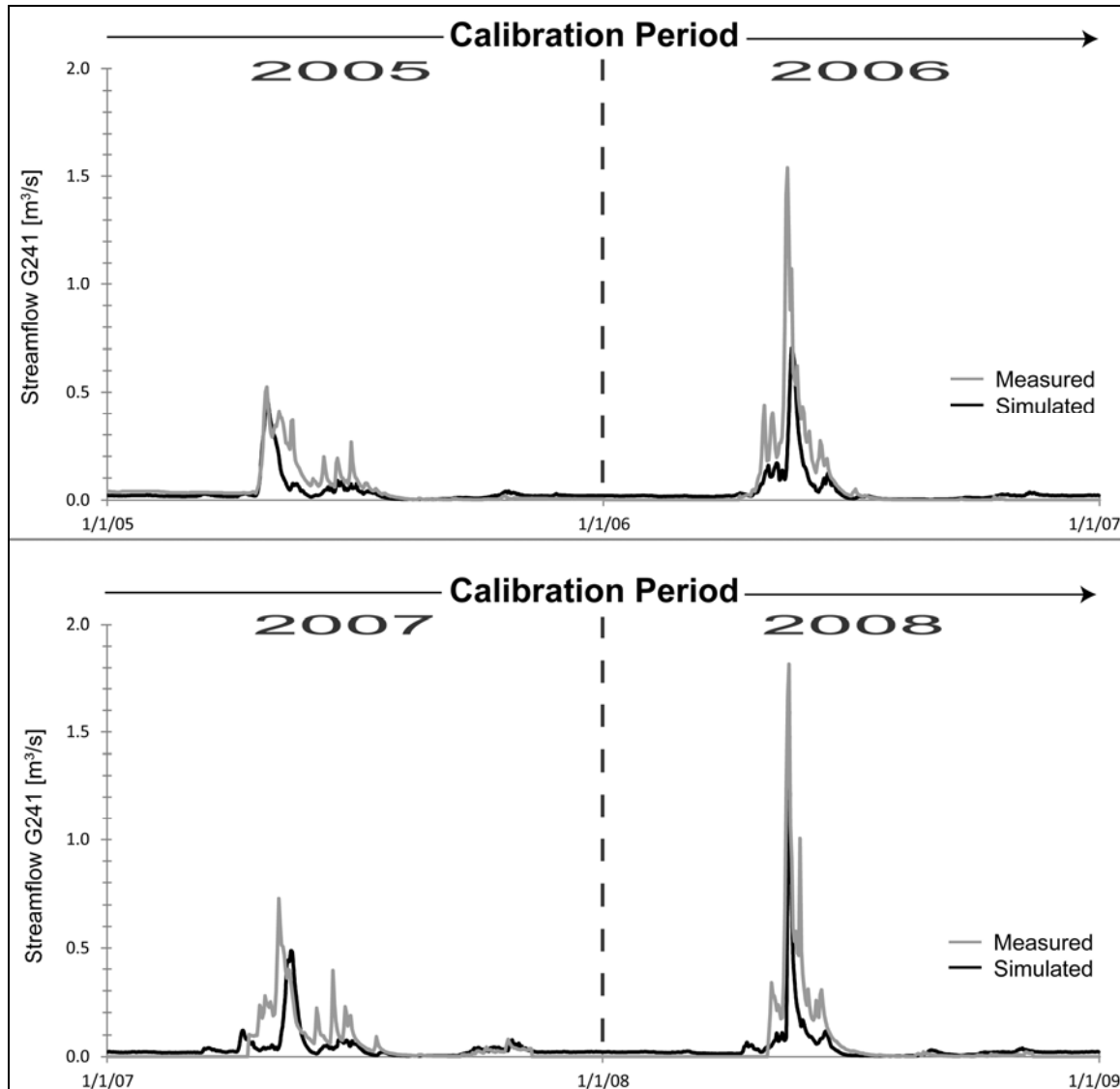
Figure 5.14. Hydrographs of measured (grey) and simulated (black) streamflow at the gauge G241 for the calibration period (2005-2008).

The simulation for the validation period of the years 2009 and 2010 also produces lower main peak flow responses (Figure 5.15). The smaller, earlier and later peaks during

the snowmelt seasons within the rising and recession limbs of the main peak of the two validation years were also simulated, but had with much lower discharge than observed. Some baseflow responses later in fall of year 2009 were simulated well.
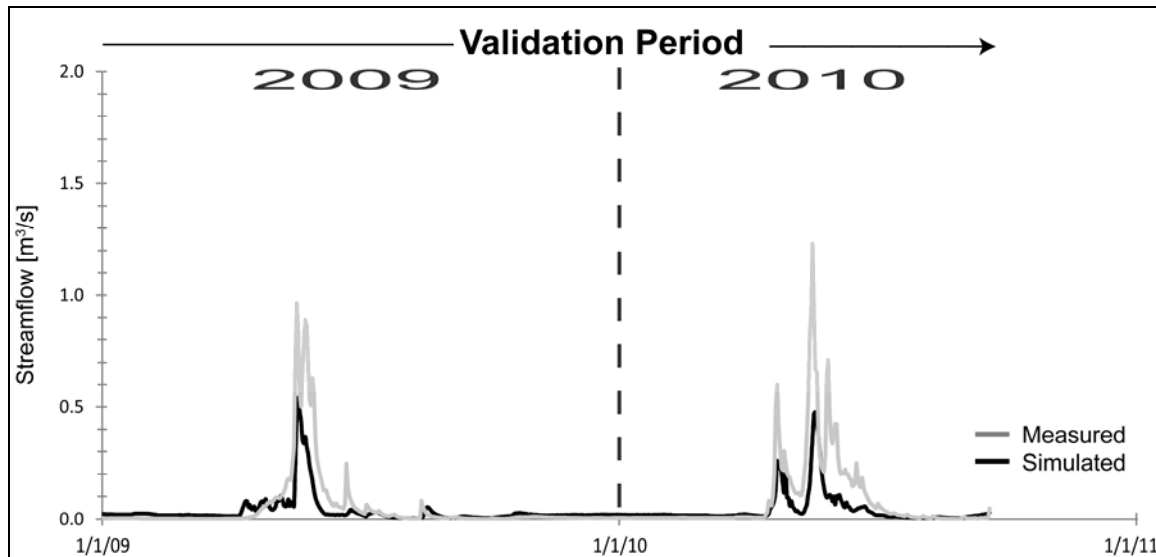
Figure 5.15. Hydrographs of measured (grey) and simulated (black) streamflows at the gauge G241 for the validation period (2009-2010).

Table 5.6 shows the model performance results for streamflow for both the calibration and validation years. Values for both periods are similar, with a slightly higher R correlation value of 0.86 for the validation period. A slightly higher Nash Sutcliffe R^2 correlation value of 0.59 was achieved for the calibration period. In general, the model performances for both the calibration and validation periods for streamflow show good correlation (above 80%) but poor Nash Sutcliffe results.

Table 5.6. Model performance statistics for the streamflow calibration and validation periods.

Stream Gauge	Calibration Period		Validation Period	
	R (Corr.)	Nash-Sutcliffe	R (Corr.)	Nash-Sutcliffe
Station G241	0.81	0.59	0.86	0.53

Nash Sutcliffe R^2 efficiency values for streamflow simulation from other recently published MIKE SHE modeling studies (e.g., Hammersmark et al., 2008; Sultana and Coulibaly, 2010; Rahim et al., 2012; Sahoo et al., 2005) show similar results. Some Nash Sutcliffe values are a little higher and some are a little lower, but in general they lie within similar ranges, except for the Hammersmark et al. (2008) study, where extremely good matches with R^2 values ranging from 0.93 to 0.97 were achieved. Results from the three other MIKE SHE modeling studies were within ranges of 0.07 to 0.44 (Sultana and Coulibaly, 2010), 0.43 to 0.83 (Rahim et al., 2012) and 0.57 to 0.75 (Sahoo et al., 2005) respectively. Streamflow model performances from two studies (Thyer et al., 2004 and Kuras et al., 2011), where the same headwater catchment was simulated, but a different code (DHSVM) was used, were better, compared to this study. Nash Sutcliffe values in Thyer et al. (2004) were within ranges of 0.77 to 0.93. In Kuras et al. (2011) values within 0.86 to 0.93 were achieved.

5.4.1.3. Deep groundwater levels

The primary objective of this modeling study was to simulate recharge to the deep bedrock and to the surrounding mountain block. Overall, the deep groundwater elevations

simulated for the model are realistic for a mountainous watershed. Figure 5.16 shows the simulated head elevations for the saturated zone during the high spring snowmelt season of 2009. Heads are highest in the upper portions of the watershed and decline toward the watershed outlet. The total range in elevation is ~1640 to 2040 masl.
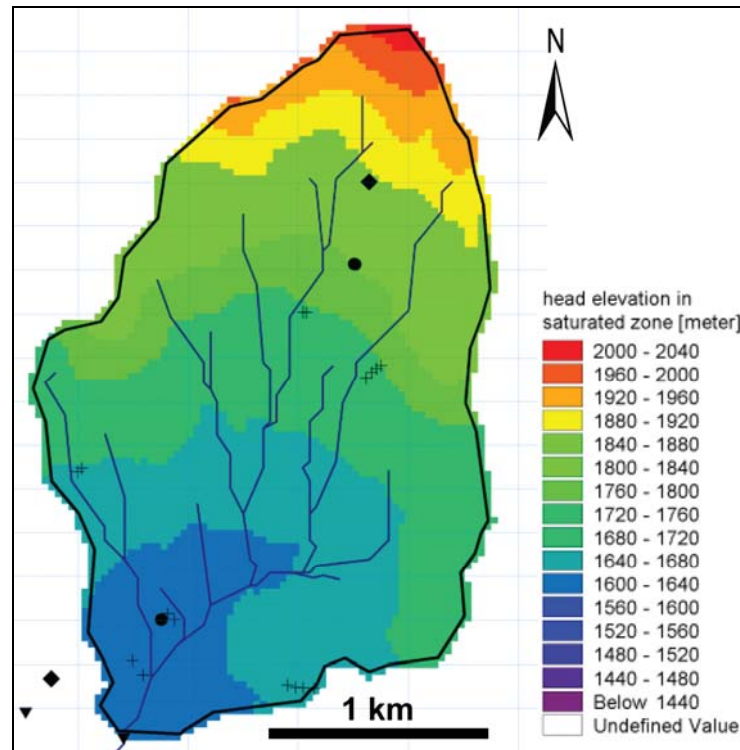
Figure 5.16. Simulated head elevations for the saturated zone during high flow spring snowmelt season of 2009 (25/05/09).

Figure 5.17 shows the measured (grey) deep water table elevation and the simulated one (black) in bedrock well 1 (W1) for the calibration period of 2007 and 2008. The scale employed emphasizes the range of values measured and simulated. Over the full range in elevation in the model, the error in simulated heads is roughly 0.1%. Measured data are only available beginning in July 2007, when the bedrock wells were

drilled. The peak simulated groundwater elevation at the beginning of the calibration period, around August 2007, is very similar to the measured one at around 1,804 masl. The simulated summer recession terminates at a groundwater level of about 1,797 masl, some 2 m lower than the observed lowest groundwater level. However, more importantly, the groundwater level in the model does not respond to the fall rain events. In Figure 5.17 the grey measured values are shown to increase during the fall and this increase is not apparent in the simulated values. As a result, the double recession is not simulated. Rather, the model simulates a continuous decrease of water table elevation from the high elevation spring snowmelt period of 2007 down to low elevation of about 1798 masl in late winter/early spring of 2008.

Similarly, the rise in groundwater level associated with the spring snowmelt of 2008 is well simulated, but the final groundwater elevation is not as high as the measured elevation. The simulated water table rises only up to an elevation of about 1804 masl, in comparison to the measured elevation of 1806 masl, and the simulated response is delayed by one month. The post spring snowmelt recession is similar in character to that of 2007, with the water level dropping down continuously. Again, the rise in the groundwater level due to fall rain events is not represented in the model. Note that the Fall 2008 rain events did occur, but were not observed on the groundwater level log because the datalogger was not operational from the end of July 2008 to the end of October 2008 (see data gap in Figure 5.17).
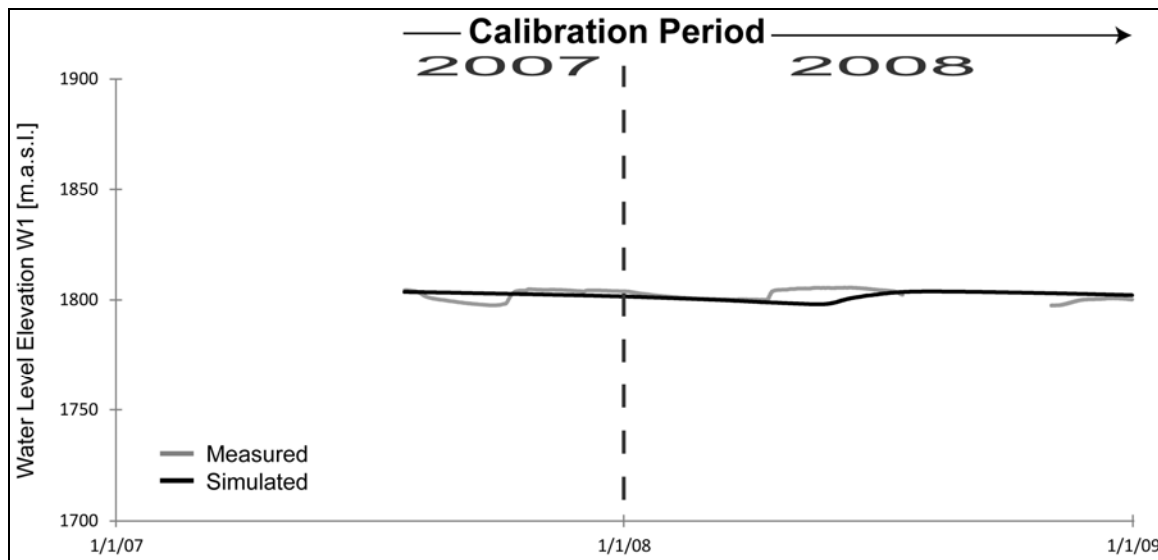
Figure 5.17. Measured water table fluctuation (grey) and simulated (black) in the deep bedrock well 1 for the calibration period (2007-2008).

No measured data are available for the calibration period 2007/2008 for wells 2 and 3 (W2 and W3), because the data loggers had malfunctioned (due to freezing). It is expected that data from W2 would look similar to W1 (see well 1 and well 2 for validation period), because those two wells are located within 2 m of each other in the upper elevation of the watershed. In contrast, W3 is a flowing well throughout most of the spring snowmelt period, so the groundwater level data are not representative as discussed below.

Figure 5.18 shows the simulated and measured groundwater level elevation for W1 for the validation period of 2009 and 2010. The water table fluctuation for this period looks similar that of the calibration period for W1. The simulated water level reaches a peak in mid to late April of 2009 (1803 masl), but the peak is not as high as measured (1805 masl). The simulated peak is also shifted later by about one month. A continuous

recession is simulated to an elevation of 1,794 masl - much lower than the measured

elevation of 1,800 masl and similarly delayed by about two months. Similar to the

calibration period, the fall rain events, which affect the measured groundwater levels, are

not captured by the model. Due to the strong similarity of the water table elevations in

W1 and W2, the validation period for W2 is not shown in this chapter, but can be found

in Appendix C.1.
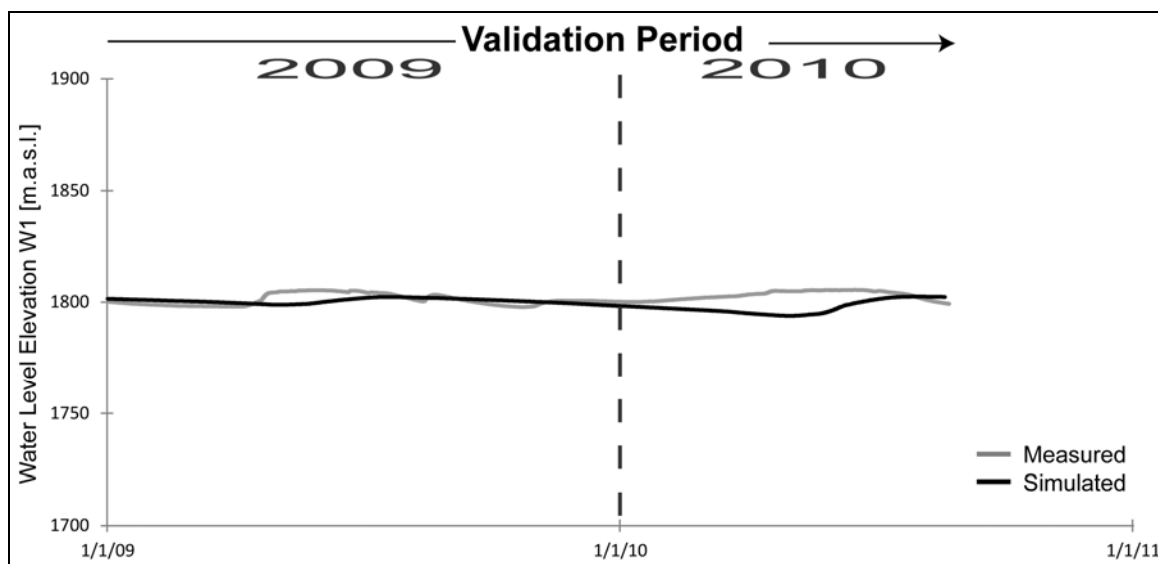
Figure 5.18. Measured water level fluctuation (grey) and simulated (black) in the deep
bedrock well 1 (W1) for the validation period (2009-2010).

Figure 5.19 shows the simulated and measured water level elevations/fluctuations

for bedrock well 3 (W3) for the validation period 2009/2010. This well is located close to

the outlet of the watershed at low elevation. Due to its low elevation and short surface

casing height, this well flows during the spring snowmelt period (i.e., the water levels

appear to "flatline" on the measured graph). The shape and the timing of the simulated

response compared to the measured one are good, but the simulated response is about 5 m lower than measured at this well.
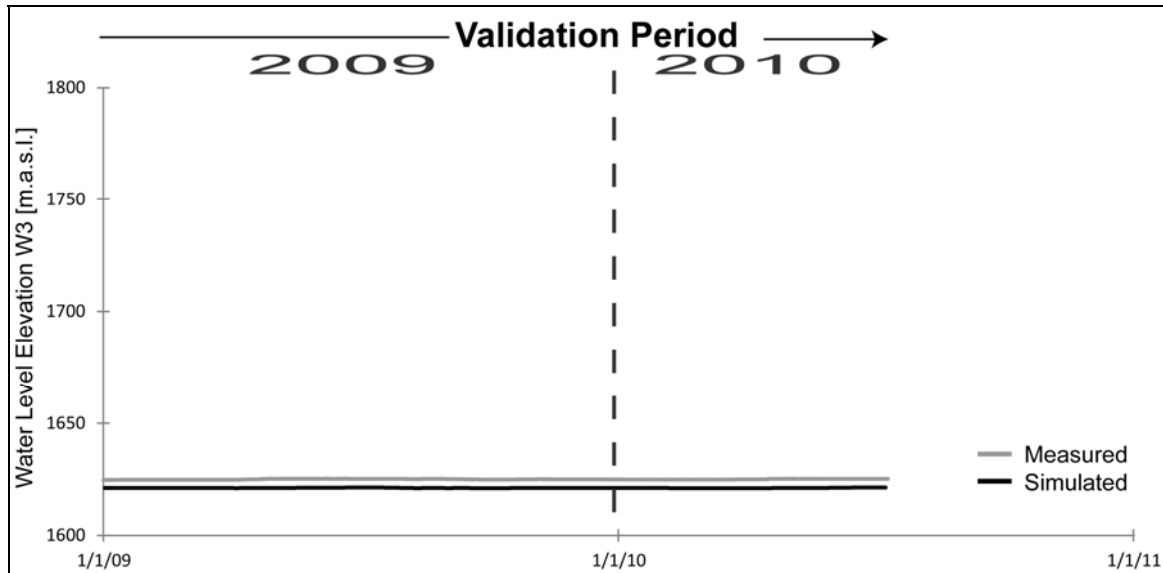
Figure 5.19. Measured water table fluctuation (grey) and simulated (black) in the deep bedrock well 3 (W3) for the validation period (2009-2010).

As seen in Table 5.7, model performance statistics are poor for the calibration and validation periods of W1 and W2. Even though highest and lowest water levels were reasonably well simulated for the spring snowmelt seasons and the winter low flow seasons, the simulated peaks in both wells are shifted to later times by about one to two months, resulting in poor negative R correlation values and negative R^2 Nash Sutcliffe correlation values. For W3 the R correlation value is reasonable with 0.64, whereas the R^2 Nash Sutcliffe value is also negative with a very high value of -1092.54.

Overall, the deep groundwater levels at high elevation in the model (as represented by W1) do not appear to be sensitive to the shorter term variations associated with fall rains. Thus, rather than two distinct recessions in groundwater level being simulated, only

one continuous response is captured by the model. The peak response is also delayed by at least one month and the recession low is delayed by close to two months. In addition, at W3 the simulated groundwater levels are considerably lower than measured, although the responses are much closer to observed. The simulated responses are discussed further in Section 5.5.4.

Table 5.7. Model performance statistics of the deep bedrock water level fluctuation for calibration and validation periods.

Bedrock Well	Calibration Period		Validation Period	
	R (Corr.)	Nash-Sutcliffe	R (Corr.)	Nash-Sutcliffe
W1	-0.57	-1.65	-0.28	-1.82
W2	not available – data logger		-0.35	-1.51
W3	malfunctioned		0.64	-1092.54

With respect to the groundwater level calibration results, no comparisons to other MIKE SHE modeling studies nor to the simulation of the same catchment using DHSVM code can be made, since none of those studies include deep fractured bedrock aquifers and perched soil water tables together and thus do not simulate their interaction.

5.4.1.4. Pressure heads in the soil zone

Figures 5.20 to 5.31 show the simulated and measured responses of the soil pressure heads in selected piezometers for the calibration and validation periods. In all graphs, a pressure head of zero corresponds to the depth of the data logger at the bottom of the piezometers. As mentioned (see Section 5.3.6), a total of 15 soil piezometers (6 transects in forested and logged areas at high and low elevations) were installed throughout the watershed. The piezometers with the best calibration and validation results

of each transect are shown here. The calibration and validation graphs for the remaining piezometers can be found in Appendix C.2.

The simulated pressure heads at piezometers P2 and P10 (Figures 5.20 and 5.23) are too low by about 1.0 m compared to the measured pressure heads. The shapes and timing of the responses, however, are well simulated. In contrast, the simulated pressure heads in piezometers P5, P7, P13 and P14 (Figures 5.21, 5.22, 5.24 and 5.25) are all too high, with the soil water level rising above ground surface throughout most of the simulation (as identified in the parts of the graphs which level off as horizontal lines).
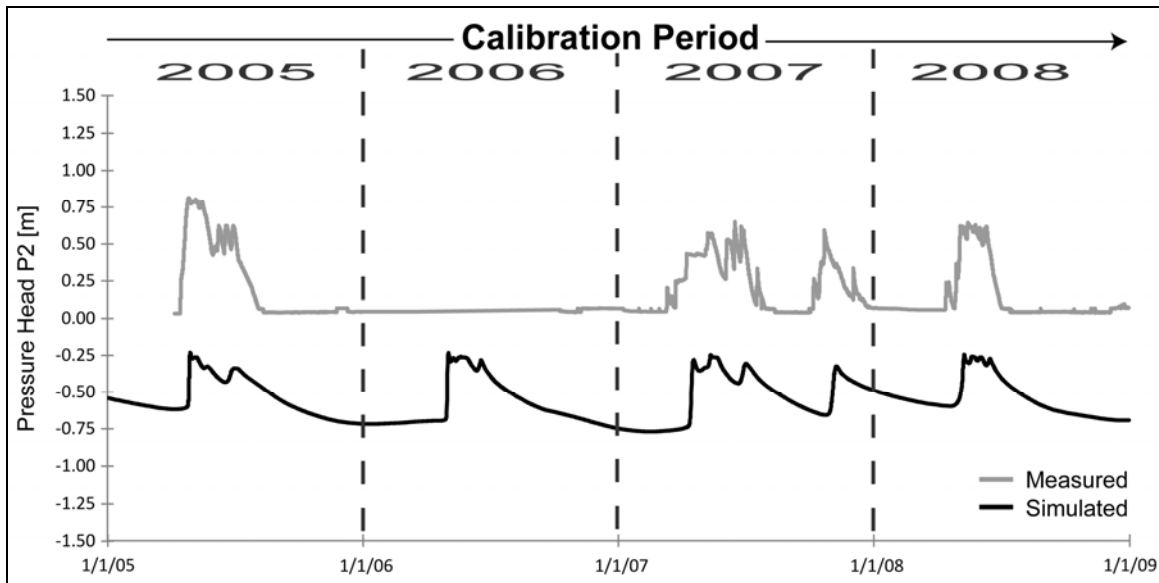
Figure 5.20. Measured soil water pressure head (grey) and simulated (black) in piezometer P2 for the calibration period (2005-2008).
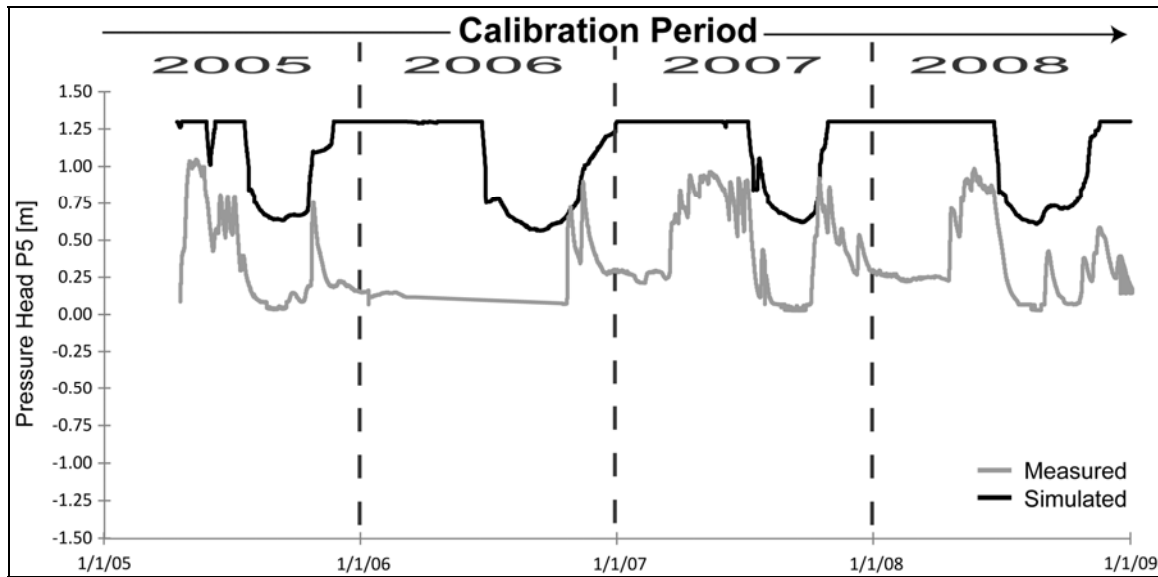
Figure 5.21. Measured soil water pressure head (grey) and simulated (black) in piezometer P5 for the calibration period (2005-2008).
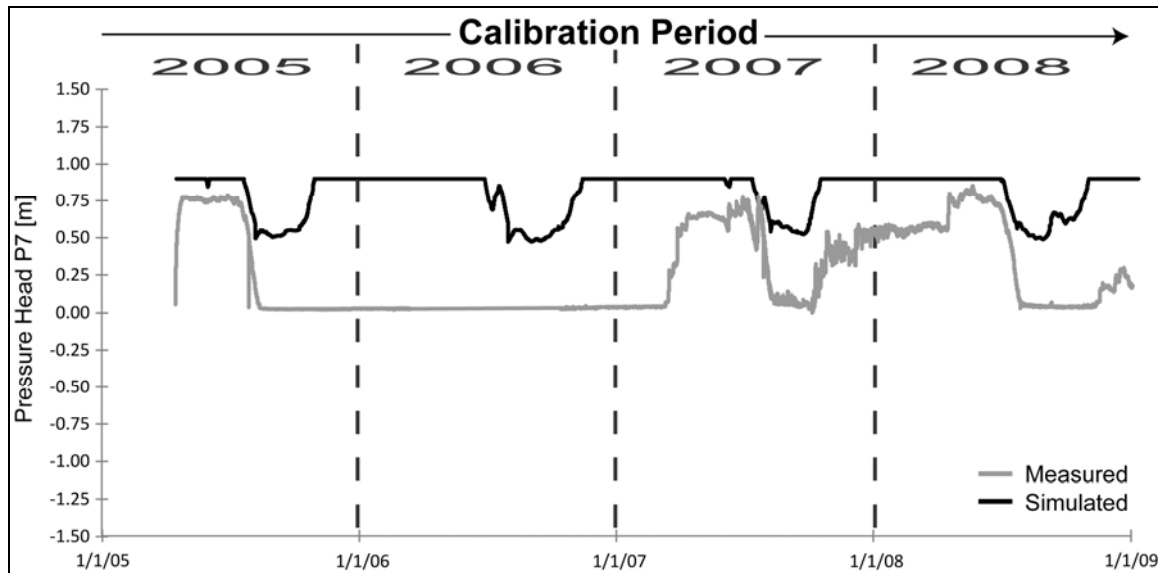
Figure 5.22. Measured soil water pressure head (grey) and simulated (black) in piezometer P7 for the calibration period (2005-2008).
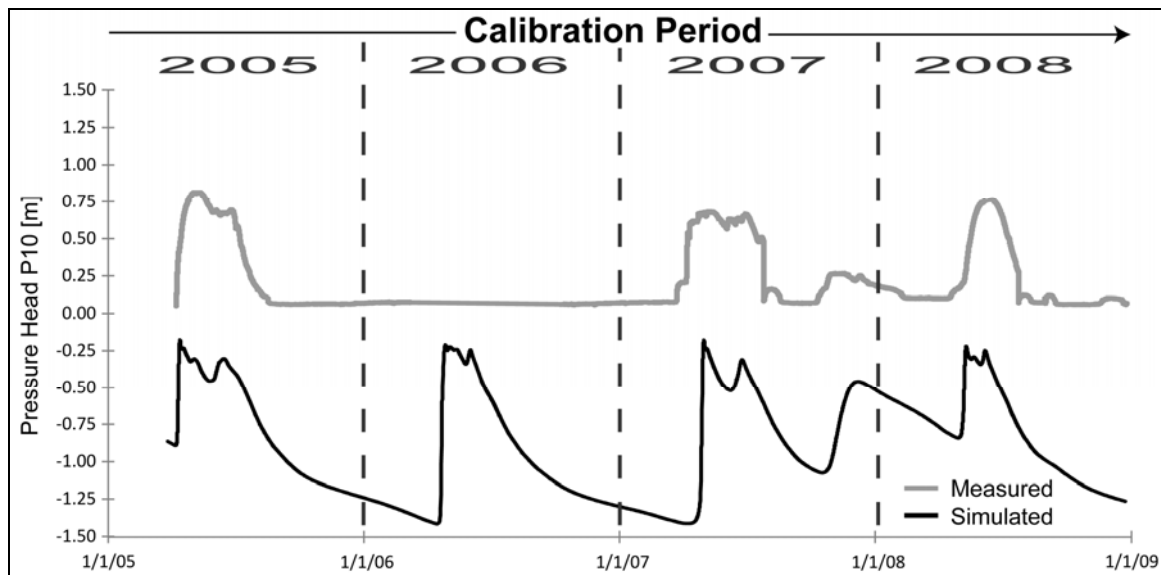
Figure 5.23. Measured soil water pressure head (grey) and simulated (black) in piezometer P10 for the calibration period (2005-2008).
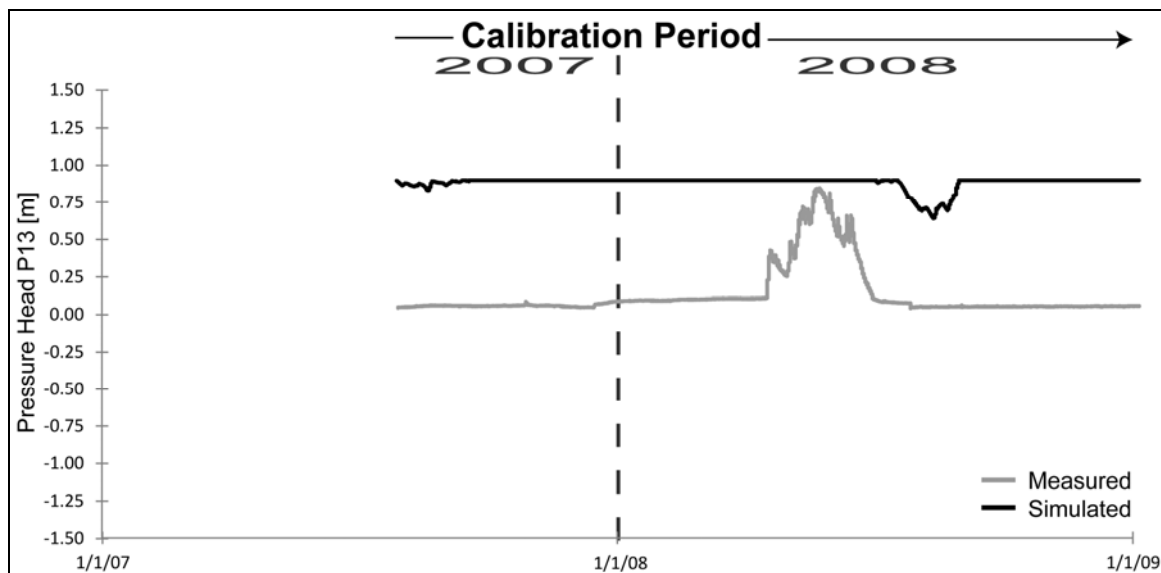
Figure 5.24. Measured soil water pressure head (grey) and simulated (black) in piezometer P13 for the calibration period (2005-2008).
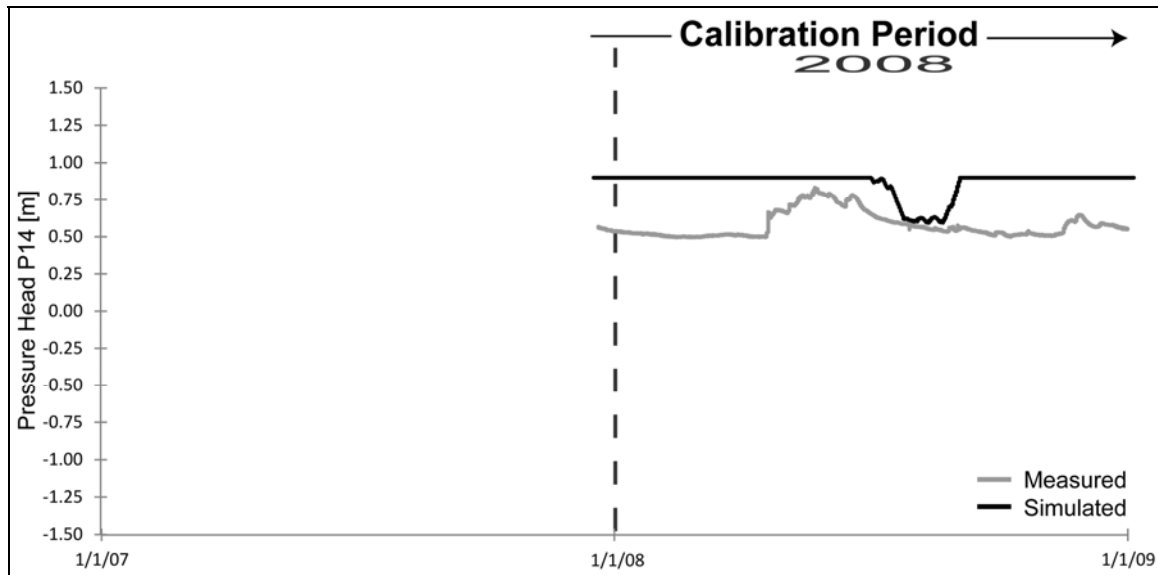
Figure 5.25. Measured soil water pressure head (grey) and simulated (black) in piezometer P14 for the calibration period (2005-2008).

Figures 5.26 to 5.31 show the simulated and measured pressure heads for the validation period for the selected piezometers. Similar results as for the calibration period were achieved.
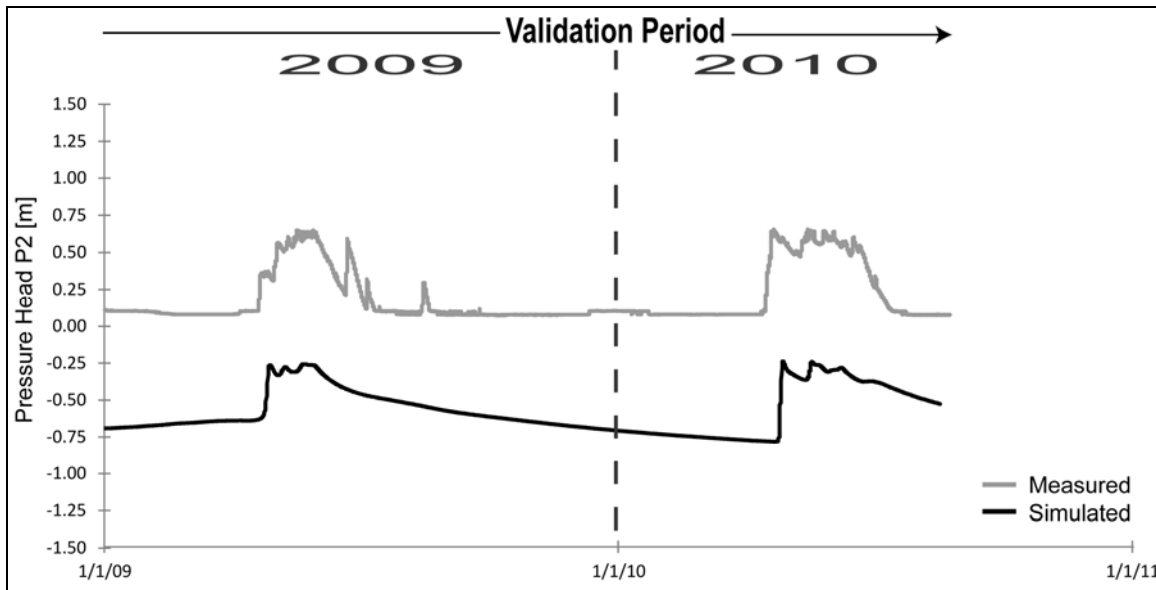
Figure 5.26. Measured soil water pressure head (grey) and simulated (black) in piezometer P2 for the validation period (2009-2010).
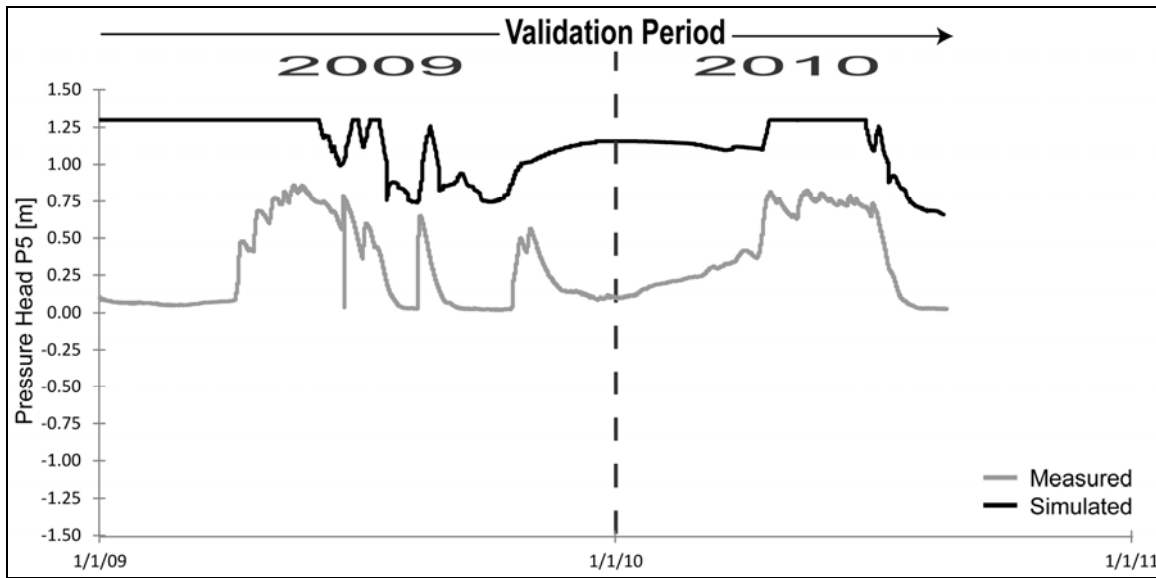
Figure 5.27. Measured soil water pressure head (grey) and simulated (black) in piezometer P5 for the validation period (2009-2010).
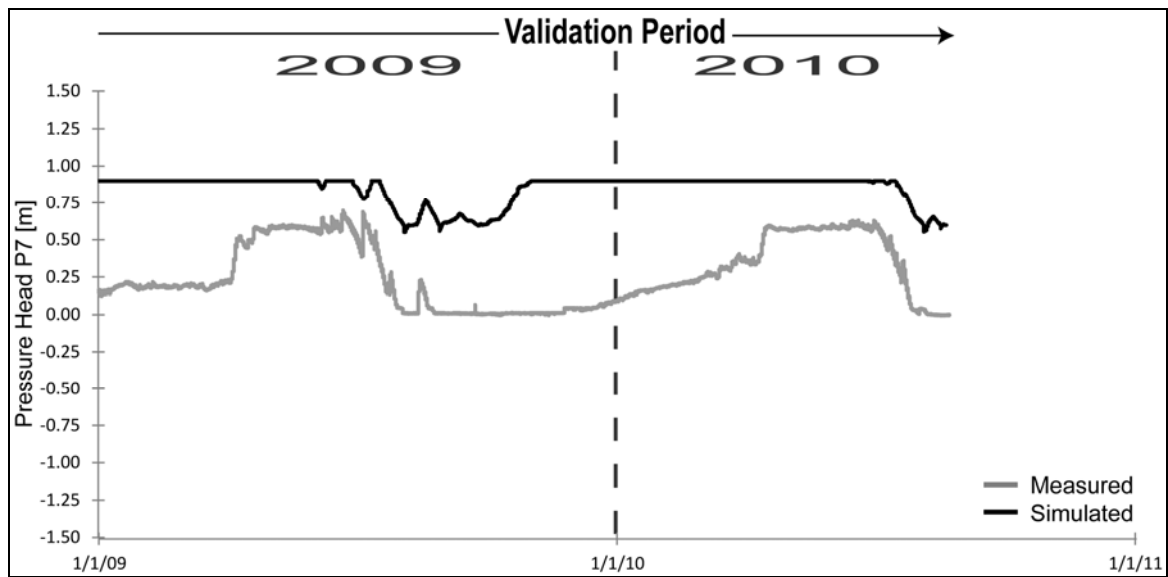
Figure 5.28. Measured soil water pressure head (grey) and simulated (black) in piezometer P7 for the validation period (2009-2010).
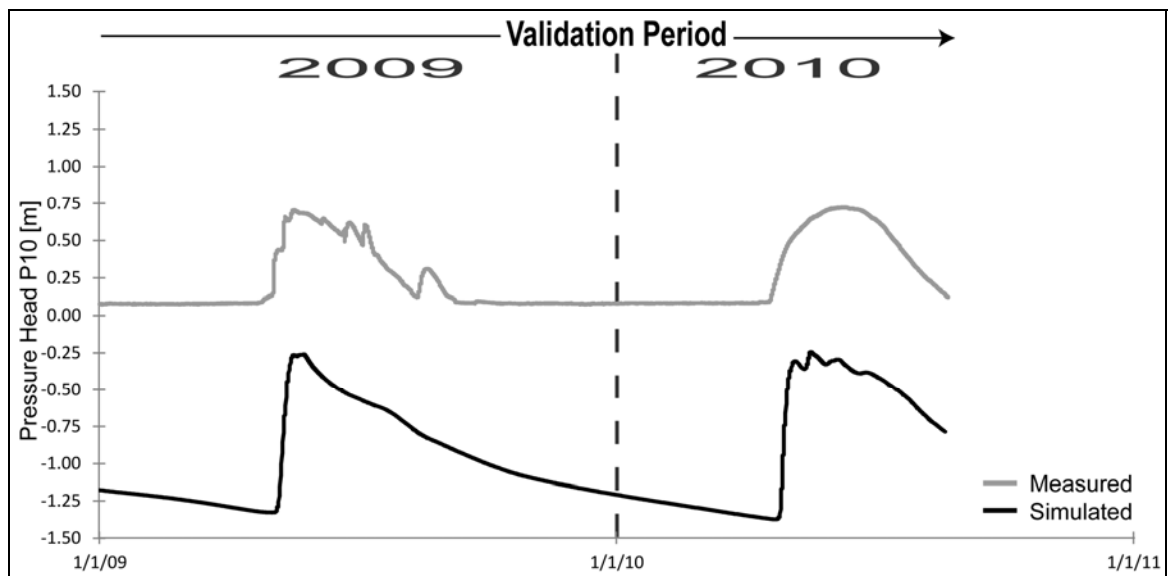
Figure 5.29. Measured soil water pressure head (grey) and simulated (black) in piezometer P10 for the validation period (2009-2010).
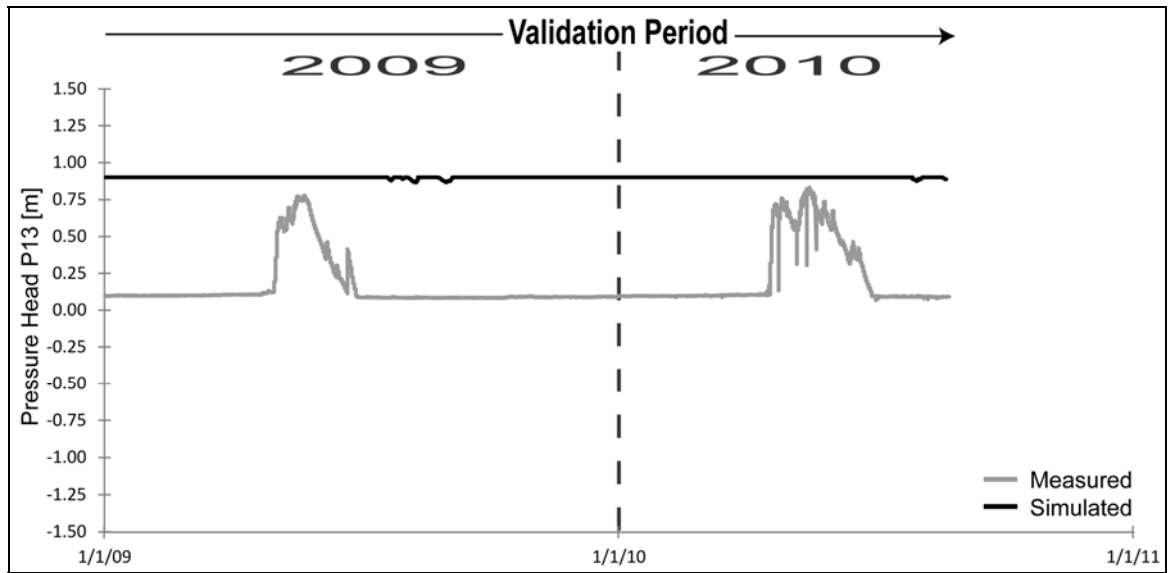
Figure 5.30. Measured soil water pressure head (grey) and simulated (black) in piezometer P13 for the validation period (2009-2010).
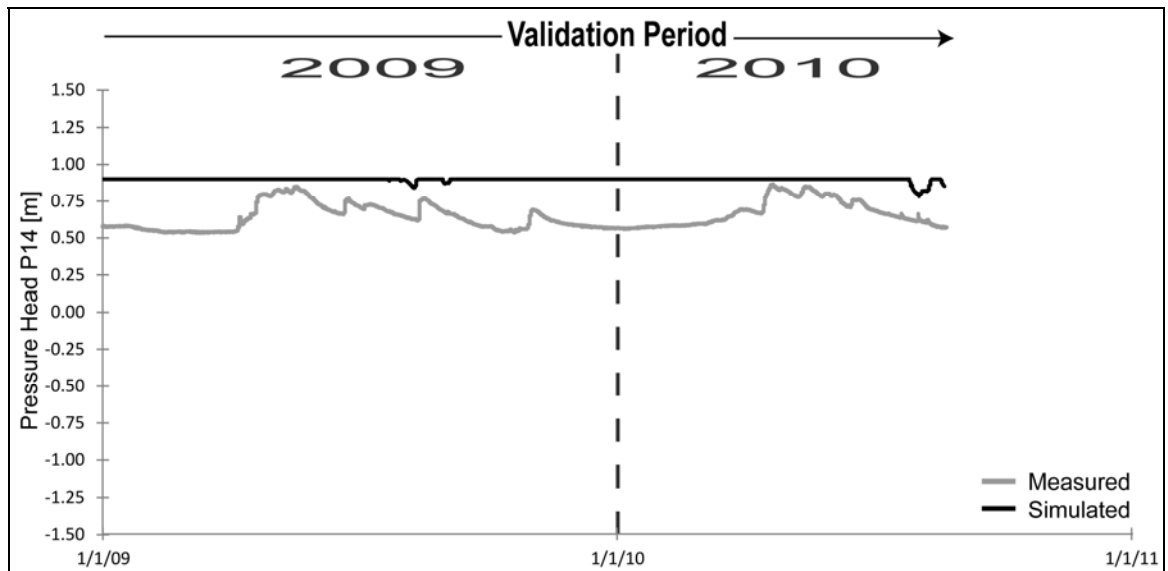
Figure 5.31. Measured soil water pressure head (grey) and simulated (black) in piezometer P14 for the validation period (2009-2010).

Table 5.8 gives an overview of the model performance results for the simulated pressure heads of all piezometers for both the calibration period and the validation period. Piezometers P1, P2, P3, P4, P9, P10 and P11, the ones where the simulated pressure heads are too low, give R correlation values above 50%. All the other piezometers (P5, P6, P7, P8, P12, P13, P14 and P15), which are the ones where the simulated pressure heads are too high and water seeps at surface, show very poor results, with R correlation values below 50%. The Nash Sutcliffe R^2 correlation values of all piezometers are negative.

The overall results for the soil piezometers suggest that the model is generating heads that are too high in some areas and too low in others, but that the timing of the response of the soil zone is reasonable. Other MIKE SHE modeling studies recently published did not include simultaneous simulation of pressure heads in the unsaturated soil zone and deep fractured bedrock aquifers in the saturated zone. Due to that, no comparisons with the results can be made concerning soil water dynamics. Kuras et al. (2011) did simulate soil water dynamics in 9 of the 15 piezometers installed in the watershed with DHSVM code. Overall, results from that study reproduce soil water dynamics better than the MIKE SHE model; however, that model did not include the deep fractured bedrock.

Table 5.8. Model performance statistics for the soil water levels in the different piezometers for the calibration and validation periods.

Soil Piezometer	Calibration Period		Validation Period	
	R (Corr.)	Nash-Sutcliffe	R (Corr.)	Nash-Sutcliffe
P1	0.29	-13.56	0.64	-12.67
P2	0.73	-12.26	0.76	-16.02
P3	0.46	-14.39	0.76	-14.59
P4	0.62	-59.89	0.66	-116.32
P5	0.45	-7.83	0.49	-7.97
P6	0.21	-24.00	0.27	-6.87
P7	0.40	-2.92	0.52	-5.98
P8	0.06	-22.86	-1	-24.70
P9	0.31	-46.08	0.54	-41.22
P10	0.73	-18.23	0.91	-26.79
P11	0.80	-9.22	0.86	-12.11
P12	-1	-8.21	-1	-4.27
P13	0.15	-18.68	0.11	-13.84
P14	0.07	-11.09	0.08	-8.45
P15	-0.28	-336.49	0.18	-337.52

5.4.2. Water balance

This section gives an overview of the water balance results for the UPC 241 catchment calculated with the MIKE SHE water balance tool.

The MIKE SHE water balance utility is a flexible, post-processing tool for generating water balance data for MIKE SHE simulations. The different output types from the water balance utility include area normalized flows, measured as storage depths in mm; storage changes; and model errors resulting from convergence problems. Water balance data can be generated at a variety of spatial and temporal scales and in a number of different formats (DHI, 2007).

Table 5.9 shows the total water balance for the area of the catchment including the total error [mm/year] for each water year of the calibration and validation periods (2005-2010) for all components of the water balance in the unsaturated and saturated zone. A yearly average value was also calculated from the five individual water years. In addition to the storage depth values in [mm/year] for each component of the yearly average, values in [% of precip.] are also shown.

All the water input to the system (100%) comes from precipitation. Precipitation input values are reported as positive numbers in Table 5.9. All other components of the water balance are either fluxes out of the system, which are always negative, or storage changes, which can be positive or negative and which differ for each individual water year. For each individual water year, water balance errors range from 9 mm/year to -16 mm/year, resulting in a 5 year average error of -3 mm/year or 0.4%. Figure 5.32 shows a conceptual block diagram of the total water budget for the yearly average of 5 years corresponding to the calibration and validation period from 2005 to 2010. The directions of the arrows indicate fluxes in or out of the system, and the lengths of the arrows represent the magnitudes of the fluxes.

Each one of these is highly uncertain due to model error, calibration error, and most importantly, parameter uncertainty. The estimated uncertainty for precipitation could be as high as ±50 mm (7% of total precipitation). Evapotranspiration (ET) is likely more uncertain due to the large number of parameters required to estimate potential ET and the various land surface and shallow subsurface parameters needed to simulate this process in MIKE SHE. Similar uncertainty exists for all other components of the water

balance. Thus, with such small estimates resulting for recharge to bedrock (29 mm/yr or 4%), it is important to recognize that these are highly uncertain. Similarly, the outflow from the catchment (2-6%) is uncertain.

Table 5.9. Total water balance for each individual water year (WY) and the yearly average (Yearly Ave.) for the calibration and validation periods spanning 2005 to 2010. Values in brackets represent % of precipitation for each component of the yearly average.

	Unsaturated Zone							Saturated Zone				
	P [mm/y]	ET [mm/y]	Snow-Storage change [mm/y]	OL-Flow to river [mm/y]	OL-Storage change [mm/y]	UZ-Storage change [mm/y]	BF-out [mm/y]	Recharge to SZ [mm/y]	Baseflow to river [mm/y]	SZ-Storage change [mm/y]	BF-out [mm/y]	Total Error [mm/y]
WY 05-06	719	-380	0	-254	0	40	-30	104	-15	-77	-12	-10
WY 06-07	673	-406	-1	-230	-2	-32	-26	-33	-15	59	-12	9
WY 07-08	714	-374	1	-279	2	6	-34	52	-15	-25	-12	-16
WY08-09	686	-449	0	-228	0	-25	-26	-51	-14	76	-12	9
WY 09-10	667	-356	0	-218	-5	2	-25	74	-14	-48	-12	-9
Yearly Ave.	692 (100%)	-393 (57%)	0 (0%)	-242 (35%)	-1 (0.1%)	-2 (0.3%)	-28 (4%)	29 (4%)	-15 (2%)	-3 (0.4%)	-12 (2%)	-3 (0.4%)

P= Precipitation; ET= Evapotranspiration; OL= Overland; UZ= Unsaturated Zone; BF= Boundary Flow; SZ= Saturated Zone; WY= Water Year
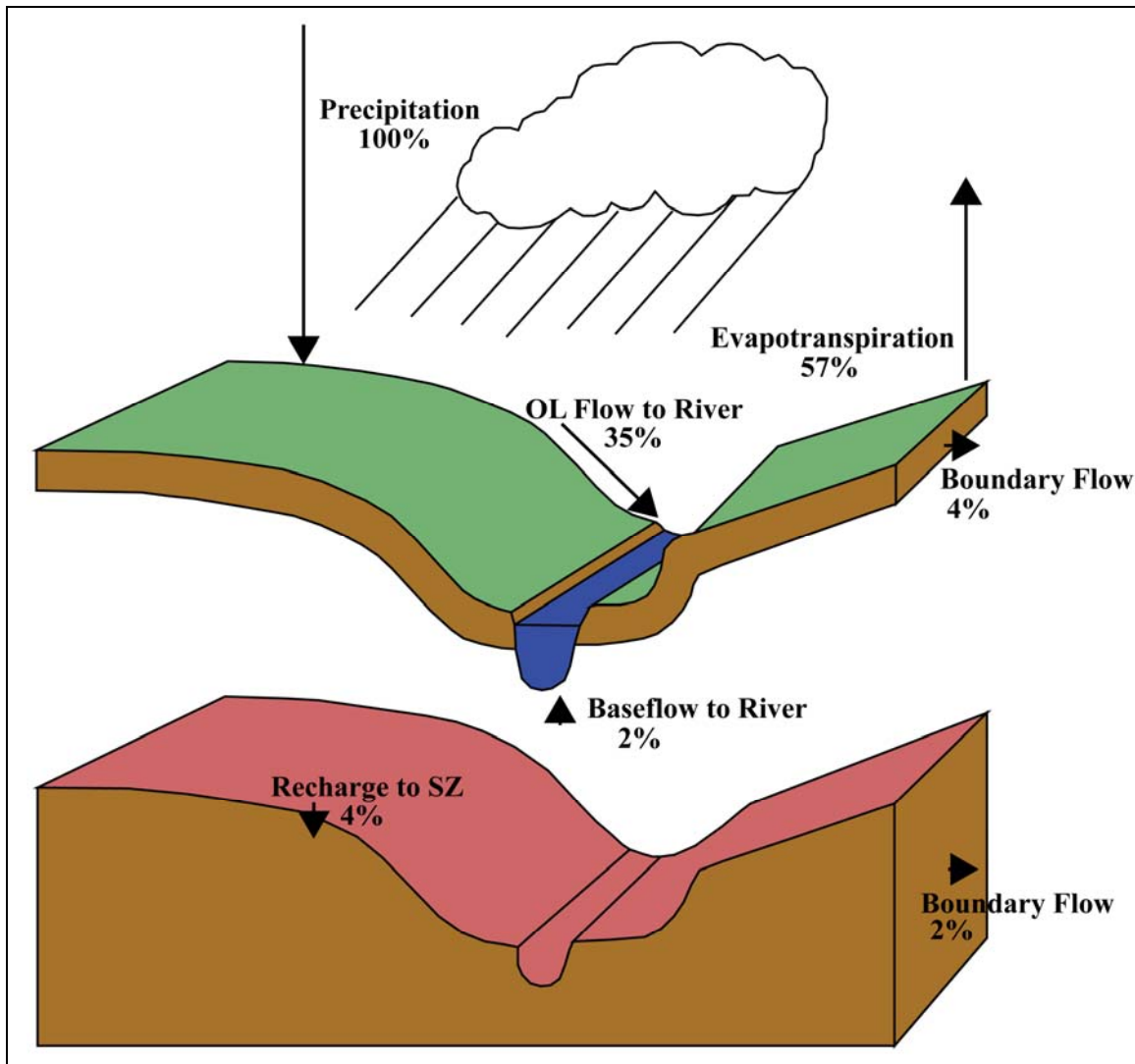
Figure 5.32. Conceptual diagram of the water budget based on the average water balance results for a 5 year period corresponding to the validation period (shown in %). The lengths of the arrows represent the magnitudes of the fluxes and the directions indicate if the fluxes are into or out of the system.

Within the unsaturated zone, the water balance is calculated as follows:

P – ET ± ΔSnow Storage – OL Flow to River ±Δ OL Storage ±ΔUZ Storage – BF Out =

Recharge to SZ   (5.1)

The component of the water balance responsible for the highest amount of water being transferred out of the unsaturated zone is evapotranspiration (EVT), which makes up about 57% of the whole water budget for the yearly average. About 35% of the water leaves the unsaturated zone through the main river at the outlet of the watershed with water entering the rivers from overland (OL) flow. Small positive or negative values are reported for changes to Snow Storage and OL Flow Storage, and variable changes to UZ Storage. On average, the unsaturated zone contributes 29 mm/year (4% of precipitation) to recharge to the saturated zone, although this recharge amount varies considerably from year to year and ranges from -51 to +104 mm/year.

Within the saturated zone, the water balance is calculated as follows:

Recharge from SZ = BF to River $\pm\Delta$ SZ Storage – BF Out $\qquad\qquad$ (5.2)

About 2% of unsaturated zone water enters the rivers from the saturated zone as baseflow and subsequently leaves the whole system. There are variable positive and negative changes to the SZ Storage.

Boundary flow (BF) occurs through both the unsaturated and saturated zones. As discussed earlier, a sensitivity analysis was performed and a plausible outward flux was assigned to the bedrock within the saturated zone. This means that as the water table changes in elevation, the amount of outward flux will change. As shown in Figure 5.7, the bedrock extends across the full thickness of the saturated zone upwards into the unsaturated zone. The assignment of unsaturated zone versus saturated zone in MIKE SHE is somewhat arbitrary, in that while the actual relative thickness of these two zones will change from day to day and year to year, the model assumes that the zone called

"saturated" has a fixed depth and the zone called "unsaturated" has a fixed depth. The saturated zone fully contains the bedrock, so the water balance results indicate a constant and uniform outward flux from the bedrock of 12 mm/year (or 2% of precipitation). However, the outward flux in the unsaturated zone, across the entire depth of the unsaturated zone flux boundary of 200 m, varies from year to year, with an average of 28 mm/year (or 4% of precipitation).

In total, an average of 40 mm/year (6% of precipitation) leaves the model through the bedrock. This flux out of the headwater catchment recharges the adjacent larger-scale intermediate or regional flow systems contributing to mountain block recharge. More details on this boundary outflow and its sensitivity will be given in Section 5.4.3.

The simulated values from this study correspond well with values found in the literature. Smerdon et al. (2008) estimated that groundwater recharge varied from 20 to 50 mm/yr at high elevations in a mountain watershed. That modeling study was conducted at the scale of the mountain block (headwaters to valley bottom), and at that scale, 20% of precipitation was found to exit the system via the deep bedrock as mountain block recharge.

5.4.3. Model sensitivity to groundwater outflow

One of the main objectives of this study was to estimate how much deep groundwater exits the system. Because the base of the model was assigned a no flow boundary, any outgoing flux was permitted to leave the model only through the lower edges of the model domain as shown in Figure 5.8. An initial flux during calibration (see

Section 5.3.9.) of -5.0 x 10^{-3} m/s (per 5 m depth of saturated zone) was estimated for this particular boundary condition. This corresponds to a total outward flux of 4,654 mm over four years (calibration period 2005-2008) or a yearly flux of 1,164 mm across the entire boundary. This would be 170% of the precipitation, which means that almost double the amount of water leaves the model than water enters the system through precipitation. Not surprisingly, this model simulation resulted in a very high total water balance error of about 140%. Also the simulation time was very long. Thus, the results of that simulation were unreasonable and a lower flux was needed. Lowering the initial flux value during calibration by two orders of magnitude resulted in a much shorter simulation time (3 hours compared to about 20 hours) and an acceptable water balance error of 0.7%. While still uncertain, the final outward flux in the calibrated model was set to -5.0 x 10^{-5} m/s or 47 mm over four years across the entire boundary during the calibration period of 2005 to 2008. This corresponds to 2% of the precipitation.

Table 5.10 shows the change in water balance results for each component for the two different groundwater outflow fluxes from the saturated zone (SZ), expressed as a percentage of precipitation. The calibrated model, with outflow from the saturated zone as 2% of precipitation is shown on the top line and is shaded grey – all values are zero as this represents the base case for comparison. For the case where outflow is 0% of precipitation (i.e., no outflow), there is slightly more EVT, overland (OL) flow to river, unsaturated zone (UZ) storage change, unsaturated boundary outflow, and baseflow to river. The recharge to the saturated zone decreases slightly. For the case of outflow from the saturated zone of 17% (likely a very upper limit of how much groundwater could exit

215

the system), EVT, OL flow to river, UZ storage change, unsaturated boundary outflow, and baseflow to river all decrease substantially as a percentage, while the infiltration to the SZ and the SZ storage change are both positive. It is important to note, however, that the change in the model error is high, particularly for the case of 17% of precipitation.

Table 5.10. Change in water balance results for each component of the water balance expressed as a percentage of precipitation for two different groundwater outfluxes at the southern boundary. The base case with the calibrated outflux value of 2% is shaded in grey.

SZ – BF-out [% - of precip.]	Unsaturated Zone				Saturated Zone			
	EVT	OL- Flow to river	UZ– Storage change	BF- out	Recharge to SZ	SZ- Storage change	Baseflow to River	Total Error
	[% change]							
2% at southern boundary	0	0	0	0	0	0	0	0
0% at southern boundary	0.5	2	10	1	-1	0	3	25
17% at southern boundary	-5	-21	-43	-2	13	27	-55	205

EVT= Evapotranspiration; OL= Overland; UZ= Unsaturated Zone; BF= Boundary Flow;
SZ= Saturated Zone

Figure 5.33 shows the sensitivity of simulated streamflow to the outward groundwater flux, expressed as a percentage of precipitation. Shown are the R correlation and Nash Sutcliffe R^2 values from model calibration period 2005 to 2008. The graph suggests that streamflow is not particularly sensitive to the outward groundwater flux. This result has important implications for modeling headwater catchments in that it suggests that a reasonable streamflow calibration can be achieved for a range of groundwater losses from the system.
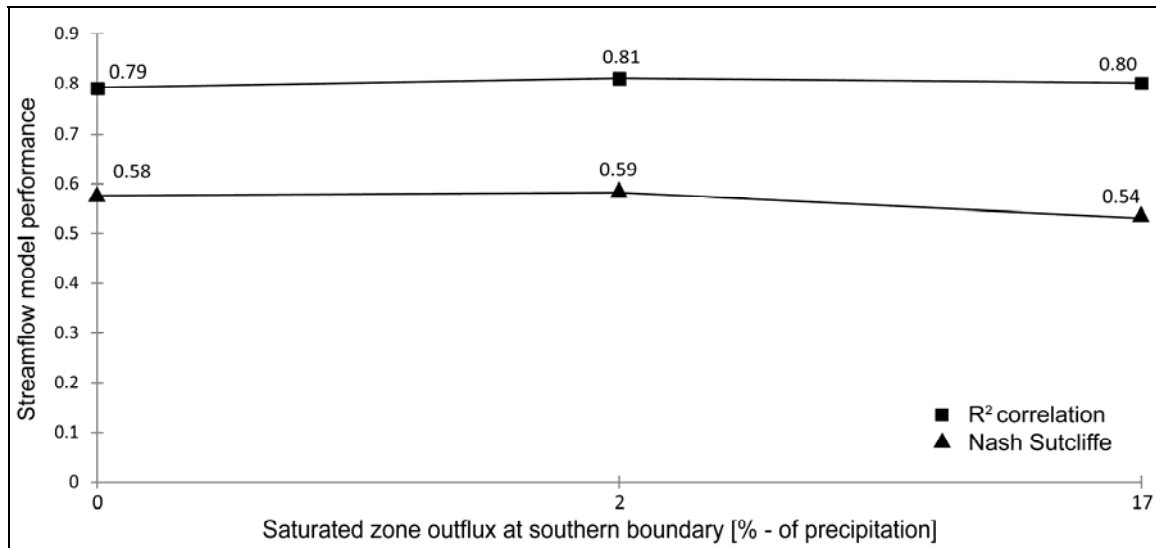
Figure 5.33. Sensitivity of simulated streamflow to the three outward groundwater fluxes. Sensitivity of streamflow is expressed through changes in the R correlation and R^2 Nash-Sutcliffe correlation model performance values.

5.5. Discussion

5.5.1. Model warm up period and calibration challenges

As seen in Figure 5.9, the model took a long time to warm up, about 10 years, from 1994 to 2004. From 2004 on, a generally visible stable state of the aquifer response was reached (i.e., the water level response in the wells appeared to no longer decline). This long warm up period may have been a consequence of the initial high water table of zero metres, which means the model is completely filled with water when it starts. Choosing a lower water level for the initial saturated zone settings might have resulted in a shorter warm up period. To test whether a lower initial water level might decrease the warm up period, the initial water level was lowered to -4 m below the ground surface uniformly distributed throughout the watershed. Unfortunately, simulation times increased

drastically by about five times. Because of that, a starting water level of zero metres was used for all remaining simulations. So it was not possible to verify whether a lower water level at the start of the simulation would have reduced the warm up period, since the simulation was cancelled due to a very long simulation time. Concerning model calibration, which began after the warm up period and ended in 2004, the model overall was found to be very sensitive to most of the input parameters. As noted earlier, over 300 model runs were completed to try and achieve the best possible calibration.

5.5.2. Snowmelt

As mentioned earlier, snowmelt during the 2004/2005 snow season was the first component targeted for calibration in the model, even though snowmelt parameters affect streamflow as well. Of course data for only a single snow season (2004/2005) were available, making the calibration period very short.

In general, the snowmelt was simulated reasonably well as seen in Figures 5.10 to 5.13 and Table 5.5. For the snow measurement locations located in clearcuts (see Figure 5.2.), SWE model results were better than those simulated for the forested locations. Compared to the results of Kuras et al. (2011), which used the DHSVM model to simulate the same watershed, forested location results were poorer using MIKE SHE, but results for clearcuts were similar. A reason why MIKE SHE modeling results for SWE in forested locations are poorer for the same watershed might be related to fact that a more sophisticated approach is used to simulate SWE in DHSVM. The approach uses a two-layer energy-balance model including a forest radiation balance (Wigmosta et al., 1994),

in which clearcut and forest snow albedo are included. The snow albedo is a measurable reflection coefficient and is different for snow accumulation in forested and clearcut areas. Instead of an energy balance model, which requires considerably more detailed input data (i.e. snow albedo), MIKE SHE uses a modified degree-day method (DHI, 2007), which does not account for different melting conditions within different vegetation covers. Degree-day based calculations require limited additional data and are relatively simple to calibrate compared to energy-balance models, but results are reasonable as seen in this study.

5.5.3. Streamflow

The simulated streamflow hydrographs at the outlet of the catchment for the calibration and validation period are always underestimated compared to the observed ones as seen in Figures 5.14 and 5.15. The model does not generate enough volume in the streams during the snowmelt high flow season, while during the fall season, baseflow is overestimated. The main peaks of the simulated hydrographs are always too low, but the timing is reasonable. In general, hydrograph simulations with R correlation values between 0.81 and 0.86 for the calibration and validation periods are reasonable, but the Nash Sutcliffe R^2 values between 0.53 and 0.53 less so. These are also lower than those achieved by Kuras (2011) using DHSVM for modeling the same watershed. DHSVM, compared to MIKE SHE, is able to include forest roads into the model, routing water through a road ditch-culvert system into the closest stream crossing a forest road. In MIKE SHE (without forest roads) this water would be delayed in reaching the streams as

a consequence of not being routed into them, while traveling longer through the unsaturated soil zone. Some of the water might even recharge the saturated zone and then leave the model through boundary outflow (see Figure 5.8 and Section 5.4.3). It is also possible that some of the water could evaporate from the soils while traveling through them. All these factors related to forest roads could result in lower peaks during the high flow season and some delayed increased flows of water in the streams during later summer/fall baseflow season as seen for the hydrograph simulations in this study. General consensus (i.e., Kuras, 2006; Bowling and Lettenmaier, 1997; Gucinski et al., 2001; Beckers and Alila, 2004) suggests that forest road segments draining directly into streams will speed up the catchment response time and contribute more to the rising limb of the hydrograph, potentially increasing peak discharge. Stream culverts are designed to allow water flow from streams to pass under the surface of a road, and it is quite common for streams to have ditch system flows of forest roads channelled directly into them. It has to be mentioned that in some cases, as seen in a recent study published by Kuras et al. (2012) for the same UPC 241 catchment, certain road segments can route intersecting subsurface runoff out of the watershed, thereby reducing streamflow for that volume. This indicates that the missing forest roads in the MIKE SHE model may not be the only cause for poor performance in reproducing measured streamflow and shallow soil water levels.

Another possible reason for underestimating streamflow volume in the model could be missing winter precipitation factors, which were not applied to the meteorological input data for the MIKE SHE model as was done by Kuras (2011). Not including those factors in snow dominated catchments may partially account for

discrepancies in simulated versus measured streamflows, and may be responsible for underestimating peaks of the streamflow hydrograph during the spring snowmelt peak flow season, as seen for all of the calibration and validation years in this study (see Figures 5.14 and 5.15).

Aside from these three possible reasons for partially underestimating streamflow volume, in general, the MIKE SHE code might not perform well for simulating a headwater catchment in mountainous steep terrain with significant elevation gain if the deep bedrock aquifer is included in the model, as is the case in this study. Models such as MIKE SHE, which have the ability to simulate the terrestrial portion of the hydrologic cycle, often depend on a formulation of the unsaturated flow equation (i.e., Richards' equation) that has a high degree of parameter uncertainty when groundwater recharge is calculated (Scanlon et al., 2002). Furthermore integrated surface flow, infiltration, and subsurface flow is computationally intensive for mountainous terrain, considering the steepness of the ground topography and a wide range in unsaturated zone thickness (i.e., shallow water table in the lower riparian zones and a potentially deep water table in the higher and steeper hillslope areas close to the ridge of the watershed (Smerdon et al., 2009). To account for a deep water table in the high areas, the unsaturated soil zone settings had to include bedrock below the soil layers up to a depth of 200 m, the same depth as for the saturated zone, as mentioned earlier (see Sections 5.3.6 and 5.4.2 and Figure 5.7). In the high elevation portions of the watershed, the simulated deep water table is up to 150 m deep (see blue to green zones in Figure 5.34 a and b). Those high steep areas are the primary recharge zones, meaning that the infiltrating water has to

percolate a long way through fractured bedrock to reach the phreatic surface. Through this vadose zone, there is a high degree of parameter uncertainty. Infiltration through discrete fractures is not simulated in MIKE SHE, nor is the process well understood (e.g., Glass et al., 1995; Evans et al., 2001; Bodvarsson et al., 2003). The bedrock itself was assigned a uniform hydraulic conductivity, which may in fact be spatially variable. Moreover, the van Genuchten parameters for unsaturated flow, especially those for fractured bedrock, are highly uncertain as there have been few studies of this kind to test ranges of potential values. As mentioned earlier, MIKE SHE always assigns a flow boundary along the outline of the watershed and then calculates the flow across this boundary automatically (see Table 5.9). This flux is active in the saturated zone, so as the depth of the saturated zone changes, so does the flux. The amount of water leaving the model through the bedrock within the saturated zone is a fixed amount (see Table 5.9), but the amount that leave the upper bedrock and soil varies depending on how thick the saturated zone is within the unsaturated zone column. If the flux is too high in the model, then too much water will be lost across this boundary and less water will be available for streamflow. However, streamflow appeared to be relatively insensitive to minor changes in this specified flux.

5.5.4. Groundwater levels

Simulated deep bedrock groundwater levels (see Figures 5.17 to 5.19), which have not previously been evaluated at the UPC 241 catchment, were in general lower than observed levels in all three bedrock wells. Water levels in W1 and W2 were just slightly

lower (~1.5 m below observed), while water levels in W3 were about 3 m below observed.

Overall, the deep water table surface reflects the shape of the topography (see Figure 5.2 and Figure 5.16), but is deeper at high elevation compared to low elevation. At low elevation, the deep water table appears to coincide with the shallow soil water table and is near surface (see Figure 5.33 a, b). Whereas in the higher and steeper areas of the watershed the saturated zone water is only located within the bedrock. This interface is located somewhere within the orange zones seen in Figure 5.34 a, b, and deepens during low flow season. The simulated water table of the saturated zone does not change a much during low flow season in summer.

During calibration of the water table in the saturated zone, K and Ss were varied in an attempt to raise the water table in the wells, but this did not work for a range of reasonable values. An important point to mention is that the observed values are from fractured bedrock and are monitored in a well that may only sample one or two main fractures. So, it could be that these wells are not giving a reasonable large-scale representation of the actual groundwater level. In W3, there might have been the added problem that it is close to a main fracture that was not included into the model. The bedrock is represented in MIKE SHE as homogenous geological medium and is simulated as an equivalent porous medium (DHI, 2007). The simulated groundwater response also totally misses the fall rain events observed in W1 and W2 (Figures 5.17 and 5.18). It peaks in spring and goes through one continuous recession, rather than two peaks and two recessions. A possible reason for this response might be the K value for the bedrock,

which is assigned as a homogenous distribution across the entire model domain. As such, it may not represent the actual local scale responses at a well due to intersecting fractures, which will respond very quickly to rain events. To see these rapid responses, a discrete fracture network would be needed, but this would require a discrete fracture simulation code and the model itself would be highly parameterized. A better representation of the fracture rock using an equivalent porous media code (such as MIKE SHE) could involve generating a heterogeneous bedrock K distribution using FRED software (Golder, 2006) (see Chapter 4.3.4) and importing it into MIKE SHE, although the well responses may be no better. Nonetheless, this approach is recommended for future study.

As mentioned earlier, the flux out of the model across the lower edges of the domain was also invariant with time. In reality, the flux would likely be greater during the snowmelt period. Allowing more water out of the model during the snowmelt period relative to the summer low flow period could affect the dynamics of the deep groundwater levels (levels, timing and shape of the simulated graphs). Therefore, future work could attempt to assign a more realistic time varying flux across this boundary.
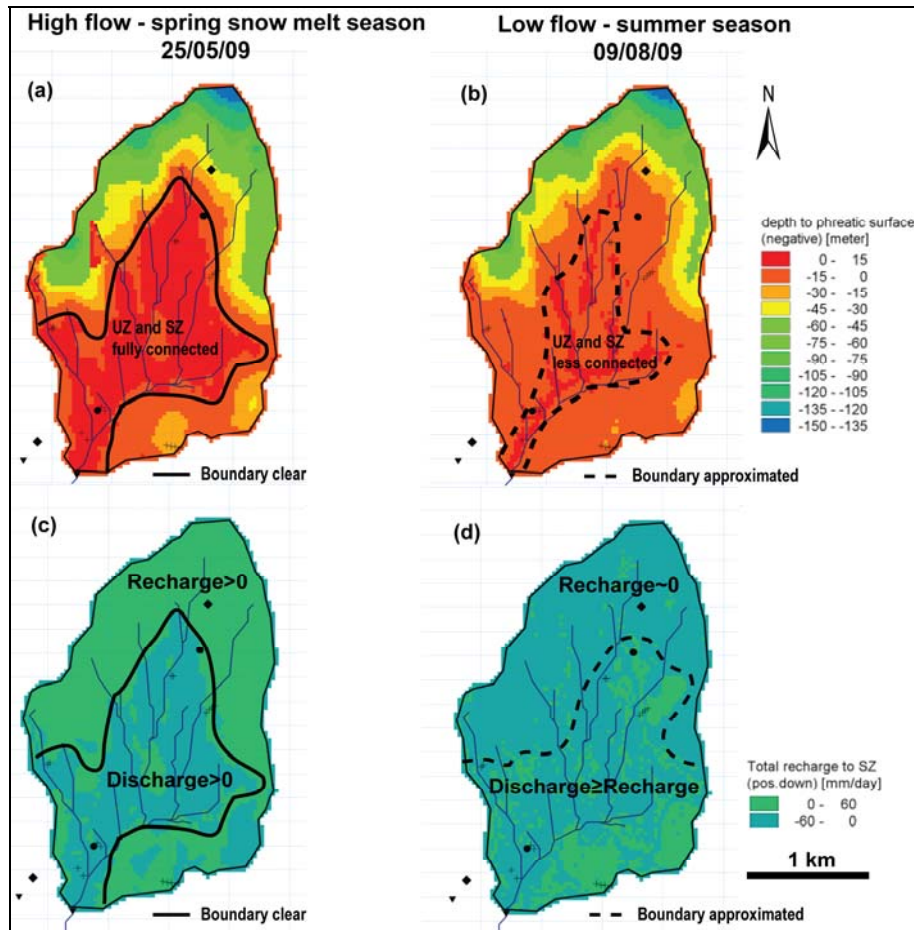
Figure 5.34. Simulation results of depth to phreatic zone for (a) a high flow spring snowmelt season, and (b) a low flow summer season. Resulting recharge to saturated zone is shown during (c) the high flow spring snowmelt season and (d) the low flow summer season.

5.5.5. Soil water levels

For the soil piezometers, the timing of responses for the simulated pressure heads in the unsaturated zone overall were quite good, in comparison to the actual elevations, which were poorly simulated. This resulted in poor model performance as indicated by the R correlation values and the Nash Sutcliffe R^2 values for some piezometers (see Table 5.8).

Piezometers of transects L1 and L3 had simulated responses that were too high. These are all located in the low elevation, less steep areas of the catchment, in riparian zones or riparian/hillslope interface zones, and in close vicinity to the main creek (see Figure 5.2).

Piezometers of transects U1 and U3 (see Figure 5.2), which are located in the higher and steeper elevation of the catchment, had simulated responses that were too high. These piezometers are all located close to the main creek within its riparian zone or interface zone, with exception of one piezometers (P15) of transect U3, which is located on the hillslope (its response was too low).

Piezometers of transects L2 and U2 (see Figure 5.2) are located in hillslopes with exception of two piezometers in transect U2, which are located in the interface zone and the riparian zone. All three piezometers of transect L2 are located in unlogged forest, whereas all four piezometers of U2 are located in a clearcut. The simulated responses at piezometers within L2 and U2 were too low. These are located at greater distance from main creeks.

The piezometers with overestimated pressure heads (i.e., P5 and P7 in Figure 5.21 and 5.22 or Figure 5.27 and Figure 5.28) show horizontal flat lines in the simulated pressure head graph, indicating that water from the saturated zone discharges and connects with soil water in the unsaturated zone and finally seeps to the surface as indicated by the red areas in Figure 5.33 (a, b). As indicated by Kuras (2011), these lower riparian zone areas have demonstrated a strong interaction between streams and subsurface soil water. It is also suspected that these low elevation areas of the watershed

are influenced by upwelling deep groundwater flows from the fractured bedrock as evidenced by the modeling results of this study, which included a deep aquifer in the model (see Figure 5.16). As mentioned earlier, uncertainty in the possible local changes in hydraulic conductivity within the mountain block and a high degree of parameter uncertainty overall, especially for the van Genuchten parameters for the bedrock, could influence infiltration rates to the saturated zone in the higher areas. If the simulated recharge to bedrock is too high in the high elevation areas, this may lead to an overestimation of discharge to the riparian zones of the watershed, resulting in an overestimation of the simulated pressure heads in the piezometers located in those areas.

Simulated underestimated pressure heads mostly occur in piezometers located in higher and steeper hillslope elevations of the watershed (i.e., P2 and P10 in Figure 5.20 and 5.23 or Figure 5.26 and Figure 5.29). As the specified flux boundaries were located along the bottom edges of the model domain, it is unlikely that the boundary would affect the soil water levels at high elevation, particularly given the fact that the low elevation piezometers generally had higher simulated heads. If all piezometers had underestimated heads, then a too high specified flux may be the cause. But this does not appear to be the case. Another possible explanation for the underestimation of pressure heads, which also ties to the underestimated streamflow results, is the inability to incorporate logging roads and ditches in MIKE SHE, which affect how water moves as overland flow or flow within the unsaturated zone.

It is also important to mention that microtopography at some locations might be inadequately represented by the model, since simulated pressure heads in the soil

piezometers are averaged over an entire 30 x 30 m pixel. In general, the soil water dynamics in the riparian zones closely follow runoff dynamics of the stream and areas further upslope are a propagation of this trend (Seibert et al., 2003; Kuras et al., 2011). However, the MIKE SHE simulations did not appear to capture this trend. This inability of the models not capturing this trend, where soil water levels further away from the streams are often independent of streamflow, has raised a topic of concern in catchment hydrology modeling (Seibert et al., 2003).

5.5.6. Groundwater recharge and groundwater outflow

Groundwater recharge to the saturated zone was estimated from the model water balance. Recognizing the uncertainty in the model results, on average, the unsaturated zone contributes 29 mm/year (4% of precipitation) to recharge to the saturated zone, although this recharge amount varies considerably from year to year and ranges from -51 to +104 mm/year. For years when the recharge is negative, EVT tends to be a greater proportion of precipitation and there is a coinciding lower volume of water that discharges to rivers from the unsaturated zone, although discharge from the saturated zone as baseflow remains relatively unchanged as does the fixed groundwater outflow from the saturated zone. The lower recharge amount results in a loss of water from storage in the saturated zone, and a lower water table (results not shown). The groundwater outflow from unsaturated zone changes only slightly due to the lowering of the water table.

Groundwater outflow was fixed in the simulation because there was no other way to simulate the outflow, apart from assigning variable heads along the southern boundary. But these are unknown and are required to change with time, so they are difficult to assign. Nevertheless, the sensitivity analysis did constrain the values to some degree. The results suggest that outflow from the watershed via deep groundwater flow is a likely component of the water balance; however, the exact amount remains uncertain. Certainly, including outflow did not significantly affect streamflow or the other components of the water balance because of the low values assigned. A potential estimate for groundwater outflow (partitioned between the unsaturated zone and the saturated zone in the model is roughly 40 mm/year (or 6% of precipitation).

Figure 5.34 showed simulated maps of the depth to the phreatic zone and recharge/discharge to/from the saturated zone for the high flow spring snowmelt season and the low flow summer season for the calibration year of 2009. During high flow season, a clear boundary between the recharge area and the discharge area can be drawn (Figure 5.34c). The higher and steeper areas in the watershed clearly serve as recharge zones (green color) and the lower riparian areas as discharge zones (blue color) where deep groundwater connects with the perched water tables in the unsaturated soil zone. The additional water forms surface runoff, resulting in a phreatic surface that lies millimetres above the surface creating fully saturated swampy areas as indicated through the red zones in map (a). Those fully saturated swampy areas do occur in areas close to the watershed outlet, but they might not be simulated correctly. They appear to be too

large and reach too far up into the watershed. Possible reasons for overestimated pressure heads in certain piezometers of the riparian zone were already discussed in Section 5.5.5.

During summer low flow season simulated recharge is nearly zero in the upper areas of the watershed and in the lower areas discharge nearly equals recharge, although discharge is still generally higher than recharge (Figure 5.34d). This indicates that unsaturated and saturated zones interact less during low flow season, while for the high flow season those zones seem to fully connect. Drawn boundaries for the low flow season (see Figure 5.34b,d) are approximated and are not as clear as for the high flow season (see Figure 5.34a,c). As a main result, recharge to the saturated zone seems to predominantly occur during high flow spring snowmelt season.

6. Conclusions

6.1. DFN hydraulic conductivity study for fractured bedrock

The first main part of this study, the DFN modeling, presented an approach for informally upscaling small scale, outcrop fracture data to derive estimates of larger scale fractures (lineaments) that could be used to estimate mountain block K_{mb} at the regional scale. Small scale fractures were mapped at outcrop locations throughout the study area using a scanline approach. Large scale lineaments were mapped using orthophotos and LANDSAT imagery. Those remote sensing techniques do not give information on dip angles and dip directions, which are needed for the large scale discrete fracture network (DFN) model generation. Due to the similarity of fracture sets occurring at both scales throughout the study area, unknown dip angles and directions were taken from the small scale fracture sets for generating the large scale DFN models. In an extensional tectonic setting, small scale fractures and large scale lineaments from the same tectonic event should show similar orientation patterns.

Outcrop scale simulated DFN K_m values are on the order of 10^{-8} to 10^{-7} m/s with the highest values in the high density zone (Table 4.5). Similar patterns can be seen for the outcrop scale specific storage values (Ss_m), which are on the order of 10^{-4} m^{-1}. Considering the directional K_m values for the outcrop scale models, the highest values were found in N-S (y) direction. E-W (x) and T-B (z) values were similar. This distribution is the same for all three zones.

For the large scale lineament mountain block DFN models, the estimated K_{mb} values are the highest for the high density zone and the lowest for the low density zone, ranging from about 10^{-8} to 10^{-7} m/s (Table 4.6). In the low and medium density zones, the K_{mb} values are similar too, although very slightly lower than, the outcrop scale values. In the high density zone, the K_{mb} values appear to be roughly 3 times as great as the K_m values, suggesting perhaps a greater influence of larger scale fractures when fracture density is high. Specific storage values for the mountain block (Ss_{mb}) follow the same pattern, ranging from about 10^{-3} to 10^{-2} m^{-1} for the high density zone. Compared to the outcrop scale models for the same zones, the Ss_{mb} values are about one order of magnitude higher for the large scale models. The directional K_{mb} behaviour is the same as the outcrop scale with highest values in N-S (y) direction. This direction coincides with the dominant strike direction of fractures and lineaments throughout the study area and is similar to the main strike orientation (N-S) of the Okanagan Valley Fault Zone (OVFZ).

This component of the research offers a new approach for estimating fractured bedrock permeability at the regional scale. The most surprising outcome was the overall similarity of K_m and K_{mb} values at the two scales (outcrop and lineament) as well as the agreement of these values with an average value for crystalline rock from a recent compilation of regional scale K values from modeling (Gleeson et al., 2011). Further testing of this methodology in other study areas, particularly using more than one pumping test to constrain K_{eff}, would strengthen these observations.

6.2. MIKE SHE modeling study – bedrock recharge estimation

The second part of this study presented a modeling exercise using the MIKE SHE/MIKE 11 code for estimating recharge from a small snowmelt dominated headwater catchment to the surrounding mountain block. Simulated conductivity (K) and storativity (S) values from the DFN modeling carried out in the first part of this study were used in MIKE SHE as input data for the saturated zone aquifer settings. MIKE SHE had not previously been tested in steep mountainous terrain. In these mountain settings, the water table is found at depth in the fractured bedrock forming the steep hillslope areas of the catchment, while in the lower and flatter riparian zones of the catchment, the water table is very shallow and groundwater discharges to the overlying soils and streams contributing to baseflow. The MIKE SHE modeling exercise carried out as part of this study is one of the first in catchment hydrology modeling within steep mountainous terrain in which the lower boundary of the model is not treated as impermeable, and in which recharge to the deep bedrock and discharge to the surrounding mountain block can be estimated.

Due to the large number of model parameters, this complex model was very hard to calibrate and time intensive. Hydraulic conductivity values of the soils and bedrock within both the unsaturated zone and the saturated zone needed to be adjusted simultaneously in order to calibrate streamflow, soil pressure heads and the deep water table. MIKE SHE modeling performance results are reasonable for the streamflow and shed more light on the connection between the bedrock and the overlying soils in a mountainous headwater catchment.

The model results (simulated streamflow and water levels) and the water balance are highly uncertain due to model error, calibration error, and most importantly, uncertainty in the model input parameters. Recognizing this uncertainty, the average water balance results over the 5 year calibration/validation period indicate recharge to the bedrock of 4% of the annual precipitation. This is the amount of water that typically is not simulated in a surface water model that treats the bedrock as impermeable. In this study, this deep bedrock recharge was permitted to leave the model domain (catchment boundary) through specified flux boundaries placed at the bottom edges of the catchment. It should be noted that in real systems, this deep groundwater flow may leave the catchment across the base of the catchment and contribute to cross-catchment flow. In this study, this outward flux was assigned to the catchment edges (to the left and right of the main stream and partway up the catchment (Figure 5.8). The estimated flux of deep groundwater leaving the catchment and contributing groundwater to the mountain block outside of the catchment (approx.. 6% of the annual water budget) suggests that a tight water balance, as is often assumed in catchment hydrology modeling, may not reflect the real dynamics of the different water sources in a headwater catchment and their interaction. This study demonstrated that there is a strong connection between the bedrock and the soils, especially in the lower riparian zones of the headwater catchment. The study also delineated reasonable recharge and discharge zones during high- and low flow seasons. The 6% outflow to the surrounding mountain block is an estimated value in that a specified outward flux was assigned to all layers in the model along the bottom edges of the model domain. The flux was estimated through model calibration. Of this

6%, approximately 2% leaves the catchment through the saturated zone boundary and 4% leaves through the saturated layers that lie within the model unsaturated zone. In MIKE SHE the unsaturated zone is set to a pre-defined depth, and it may become saturated at different times during a simulation. As such, outflow across the unsaturated zone boundary varies seasonally depending on the depth to the water table, but the flux per model layer was fixed in the simulation and was invariant in time despite the likely time varying nature of the actual flux. At the lower edges of the model, where this outflow is assigned, both soil and bedrock layers are present; therefore, some flow may exit via the soil zone if it becomes saturated. This could lead to an overestimation of the flux in the unsaturated zone because generally the soil zone in a catchment would drain toward the main stream and not exit the catchment. In the saturated zone, outflow was similarly defined; however, in this case, only the bedrock comprises the saturated zone, so there is confidence that the water exiting the model is through the bedrock. The total amount leaving through the bedrock in the saturated zone likely represents a small amount of the water budget, but nonetheless it is important and should not be neglected because this water contributes to deep groundwater flow entering lower elevation catchments down the mountain side, and ultimately may contribute to mountain block recharge at the valley bottom. Of course there is considerable uncertainty in the actual outflow across catchment boundary, but this study has shown that if such a flux is included in a model, small changes in this flux do not have a large impact on the streamflow. On the one hand, this suggests that surface water models (that do not include deep groundwater flow) can be reasonably calibrated without consideration for deep groundwater loss from the

catchment. On the other hand, including some deep groundwater loss will not significantly impact streamflow and soil water calibration, but will perhaps be more realistic, particularly if cross-catchment flow is important.

The overall model performance for streamflow was not strong, but nevertheless compared well to that of other studies. However, the model performance for the saturated zone (water table response within the deep bedrock) was generally poor. This was due to a simulated time lag relative to observed and a slightly different shape of the water table response. But the general trend of highest water tables during the spring snowmelt season and lowest during the baseflow season in summer were well captured by the model. Seasonal changes in the water table height during the fall due to fall rain events were not adequately captured by the model. The saturated zone hydraulic conductivity and storativity values were assigned as homogenous throughout the entire bedrock aquifer and do not account for discrete fractures that might significantly influence the response in an observation well. Small scale fracture zones as well as larger scale lineaments might locally increase recharge rates and lead to very fast responses in deep bedrock wells where they intersect those features. Assuming a homogenous medium for the aquifer is most likely responsible for the delayed simulated water table fluctuations and its different shape. In addition, high parameter uncertainty, especially for the van Genuchten parameters of the bedrock within the unsaturated zone likely affect the modeling results.

Overall, MIKE SHE was able to simulate the general trends of all components of the water budget for a complex setting in a mountainous headwater catchment within a fractured bedrock mountain block, but the detailed responses were poor. The study

contributed to a better understanding of groundwater processes in snowmelt dominated mountainous headwater catchments and how groundwater interacts with surface water. These results are important for future modeling exercises that might consider the entire mountain block for estimating mountain block recharge (MBR) to valley bottom aquifers, for example the Okanagan Valley, but also other large mountainous valleys throughout the world.

6.3. Future opportunities

The calibrated MIKE SHE model of the UPC 241 headwater catchment is ideally suited to future modeling. In particular, future research could include an investigation of different climate change scenarios and different land use scenarios due to intense forest logging and their impact on components of the water balance. The use of climate change projections, based on downscaled global climate model results, has been done for climate change scenario groundwater modeling in the lower areas of the Okanagan valley bottom aquifer by Toews and Allen (2009a,b), but no groundwater-focused modeling studies have been attempted for the upper snowmelt dominated recharge zones of the mountain block.

Results of this MIKE SHE modeling study could also be useful for future modeling exercises of similar mountainous catchments, but in more developed regions where deep bedrock groundwater is pumped and used as a water supply. Since MIKE SHE has been shown to reasonably simulate the interaction between deep groundwater and shallow subsurface water, different pumping scenarios of bedrock wells could be

simulated and the impacts on streamflow, changes in soil water levels, and the altering of the fully saturated swampy or even flooded areas in the riparian zones could be investigated.

Future work at the UPC 241 catchment could also include the use and importation of a dual porosity grid for the saturated zone, which accounts for discrete fracture/lineament zones and the fractured matrix in between. Such heterogeneous permeability grids for fractured aquifers can be constructed with a DFN modeling software, for example FRED, which was used in the first main part of this study for estimating fractured bedrock permeability at different scales.

Bibliography

Allen, D.M., and Michel, F.A., 1998, Evaluation of Multi-Well Test Data in a Faulted Aquifer Using Linear and Radial Flow Models: Ground Water, v. 36, no. 6, p. 938-948, doi: 10.1111/j.1745-6584.1998.tb02100.x.

Allen, R.G., Pereira, L.S., Raes, D., and Smith, M., 1998, Crop evapotranspiration. Guidelines for Computing Crop Water Requirements: FAO Irrigation and Drainage Paper, no. 56. FAO: Rome; 328p.

Anderson, S.P., Dietrich, W.E., Montgomery, D.R., Torres, R., Conrad, M.E., and Loague, K., 1997, Subsurface flow paths in a steep, unchanneled catchment: Water Resources Research, v. 33, no. 12, p. 2637-2653, doi: 10.1029/97WR02595.

AWSET version 3.0, 2002, Cranfield University Silsoe.

Baecher, G.B., and Lanney, N.A., 1978, Trace length biases in joint surveys: Proc. 19[th]U.S. Symposium on Rock Mechanics, Mackay School of Mines, p. 56-65.

Bodvasson, G.S., Wu, Y.S., and Zhang, K., 2003, Development of discrete flow paths in unsaturated fractures at Yucca Mountain: Journal of Contaminant Hydrology, v. 62-63, p. 23-42.

Bosch, J.M. and Hewlett, J.D., 1982, A review of catchment experiments to determine the effect of vegetation changes on water yield and evapotranspiration: Journal of Hydrology, v. 55, Issue: 1-4, p. 3-23, doi: 10.1016/0022-1694(82)90117-2.

Boussinesq, J., 1872, "Théorie des ondes et des remous qui se propagent le long d'un canal rectangulaire horizontal, en communiquant au liquide contenu dans ce canal des vitesses sensiblement pareilles de la surface au fond": Journal de Mathématiques Pures et Appliquées. Deuxième Série 17: 55–108

Boussinesq, J., 1872, Essai sur la theorie des eaux courantes: Mem. Pres. Acad. Sci., Paris, v. 23, 680p.

Boutt, D.F., Diggins P., and Mabee, S., 2010, A field study (Massachusetts, USA) of the factors controlling the depth of groundwater flow systems in crystalline fractured rock terrain: Hydrogeology Journal v. 18, p. 1839-1854.

Bouwer, H., and Rice, R.C., 1976, A Slug Test for Determining Hydraulic Conductivity of Unconfined Aquifers With Completely or Partially Penetrating Wells: Water Resources Research, v. 12, no. 3, p. 423-428.

Brown, R.L., and Journeay, J.M., 1987, Tectonic denudation of the Shuswap metamorphic terrane of southeastern British Columbia: Geology, v. 15, p. 142-146, doi: 10.1130/0091-7613(1987)15<142:TDOTSM>2.0.CO;2.

Caine, J.S., Evans, J.P., and Forster, C.B., 1996, Fault zone architecture and permeability structure: Geology, v. 24, no. 11, p. 1025-1028, doi: 10.1130/0091-7613(1996) 024<1025:FZAAPS>2.3.CO;2.

Caine, J.S., and Tomusiak, S.R.A., 2003, Brittle structures and their role in controlling porosity and permeability in a complex Precambrian crystalline-rock aquifer system in the Colorado Rocky Mountain Front Range: Geological Society of America Bulletin, v. 115, no. 11, p. 1410, doi: 10.1130/B25088.1.

Caine, J.S., Manning, A.H., Verplanck, P.L., Bove, D.J., Kahn, K.G., and Ge, S., 2006, Well Construction Information, Lithologic Logs, Water Level Data, and Overview of Research in Handcart Gulch, Colorado: An Alpine Watershed Affected by Matalliferous Hydrothermal Alteration: U.S. Geological Survey Open-File Report 2006–1189, http://pubs.usgs.gov/of/2006/1189/downloads/pdf/of06-1189_508.pdf (03/04/2009).

Clague, J.J., 1991, Quaternary glaciation and sedimentation. In: Gabrielse, H., Yorath, C. J. (eds.), Geology of the Cordilleran Orogen in Canada, no. 4, in Geology of Canada, chap. 12, Geological Survey of Canada, p. 419–434.

Cohen, S., and Kulkarni, T., 2001, Water management and climate change in the Okanagan Basin, Project A206, Environment Canada and University of British Columbia. Submitted to the Adaptation Liason Office, Climate Change Action Fund: Natural Resources Canada, Ottawa, 75 pp.

Cohen, S., Neilsen, D., and Welbourn, R., 2004, Expanding the dialogue on climate change and water management in the Okanagan Basin, British Columbia, Final report, January 1, 2002 to June 30, 2004: Environment Canada, Agriculture and Agri-Food Canada, University of British Columbia, 230 pp.

Constantz, J., 1998, Interaction between stream temperature, streamflow, and groundwater exchanges in alpine streams: Water Resources Research, v. 34, Issue: 7, p. 1609-1615, doi: 10.1029/98WR00998.

Cooper, H.H., and Jacob, C.E., 1946, A generalized graphical method for evaluating formation constants and summarizing well field history. Transactions: American Geophysical Union, v. 27, p. 526-534.

Degnan, J.R., ad Clark, S.F. Jr., 2002, Fracture-Correlated Lineaments at Great Bay, Southeastern New Hampshire: U.S. Geological Survey Open-File Report 02-13.

Dershowitz, W., Carvahlo, J., and Foxford, T., 1995, FracMan/RockBlock, Discrete fracture rock block stability analysis, version 1.0: Redmond, Washington, Golder Associates, User Documentation.

Dershowitz, W.S., and Herda, H.H., 1992, Interpretation of fracture spacing and intensity, In: Tillerson, J.R., and Wawersik, W.R. (eds.), Proc. 33rd U.S. Symposium on Rock Mechanics, Balkema, Rotterdam, p. 757-766.

DHI, 2005, MIKE 11: A Modeling System for Rivers and Channels-Short Introduction and Tutorial, Danish Hydraulic Institute: Denmark.

DHI, 2007, MIKE SHE User Manual, Volume 2: Reference Guide, Danish Hydraulic Institute: Denmark.

Environment Canada, Accessed 2006, National Climate Data and Information Archive: http://climate.weatheroffice.ec.gc.ca/Welcome_e.html (23/07/2010).

ERSI (Environmental Systems Research Institute, Inc.), 2008, ArcGIS, version 9.3: Redlands, California.

Evans, D.D., Rasmussen, T.C., and Nicholson, T.J., 2001, Flow and Transport Through Unsaturated Fractured Rock: An Overview, second edition: Geophysical Monograph, AGU, 196 pp.

Eyles, N., Mullins, H.T., and Hine, A.C., 1990, Thick and fast: Sedimentation in a Pleistocene fiord lake of British Columbia, Canada: Geology, v. 18, p. 1153-1157.

Feth, J.H., 1964, Hidden Recharge: U.S. Geological Survey, Water Resources Division, Menlo Park, California, p. 14-17.

Fisher, R.A., 1953, Dispersion on a sphere: Proceedings of the Royal Society London, ser. A, v. 217, p. 295-305.

Fisher, H.N., and Tester, J.W., 1980, The Pressure Transient Testing of a Manmade Fractured Geothermal Reservoir: An Examination of Fracture Versus Matrix Dominated Flow Effects: United States Department of Energy Informal Report LA-8535-MS, http://www.osti.gov/energycitations/servlets/purl/5049862-qCLMlD/native/5049862.pdf, doi: 10.2172/5049862.

Fisher, N.I., Lewis, T., and Embleton, B.J.J., 1987, Statistical analysis of spherical data: Cambridge University Press, 329 p.

Flint, R.F., 1935, "White-silt" deposits in the Okanagan Valley, British Columbia: Royal Society of Canada, Transactions 29, p. 107–114.

Flint, A.L., Flint, L.E., Bodvarsson, G.S.W., Kwicklis, E.M., and Fabryka-Martin, J., 2001, Evolution of the conceptual model of unsaturated zone hydrology at Yucca Mountain, Nevada: Journal of Hydrology, v. 247, p. 1-30, doi: 10.1016/S0022-1694(01)00358-4.

Folger, P.F., 1995, A multidisciplinary study of the variability of dissolved 222Rn in groundwater in a fractured crystalline rock aquifer and its impact on indoor air [Ph.D. thesis]: Golden, Colorado School of Mines, U.S.A., 181 p.

Forster, C., and Smith, L., 1988, Groundwater flow systems in mountainous terrain: 2. Controlling factors: Water Resources Research, v. 24, no. 7, p. 1011-1023, doi: 10.1029/WR024i007p01011.

Freer, J., McDonnell, J.J., Beven, K.J., Peters, N.E., Burns, D.A., Hooper, R.P., Aulenbach, B., Kendall, C., 2002, The role of bedrock topography on subsurface storm flow: Water Resources Research, v. 38, Issue: 12, doi: 10.1029/2001WR000872.

Freeze, R.A., and Witherspoon, P.A., 1967, Theoretical analysis of regional groundwater flow: 2. Effect of water-table configuration and subsurface and permeability variation: Water Resources Research, v. 3, no. 2, p. 623-634, doi: 10.1029/WR003i002p00623.

FRED (FracManReservoirEdition), 2006, version 6.54: Redmond, Washington, Golder Associates.

Fulton, R.J., 1972, Stratigraphy of the unconsolidated fill and Quaternary development of north Okanagan Valley: GSC Paper 72-8, Part B, Geological Survey of Canada.

Fulton, R.J., and Smith, G.W., 1978, Late Pleistocene stratigraphy of south-central British Columbia: Canadian Journal of Earth Sciences, v. 15, p. 971–980.

Geiger, S., Niessner, J., Matthai, S.K., and Helmig, R., 2006, Three-phase flow simulations in discrete fracture networks: AGU Fall Meeting, Oral Presentation.

Glass, R.J., Nicholl, M.J., and Tidwell, V.C., 1995, Challenging models for fluid flow in unsaturated, fractured rock through exploration of small scale processes: Geophysical research Letters, v. 22, no. 11, p. 1457-1460, doi: 10.1029/95GL01490.

Gleeson, T., and Manning, A.H., 2008, Regional groundwater flow in mountainous terrain: Three-dimensional simulations of topographic and hydrogeologic controls: Water Resources Research, v. 44, W10403, 16 pp., doi: 10.1029/2008WR006848.

Gleeson, T., and Novakowski, K., 2009, Identifying watershed-scale barriers to groundwater flow: Lineaments in the Canadian Shield: Geological Society of America Bulletin, v. 121, no. 3/4, p. 333-347, doi: 10.1130/B26241.1.

Gleeson, T., Smith, L., Moosdorf, N., Hartmann, J., Dürr, H.H., Manning, A.H., van Beek, L.P.H., and Jellinek, A.M., 2011, Mapping permeability over the surface of the Earth: Geophysical Research Letters v. 38: L02401., doi:10.1029/2010GL045565

Gringarten, A.C., and Witherspoon, P.A., (1971), A method of analyzing pump test data from fractured aquifers: Percolation through Fissured Rock: Deutsche Gesellschaft fuer Erd- und Grundbau, Stuttgart, Germany, T3B1-3B8.

Hammersmark, C.T., Rains, M.C., and Mount, J.F., 2008, Quantifying the hydrological effects of stream restoration in a montane meadow, Northern California, USA: River Research and Applications, v.24, p. 735-753, doi: 10.1002/rra.1077.

Haneburg, W.C., 1995, Steady state groundwater flow across idealized faults: Water Resources Research, v. 31, p. 1815-1820, doi: 10.1029/95WR01178.

Harte, P.T., and Winter, T.C., 1995, Simulations of Flow in Crystalline Rock and Recharge from Overlying Glacial Deposits in a Hypothetical New England Setting: GroundWater, v. 33, no. 6, p. 953-964, doi: 10.1111/j.1745-6584.1995.tb00041.x.

Haught, D.R.W., and Meerveld, H.J., 2011, Spatial variation in transient water table responses: differences between an upper and lower hillslope zone: Hydrological Processes, v. 25, Issue: 25, Special Issue: SI, p. 3866-3877, doi: 10.1002/hyp.8354.

Herschy, R.W., 1995, Streamflow Measurement (2nd edition): E & FN Spon, London, UK, 524p.

Hope, G., 2001, Soil descriptions for Penticton Creek experimental watersheds, report, B.C. Ministry of Forests, Kamloops Region, Kamloops, B.C., Canada, 19 pp.

Hvorslev, M.J., 1951, Time Lag and Soil Permeability in Ground-Water Observations: Bull. no. 36, Waterways Exper. St., Corps of Engineers, U.S. Army, Vicksburg, Mississippi, p. 1-50.

Johnson, B.J., 2006, Extensional shear zones, granitic melts, and linkage of overstepping normal faults bounding the Shuswap metamorphic core complex, British Columbia: Geological Society of America Bulletin, v. 118, p. 336-382, doi: 10.1130/B25800.1.

Keith, S.J., 1980, Mountain front recharge: Regional Recharge Research for Southwest Alluvial Basins, edited by L.G. Wilson et al., pp. 4-1 to 4-44, Chapter 4, Tuscon, University of Arizona.

Kirkby, M., 1988, Hillslope runoff processes and models: Journal of Hydrology, v. 100, Issue: 1-3, p. 315-339, doi: 10.1016/0022-1694(88)90190-4.

Koike, K., and Ichikawa, Y., 2006, Spatial correlation structures of fracture systems for deriving a scaling law and modeling fracture distributions: Computers & Geosciences, v. 32, p. 1079-1095, doi: 10.1016/j.cageo.2006.02.013.

Kosugi, K., Fujimoto, M., Karsura, S., Kato, H., Sando, Y., and Mizuvama, T., 2011, Localized bedrock aquifer distribution explains discharge from a headwater catchment: Water Resources Research, v. 47, W07530, doi: .1029/2010WR009884.

Kristensen, K.J., and Jensen, S.E., 1997, A model for estimating actual evapotranspiration from potential evapotranspiration: Nordic Hydrology, v. 6, no. 3, p. 170-188, doi: 10.2166/nh.1975.012.

Kruseman, G.P., and de Ridder N.A., 1990, Analysis and evaluation of pumping test data, Second Edition: International Institute for Land Reclamation and Improvement, Publication no. 47, Wageningen, The Netherlands, 377 p.

Kuras, P.K., 2006, Forest Road and Harvesting Effects on the Hydrology of A Snow-Dominated Catchment in South-Central British Columbia [M.S. thesis]: Vancouver, University of British Columbia, Canada, 159 p.

Kuras, P.K., Alila, Y., Weiler, M., Spittlehouse, D., and Winkler, R., 2011, Internal catchment process simulation in a snow-dominated basin: performance evaluation with spatiotemporally variable runoff generation and groundwater dynamics: Hydrological Processes, v.25, p. 3187-3203, doi: 10.1002éhyp.8037

Kuras, P.K., Alila, Y., and Weiler, M., 2012, Forest harvesting effects on the magnitude and frequency of peak flows can increase with return period: Water Resources Research, v. 48, W01544, p. 1-19, doi: 10.1029/2011WR01705.

Lerner, D.N., Issar, A.S., and Simmers, I., 1990, Groundwater recharge: a guide to understanding and estimating natural recharge: International Association of Hydrogeologists, Kenilworth, Rep 8, 345 pp.

Lesemann, J.E., Brennand, T.A., and Shaw, J., 2005, A revised conceptual model for growth and decay of the Cordilleran Ice Sheet in British Columbia, Canada, unpublished.

Lowry, C.S., Deems, J.S., Loheide, S.P., and Lundquist, J.D., 2010, Linking snowmelt-derived fluxes and groundwater flow in a high elevation meadow system, Sierra Nevada Mountains, California: Hydrological Processes, v. 24, Issue: 20, p. 2821-2833, doi: 10.1002/hyp.7714.

Mabee, S.B., Hardcastle, K.C., and Wise, D.U., 1994, A method of collecting and analyzing lineaments for regional-scale bedrock aquifer studies: Ground Water v. 32, no. 6, p. 884-894.

MacAulay, H.A., Hobson, G.D., 1972, A seismic refraction survey of the north Okanagan and south Shuswap Valleys: GSC Paper 72-8, Part A, Geological Survey of Canada.

Mackie, D.C., 2002, An integrated structural and hydrogeologic investigation of the fracture system in the Upper Cretaceous Nanaimo Group, Southern Gulf Islands, British Columbia [M.S. thesis]: Burnaby, Simon Fraser University, Canada, 358 p.

Mailloux, B.J., Person, M., Kelley, S., Dunbar, N., Cather, S., Strayer, L., and Hudleston, P., 1999, Tectonic controls on the hydrogeology of the Rio Grande Rift, New Mexico: Water Resources Research, v. 35, p. 2641-2659, doi: 10.1029/1999WR900110.

Manning, A.H., and Solomon, D.K., 2003, Using noble gases to investigate mountain-front recharge: Journal of Hydrology v. 275, p. 194-207.

Manning, A.H., and Solomon, D.K., 2005, An integrated environmental tracer approach to characterizing groundwater circulation in a mountain block: Water Resources Research v. 41, W12412.

Mantua, N.J., Hare, S.R., Zhang, Y., Wallace, J.M., and Francis, R.C., 1997, A Pacific interdecadal climate oscillation with impacts on salmon production: Bulletin of the Meteorological Society, v. 78, p. 1069-1079.

Massey, N.W.D., MacIntyre, D.G., Desjardins, P.J., and Cooney, R. T., 2005, Digital geology map of British Columbia, whole province: Geofile 2005-1, Ministry of Energy and Mines.

Mau, D.P., and Winter, T.C., 1997, Estimating ground-water recharge from streamflow hydrographs for a small mountain watershed in a temperate humid climate, New Hampshire, USA: Ground Water, v. 35, Issue: 2, p. 291-304, doi: 10.1111/j.1745-6584.1997.tb00086.x.

Maurer, D.K., Prudic, D.E., Berger, D.L., and Thodal, C.E., 1999, Sources of water flowing into basin-fill aquifers underlying Carson City, Nevada: Geological Society of America, Annual Meeting, Abstracts with Programms, 31(7), 87.

Mayo, A.L., Morris, T.H., Peltier, S., Petersen, E.C., Payne, K., Holman, L.S., Tingey, D., Fogel, R., Black, B.J., and Gibbes, R.D., 2003, Active and inactive groundwater flow systems: Evidence from a stratified mountainous terrain: Geological Society of America Bulletin, v. 115, p. 1456-1472, doi: 10.1130/B25145.1.

McCabe, G.J., Clark, M.P., and Hay, L.E., 2007, Rain-On-Snow Events in the Western United States: American Meteorological Society, p. 319-328.

McGlynn, B.L., McDonnell, J.J., and Brammer, D.D., 2002, A review of the evolving perceptual model of hillslope flowpaths at the Maimai catchments, New Zealand: Journal of Hydrology, v. 257, p. 1-26.

Merritt, W.S., Alila, Y., Barton, M., Taylor, B., Cohen, S., and Neilsen, D., 2006, Hydrologic response to scenarios of climate change in sub watersheds of the Okanagan basin, British Columbia: Journal of Hydrology, v. 326, Issues 1-4, p. 79-108, doi: 10.1016/j.jhydrol.2005.10.025.

Miller, I., Lee, G., and Dershowitz, W., 1995, Mafic, Matrix/fracture interaction code with heat and solute transport, version 1.6: Redmond, Washington, Golder Associates, User Documentation.

Monger, J., and Price, R., 2002, The Canadian Cordillera: Geology and Tectonic Evolution: CSEG Recorder, p. 17-36.

Montgomery, D.R., Dietrich, W.E., Torres, R., Anderson, S.P., Heffner, J.T., and Loague, K., 1997, Hydrologic response of a steep, unchanneled valley to natural and applied rainfall: Water Resources Research, v. 33, no. 1, p. 91-109.

Nash, I.E., and Sutcliffe, I.V., 1970, River flow forecasting through conceptual models: Journal of Hydrology, v. 10, p. 282-290.

Nasmith, H., 1962, Late glacial history and surficial deposits of the Okanagan Valley, British Columbia: Bulletin 46, BC Ministry of Energy, Mines and Petroleum Resources.

Nippgen, F., McGlynn, B.L., Marshall, L.A., and Emanuel, R.E., 2011, Landscape structure and climate influences on hydrologic response: Water Resources Research, v. 47, W12528, doi: 10.1029/2011WR011161.

National Research Council, 1996, Rock Fractures and Fluid Flow: Contemporary Understanding and Applications: Committee on Fracture Characterization and Fluid Flow, National Academy Press, Washington, D.C., 551 pp.

Obedkoff, W., 1973, Regionalization of sub-basin hydrology: Preliminary Report no. 38, prepared for the Okanagan Study Committee.

Oda, M., 1985, Permeability tensor for discontinuous rock masses: Geotechnique, v. 35, p. 483-495.

Oehman, J., and Niemi, A., 2003, Upscaling of fracture hydraulics by means of an orientated correlated stochastic continuum model: Water Resources Research, v. 39, no. 10, 1277, 13 pp., doi: 10.1029/2002WR001776.

Ohlmacher, G.C., 1999, Structural domains and their potential impact on recharge to intermontane-basin aquifers: Environmental and Engineering Geoscience, v. 1, no. 1, p. 61-71.

Okanagan Basin Water Board (OBWB), 2010, Water Supply & Demand Project: http://www.obwb.ca/water_supply_demand/ (23/07/2010).

Okanagan Valley Tree Fruit Authority, 1995, Tree Fruit Suitability in the Okanagan, Similkameen, and Creston Valleys.

Penna, D., .J., Tromp-van Meerveld, H.J., Gobbi, A., Borga, M., and Dalla Fontana, G., 2011, The influence of soil moisture on threshold runoff generation processes in an alpine headwater catchment: Hydrology and Earth System Sciences, v. 14, Issue: 3, p. 689-702, doi: 10.5194/hess-15-689-2011.

Peters, D.L., Buttle, J.M., Taylor, C.H., and LaZerte, B.D., 1995, Runoff production in a forested, shallow soil, Canadian Shield basin: Water Resources Research, v. 31, no. 5, p. 1291-1304.

Rahim, E.A., Yusoff, I., Jafri, A.M., Othman, Z., and Ghani, A.A., 2012, Application of MIKE SHE modelling system to set up a detailed water balance computation: Water and Environmental Journal, p. 1-14, doi:10.1111/j.1747-6593.2012.00309.x

Rahiman, T.I.H., and Pettinga, J.R., 2008, Analysis of lineaments and their relationship in Neogene fracturing: Geological Society of America Bulletin v. 120, no. 11-12, p. 1544-1555.

Rawls, W.J., Brakensiek, D.L., and Logsdon, S.D., 1993, Predicting saturated hydraulic conductivity utilizing fractal principles: Soil Sci. Soc. Am. J., v. 57, p. 1193-1197.

Renard, P., Glenz, D., and Mejias, M., 2009, Understanding diagnostic plots for well-test interpretation: Hydrogeology Journal, v. 17, p. 589-600.

Rohrbaugh Jr, M.B., Dunne, W.M., and Mauldon, M., 2002, Estimating fracture trace intensity, density, and mean length using circular scan lines and windows: AAPG Bulletin, v. 86, no. 12, p. 2089-2104.

Sahoo, G.B., Ray, C., and De Carlo, E.H., 2004, Calibration and validation of a physically distributed hydrological model, MIKE SHE, to predict streamflow at high frequency in a flashy mountainous Hawaii stream: Journal of Hydrology, v. 327, Issues 1-2, p. 94-109.

Scanlon, B.R., Healy, R.W., and Cook, P.G., 2002, Choosing appropriate techniques for quantifying groundwater recharge: Hydrogeology Journal, v. 10, no. 1, p. 18-39, doi: 10.1007/s10040-001-0176-2.

Schlumberger Water Services, 2010, AquiferTest Pro v. 4.2: Waterloo, Ontario.

Schnorbus, M., and Alila, Y., 2004, Forest harvesting impacts on the peak flow regime in the Columbia Mountains of southeastern British Columbia: An investigation using long term numerical modeling: Water Resources Research, v. 40, W05205, p. 1-16, doi: 10.1029/2003WR002918.

Seibert, J., Bishop, K., Rodhe, A., and McDonnel, J.J., 2003, Groundwater dynamics along a hillslope: A test of the steady state hypothesis: Water resources Research, v.39, no. 1, 1014, p. 1-9, doi: 10.1029/2002WR001404.

Shaw, J., Munro-Stasiuk, M., Sawyer, B., Beaney, C., Leseman, J.E., Musacchio, A., Rains, B., and Young, R.R., 1999, The Channeled Scabland: Back to Bretz?: Geology, v. 27, no. 7, p. 605-608.

Singhal, R.B.S., and Gupta, R.P., 1999, Applied Hydrogeology of Fractured Rocks: Kluwer, Dordrecht, The Netherlands.

Smerdon, B.D., Allen, D.M., Berg, M.A., and Grasby, S.E., 2009, An approach for predicting groundwater recharge in mountainous watersheds: Journal of Hydrology, v. 365, Issues 3-4, p. 156-172, doi: 10.1016/j.jhydrol.2008.11.023.

Snow, D.T., 1968, Rock fracture spacings, openings, and porosities: J. Soil Mech. Found. Div., ASCE v. 94, p. 73-91.

SpheriStat for windows, 1998, version 2.2.: Pangea Scientific, Brockville Ontario, Canada.

Starzec, P., and Andersson, J., 2002, Probabilistic predictions regarding key blocks using stochastic discrete fracture networks-example from a rock cavern in south-east Sweden: Bulletin of Engineering Geology and the Environment, v. 61, no. 4, p. 363-378, doi: 10.1007/s10064-002-0154-5.

Statistics Canada, 2001 Census, Population and Dwelling Counts: http://www12.statcan.gc.ca/english/census01/products/standard/popdwell/Tables.cfm (15/08/2010).

Statistics Canada, 2003, Human Activity and the Environment: Annual Statistics, Catalogue no. 16-201-XIE (15/08/2010).

Sultana, Z., and Coulibaly, P., 2010, Distributed modelling of future changes in hydrological process of Spencer Creek watershed: Hydrological Processes, v. 25, Issue: 8, p. 1254-1270, doi: 10.1002/hyp.7891.

Surrette, M., Allen, D.M. and Journeay, M., 2008, Regional evaluation of hydraulic properties in variably fractured rock using a hydrostructural domain approach: Hydrogeology Journal, v. 16, no.1, p. 11-30, doi: 10.1007/s10040-007-0206-9.

Surrette, M., and Allen, D.M., 2008, Quantifying heterogeneity in fractured sedimentary rock using a hydrostructural domain approach: Geological Society of America Bulletin, v. 120, no. 1/2, p. 225–237, doi: 10.1130/B26078.1.

Tani, M., 1997, Runoff generation processes estimated from hydrological observations on a steep forested hillslope with a thin soil layer: Journal of Hydrology, v. 200, Issue: 1-4, p. 84-109, doi: 10.1016/S0022-1694(97)00018-8.

Taque, C., and Grant, G.E., 2009, Groundwater dynamics mediate low-flow response to global warming in snow-dominated alpine regions: Water Resources Research, v. 45, W07421, doi: 10.1029/2008WR007179.

Tempelman-Kluit, D., and Parkinson, D., 1986, Extension across the Eocene Okanagan crustal shear in southern British Columbia: Geology, v. 14, no. 4, p. 318-321, doi: 10.1130/0091-7613(1986)14<318:EATEOC>2.0.CO;2.

Terzaghi, R.D., 1965, Sources of error in joint surveys: Geotechnique, v. 15, p. 287-304.

Theis, C.V., 1935, The relation between the lowering of the piezometric surface and the rate of discharge of a well using ground-water storage. Transactions: American Geophysical Union, v. 16, p. 519-524.

Thomson, J.R., Strenson, H.R., Gavin, H., and Refsgaard, A., 2004, Application of the coupled MIKE SHE/MIKE11 modelling system to a lowland wet grassland in southeast England: Journal of Hydrology, v. 293, p. 151-179.

Thyer, M., Beckers, J., Spittlehouse, D., Alila, Y., and Winkler, R., 2004, Diagnosing a distributed hydrologic model for two high-elevation forested catchments based on detailed stand- and basin-scale data: Water Resources Research, v. 40, W01103, 20 pp., doi:10.1029/2003WR002414.

Toews, M.W., 2007, Modelling the effects of climate change on groundwater in Oliver, British Columbia [Ph.D. thesis]: Vancouver, Simon Fraser University, Canada, 201 p.

Toews, M.W., and Allen, D.M., 2009, Simulated Response of Groundwater to Predicted Recharge in a Semi-Arid Region Using A Scenario of Modelled Climate Change: Environmental Research Letters, 4, 035003. doi.org/10.1088/1748-9326/4/3/035003

Toews, M.W., and Allen, D.M., 2009, Evaluating Different GCMs for Predicting Spatial Recharge in an Irrigated Arid Region: Journal of Hydrology, 374: 265-281. doi:10.1016/j.jhydrol.2009.06.022

Toth, J., 1963, A Theoretical Analysis of Groundwater Flow in Small Drainage Basins: Journal of Geophysical Research, v. 68, no. 16, p. 4795-4812.

Trenberth, K.E., and Hurrel, J.W., 1994, Decadal atmosphere-ocean variations in the Pacific: Climate Dynamics, v. 9, p. 303-319.

Tromp- van Meerfeld, H.J., Peters, N.E., and McDonnel, J.J., 2007, Effect of bedrock permeability on subsurface stormflow and the water balance of a trenched hillslope at the Panola Mountain Research Watershed, Georgia, USA: Hydrological Processes, v. 21, p. 750-769, doi: 10.1002/hyp.6265.

Tromp-van Meerveld, H.J., James, A.L., McDonnell J.J., et al., 2008, A reference data set of hillslope rainfall-runoff response, Panola Mountain Research Watershed, United States: Water Resources Research, v. 44, Issue: 6, W06502, doi: 10.1029/2007WR006299.

Tsujimura, M., Onda, Y., and Ito, J., 2001, Stream water chemistry in a steep headwater basin with high relief: Hydrological Processes, v. 15, p. 1847-1858, doi: 10.1002/hyp.243.

Vanderburgh, S., and Roberts, M.C., 1996, Depositional systems and seismic stratigraphy of a Quaternary basin: north Okanagan Valley, British Columbia: Canadian Journal of Earth Sciences, v. 33, p. 917-927.

Van Genuchten, M.T., 1996, Estimating unsaturated soil hydraulic properties from tension disc infiltrometer data by numerical inversion: Water Resources Research, v. 32, No. 9, p. 2683-2696.

Viviroli, D., Dürr H.H., Messerli, B., Meybeck, M., and Weingartner, R., 2007, Mountains of the world, water towers for humanity: typology, mapping, and global significance: Water Resources Research v. 43, W07447.

Voeckler, H., and Allen, D.M., In press., Estimating regional-scale fractured bedrock hydraulic conductivity using discrete fracture network (DFN) modeling: Hydrogeology Journal.

Wallace, J.M., and Gutzler, D.S., 1981, Teleconnections in the Geopotential Height Field during the Northern Hemisphere Winter: Monthly Weather Review, American Meteorological Society, v. 109, p. 784-812.

Wenninger, J. Uhlenbrock, S., Tilch, N., and Leibundgut, C., 2004, Experimental evidence of fast groundwater responses in a hillslope/floodplain area in the Black Forest Mountains, Germany: Hydrological Processes, v. 18, Issue: 17, p. 3305-3322, doi: 10.1002/hyp.5686.

Whitaker, A., Alila, Y., Beckers, J., and Toews, D., 2003, Application of the Distributed Hydrology Soil Vegetation Model to Redfish Creek, British Columbia: model evaluation using internal catchment data: Hydrological Processes, v. 17, p. 199-224, doi: 10.1002/hyp.1119.

Whitfield, P.H., and Spence, C., 2011, Estimates of Canadian Pacific Coast runoff from observed streamflow data: Journal of Hydrology, v. 410, Issue: 3-4, p. 141-149, doi: 10.1016/j.jhydrol.2011.05.057.

Wigmosta, M.S., Vail, L.W., and Lettenmaier, D.P., 1994, A distributed hydrology-vegetation model for complex terrain: Water Resources Research, v. 30(6), p. 1665-1679.

Wilson, J.L., and Guan, H., 2004, Mountain-block hydrology and mountain-front recharge, In Groundwater Recharge in a Desert Environment: The Southwestern United States, Water Science and Applications Series, v. 9, edited by Hogan J.F., Phillips, F.M., and Scanlon, B.R., American Geophysical Union: Washington, DC, p. 113-137.

Winkler, R.D., Spittlehouse, D.L., and Golding, D.L., 2005, Measured differences in snow accumulation and melt among clearcut, juvenile, and mature forests in southern British Columbia: Hydrological Processes, v. 19, p. 51–62

Winkler, R., Spittlehouse, D., Allen, D., Redding, T., Giles, T., Hope, G., Alila, Y., and Voeckler, H., 2008, The Upper Penticton Creek Watershed Experiment, Integrated Water Resource Research: One Watershed – One Water Conference Proceedings, Kelowna, BC, Canada, p. 38-47.

Wohl, E., 2000, Mountain Rivers: American Geophysical Union, Washington, DC, 320 p.

Wolf, J., Barthel, R., and Braun, J., 2008, Modeling Ground Water Flow in Alluvial Mountainous Catchments on a Watershed Scale: GroundWater, v. 46, no. 5, p. 695-705, doi: 10.1111/j.1745-6584.2008.00456.x.

Zahm, C.K., and Hennings, P.H., 2009, Complex fracture development related to stratigraphic architecture: Challenges for structural deformation prediction, Tensleep Sandstone at the Alcova anticline, Wyoming: AAPG Bulletin, v. 93, no. 11, p. 1427-1446, doi: 10.1306/08040909110.

Zhang, Z., Wang, S., Sun, G., McNulty, S.G., Zhang, H., Li, J., Zhang, M., Klaghofer, E., and Strauss, P., 2008, Evaluation of the MIKE SHE model for application in the Loess Plateau, China: Journal of the American Water Resources Association, v. 44, no. 5, doi: 10.1111/j.1752-1688.2008.00244.x.

Appendices

Appendix A: Data Collection, Processing and Interpretation

A.1. Scanline outcrop scale fracture data

Outcrop #: 1

One or more separate scanlines

			Dip Dir. [°]	Dip [°]	Outcrop Face Dimensions [m]:
Photo #:	1	approximate surface orientation:	245	76	y = 11
					z = 4

Scanline b)

Waypoint	E [m]	N [m]	Elev. [m]	SL length [m]	Trend [°]	Plunge [°]	Direction
1b	313039	5498098	446	3.1	233	-77	U-D

DATA

Fracture SL Intersection [m]	Dip Dir [°]	Dip [°]	Trace Length strike [m]	Trace Length dip [m]	Upper Termin.	Lower Termin.	Aperture [mm]	Primary roughness	Secondary roughness	Fillings	Movement	Comment
1.01	246	63		1.9	U	B	0	u	s	none	none	1.01
1.49	252	30		2.3	U	B	0	u	r	none	none	1.49
1.79	265	35		6.65	U	U	2.44	u	r	none	none	1.79
2.25	273	54		2.8	U	B	0	u	r	none	none	2.25
2.81	251	39		1.8	U	B	1.73	u	r	none	none	2.81

One or more separate scanlines					Dip Dir. [°]	Dip [°]	Outcrop Face Dimensions [m]:		
Photo #:	2	approximate surface orientation:			265	25	x =20		
							y =10		

Scanline c)

Waypoint	E [m]	N [m]	Elev. [m]	SL length [m]	Trend [°]	Plunge [°]	Direction
1c	0313048	5498099	447	13	320	-10	S-N

DATA

Fracture SL Intersection [m]	Dip Dir [°]	Dip [°]	Trace Length strike [m]	Trace Length dip [m]	Upper Termin.	Lower Termin.	Aperture [mm]	Primary roughness	Secondary roughness	Fillings	Movement	Comment
0.38	330	16	3.66		U	U	0	u	r	none	none	
0.81	145	81	2.62		T	U	0	p	s	none	none	
1.04	156	53	1.91		T	B	0	p	r	none	none	
1.25	290	50	3.7		U	B	0	u	r	none	none	
3.23	145	82	2.15		U	U	0	st	r	none	none	
3.86	40	87	1.1		U	U	0	p	r	none	none	
7.02	140	46	2.95		T	B	0	p	r	none	none	
9.49	255	81	6.2		B	T	0	p	r	none	none	
10.44	266	86	1.82		B	B	0	p	r	none	none	
11.09	268	82	0.97		A	B	0	p	s	none	none	
11.24	268	85	3.5		B	B	0	p	s	none	none	
11.59	271	86	4.6		B	B	0	p	s	none	none	
12.52	265	59	2.73		B	B	0	p	s	none	none	

Outcrop #	2
General Data	
Date	2
Name Surveyor	17-May-06
Character/dimension of outcrop	HV/MAB
near or away of faulzone?	Walls (A: 2.5mX1.5m) (B:3mX4.5m): Top about 10m away from walls (C,D: 4.5mX2m)
Lithology description	
Rocktype	Quartzofeldspathic gneiss
colour fresh/weathered	Fresh: whitish grey with bands of large porphyoblasts (2 cm). Bands are white with hornblende. Weathered: dark grey, abundant lichen and moss.
homegeneous vs heterogeneous	Heterogeneous
sample taken?	
Structures	
Foliation/bedding (Dip Dir./Dip)	nr
Liniation (Trend/plunge)	nr
folds (amplitude, wavelength, fold axis, fold plane)	
fault (width, trace, gouge, orientation)	
Shear zone (width, trace)	
Rock mass description	
Block shape	co
Block size	ms
weathering class	II
seepage (presence/absence)	absent

Outcrop #: 2

One or more separate scanlines

			Dip Dir. [°]	Dip [°]	Outcrop Face Dimensions [m]:
Photo #:	3	approximate surface orientation:	285	83	y =2.5
					z =1.5

Scanline a)

Waypoint	E [m]	N [m]	Elev. [m]	SL length [m]	Trend [°]	Plunge [°]	Direction
2a	0318517	5489386	1056	4.5	197	-18	N-S

DATA

Fracture SL Intersection [m]	Dip Dir [°]	Dip [°]	Trace Length strike [m]	Trace Length dip [m]	Upper Termin.	Lower Termin.	Aperture [mm]	Primary roughness	Secondary roughness	Fillings	Movement	Comment
1.11	310	75		0.7	T	U	1.89	u	r	none	none	
1.53	81	83		1	U	T	1.34	p	r	none	none	
1.91	32	69		0.69	B	U	0	p	r	none	none	
2.32	72	80		0.39	B	B	0	u	r	none	none	
2.95	60	81		0.38	T	B	0.66	p	r	none	none	
3.47	40	62		0.49	T	T	0	p	s	none	none	
3.62	38	65		0.19	T	B	0	p	s	none	none	
3.86	36	64		0.42	T	T	0	p	s	none	none	
4.18	37	57		0.55	B	T	0	p	s	none	none	
4.48	39	64		0.64	B	B	0.67	p	s	none	none	

One or more separate scanlines

			Dip Dir. [°]	Dip [°]
Photo #:	3	approximate surface orientation:	200	70

Outcrop Face Dimensions [m]:
x =4.5
z = 3

Scanline b)

Waypoint	E [m]	N [m]	Elev. [m]	SL length [m]	Trend [°]	Plunge [°]	Direction
2b	0318516	5489389	1058	3.1	185	-70	U-D

DATA

Fracture SL Intersection [m]	Dip Dir [°]	Dip [°]	Trace Length strike [m]	Trace Length dip [m]	Upper Termin.	Lower Termin.	Aperture [mm]	Primary roughness	Secondary roughness	Fillings	Movement	Comment
0.32	194	17	2.5		T	U	0	p	r	none	none	
0.75	192	19	1.5		T	A	0	p	r	none	none	
1.38	200	20	3.5		U	U	0	p	r	none	none	
1.59	198	25	3.5		U	B	0	p	r	none	none	
2.05	194	28	3.1		B	U	0	p	r	none	none	
2.5	198	25	3.5		U	B	0	p	r	none	none	

One or more separate scanlines

			Dip Dir. [°]	Dip [°]	Outcrop Face Dimensions [m]:
Photo #:	4	approximate surface orientation:	255	12	x =4.5
					y = 2

Scanline c)

Waypoint	E [m]	N [m]	Elev. [m]	SL length [m]	Trend [°]	Plunge [°]	Direction
2c	0318522	5489402	1059	2.45	255	12	W-E

DATA

Fracture SL Intersection [m]	Dip Dir [°]	Dip [°]	Trace Length strike [m]	Trace Length dip [m]	Upper Termin.	Lower Termin.	Aperture [mm]	Primary roughness	Secondary roughness	Fillings	Movement	Comment
0.23	74	82	0.8		U	B	0	p	r	none	none	
0.36	90	69	1.05		H	B	0	p	s	none	none	
0.49	82	68	0.6		B	B	0	p	s	none	none	
0.71	74	88	1.01		B	B	0	p	s	none	none	
0.82	72	86	1.75		B	B	0	p	s	none	none	
1.28	77	70	1.85		B	U	0	p	r	none	none	
1.48	72	74	2.89		U	B	0	p	r	none	none	
1.49	78	81	2.13		B	U	0	p	r	none	none	
1.57	79	77	3.94		A	U	0	p	r	none	none	
1.67	77	81	1.53		B	B	0	p	r	none	none	
1.73	295	89	0.63		U	A	0	p	r	none	none	
1.87	294	88	0.69		U	B	0	p	r	none	none	
2.43	292	87	1.03		U	U	0	p	r	none	none	

One or more separate scanlines

			Dip Dir. [°]	Dip [°]	Outcrop Face Dimensions [m]:
Photo #:	4	approximate surface orientation:	295	8	x =4.5
					y = 2

Scanline d)

Waypoint	E [m]	N [m]	Elev. [m]	SL length [m]	Trend [°]	Plunge [°]	Direction
2d	0318521	5489395	1059	2.2	301	-12	E-W

DATA

Fracture SL Intersection [m]	Dip Dir [°]	Dip [°]	Trace Length strike [m]	Trace Length dip [m]	Upper Termin.	Lower Termin.	Aperture [mm]	Primary roughness	Secondary roughness	Fillings	Movement	Comment
0.23	292	88	0.66		B	B	0	p	r	none	none	
0.5	295	84	0.61		B	A	0	p	r	none	none	
0.68	292	85	0.78		B	B	1.95	p	r	Quartz	none	
0.72	297	83	0.61		B	B	1.34	p	r	Quartz	none	
0.83	296	83	2.89		T	B	2.98	p	r	Quartz	none	
0.92	110	60	0.53		B	B	0	p	r	none	none	
1.31	130	81	0.54		B	B	0	p	r	none	none	
1.57	71	68	0.44		B	B	0	p	r	none	none	
1.6	296	79	0.43		B	B	0	p	r	none	none	
1.65	294	70	0.48		B	B	0	p	r	none	none	
2.08	290	85	0.91		U	T	2.34	p	r	Quartz	none	

Outcrop #	3
General Data	
Date	18-May-06
Name Surveyor	MAB/HV
Character/dimension of outcrop	Surface (A,B; 5mx26m). Wall (C; 1.5X7m)
near or away of faulzone?	
Lithology description	
Rocktype	Quartzofeldspathic gneiss
colour fresh/weathered	Fresh: Medium grained, light grey with reddish staining. Few augen, no hornblende. Weathered: Medium to dark grey, moderate lichen.
homegeneous vs heterogeneous	homogeneous
sample taken?	
Structures	
Foliation/bedding (Dip Dir./Dip)	005/24
Liniation (Trend/plunge)	296/10
folds (amplitude, wavelength, fold axis, fold plane)	
fault (width, trace, gouge, orientation)	
Shear zone (width, trace)	
Rock mass description	
Block shape	b
Block size	I
weathering class	II
seepage (presence/absence)	absent

Outcrop #: 3

One or more separate scanlines

			Dip Dir. [°]	Dip [°]
Photo #:	3	approximate surface orientation:	309	20

Outcrop Face Dimensions [m]:

x = 5

y = 26

Scanline a)

Waypoint	E [m]	N [m]	Elev. [m]	SL length [m]	Trend [°]	Plunge [°]	Direction
3a	0316953	5484694	819	11	302	-20	E-W

DATA

Fracture SL Intersection [m]	Dip Dir [°]	Dip [°]	Trace Length strike [m]	Trace Length dip [m]	Upper Termin.	Lower Termin.	Aperture [mm]	Primary roughness	Secondary roughness	Fillings	Movement	Comment
0.42	130	73	1.55		T	B	1.11	u	r	n	n	
0.6	131	70	1.03		T	A	0	p	r	n	n	
0.67	304	80	0.62		T	A	0	p	r	n	n	
1.85	300	83	1		U	B	0	st	r	n	n	
2.14	300	75	1.47		B	B	0	st	r	n	n	
2.39	303	83	1.96		U	T	0	st	r	n	n	
2.79	135	70	1.07		T	T	0	p	r	n	n	
3.3	118	68	2.51		B	T	0	p	r	n	n	

Fracture SL Intersection [m]	Dip Dir [°]	Dip [°]	Trace Length strike [m]	Trace Length dip [m]	Upper Termin.	Lower Termin.	Aperture [mm]	Primary roughness	Secondary roughness	Fillings	Movement	Comment
3.4	300	82	0.6		B	B	0	st	r	n	n	
3.55	130	70	0.95		B	A	0	p	r	n	n	
4.32	115	68	2.08		T	T	0	p	r	n	n	
4.89	112	68	2.27		T	T	0	p	r	n	n	
6.24	111	66	2.57		B	B	0	p	r	n	n	
6.7	107	76	2.65		B	B	0	p	r	n	n	
7.48	110	68	5.53		B	B	0	p	r	n	n	
8.13	98	72	6.3		B	U	0	u	r	n	n	
8.76	290	87	0.57		T	B	0	p	r	n	n	
8.89	281	76	4.57		B	T	0	p	r	n	n	
9.31	294	76	6.2		B	T	0	p	r	n	n	
9.51	300	84	0.75		A	B	0	p	r	n	n	
9.55	115	75	6.8		U	B	0	p	r	n	n	
9.74	292	82	1.19		B	B	0	u	r	n	n	
10.25	299	80	0.8		B	B	0	p	r	n	n	
10.81	296	82	0.43		T	T	0	p	r	n	n	

				Dip Dir. [°]	Dip [°]	Outcrop Face Dimensions [m]:		
Photo #:	5	approximate surface orientation:		309	20	x =5		
						y = 26		

Scanline b)

Waypoint	E [m]	N [m]	Elev. [m]	SL length [m]	Trend [°]	Plunge [°]	Direction
3b	0316943	5484693	817	11	41	-1	S-N

DATA

Fracture SL Intersection [m]	Dip Dir [°]	Dip [°]	Trace Length strike [m]	Trace Length dip [m]	Upper Termin.	Lower Termin.	Aperture [mm]	Primary roughness	Secondary roughness	Fillings	Movement	Comment
0.4	206	76	3.32		T	T	0	u	r	n	n	
0.82	182	81	0.77		T	B	0	u	r	n	n	
1.21	202	75	1.54		B	T	0	u	r	n	n	
1.83	16	63	0.77		B	B	0	p	r	n	n	
3.55	203	81	7.75		B	T	0	st	r	n	n	
6.17	186	88	7.76		B	T	0	st	r	n	n	
9.17	200	89	8.96		U	U	0	u	r	n	n	
9.59	56	58	1.52		T	A	0	u	r	n	n	
10.2	20	83	3.46		T	T	0	st	r	n	n	
10.62	19	79	0.37		B	B	0	p	r	n	n	

One or more separate scanlines

			Dip Dir. [°]	Dip [°]	Outcrop Face Dimensions [m]:
Photo #:	6	approximate surface orientation:	119	71	x = 7
					z = 1.5

Scanline c)

Waypoint	E [m]	N [m]	Elev. [m]	SL length [m]	Trend [°]	Plunge [°]	Direction
3c	0316970	5484687	819	1.7	130	-87	U-D

DATA

Fracture SL Intersection [m]	Dip Dir [°]	Dip [°]	Trace Length strike [m]	Trace Length dip [m]	Upper Termin.	Lower Termin.	Aperture [mm]	Primary roughness	Secondary roughness	Fillings	Movement	Comment
0.79	298	12	0.87		U	T	0	st	r	n	n	
0.9	305	10	0.44		T	T	3.41	p	r	n	n	
0.92	18	28	0.63		B	U	0	p	r	n	n	
1.11	309	10	2.55		T	B	0	u	r	n	n	
1.54	300	14	0.66		T	U	0	st	r	n	n	

265

Outcrop #	4
General Data	
Date	18-May-06
Name Surveyor	HV/MAB
Character/dimension of outcrop	Wall (A,B: 1m x3m x 1m(top), Wall (C: 1.6m x 2.2m), surface about 15m away (D: 2.0m x 1.8m)
near or away of faulzone?	
Lithology description	
Rocktype	Quartzofeldspathic gneiss
colour fresh/weathered	Fresh: light grey with wihtish and grey bands, some bands ave concentration of augen (0.5cm). In main body, few augen. Weathered: medium to dark grey, some pinkish staining along same plane as gneissic banding
homegeneous vs heterogeneous	Homogeneous
sample taken?	
Structures	
Foliation/bedding (Dip Dir./Dip)	010/13
Liniation (Trend/plunge)	295/14
folds (amplitude, wavelength, fold axis, fold plane)	
fault (width, trace, gouge, orientation)	
Shear zone (width, trace)	

Rock mass description	
Block shape	t
Block size	ms
weathering class	II
seepage (presence/absence)	absent

Outcrop #: 4

One or more separate scanlines

			Dip Dir. [°]	Dip [°]	Outcrop Face Dimensions [m]:
Photo #:	7	approximate surface orientation:	223	77	x =1

y = 3

z =1

Scanline a)

Waypoint	E [m]	N [m]	Elev. [m]	SL length [m]	Trend [°]	Plunge [°]	Direction
4a	0318370	5485620	957	4	121	-2	W-E

DATA

Fracture SL Intersection [m]	Dip Dir [°]	Dip [°]	Trace Length strike [m]	Trace Length dip [m]	Upper Termin.	Lower Termin.	Aperture [mm]	Primary roughness	Secondary roughness	Fillings	Movement	Comment
0.35	309	81		0.61	U	U	0	st	s	n	n	0.35
0.38	127	89		0.57	B	U	0	u	r	n	n	0.38
0.43	308	88		0.4	U	T	0	p	r	n	n	0.43
0.75	131	85	0.83U	0.65	U	U	0	p	r	n	n	0.75
0.79	296	84	0.83U	0.27	U	T	0	p	r	n	n	0.79
0.84	299	83	0.83U	0.46	U	T	0	p	r	n	n	0.84
0.91	308	79	0.83U	0.62	U	U	0	p	r	n	n	0.91
1.02	138	89	0.88U	0.55	U	B	0	p	r	n	n	1.02
1.07	304	83	0.88U	0.8	U	U	0	p	s	n	n	1.07
1.24	316	87		0.74	B	U	0	p	s	n	n	1.24
1.29	305	74		0.93	T	U	0	p	s	n	n	1.29

Fracture SL Intersection [m]	Dip Dir [°]	Dip [°]	Trace Length strike [m]	Trace Length dip [m]	Upper Termin.	Lower Termin.	Aperture [mm]	Primary roughness	Secondary roughness	Fillings	Movement	Comment
1.62	134	85	1.05U	1.21	U	U	0	p	r	n	n	1.62
1.81	287	81		0.76	B	U	0	p	r	n	n	1.81
1.96	317	86	.68U	0.85	U	U	0	p	r	n	n	1.96
2.11	312	89	.78U	0.69	U	U	0	p	r	n	n	2.11
2.52	314	89	.30B	1.12	U	U	0.72	p	r	n	n	2.52
3.24	316	82		0.9	T	U	0	p	r	n	n	3.24
3.72	129	82		0.3	T	T	0	p	r	n	n	3.72

One or more separate scanlines

				Dip Dir. [°]	Dip [°]
Photo #:	7		approximate surface orientation:	223	77

Outcrop Face Dimensions [m]:
x = 1
y = 3
z = 1

Scanline b)

Waypoint	E [m]	N [m]	Elev. [m]	SL length [m]	Trend [°]	Plunge [°]	Direction
4b	0318370	5485617	957	1	218	-86	U-D

DATA

Fracture SL Intersection [m]	Dip Dir [°]	Dip [°]	Trace Length strike [m]	Trace Length dip [m]	Upper Termin.	Lower Termin.	Aperture [mm]	Primary roughness	Secondary roughness	Fillings	Movement	Comment
0.19	194	11	1.29		B	T	0	p	r	n	n	
0.24	25	2	1.12		U	T	0	u	r	n	n	
0.35	30	5	1.7		B	T	0	p	r	n	n	
0.5	40	14	1.81		U	T	0	p	r	n	n	
0.68	35	15	2.07		B	U	0	p	r	n	n	
0.9	21	2	0.52		B	T	0	p	r	n	n	
1	16	3	1.79		U	U	0	p	r	n	n	

One or more separate scanlines

			Dip Dir. [°]	Dip [°]	Outcrop Face Dimensions [m]:
Photo #:	8	approximate surface orientation:	209	88	x =2.2
					z = 1.6

Scanline c)

Waypoint	E [m]	N [m]	Elev. [m]	SL length [m]	Trend [°]	Plunge [°]	Direction
4c	0318372	5485618	959	1.6	209	-85	U-D

DATA

Fracture SL Intersection [m]	Dip Dir [°]	Dip [°]	Trace Length strike [m]	Trace Length dip [m]	Upper Termin.	Lower Termin.	Aperture [mm]	Primary roughness	Secondary roughness	Fillings	Movement	Comment
0.11	359	8	2	2.44B	U	U	0	p	r	n	n	
0.23	355	16	1.55		T	B	0	u	r	n	n	
0.31	353	11	1.6	2.87U	B	U	0	p	r	n	n	
0.37	354	13	1.18		B	B	0	p	r	n	n	
0.49	345	9	1.63	.64B	U	B	0	u	r	n	n	
0.55	350	7	2.5	1.4B/.9A	U	U	0	p	r	n	n	
0.61	349	12	2.08	.56B	U	A	0	p	r	n	n	
0.7	348	3	2.39	/.62B	U	T	0	p	r	n	n	
0.74	345	5	1.87	/.94T	U	T	0	p	r	n	n	
0.81	345	4	2.08		T	B	0	p	r	n	n	
0.86	348	13	0.72		B	T	0	p	r	n	n	
0.92	348	13	2.46		U	U	0	p	r	n	n	
1.31	351	14	2.06	/.15U	U	T	0	p	r	n	n	
1.53	347	12	2.09		U	U	0	p	r	n	n	
1.6	347	11	1.32		B	U	0	p	r	n	n	

				Dip Dir. [°]	Dip [°]	Outcrop Face Dimensions [m]:		
Photo #:	9	approximate surface orientation:		272	19	x =1.8		
						v = 2.0		

Scanline d)

Waypoint	E [m]	N [m]	Elev. [m]	SL length [m]	Trend [°]	Plunge [°]	Direction
4d	0318367	5485628	960	1.8	218	7	S-N

DATA

Fracture SL Intersection [m]	Dip Dir [°]	Dip [°]	Trace Length strike [m]	Trace Length dip [m]	Upper Termin.	Lower Termin.	Aperture [mm]	Primary roughness	Secondary roughness	Fillings	Movement	Comment
0.25	217	89	0.75		B	U	0	p	s	n	n	
0.71	216	89	1.56		U	B	0	p	s	n	n	
0.85	214	88	3.03		U	U	0	p	s	n	n	
1.13	215	89	3.21		U	U	0	p	s	n	n	
1.57	213	87	0.95		U	U	0	p	s	n	n	
1.74	214	88	0.69		U	U	0	p	s	n	n	

Outcrop #	5
General Data	
Date	19-May-06
Name Surveyor	HV/MAB
Character/dimension of outcrop	surface (A,B: 4mx6m), wall about 10m away (C: 5mx1.5)
near or away of faultzone?	
Lithology description	
Rocktype	Granodiorite
colour fresh/weathered	Fresh: whitish (quarz, feldspar and hornblende contribution - medium grained. No large phorphyroclasts seen), Weathered: medium to dark grey, moderate lichen
homegeneous vs heterogeneous	homogeneous
sample taken?	yes
Structures	
Foliation/bedding (Dip Dir./Dip)	no foliation, because granodiorite
Liniation (Trend/plunge)	no foliation, because granodiorite
folds (amplitude, wavelength, fold axis, fold plane)	
fault (width, trace, gouge, orientation)	In center of outcrop (photo 11) appears to be a small faultzone, strongly fractured. No indication of movement and no obvisious offsett in any of cross cutting fractures. On both sides more massive with block size
Shear zone (width, trace)	
Rock mass description	
Block shape	irregular
Block size	ms
weathering class	II
seepage (presence/absence)	absent

Outcrop #: 5

One or more separate scanlines

			Dip Dir. [°]	Dip [°]	Outcrop Face Dimensions [m]:
Photo #:	10, 11	approximate surface orientation:	265	29	x = 4
					y = 6

Scanline a)

Waypoint	E [m]	N [m]	Elev. [m]	SL length [m]	Trend [°]	Plunge [°]	Direction
5a	0314713	5500513	972	3.3	238	-40	E-W

DATA

Fracture SL Intersection [m]	Dip Dir [°]	Dip [°]	Trace Length strike [m]	Trace Length dip [m]	Upper Termin.	Lower Termin.	Aperture [mm]	Primary roughness	Secondary roughness	Fillings	Movement	Comment
0.41	112	48	2.01		U	B	0	p	r	n	n	
2.54	105	74	2.56		U	B	0	p	r	n	n	
3.14	109	59	1.99		T	B	0	p	r	n	n	

Scanline b)

Waypoint	E [m]	N [m]	Elev. [m]	SL length [m]	Trend [°]	Plunge [°]	Direction
5b	0314707	5500526	971	3.5	290	-28	E-W

DATA

Fracture SL Intersection [m]	Dip Dir [°]	Dip [°]	Trace Length strike [m]	Trace Length dip [m]	Upper Termin.	Lower Termin.	Aperture [mm]	Primary roughness	Secondary roughness	Fillings	Movement	Comment
0.29	116	64	1.89		B	B	0	u	r	n	n	
0.65	129	76	0.6		B	B	0	p	r	n	n	
0.79	138	70	1.13		B	B	0	p	r	n	n	
1.05	140	70	1.15		B	B	0	p	r	n	n	
1.17	146	70	1.73		U	A	0	p	r	n	n	
1.27	146	70	2.04		B	B	0	p	r	n	n	
1.29	138	69	0.65		A	A	0	p	r	n	n	
1.38	144	80	2.8		A	B	0	p	r	n	n	
1.42	145	76	1.89		A	B	0	p	r	n	n	
1.54	140	69	0.78		B	B	0	p	r	n	n	
1.65	276	81	0.69		B	B	0	p	r	n	n	
1.78	279	81	1.46		U	A	0	p	r	n	n	
1.98	141	68	0.35		B	B	0	p	r	n	n	
2.04	142	74	1.65		U	B	0	p	r	n	n	
2.15	100	74	0.52		A	B	0	p	r	n	n	
2.28	103	71	0.47		A	B	0	p	r	n	n	
2.4	141	76	0.65		B	B	0	p	r	n	n	
2.7	104	67	1.03		U	U	0	p	r	n	n	
2.95	102	72	1.04		U	B	0	p	s	n	n	
3.09	102	68	0.49		U	B	0	p	r	n	n	
3.34	109	71	0.82		U	U	0	p	r	n	n	
3.36	274	89	0.45		B	B	0	p	r	n	n	
3.41	274	89	0.64		U	U	0	p	r	n	n	

One or more separate scanlines

			Dip Dir. [°]	Dip [°]
Photo #:	12	approximate surface orientation:	26	77

Outcrop Face Dimensions [m]:

y =5

z = 1.5

Scanline c)

Waypoint	E [m]	N [m]	Elev. [m]	SL length [m]	Trend [°]	Plunge [°]	Direction
5c	0314698	5500515	968	4.2	285	-34	E-W

DATA

Fracture SL Intersection [m]	Dip Dir [°]	Dip [°]	Trace Length strike [m]	Trace Length dip [m]	Upper Termin.	Lower Termin.	Aperture [mm]	Primary roughness	Secondary roughness	Fillings	Movement	Comment
0.18	241	28	1.09		U	T	0	p	r	n	n	
0.4	276	77		0.8	U	U	0	p	r	n	n	
0.52	78	67		0.41	T	U	0	p	r	n	n	
0.71	306	85		0.49	U	B	0	p	r	n	n	
0.98	299	87		0.61	T	U	0	p	r	n	n	
1.47	162	2	2.5		U	U	0	p	r	n	n	
1.85	109	70		0.44	A	U	0	p	r	n	n	
2.41	210	20	2.5		A	B	0	p	r	n	n	
2.59	100	59		0.93	U	U	0	p	r	n	n	
3.15	222	22	1		B	U	0	p	r	n	n	

274

Outcrop #	6
General Data	
Date	20-May-06
Name Surveyor	MAB/HV
Character/dimension of outcrop	Wall(A,B-3mx10m), upper surface oval (C 11mx7m about 20m away from wall)
near or away of faulzone?	
Lithology description	
Rocktype	Quartzofeldspathic gneis
colour fresh/weathered	Fresh: Alternating bands; fine grained, medium grey, homogenous with white, medium grey, porphyoblasts (05-1cm). Weathered: Dark grey, abundant pink coloration and staining.
homegeneous vs heterogeneous	hetergeneous
sample taken?	no
Structures	
Foliation/bedding (Dip Dir./Dip)	175/17
Liniation (Trend/plunge)	290/15
folds (amplitude, wavelength, fold axis, fold plane)	
fault (width, trace, gouge, orientation)	Abundant fractures suggest near fault or lineament (at upper oval surface- photo 15). Very broken where fractures meet, random array of fractures at intersection point. Appears to be 2 directions (~10 degrees different)
Shear zone (width, trace)	
Rock mass description	
Block shape	irregular
Block size	ms
weathering class	II
seepage (presence/absence)	absent

275

Outcrop #: 6

One or more separate scanlines

			Dip Dir. [°]	Dip [°]	Outcrop Face Dimensions [m]:
Photo #:	13	approximate surface orientation:	274	70	y =10
					z = 3

Scanline a)

Waypoint	E [m]	N [m]	Elev. [m]	SL length [m]	Trend [°]	Plunge [°]	Direction
6a	0314400	5498190	772	3.7	205	11	S-N

DATA

Fracture SL Intersection [m]	Dip Dir [°]	Dip [°]	Trace Length strike [m]	Trace Length dip [m]	Upper Termin.	Lower Termin.	Aperture [mm]	Primary roughness	Secondary roughness	Fillings	Movement	Comment
0.01	151	79		1.72	U	B	0	p	r	none	none	
0.43	80	46	0.57		B	B	0	p	r	none	none	
0.47	153	78		0.6	B	T	0	p	r	none	none	
0.68	155	79		1.8	U	B	0	p	r	none	none	
0.9	269	85		1.94	U	U	0	p	r	none	none	
0.96	255	78		0.46	T	T	0	p	r	none	none	
0.99	260	81		0.48	B	B	0	p	r	none	none	
1	4	86		0.41	B	B	0	p	r	none	none	
1.16	256	76		1	B	B	0	p	r	none	none	
1.2	152	75		1.39	U	B	0	p	r	none	none	
1.34	260	67		1	B	U	0	p	r	none	none	
1.82	30	69		1.12	T	B	0	u	r	none	none	
2.57	5	81		2.03	U	T	0	u	r	none	none	
2.6	182	84		1.14	T	B	0	u	r	none	none	
3.38	158	85		0.46	B	B	0	p	r	none	none	
3.58	159	86		1.26	B	B	0	p	r	none	none	

One or more separate scanlines

			Dip Dir. [°]	Dip [°]	Outcrop Face Dimensions [m]:
Photo #:	13	approximate surface orientation:	274	70	y = 10
					z = 3

Scanline b)

Waypoint	E [m]	N [m]	Elev. [m]	SL length [m]	Trend [°]	Plunge [°]	Direction
6b	0314499	5498184	774	3.2	282	-74	U-D

DATA

Fracture SL Intersection [m]	Dip Dir [°]	Dip [°]	Trace Length strike [m]	Trace Length dip [m]	Upper Termin.	Lower Termin.	Aperture [mm]	Primary roughness	Secondary roughness	Fillings	Movement	Comment
1.16	312	6	1.2		T	T	0	u	r	none	none	
1.47	310	5	0.68		U	B	0	p	r	none	none	
1.75	100	15	1.06		T	T	0	u	r	none	none	
2.23	64	35	0.88		B	T	0	p	r	none	none	
3.03	197	18	0.86		T	B	0	p	r	none	none	
3.24	100	16	1.43		U	U	0	u	r	none	none	

One or more separate scanlines

				Dip Dir. [°]	Dip [°]	Outcrop Face Dimensions [m]:
Photo #:	14, 15	approximate surface orientation:		180	5	x = 11
						y = 7

Scanline c)

Waypoint	E [m]	N [m]	Elev. [m]	SL length [m]	Trend [°]	Plunge [°]	Direction
6c	0314510	5498162	775	4.9	248	6	W-E

DATA

Fracture SL Intersection [m]	Dip Dir [°]	Dip [°]	Trace Length strike [m]	Trace Length dip [m]	Upper Termin.	Lower Termin.	Aperture [mm]	Primary roughness	Secondary roughness	Fillings	Movement	Comment
0.49	31	80	2.7		U	B	0	p	r	none	none	
0.61	272	87	1.05		B	B	0	p	r	none	none	
0.83	276	83	6.25		B	B	0	p	r	none	none	
1.12	34	76	1.35		B	B	0	p	r	none	none	
1.29	33	74	0.3		B	B	0	st	r	none	none	
2.02	284	81	6.1		U	A	0	st	r	none	none	
2.41	270	87	0.94		A	A	0	u	r	none	none	
3.21	290	80	10.8		B	U	3	u	r	none	none	
3.68	283	86	2.55		B	B	0	st	r	none	none	
3.85	285	82	2.6		B	B	0	p	r	none	none	
3.96	276	75	1.81		B	B	0	p	r	none	none	
4.13	278	81	1.34		T	B	0	p	r	none	none	
4.51	290	81	2.27		B	T	0	p	r	none	none	
4.78	287	75	3.7		B	B	0	st	r	none	none	

Outcrop #	7
General Data	
Date	21-May-06
Name Surveyor	HV/MAB
Character/dimension of outcrop	Wall (A: 7mx1.5); Wall (B: 3mx2m)
near or away of faulzone?	
Lithology description	
Rocktype	Quartzofeldspathic gneiss but less foliated close to granodiorite, 3 different types
colour fresh/weathered	Type 1- fresh: greyish white fine grained quarzo feldsp. gneiss but less foliated without phorphyroclasts (up to 1cm); Type 2- fresh: pinkish greyish white medium to coarse grained with little foliation, mostly feldspat, some quarzo and some mafic minerals (20%); Type 3-fresh: whitish grey fine to medium grained mafic minerals and hornblende grains with phorphyroclasts (up to 1 cm) about 50%; Weathered (all 3 types the same): medium to dark grey with lichen and moss
homegeneous vs heterogeneous	Type 1: homogeneous; Type 2: hetrogeneous; Type 3: homogeneous/hetrogeneous
sample taken?	yes
Structures	
Foliation/bedding (Dip Dir./Dip)	12/50 Type1
Liniation (Trend/plunge)	absent
folds (amplitude, wavelength, fold axis, fold plane)	
fault (width, trace, gouge, orientation)	
Shear zone (width, trace)	
Rock mass description	
Block shape	t
Block size	ms
weathering class	II
seepage (presence/absence)	absent

279

Outcrop #: 7

One or more separate scanlines

			Dip Dir. [°]	Dip [°]
Photo #:	16	approximate surface orientation:	205	73

Outcrop Face Dimensions [m]:

x =7

z = 1.5

Scanline a)

Waypoint	E [m]	N [m]	Elev. [m]	SL length [m]	Trend [°]	Plunge [°]	Direction
7a	0315314	5499603	956	5.8	300	-15	E-W

DATA

Fracture SL Intersection [m]	Dip Dir [°]	Dip [°]	Trace Length strike [m]	Trace Length dip [m]	Upper Termin.	Lower Termin.	Aperture [mm]	Primary roughness	Secondary roughness	Fillings	Movement	Comment
0.06	128	71		0.61	U	U	0	p	r	n	n	
0.21	116	59		0.6	B	U	0	p	r	n	n	
0.37	107	46		0.59	B	U	0	p	r	n	n	
0.4	118	76	3.65B	1.13	U	U	0	u	r	n	n	
0.56	111	45		1.16	U	A	0	u	r	n	n	
0.85	126	44		0.33	B	B	0	p	r	n	n	
0.89	116	69		0.56	H	B	0	p	r	n	n	
0.95	114	60	1.17B	1.23	U	U	0	st	r	n	n	
1.24	95	57		1.28	U	B	0	st	r	n	n	
1.34	87	58		0.78	U	B	0	p	r	n	n	
1.81	94	56		0.66	B	B	0	p	r	n	n	

Fracture SL Intersection [m]	Dip Dir [°]	Dip [°]	Trace Length strike [m]	Trace Length dip [m]	Upper Termin.	Lower Termin.	Aperture [mm]	Primary roughness	Secondary roughness	Fillings	Movement	Comment
1.87	114	57		0.68	B	B	0	p	r	n	n	
1.97	104	59	.93B	1.42	U	U	0	p	r	n	n	
2.03	108	63		0.65	U	B	0	u	r	n	n	
2.13	112	58	2.8B	1	B	U	0	st	r	n	n	
2.15	110	56		0.93	U	B	0	p	r	n	n	
2.31	102	58	.79B	1.1	T	U	0	p	r	n	n	
2.41	104	57		1.55	U	B	0	p	r	n	n	
2.67	96	57		0.24	B	B	0	p	r	n	n	
2.74	109	59		0.38	U	B	0	p	r	n	n	
2.81	112	56	.89B	1.38	U	U	0	p	r	n	n	
3.04	102	59	.51H	1.28	U	U	0	p	r	n	n	
3.08	117	59		1.12	B	B	0	u	r	n	n	
3.2	114	68		0.62	U	B	0	u	r	n	n	
3.39	117	57		0.53	B	B	0	u	r	n	n	
3.5	115	57		0.63	B	B	0	p	r	n	n	
3.63	106	54	1.22B	1.23	U	U	0	u	r	n	n	
3.8	116	60		0.92	B	U	0	u	r	n	n	
3.85	116	60		1.26	U	B	0	u	r	n	n	
3.95	106	61		1	U	B	0	u	r	n	n	
4.5	114	67	1.23B	0.96	B	U	0	st	r	n	n	
4.53	109	68		0.93	U	B	0	u	r	n	n	
4.59	116	54	0.91B	1.1	U	U	0	st	r	n	n	
4.66	113	59	0.43B	1.18	U	U	0	st	r	n	n	
4.84	106	74	0.34B	1.31	U	U	0	u	r	n	n	
5.13	112	77		0.47	B	B	0	p	r	n	n	
5.14	113	63		0.62	B	B	0	u	r	n	n	
5.23	102	69	.63B	1.29	U	U	0	u	r	n	n	
5.39	116	68	2.14U	1.27	U	U	0	u	r	n	n	
5.69	108	58	.72B	1.12	U	U	0	u	r	n	n	

One or more separate scanlines

				Dip Dir. [°]	Dip [°]
Photo #:	17	approximate surface orientation:		195	75

Outcrop Face Dimensions [m]:

y = 3
z = 2

Scanline b)

Waypoint	E [m]	N [m]	Elev. [m]	SL length [m]	Trend [°]	Plunge [°]	Direction
7b	0315317	5498587	954	4	274	-35	E-W

DATA

Fracture SL Intersection [m]	Dip Dir [°]	Dip [°]	Trace Length strike [m]	Trace Length dip [m]	Upper Termin.	Lower Termin.	Aperture [mm]	Primary roughness	Secondary roughness	Fillings	Movement	Comment
0.46	195	9	1.24		U	T	0	p	r	n	n	
0.49	196	21	1.08		U	B	0	p	r	n	n	
0.63	98	8		0.43	A	B	0	u	r	n	n	
0.64	96	69	0.53		U	U	0	p	r	n	n	
0.98	228	12	1.77		U	A	0	p	r	n	n	
1.23	227	11	3.06		U	B	0	u	r	n	n	
1.27	100	61		1.23	U	B	0	u	r	n	n	
1.43	96	65		1.3	U	B	0	p	r	n	n	
1.74	101	65	1.5U	1.44	U	U	2.85	p	r	n	n	
1.91	104	72		1.01	T	B	0	p	r	n	n	
2.08	104	65		0.96	B	B	0	p	r	n	n	
2.43	100	66		0.98	T	B	0	p	r	n	n	
2.74	98	72		1.1	B	U	0	p	r	n	n	
2.84	273	30	0.98		T	T	0	p	r	n	n	
3.65	98	65		1.04	B	B	0	p	r	n	n	

Outcrop #	8
General Data	
Date	22-May-06
Name Surveyor	HV/MAB
Character/dimension of outcrop	Wall (A, B, C (B,C=leg1,2): 28mx3m); oval surface about 40m away (D: 2.8mx2.5m)
near or away of faulzone?	
Lithology description	
Rocktype	Quarzo feldsp. Gneiss
colour fresh/weathered	Fresh: medium grey with bands of pinkish white; grey is mafic minerals and phorphyroclasts (up to 1cm)-little foliated, mafic generally fine grained; feldsp bands medium to coarse very little foliated; Weathered: whitish grey to dark grey with minor moss
homegeneous vs heterogeneous	heterogeneous
sample taken?	yes
Structures	
Foliation/bedding (Dip Dir./Dip)	280/17
Liniation (Trend/plunge)	(296/8?)
folds (amplitude, wavelength, fold axis, fold plane)	
fault (width, trace, gouge, orientation)	
Shear zone (width, trace)	
Rock mass description	
Block shape	i
Block size	ms
weathering class	II
seepage (presence/absence)	absent

Outcrop #: 8

One or more separate scanlines

		Dip Dir. [°]	Dip [°]
Photo #:	18	approximate surface orientation:	290	85

Outcrop Face Dimensions [m]:
y = 23
z = 3

Scanline a)

Waypoint	E [m]	N [m]	Elev. [m]	SL length [m]	Trend [°]	Plunge [°]	Direction
8a	0317967	5490946	1089	2.2	16	-72	U-D

DATA

Fracture SL Intersection [m]	Dip Dir [°]	Dip [°]	Trace Length strike [m]	Trace Length dip [m]	Upper Termin.	Lower Termin.	Aperture [mm]	Primary roughness	Secondary roughness	Fillings	Movement	Comment
0.41	260	10	2		T	U	0	u	r	n	n	
0.56	263	12	2.2		A	U	0	u	r	n	n	
0.75	235	9	0.7		B	T	0	p	r	n	n	
0.88	237	7	0.87		B	A	0	u	r	n	n	
1.02	242	7	1.02		B	B	0	u	r	n	n	
1.3	259	9	3.1		T	A	0	u	r	n	n	
2.06	270	12	1.17		B	A	0	u	r	n	n	

One scanline portioned in different legs

Outcrop Face Dimensions [m]:
y = 23
z = 3

approximate surface orientation

Photo #:	18

Waypoint	E [m]	N [m]	Elev. [m]	SL start point [m]	Leg #	Trend [°]	Plunge [°]	Direction	Dip Dir. [°]	Dip [°]
8b	317969	5490933	1087	0	1	215	1	S-N	291	83
8c	317968	5490936	1087	3 to 9	2	208	9	S-N	290	85

DATA

Fracture SL Intersection [m]	Leg #	Dip Dir [°]	Dip [°]	Trace Length strike [m]	Trace Length dip [m]	Upper Termin.	Lower Termin.	Aperture [mm]	Primary roughness	Secondary roughness	Fillings	Movement	Comment
0.24	1	28	63		0.36	B	B	0	st	r	n	n	
0.37	1	21	67		0.68	U	B	0	st	r	n	n	

Fracture SL Intersection [m]	Leg #	Dip Dir [°]	Dip [°]	Trace Length strike [m]	Trace Length dip [m]	Upper Termin.	Lower Termin.	Aperture [mm]	Primary roughness	Secondary roughness	Fillings	Movement	Com-ment
0.56	1	14	65		0.33	B	B	0	st	r	n	n	
0.61	1	358	59		1.03	B	U	0	u	r	n	n	
0.77	1	232	8	1.06		B	T	0	p	r	n	n	
0.96	1	239	8	0.33		A	T	0	p	r	n	n	
1.33	1	290	83		1.38	U	U	0	p	r	n	n	
1.69	1	10	66		0.23	T	T	0	p	r	n	n	
1.85	1	292	12	2.59		B	T	0	st	r	n	n	
1.88	1	11	71		0.18	T	B	0	p	r	n	n	
1.95	1	11	59		0.22	B	B	0	st	r	n	n	
2.12	1	5	71		0.25	B	B	0	u	r	n	n	
2.44	1	287	81		1.12	U	U	0	u	r	n	n	
3.02	2	51	87		0.38	T	T	0	p	r	n	n	
3.05	2	22	55		0.32	T	B	0	p	r	n	n	
3.11	2	264	13	1.77		T	T	0	st	r	n	n	
3.24	2	13	44		0.46	B	B	0	u	r	n	n	
3.3	2	21	59		0.25	B	B	0	u	r	n	n	
3.5	2	8	54		0.28	B	B	0	p	r	n	n	
3.94	2	355	53		2.03	U	B	0	u	r	n	n	
3.99	2	7	52		0.48	B	B	0	u	r	n	n	
4.18	2	357	56		0.9	B	B	0	u	r	n	n	
4.61	2	359	36		1.32	U	B	0	u	r	n	n	
4.75	2	11	48		2.17	T	U	0	u	r	n	n	
5.18	2	28	63		0.25	B	B	0	u	r	n	n	
5.42	2	9	37		1.11	B	A	0	u	r	n	n	
5.93	2	13	42		0.67	B	B	0	p	r	n	n	
6.07	2	18	43		0.51	T	T	0	u	r	n	n	
6.1	2	252	12	1.82		T	T	0	st	r	n	n	
6.25	2	11	51		0.71	T	B	0	u	r	n	n	
6.9	2	12	49		1.27	T	B	0	u	r	n	n	
7.6	2	11	50		3.3	U	U	0	u	r	n	not detect.	fault?
8.41	2	12	57		0.68	B	B	0	u	r	n	n	

One or more separate scanlines

			Dip Dir. [°]	Dip [°]	Outcrop Face Dimensions [m]:
Photo #:	19	approximate surface orientation:	236	11	x = 2.8
					y = 2.5

Scanline d)

Waypoint	E [m]	N [m]	Elev. [m]	SL length [m]	Trend [°]	Plunge [°]	Direction
8d	0317938	5490948	1090	2.5	320	2	N-S

DATA

Fracture SL Intersection [m]	Dip Dir [°]	Dip [°]	Trace Length strike [m]	Trace Length dip [m]	Upper Termin.	Lower Termin.	Aperture [mm]	Primary roughness	Secondary roughness	Fillings	Movement	Comment
0.02	299	78	1.79		U	U	0	p	r	n	n	
0.11	296	78	0.32		B	B	0	p	s	n	n	
0.16	292	84	0.72		B	B	0	st	s	n	n	
0.27	297	85	0.83		B	B	0	p	s	n	n	
0.33	292	85	1.57		U	B	0	st	s	n	n	
0.41	293	81	0.59		B	B	0	st	s	n	n	
0.55	298	86	0.77		B	B	0	p	s	n	n	
0.6	296	77	0.4		A	B	0	p	s	n	n	
0.72	299	70	0.45		B	B	0	p	s	n	n	
0.77	300	77	0.42		B	B	0	u	s	n	n	
0.78	293	84	0.36		B	B	0	u	s	n	n	
1.39	297	86	0.61		B	B	0	p	s	n	n	
1.42	298	81	0.3		B	B	0	p	s	n	n	
1.45	296	85	0.24		B	B	0	p	s	n	n	

286

Fracture SL Intersection [m]	Dip Dir [°]	Dip [°]	Trace Length strike [m]	Trace Length dip [m]	Upper Termin.	Lower Termin.	Aperture [mm]	Primary roughness	Secondary roughness	Fillings	Movement	Comment
1.64	300	86	1.26		B	B	0	st	s	n	n	
1.69	297	83	0.39		B	B	0	p	s	n	n	
1.78	300	86	0.45		B	B	0	p	s	n	n	
2.04	299	88	0.53		B	A	0	p	s	n	n	
2.16	300	89	1.15		B	B	0	p	r	n	n	
2.29	298	89	0.53		U	B	0	p	r	n	n	
2.34	297	87	0.33		B	B	0	p	r	n	n	
2.41	299	89	0.56		B	B	0	p	s	n	n	
2.43	298	88	0.39		B	B	0	p	r	n	n	

Outcrop #	9
General Data	
Date	23-May-06
Name Surveyor	HV/MAB
Character/dimension of outcrop	Wall (A: 27mx5m); Surface about 40m above lower wall A (B: 12mx5m); Wall close to surface B (C: 3mx10m)
near or away of faulzone?	
Lithology description	
Rocktype	quarzo feldsp. Gneiss with lots of mafic minerals probably amphibol
colour fresh/weathered	Fresh: medium grey with pinkish white feldsp. bands (also phorphyroclasts up to 1cm); medium grained, dark colors are mafic minerals (probably amphibol or hornblende) of about 60% and lighter minerals is quarz (about 40%); small grains of pyrite and copper color minerals and maybe parts of green epidot; Weathered: light yellowish brown with pink staining and in some sections light green coating on surface
homegeneous vs heterogeneous	homogeneous
sample taken?	yes
Structures	
Foliation/bedding (Dip Dir./Dip)	little foliation, hard to measure
Liniation (Trend/plunge)	nd
folds (amplitude, wavelength, fold axis, fold plane)	
fault (width, trace, gouge, orientation)	~1m, gouge & becciated material. 323/87; maybe fault zone?
Shear zone (width, trace)	

Rock mass description	
Block shape	i
Block size	ms
weathering class	II
seepage (presence/absence)	absent

Outcrop #: 9

One or more separate scanlines

			Dip Dir. [°]	Dip [°]
Photo #:	01b	approximate surface orientation:	260	86

Outcrop Face Dimensions [m]:
y = 27
z = 5

Scanline a)

Waypoint	E [m]	N [m]	Elev. [m]	SL length [m]	Trend [°]	Plunge [°]	Direction
9a	0312203	5502696	740	23	172	-1	N-S

DATA

Fracture SL Intersection [m]	Dip Dir [°]	Dip [°]	Trace Length strike [m]	Trace Length dip [m]	Upper Termin.	Lower Termin.	Aperture [mm]	Primary roughness	Secondary roughness	Fillings	Movement	Comment
1.48	316	87		4.2	U	U	0	u	r	n	n	
3.08	314	89		2.3	B	B	0	u	r	n	n	
3.53	325	79		1.25	B	B	0	u	r	n	n	
3.71	322	71		3.4	B	U	0	u	r	n	n	
3.83	325	75		2.9	B	B	0	u	r	n	n	
4.86	327	80		4.6	B	U	0	st	r	n	n	
5.51	324	85		1.25	B	B	0	p	r	n	n	
6.63	325	81		2.7	B	U	0	u	r	n	n	
6.46	325	84		1.04	B	B	0	u	r	n	n	
6.83	323	89		3.1	T	U	0	p	r	n	n	
7.18	320	85		4.5	U	B	0	u	r	gouge	n/d	Possibly in a fault zone (~1m wide)
7.34	322	86		3.3	B	U	0	u	r	gouge	n/d	

Fracture SL Intersection [m]	Dip Dir [°]	Dip [°]	Trace Length strike [m]	Trace Length dip [m]	Upper Termin.	Lower Termin.	Aperture [mm]	Primary roughness	Secondary roughness	Fillings	Movement	Comment
7.35	4	47		3.3	B	U	0	p	r	n	n/d	(~1m wide). Movement not detectable.
7.83	329	88		4.6	U	U	0	u	r	n	n/d	
7.99	195	22		2.06	T	T	0	p	r	n	n/d	
8.21	319	89		3.2	A	U	0	u	r	n	n/d	
9.27	22	30		2.99	B	U	0	u	r	n	n	
10.33	306	75		1.7	B	B	0	p	r	n	n	
10.44	27	14		1.11	T	B	0	p	r	n	n	
10.72	1	16		1.31	T	B	0	u	r	n	n	
11.06	132	83		0.52	T	A	0	p	r	n	n	
11.7	296	86		3.9	B	U	0	u	r	n	n	
11.81	359	7		5.38	B	B	0	u	r	n	n	

One or more separate scanlines

			Dip Dir. [°]	Dip [°]	Outcrop Face Dimensions [m]:
Photo #:	2b	approximate surface orientation:	296	14	x =12
					y = 5

Scanline b)

Waypoint	E [m]	N [m]	Elev. [m]	SL length [m]	Trend [°]	Plunge [°]	Direction
9b	0312229	5502649	749	6.3	251	-14	E-W

DATA

Fracture SL Intersection [m]	Dip Dir [°]	Dip [°]	Trace Length strike [m]	Trace Length dip [m]	Upper Termin.	Lower Termin.	Aperture [mm]	Primary roughness	Secondary roughness	Fillings	Movement	Comment
0.13	282	85	2.17		A	U	0	p	r	n	n	
0.55	260	81	2.97		B	B	0	p	r	n	n	
0.87	257	80	3.23		B	B	0	p	r	n	n	
1.3	30	33	2.79		B	U	0	p	r	n	n	
1.46	261	84	0.45		B	B	0	st	r	n	n	
1.59	25	78	2.24		B	B	0	p	r	n	n	
1.84	264	72	2.78		T	U	0	p	r	n	n	
2.39	35	62	1.23		A	B	0	p	r	n	n	
2.49	255	79	1.37		A	B	0	p	r	n	n	
2.58	257	71	0.52		A	B	0	p	r	n	n	
2.73	38	49	1.27		A	A	0	p	r	n	n	
2.88	30	34	0.7		A	B	0	p	r	n	n	
3	260	87	0.5		B	B	0	p	r	n	n	
3.08	20	30	0.89		A	B	0	p	r	n	n	
4	40	45	0.75		B	B	0	p	r	n	n	

One or more separate scanlines

			Dip Dir. [°]	Dip [°]
Photo #:	3b	approximate surface orientation:	135	68

Outcrop Face Dimensions [m]:

y = 10

z = 3

Scanline c)

Waypoint	E [m]	N [m]	Elev. [m]	SL length [m]	Trend [°]	Plunge [°]	Direction
9c	0312241	5502657	749	2.7	135	-68	U-D

DATA

Fracture SL Intersection [m]	Dip Dir [°]	Dip [°]	Trace Length strike [m]	Trace Length dip [m]	Upper Termin.	Lower Termin.	Aperture [mm]	Primary roughness	Secondary roughness	Fillings	Movement	Comment
0.42	240	17		1	B	B	0	p	r	n	n	
0.53	239	18		1.2	B	B	0	p	r	n	n	
0.91	242	17		1.3	B	B	0	u	r	n	n	
1.64	23	24		2.4	B	B	0	p	r	n	n	
1.77	250	28		3.1	B	B	0	u	r	n	n	
1.87	37	16		1.8	B	B	0	p	r	n	n	

291

Outcrop #	10
General Data	
Date	5/24/2006
Name Surveyor	HV/MAB
Character/dimension of outcrop	A leg1 (wall:6mx2.5m), B leg2 (wall:9mx3.5m), C(wall: 5mx3x), D(wall: 20mx5m)
near or away of faulzone?	
Lithology description	
Rocktype	Quartzofeldspathic gniess, and ampholibite gneiss in layers, 0.5-2m thick
colour fresh/weathered	Fresh: quartzofeldspathic; pinkish white, fine grained, no augen or apparent foliation. Amphibolite; dark grey, medium grained, with moderate amounts of augen, ≤1cm. Dark grey matrix, with some quartz and felsdspar in the matrix, and some bands of feldspathic material <5cm wide. Weathered: Quartzofeldspathic; light orangish brown, planar surfaces, little lichen or moss. Amphibolite; dark grey to black, very rough surfaces, moderately weathered out, some moss.
homegeneous vs heterogeneous	quartzofeldspathic; homogenous. Amphibolite; hetergeneous.
sample taken?	no
Structures	
Foliation/bedding (Dip Dir./Dip)	210/28
Liniation (Trend/plunge)	none observed to measure
folds (amplitude, wavelength, fold axis, fold plane)	
fault (width, trace, gouge, orientation)	1: width 20cm, trace 1.29m on line C, breccia and gouge, 152/51. 2: 3.9-4.6 on line D., trace, 4.1m, tabular breccia in quartzofeldsapthic, angular breccia and gouge in amphibolite 335/75 . 3: width 20cm (@7.8 on line D), trace 3.3m, breccia and gouge, ends at upper contact of quartzofeldspathic gneiss, 330/71
Shear zone (width, trace)	
Rock mass description	
Block shape	i
Block size	ms
weathering class	III
seepage (presence/absence)	absent

Outcrop #: 10

One scanline portioned in different legs

Outcrop Face Dimensions [m]:

y = 9

z = 3.5

Photo #:	4b

approximate surface orientation

Waypoint	E [m]	N [m]	Elev. [m]	SL start point [m]	SL End Point [m]	Leg #	Trend [°]	Plunge [°]	Direction	Dip Dir. [°]	Dip [°]
10a	314848	5490464	508	0	6.4	1	190	-23	N-S	97	82
10b	314828	5490446	507	6.4	15	2	183	-22	N-S	94	81

DATA

Fracture SL Intersection [m]	Leg #	Dip Dir [°]	Dip [°]	Trace Length strike [m]	Trace Length dip [m]	Upper Termin	Lower Termin	Aperture [mm]	Primary roughness	Secondary roughness	Filling	Movement	Com-ment
0.11	1	148	49		2.61	A	B	0	p	r	n	n	
0.72	1	173	88		0.52	T	T	0	p	r	n	n	
1.47	1	10	68		1.03	T	T	0	u	r	n	n	
1.95	1	142	46		2.99	B	B	0	p	s	n	n	
2.2	1	181	89		2.32	B	T	0	u	r	n	n	
2.62	1	188	84		0.96	A	B	0	u	r	n	n	
2.82	1	190	80		0.88	A	A	0	u	r	n	n	
3.24	1	5	57		0.85	A	U	0	u	r	n	n	
3.28	1	195	75		0.94	A	A	0	u	r	n	n	
3.7	1	141	48		2.92	B	B	0	p	r	n	n	
4.33	1	145	46		2.17	B	B	0	p	r	n	n	
4.65	1	193	89		0.39	A	T	0	u	r	n	n	
4.81	1	196	89		0.34	A	T	0	u	r	n	n	
4.99	1	185	86		0.29	A	T	0	u	r	n	n	
5.03	1	175	85		0.49	A	T	0	u	r	n	n	
5.04	1	195	87		0.27	A	B	0	p	r	n	n	
5.27	1	190	89		0.55	B	B	0	u	r	n	n	
5.55	1	178	85		0.44	B	B	0	u	r	n	n	
5.7	1	185	75		0.51	T	B	0	u	r	n	n	
6.64	2	170	81		1.02	B	B	0	u	r	n	n	

Fracture SL Intersection [m]	Leg #	Dip Dir [°]	Dip [°]	Trace Length strike [m]	Trace Length dip [m]	Upper Termin	Lower Termin	Aperture [mm]	Primary roughness	Secondary roughness	Filling	Movement	Com-ment
6.7	2	171	86		0.9	B	B	0	p	r	n	n	
6.98	2	143	50		0.67	B	B	0	p	r	n	n	
7.42	2	142	48		2.44	B	B	0	st	r	n	n	
7.61	2	356	65		0.7	A	B	0	u	r	n	n	
7.76	2	356	60		0.6	B	T	0	p	r	n	n	
7.85	2	10	45		0.79	B	B	0	u	r	n	n	
7.99	2	350	61		0.81	T	T	0	u	r	n	n	
8.28	2	354	56		0.78	T	B	0	u	r	n	n	
8.33	2	139	45		0.9	T	T	0	st	r	n	n	
8.46	2	10	49		3	U	B	0	u	r	n	n	
8.71	2	159	46		1.16	T	T	0	u	r	n	n	
8.81	2	352	54		0.37	T	B	0	u	r	n	n	
8.84	2	350	46		1.07	B	B	0	u	r	n	n	
8.88	2	349	49	3.5U	1.35	T	U	1	u	r	n	n	
9.06	2	6	46		2.6	U	B	0	u	r	n	n	
9.47	2	0	48		0.56	B	B	0	p	r	n	n	
9.6	2	0	40		2.9	U	B	0	u	r	n	n	
9.72	2	142	48		0.84	T	B	0	p	r	n	n	
10.06	2	138	63		1.88	T	B	0	p	r	n	n	
10.45	2	348	59		3.2	U	U	0	u	r	n	n	
10.73	2	347	64		2.1	U	B	0	u	r	n	n	
11.06	2	358	58		1.52	U	B	0	u	r	n	n	
11.42	2	352	56		3.6	U	B	0	u	r	n	n	
11.51	2	349	52		1.17	U	B	0	u	r	n	n	
11.54	2	351	39		2.2	U	A	0	u	r	n	n	
11.89	2	349	60		3.3	U	B	0	u	r	n	n	
12	2	345	60		2.1	U	U	0	u	r	n	n	
12.14	2	354	53		1.7	U	B	0	u	r	n	n	
12.25	2	9	34		1.3	U	B	0	u	r	n	n	
12.81	2	5	40		1.5	U	B	0	u	r	n	n	
13.98	2	338	68		1.3	U	T	0	u	r	n	n	

294

One or more separate scanlines

			Dip Dir. [°]	Dip [°]
Photo #:	5b,6b	approximate surface orientation:	266	68
	6b (fault)			

Outcrop Face Dimensions [m]:
y =5
z = 3

Scanline c)

Waypoint	E [m]	N [m]	Elev. [m]	SL length [m]	Trend [°]	Plunge [°]	Direction
10c	0314830	5490450	507	5	316	19	N-S

DATA

Fracture SL Intersection [m]	Dip Dir [°]	Dip [°]	Trace Length strike [m]	Trace Length dip [m]	Upper Termin.	Lower Termin.	Aperture [mm]	Primary roughness	Secondary roughness	Fillings	Movement	Comment
0.34	274	89	3.69U	1.84	B	U	0	p	r	none	none	
0.87	275	87		0.89	B	U	0	u	r	none	none	
1.3	276	83		1.66	U	U	0	u	r	none	none	
1.65	275	83		1.67	U	U	0	u	r	none	none	
1.77	99	89		1.11	U	U	0	p	r	none	none	
1.87	99	89		1	B	U	0	p	r	none	none	
2.1	96	84		0.94	B	U	0	p	s	none	none	
2.27	99	85		0.75	B	B	0	u	r	none	none	
2.5	152	51		1.29	U	B	0	u	r	none	none	Fault plane?
2.68	96	84		1.48	B	U	0	u	r	none	none	
2.88	96	88		1.04	B	U	0	u	r	none	none	
3.05	155	42		1.8	B	U	0	p	r	none	none	
3.22	100	82		1.1	U	U	0	p	r	none	none	
3.87	96	86	3.0 U	1.48	B	U	0	u	r	none	none	
4.1	97	87		0.61	B	B	0	u	r	none	none	

One or more separate scanlines

			Dip Dir. [°]	Dip [°]	Outcrop Face Dimensions [m]:
Photo #:	7b,8b,9b	approximate surface orientation:	265	72	y =20
	8b (fault)	@ 4m			z = 5
Scanline d)	9b (fault)	@ 8m			

Waypoint	E [m]	N [m]	Elev. [m]	SL length [m]	Trend [°]	Plunge [°]	Direction
10d	0314816	5490449	500	8.5	355	-5	S-N

DATA

Fracture SL Intersection [m]	Dip Dir [°]	Dip [°]	Trace Length strike [m]	Trace Length dip [m]	Upper Termin.	Lower Termin.	Aperture [mm]	Primary roughness	Secondary roughness	Fillings	Movement	Comment
0.01	236	19	20		U	U	0	p	r	n	n	contact
0.02	345	65		2.8	B	U	0	u	r	n	n	
0.16	340	66		2.3	B	U	0	u	r	n	n	
0.34	358	74		1.3	B	T	0	u	r	n	n	
0.5	342	64		2.2	U	T	0	u	r	n	n	
0.91	335	72		4.2	U	U	0	u	r	n	n	
1.66	335	68		1	B	T	0	u	r	n	n	
1.87	340	69		1.8	U	T	0	u	r	n	n	
1.98	344	78		0.93	B	B	0	p	r	n	n	
2.17	355	76		2.6	B	U	0	u	r	n	n	
2.36	356	60		1.8	B	T	0	u	r	n	n	
2.43	355	71		3.8	B	B	0	u	r	n	n	

Fracture SL Intersection [m]	Dip Dir [°]	Dip [°]	Trace Length strike [m]	Trace Length dip [m]	Upper Termin.	Lower Termin.	Aperture [mm]	Primary roughness	Secondary roughness	Fillings	Movement	Comment
2.77	345	74		3.3	B	U	0	u	r	n	n	
2.87	347	74		0.96	B	B	0	u	r	n	n	
3.04	348	78		2	B	U	0	u	r	n	n	
3.3	351	70		1.15	B	T	0	u	r	n	n	
3.4	340	77		2.15	B	B	0	u	r	n	n	
3.82	349	86		2.6	B	U	0	u	r	n	n	
4.63	353	80		3.8	U	U	0	u	r	n	n	
5.08	338	85		1.54	B	T	0	u	r	n	n	
5.74	340	71		2.2	U	B	0	u	r	n	n	
5.83	338	75		2.7	B	B	0	u	r	n	n	
6.37	345	79		1.4	B	B	0	u	r	n	n	
6.8	348	82		5.4	U	U	0	u	r	n	n	
7.18	347	78		2.5	U	B*	0	u	r	n	n	
7.93	347	74		2.9	U	B*	0	u	r	n	n	
8.49	346	79		1.7	B	B	0	u	r	n	n	

Outcrop #	11
General Data	
Date	25-May-06
Name Surveyor	HV/MAB
Character/dimension of outcrop	A-leg1 (Wall: 2.5mx4m); B-leg2 (Wall: 5mx3.5); C (Wall: 5mx4m); D (Wall: 3.4mx6m)
near or away of faulzone?	
Lithology description	
Rocktype	Amphibolite gneiss
colour fresh/weathered	Fresh: medium grey fine grained to medium grained with mafic (amphibolite) matrix and quarz +feldspat in matrix. Minor phorphyroclats (up to 3mm). Some bands of quarzo-feldsp. Material (up to 5mm); Weathered: medium to dark gey. Medium grey has pinkish and brownish stinning. dark grey has pocked surface and moss +lichen
homegeneous vs heterogeneous	more hetrogeneous
sample taken?	no

Structures	
Foliation/bedding (Dip Dir./Dip)	250/19? (was not clear!)
Liniation (Trend/plunge)	not detectable
folds (amplitude, wavelength, fold axis, fold plane)	
fault (width, trace, gouge, orientation)	width, 3.32-3.67 (35cm wide), trace, 3.8 high, both ends U, 124/81 , may be weathered out fault zone, movement, apparent vertical offset 6cm, possibly oblique. . Or maybe just a fracture, where the whole block just slided down, that's why it is so wide open!! not clear!
Shear zone (width, trace)	
Rock mass description	
Block shape	irregular
Block size	ms
weathering class	II
seepage (presence/absence)	absent

Outcrop #: 11

One scanline portioned in different legs

Outcrop Face Dimensions [m]:
y =2.5 (leg1)   y =5.0 (leg2)
z = 4.0 (leg1)   z = 3.5 (leg2)

approximate surface orientation

Photo #:	10b

Waypoint	E [m]	N [m]	Elev. [m]	SL start point [m]	SL End Point [m]	Leg #	Trend [°]	Plunge [°]	Direction	Dip Dir. [°]	Dip [°]
11a	314261	5494567	631	0	3.2	1	345	38	N-S	274	85
11b	314268	5494568	633	3.2	5.95	2	323	26	N-S	90	69

DATA

Fracture SL Intersection [m]	Leg #	Dip Dir [°]	Dip [°]	Trace Length strike [m]	Trace Length dip [m]	Upper Termin	Lower Termin	Aperture [mm]	Primary roughness	Secondary roughness	Filling	Movement	Comment
0.1	1	267	10	4.38	3.73U	U	U	20	u	r	n	n	
1.62	1	278	23	1.49		T	B	0	u	r	n	n	
2.85	1	255	31	2.56		B	B	0	u	r	n	n	
3.21	2	124	81		3.8	U	U	350	u	r	n	n	
3.67	2	123	83		3.8	U	U	350	u	r	n	n	
4.45	2	85	69	0.85U	2.42	T	U	0	u	r	n	n	
4.75	2	86	70	0.9U	3.15	B	U	0	u	r	n	n	

Fracture SL Intersection [m]	Leg #	Dip Dir [°]	Dip [°]	Trace Length strike [m]	Trace Length dip [m]	Upper Termin	Lower Termin	Aperture [mm]	Primary roughness	Secondary roughness	Filling	Movement	Com- ment
4.76	2	264	14	0.77		B	B	0	u	r	n	n	
5.15	2	87	75	2.9U	3.26	B	U	0	u	r	n	n	
5.37	2	86	73	2.3A	3.68	U	U	0	u	r	n	n	
5.57	2	100	83	2.29B	3.8	U	U	60	u	r	n	n	

One or more separate scanlines

			Dip Dir. [°]	Dip [°]	Outcrop Face Dimensions [m]:
Photo #:	11b	approximate surface orientation:	136	79	y =5 z = 4

Scanline c)

Waypoint	E [m]	N [m]	Elev. [m]	SL length [m]	Trend [°]	Plunge [°]	Direction
11c	0314255	5494539	636	4	31	-57	U-D

DATA

Fracture SL Intersection [m]	Dip Dir [°]	Dip [°]	Trace Length strike [m]	Trace Length dip [m]	Upper Termin.	Lower Termin.	Aperture [mm]	Primary roughness	Secondary roughness	Fillings	Movement	Comment
0.67	254	66		1.7	U	U	0	u	r	n	n	
0.75	255	67		1.8	B	U	0	u	r	n	n	
0.88	257	70		2.05	B	B	0	u	r	n	n	
1.51	253	75		1.4	A	U	0	u	r	n	n	
1.65	252	76		1.6	T	A	0	u	r	n	n	
1.73	249	9		1.8	U	B	0	u	r	n	n	
1.77	265	59		3.5	U	B	0	u	r	n	n	
2.2	240	85		0.95	B	B	0	u	r	n	n	
2.55	220	79		1.2	B	B	0	u	r	n	n	
2.74	223	80		1.9	B	B	0	u	r	n	n	
2.9	285	8		1.25	T	T	0	u	r	n	n	
2.99	300	30		0.84	B	T	0	u	r	n	n	
3.03	243	84		3.2	B	B	0	u	r	n	n	

Fracture SL Intersection [m]	Dip Dir [°]	Dip [°]	Trace Length strike [m]	Trace Length dip [m]	Upper Termin.	Lower Termin.	Aperture [mm]	Primary roughness	Secondary roughness	Fillings	Movement	Comment
3.2	256	80		2.1	B	A	0	u	r	n	n	
3.34	257	88		0.35	B	B	0	u	r	n	n	
3.44	255	81		1.23	T	B	0	u	r	n	n	
3.66	246	85		1.37	T	T	0	u	r	n	n	
3.86	270	13	4.38	3.62	U	U	10	u	r	n	n	

One or more separate scanlines

				Dip Dir. [°]	Dip [°]
Photo #:	12b	approximate surface orientation:		260	81

Outcrop Face Dimensions [m]:
x =3.5
z =6.0

Scanline d)

Waypoint	E [m]	N [m]	Elev. [m]	SL length [m]	Trend [°]	Plunge [°]	Direction
11d	0314244	5494519	635	5	3	-37	U-D

DATA

Fracture SL Intersection [m]	Dip Dir [°]	Dip [°]	Trace Length strike [m]	Trace Length dip [m]	Upper Termin.	Lower Termin.	Aperture [mm]	Primary roughness	Secondary roughness	Fillings	Movement	Comment
1.15	270	20	1.6		B	B	0	u	r	n	n	
1.84	260	22	2.9	1.5U	U	B	0	u	r	n	n	
2.17	270	20	3		U	B	0	u	r	n	n	
2.26	225	84		1.8	B	B	0	u	r	n	n	
2.46	265	21	1		B	B	0	u	r	n	n	
2.73	267	20	1.2		B	B	0	u	r	n	n	
3.48	260	15	4.87		B	U	0	u	r	n	n	
4.14	200	81		1.6	B	T	5	u	r	n	n	
4.87	278	18	4.33		U	B	1	u	r	n	n	

Outcrop #	12
General Data	
Date	27-May-06
Name Surveyor	HV/MAB
Character/dimension of outcrop	A-leg1, B-leg2, C (oval surface: 6mx3m); D (wall: 3mx0.5m)
near or away of faulzone?	
Lithology description	
Rocktype	quarzo feldsp. Gneiss with minor mafic minerals (about 15%); no large phorphyroclasts
colour fresh/weathered	Fresh: greyish white, fine grained; Weathered: dark grey with abundant moss, under moss weathered color is light pinkish and light yellowish
homegeneous vs heterogeneous	homogenous
sample taken?	no
Structures	
Foliation/bedding (Dip Dir./Dip)	not measurable, surface outcrop all rounded, heavily discoloured by weathering
Liniation (Trend/plunge)	220/13
folds (amplitude, wavelength, fold axis, fold plane)	
fault (width, trace, gouge, orientation)	
Shear zone (width, trace)	
Rock mass description	
Block shape	i
Block size	s
weathering class	II
seepage (presence/absence)	absent

Outcrop #: 12

One scanline portioned in different legs

Outcrop Face Dimensions [m]:
x = 6.0
y = 3.0

approximate surface orientation

Photo #:	13b

Waypoint	E [m]	N [m]	Elev. [m]	SL start point [m]	SL End Point [m]	Leg #	Trend [°]	Plunge [°]	Direction	Dip Dir. [°]	Dip [°]
12a	313855	5497737	613	0	3.65	1	165	-1	N-S	268	18
12b	313860	5497722	613	3.65	4.6	2	300	-39	E-W	262	74

DATA

Fracture SL Intersection [m]	Leg #	Dip Dir [°]	Dip [°]	Trace Length strike [m]	Trace Length dip [m]	Upper Termin	Lower Termin	Aperture [mm]	Primary roughness	Secondary roughness	Filling	Movement	Com-ment
0.1	1	307	82	1.28	0.40U	B	U	0	u	r	n	n	
0.32	1	295	89	0.82		B	A	0	u	r	n	n	
0.53	1	285	83	1.49		B	B	0	u	r	n	n	
0.72	1	304	85	0.96		B	B	0	u	r	n	n	
1.24	1	116	40	0.86		B	B	0	u	r	n	n	
1.96	1	282	80	1.03		B	A	0	u	r	n	n	
2.21	1	81	70	0.83		B	B	0	p	r	n	n	
2.53	1	347	86	0.44		A	B	0	u	r	n	n	
2.82	1	335	60	0.37		B	T	0	u	r	n	n	
3.12	1	337	82	0.59	0.51U	T	U	0	u	r	n	n	
3.24	1	86	65	3.03		B	A	0	u	r	n	n	
3.3	1	158	89	0.39		T	T	0	u	r	n	n	
3.76	2	81	21	0.3		T	T	0	u	r	n	n	
3.8	2	91	64	1.16		B	T	0	u	r	n	n	
3.95	2	94	66	1.17		B	B	0	u	r	n	n	
4.06	2	86	20	0.83		B	T	0	u	r	n	n	
4.15	2	86	66	0.47		B	A	0	u	r	n	n	
4.2	2	76	22	1.09		B	T	0	u	r	n	n	
4.21	2	82	75	0.38		T	B	0	u	r	n	n	
4.3	2	83	21	0.55		B	A	0	u	r	n	n	
4.42	2	76	36	1.66		B	B	0	u	r	n	n	
4.52	2	80	30	1.08		B	B	0	u	r	n	n	
4.55	2	80	29	0.92		B	B	0	u	r	n	n	

One or more separate scanlines

			Dip Dir. [°]	Dip [°]
Photo #:	14b	approximate surface orientation:	245	76

Outcrop Face Dimensions [m]:
x = 6.0
y = 3.0

Scanline c)

Waypoint	E [m]	N [m]	Elev. [m]	SL length [m]	Trend [°]	Plunge [°]	Direction
12c	0313872	5497699	614	3.05	231	-12	E-W

DATA

Fracture SL Intersection [m]	Dip Dir [°]	Dip [°]	Trace Length strike [m]	Trace Length dip [m]	Upper Termin.	Lower Termin.	Aperture [mm]	Primary roughness	Secondary roughness	Fillings	Movement	Comment
0.21	101	81	1.74		B	B	0	u	r	n	n	
0.52	284	78	1.04		B	B	0	u	r	n	n	
0.66	283	80	4.07		B	B	0	u	r	n	n	
0.81	288	84	1.44		B	B	0	u	r	n	n	
0.96	278	79	1.49		B	A	0	u	r	n	n	
1.11	284	76	0.45		A	B	0	u	r	n	n	
1.52	273	61	1.19		B	T	0	u	r	n	n	
1.58	274	81	0.99		B	B	0	u	r	n	n	
1.6	271	81	0.83		B	B	0	u	r	n	n	
1.73	261	59	1.97		B	B	0	u	r	n	n	
1.84	279	66	0.65		B	B	0	u	r	n	n	
1.91	270	70	0.48		B	B	0	u	r	n	n	
2.02	253	72	1.15		B	B	0	u	r	n	n	
2.12	264	85	1.4		B	B	0	u	r	n	n	
2.28	273	72	0.59		B	B	0	u	r	n	n	
2.39	259	85	2.12		A	B	0	u	r	n	n	

Fracture SL Intersection [m]	Dip Dir [°]	Dip [°]	Trace Length strike [m]	Trace Length dip [m]	Upper Termin.	Lower Termin.	Aperture [mm]	Primary roughness	Secondary roughness	Fillings	Movement	Comment
2.53	257	77	0.68		B	B	0	u	r	n	n	
2.59	257	77	0.66		B	B	0	u	r	n	n	
2.71	254	79	1.54		A	B	0	u	r	n	n	
2.76	251	88	1.07		B	B	0	u	r	n	n	
2.83	255	78	2.3		T	U	0	u	r	n	n	
3.03	75	74	0.5		B	B	0	u	r	n	n	

One or more separate scanlines

				Dip Dir. [°]	Dip [°]
Photo #:	15b	approximate surface orientation:		245	76

Outcrop Face Dimensions [m]:
x = 3.0
z = 0.5

Scanline d)

Waypoint	E [m]	N [m]	Elev. [m]	SL length [m]	Trend [°]	Plunge [°]	Direction
12d	0313860	5497718	613	2.3	170	-1	N-S

DATA

Fracture SL Intersection [m]	Dip Dir [°]	Dip [°]	Trace Length strike [m]	Trace Length dip [m]	Upper Termin.	Lower Termin.	Aperture [mm]	Primary roughness	Secondary roughness	Fillings	Movement	Comment
0.17	66	61	0.42		B	U	0	u	r	n	n	
0.39	62	67	0.31		B	U	0	u	r	n	n	
0.43	65	53	0.36		B	B	0	u	r	n	n	
0.6	60	71	0.72		T	B	0	u	r	n	n	
0.61	314	88	1.37B	0.25	T	U	0	u	r	n	n	
0.9	310	67		0.24	U	B	0	u	r	n	n	
1	311	65	0.12		U	T	0	u	r	n	n	
1.04	62	63	0.98		U	B	0	u	r	n	n	
1.2	127	82	.64B	0.38	U	U	0	u	r	n	n	
1.44	304	76	0.53		U	A	0	u	r	n	n	

Fracture SL Intersection [m]	Dip Dir [°]	Dip [°]	Trace Length strike [m]	Trace Length dip [m]	Upper Termin.	Lower Termin.	Aperture [mm]	Primary roughness	Secondary roughness	Fillings	Movement	Comment
1.59	298	69		0.33	U	T	0	u	r	n	n	
1.67	64	83	0.67		B	B	0	u	r	n	n	
1.83	61	84	0.47		U	B	0	u	r	n	n	
2.18	248	89	1.67		B	B	0	u	r	n	n	

Outcrop #	13
General Data	
Date	28-May-06
Name Surveyor	HV/MAB
Character/dimension of outcrop	A(wall: 10x4.5), B(wall: 6x2), C(surface:18x6)
near or away of faulzone?	
Lithology description	
Rocktype	ambhibolite gneiss
colour fresh/weathered	Fresh: dark grey fine to medium grained mafic minerals (ambhibole and hornblende) with bands of feldspat and quarzo, phorphyroclasts up to 0.5 cm. In some parts pinkish, orange colors from weathering of feldspar; Weathered: drak grey with moss and lichen
homegeneous vs heterogeneous	hetrogeneous
sample taken?	no
Structures	
Foliation/bedding (Dip Dir./Dip)	not measurable
Liniation (Trend/plunge)	not measurable
folds (amplitude, wavelength, fold axis, fold plane)	
fault (width, trace, gouge, orientation)	
Shear zone (width, trace)	
Rock mass description	
Block shape	t
Block size	ms
weathering class	II
seepage (presence/absence)	absent

Outcrop #: 13

One or more separate scanlines

			Dip Dir. [°]	Dip [°]
Photo #:	16b	approximate surface orientation:	81	74

Outcrop Face Dimensions [m]:

y = 10

z = 4.5

Scanline a)

Waypoint	E [m]	N [m]	Elev. [m]	SL length [m]	Trend [°]	Plunge [°]	Direction
13a	0311471	5502084	572	6.5	194	-28	U-D

DATA

Fracture SL Intersection [m]	Dip Dir [°]	Dip [°]	Trace Length strike [m]	Trace Length dip [m]	Upper Termin.	Lower Termin.	Aperture [mm]	Primary roughness	Secondary roughness	Fillings	Movement	Comment
0.45	245	10		3.52	B	B	0	u	r	n	n	
0.7	265	18		0.72	B	B	0	u	r	n	n	
0.85	240	10		2.36	B	B	1	u	r	n	n	
0.98	242	12		0.84	B	B	0	u	r	n	n	
1.19	230	10		2.91	B	B	1	u	r	n	n	
1.76	234	11		1.83	B	B	0	u	r	n	n	
2.19	229	11		2.82	B	B	0	u	r	n	n	
3.01	233	13		3.69	B	B	0.5	u	r	n	n	
4.02	232	15		3.7	B	B	0	u	r	n	n	
4.99	239	19		8.9	U	U	0	u	r	n	n	
5.54	240	16		1.45	B	T	0	u	r	n	n	
5.85	212	85		1.7	B	B	0	u	r	n	n	
5.91	238	16		2.35	B	B	0	u	r	n	n	

306

One or more separate scanlines									
				Dip Dir. [°]	**Dip [°]**	**Outcrop Face Dimensions [m]:**			
Photo #:	17b	approximate surface orientation:		84	68	x = 6.0			
						z = 2.0			

Scanline b)

Waypoint	E [m]	N [m]	Elev. [m]	SL length [m]	Trend [°]	Plunge [°]	Direction
13b	0311467	5502073	573	4.5	18	-18	S-N

DATA

Fracture SL Intersection [m]	Dip Dir [°]	Dip [°]	Trace Length strike [m]	Trace Length dip [m]	Upper Termin.	Lower Termin.	Aperture [mm]	Primary roughness	Secondary roughness	Fillings	Movement	Comment
0.01	212	7		0.79	B	B	0	u	r	n	n	
1.51	285	31	0.94		U	B	0	u	r	n	n	
1.79	214	79		1.5	U	B	0	u	r	n	n	
1.98	212	77		1.11	B	B	0	u	r	n	n	
2.96	210	81		2.3	B	B	0	u	r	n	n	
3.1	227	15		6.2	B	U	0	u	r	n	n	
3.67	237	10		1.88	B	B	0	u	r	n	n	
4	230	20		2.33	B	B	0	u	r	n	n	

One or more separate scanlines

Photo #:	18b	approximate surface orientation:	Dip Dir. [°]	Dip [°]
			235	12

Outcrop Face Dimensions [m]:
x = 18
y = 6

Scanline c)

Waypoint	E [m]	N [m]	Elev. [m]	SL length [m]	Trend [°]	Plunge [°]	Direction
13c	0311460	5502072	574	5.5	228	-12	E-W

DATA

Fracture SL Intersection [m]	Dip Dir [°]	Dip [°]	Trace Length strike [m]	Trace Length dip [m]	Upper Termin.	Lower Termin.	Aperture [mm]	Primary roughness	Secondary roughness	Fillings	Movement	Comment
0.13	297	75	0.34		B	B	0	p	r	n	n	
0.41	254	89	0.67		B	B	0	u	r	n	n	
0.46	255	88	0.43		B	B	0	u	r	n	n	
0.61	252	84	0.24		B	B	0	u	r	n	n	
0.98	81	63	0.54		B	B	0	u	r	n	n	
1.07	76	76	0.46		B	B	0	u	r	n	n	
1.27	3	80	1.45		B	B	0	u	r	n	n	
1.68	264	81	0.56		B	U	0	u	r	n	n	
1.73	264	62	0.59		B	U	0	u	r	n	n	
1.85	246	83	1.38		B	U	0	P	r	n	n	
2.08	258	69	3.32		U	U	10	u	r	n	n	
2.21	272	57	0.88		B	T	0	u	r	n	n	
2.59	252	66	0.7		B	B	0	u	r	n	n	
3.09	281	89	0.41		A	B	0	st	r	n	n	
3.21	280	88	0.81		B	B	0	st	r	n	n	
3.32	282	79	0.35		B	A	0	u	r	n	n	
4.28	34	62	0.33		B	B	0	p	r	n	n	
4.5	213	64	0.72		T	B	0	u	r	n	n	
4.71	130	88	0.59		B	B	0	u	r	n	n	
5.46	206	84	0.78		U	B	0	u	r	n	n	

308

Outcrop #	14
General Data	
Date	29-May-06
Name Surveyor	HV/MAB
Character/dimension of outcrop	A(wall: 12mx5m); B(wall: 2mx1m)
near or away of faulzone?	
Lithology description	
Rocktype	Quarzo feldspatic gneiss
colour fresh/weathered	Fresh: greyish white coarse grained quarzo feldspatic gneiss with bands of light grey fine grained mafic material up to 3cm wide. Quarz viening in matrix, some feldspar phorpyroclats up to 5cm in diameter, most of them 1 cm.; Weathered: yellowish and pinkish with some light reddish staining, little moss, some surfaces wethered to form a pitted surface
homegeneous vs heterogeneous	homogeneous
sample taken?	no
Structures	
Foliation/bedding (Dip Dir./Dip)	211/15
Liniation (Trend/plunge)	295/10
folds (amplitude, wavelength, fold axis, fold plane)	
fault (width, trace, gouge, orientation)	
Shear zone (width, trace)	
Rock mass description	
Block shape	i
Block size	ms
weathering class	II
seepage (presence/absence)	absent

Outcrop #: 14

One or more separate scanlines

Photo #:	19b	approximate surface orientation:	Dip Dir. [°]	Dip [°]
			304	84

Outcrop Face Dimensions [m]:
x =12
z = 5

Scanline a)

Waypoint	E [m]	N [m]	Elev. [m]	SL length [m]	Trend [°]	Plunge [°]	Direction
14a	0316951	5485947	643	8.4	22	-31	S-N

Fracture SL Intersection [m]	Dip Dir [°]	Dip [°]	Trace Length strike [m]	Trace Length dip [m]	Upper Termin.	Lower Termin.	Aperture [mm]	Primary roughness	Secondary roughness	Fillings	Movement	Comment
0.25	206	77		0.78	B	B	0	u	r	n	n	
0.34	124	79	0.96		U	T	0	u	r	n	n	
0.53	206	42		0.84	B	B	0	u	r	n	n	
0.8	199	56		0.74	B	B	0	u	r	n	n	
0.92	26	77		0.36	B	B	0	u	r	n	n	
1.08	247	81		0.39	B	B	0	u	r	n	n	
1.41	44	61		0.76	B	B	0	u	r	n	n	
1.62	221	61		1.16	B	B	0	u	r	n	n	
1.99	111	65		0.66	B	A	0	u	r	n	n	
2.01	19	67		0.58	B	B	0	u	r	n	n	
2.21	272	10	0.6		B	B	0	u	r	n	n	
2.65	189	71		0.82	U	U	0	u	r	n	n	
3.3	114	45	4.41		B	B	0	u	r	n	n	
4.21	217	62		0.36	B	B	0	u	r	n	n	
4.44	205	48		1.1	B	T	0	u	r	n	n	
4.59	32	82		1.47	U	U	0	u	r	n	n	
4.82	121	50	3.07		B	T	0	u	r	n	n	
4.96	218	52		1.2	T	B	0	u	r	n	n	
5.02	31	82		0.67	B	U	0	u	r	n	n	
5.25	211	52		0.57	B	T	0	u	r	n	n	
5.52	121	6	0.8		B	B	0	u	r	n	n	
5.96	211	52		1.3	B	U	0	u	r	n	n	
6.38	191	59		0.9	B	B	0	p	r	n	n	
6.53	211	63		0.41	B	B	0	u	r	n	n	
6.84	207	72		1.2	A	B	0	u	r	n	n	
7.04	28	82		0.63	T	A	0	u	r	n	n	
7.34	222	56		0.81	T	B	0	u	r	n	n	

Fracture SL Intersection [m]	Dip Dir [°]	Dip [°]	Trace Length strike [m]	Trace Length dip [m]	Upper Termin.	Lower Termin.	Aperture [mm]	Primary roughness	Secondary roughness	Fillings	Movement	Comment
7.58	196	62		0.49	B	B	0	u	r	n	n	
7.91	228	82		0.83	T	B	0	u	r	n	n	
8.15	224	63		2.1	B	A	0	u	r	n	n	
8.37	205	54		0.69	B	B	0	u	r	n	n	

One or more separate scanlines

			Dip Dir. [°]	Dip [°]
Photo #:	1	approximate surface orientation:	245	76

Outcrop Face Dimensions [m]:

y = 2

z = 1

Scanline b)

Waypoint	E [m]	N [m]	Elev. [m]	SL length [m]	Trend [°]	Plunge [°]	Direction
14b	0316949	5485937	647	1.4	320	-52	U-D

DATA

Fracture SL Intersection [m]	Dip Dir [°]	Dip [°]	Trace Length strike [m]	Trace Length dip [m]	Upper Termin.	Lower Termin.	Aperture [mm]	Primary roughness	Secondary roughness	Fillings	Movement	Comment
0.01	120	60	0.26		B	B	0	p	r	n	n	
0.03	112	55	0.55		B	B	0	p	r	n	n	
0.1	111	55	0.92		U	T	0	p	r	n	n	
0.15	116	59	0.39		B	T	0	p	r	n	n	
0.18	108	46	0.42		U	B	0	p	r	n	n	
0.19	111	52	0.56		A	B	0	p	r	n	n	
0.25	109	41	0.47		U	B	0	p	r	n	n	
0.28	114	56	1.07		U	U	0	p	r	n	n	
0.31	115	58	0.54		U	T	0	p	r	n	n	
0.43	115	57	0.56		U	T	0	p	r	n	n	
0.53	178	71		0.39	B	T	0	p	r	n	n	
0.68	118	62	1.41		U	U	0	u	r	n	n	

Fracture SL Intersection [m]	Dip Dir [°]	Dip [°]	Trace Length strike [m]	Trace Length dip [m]	Upper Termin.	Lower Termin.	Aperture [mm]	Primary roughness	Secondary roughness	Fillings	Movement	Comment
0.71	192	61		0.31	B	B	0	u	r	n	n	
0.83	191	61		0.34	B	B	0	u	r	n	n	
0.86	116	72	1.36		U	T	0	u	r	n	n	
0.98	194	75		1.17	U	U	0	u	r	n	n	
1.29	69	68		1.02	U	B	0	u	r	n	n	

Outcrop #	15
General Data	
Date	3-Jun-06
Name Surveyor	HV/JL
Character/dimension of outcrop	A,B (wall: 5mx40m); C (surface: 70mx20m)
near or away of faulzone?	
Lithology description	
Rocktype	granodiorite
colour fresh/weathered	Fresh: greyish white medium grained, mostly feldspar, some quartz (~15%) and K-feldspar (~60%) and mafic (~25%) probably biotide or hornblende; Weathered: rusty brown color with lichen and some moss
homegeneous vs heterogeneous	homogeneous
sample taken?	yes
Structures	
Foliation/bedding (Dip Dir./Dip)	no, granodiorite!
Liniation (Trend/plunge)	no, granodiorite!
folds (amplitude, wavelength, fold axis, fold plane)	
fault (width, trace, gouge, orientation)	
Shear zone (width, trace)	
Rock mass description	
Block shape	i
Block size	ms
weathering class	II
seepage (presence/absence)	absent

312

Outcrop #: 15

One or more separate scanlines

			Dip Dir. [°]	Dip [°]	Outcrop Face Dimensions [m]:
Photo #:	23b	approximate surface orientation:	261	70	y =40
					z = 5

Scanline a)

Waypoint	E [m]	N [m]	Elev. [m]	SL length [m]	Trend [°]	Plunge [°]	Direction
15a	0312195	5502881	759	7.5	180	-21	N-S

DATA

Fracture SL Intersection [m]	Dip Dir [°]	Dip [°]	Trace Length strike [m]	Trace Length dip [m]	Upper Termin.	Lower Termin.	Aperture [mm]	Primary roughness	Secondary roughness	Fillings	Movement	Comment
0.08	174	89		0.2	B	B	0	p	r	n	n	
0.29	169	88		1.01	B	T	0	u	r	n	n	
0.36	173	89		0.45	T	T	0	u	r	n	n	
1.18	175	89		1.12	B	B	0	u	r	n	n	
1.65	185	84		0.72	B	H	0	u	r	n	n	
1.85	174	85		0.51	B	B	0	u	r	n	n	
2.2	166	89		1.32	T	B	0	u	r	n	n	
2.57	175	89		1.9	T	B	0	u	r	n	n	
2.71	173	89		1.23	B	U	0	u	r	n	n	
2.93	176	87		0.49	B	T	0	u	r	n	n	
3.05	175	88		3.6	U	B	10	u	r	n	n	
3.23	173	88		1.19	B	U	0	u	r	n	n	
3.79	176	89		0.31	T	B	0	u	r	n	n	
3.84	120	31		0.64	B	B	0	p	r	n	n	
6.3	172	89		0.2	B	B	0	p	r	n	n	
6.63	175	86		2.2	U	A	10	u	r	n	n	

Fracture SL Intersection [m]	Dip Dir [°]	Dip [°]	Trace Length strike [m]	Trace Length dip [m]	Upper Termin.	Lower Termin.	Aperture [mm]	Primary roughness	Secondary roughness	Fillings	Movement	Comment
6.65	169	89		0.74	B	B	0	u	r	n	n	
6.68	174	89		1.02	A	H	0	u	r	n	n	
6.86	166	85		0.66	B	T	0	u	r	n	n	
7.25	162	83		1.12	B	T	0	u	r	n	n	

One or more separate scanlines

				Dip Dir. [°]	Dip [°]
Photo #:	23b	approximate surface orientation:		261	70

Outcrop Face Dimensions [m]:
y =40
z = 5

Scanline b)

Waypoint	E [m]	N [m]	Elev. [m]	SL length [m]	Trend [°]	Plunge [°]	Direction
15b	0312187	5502880	762	4.5	253	-69	U-D

DATA

Fracture SL Intersection [m]	Dip Dir [°]	Dip [°]	Trace Length strike [m]	Trace Length dip [m]	Upper Termin.	Lower Termin.	Aperture [mm]	Primary roughness	Secondary roughness	Fillings	Movement	Comment
1	128	20		3	B	U	u	u	r	n	n	
1.32	128	20		1.5	T	U	u	p	r	n	n	
1.68	128	20		1	T	U	u	u	r	n	n	
2.79	125	38		10.6	T	U	0	u	r	n	n	
3.06	144	37		0.75	A	B	0	p	r	n	n	
3.18	147	39		1.02	A	T	0	u	r	n	n	
3.42	135	38		0.96	T	B	0	u	r	n	n	
3.61	125	30		0.32	T	B	0	p	r	n	n	
3.85	235	24		1.38	T	T	0	u	r	n	n	
4.24	120	41		1.29	A	B	0	u	r	n	n	

One or more separate scanlines

				Dip Dir. [°]	Dip [°]	Outcrop Face Dimensions [m]:
Photo #:	24b	approximate surface orientation:		200	22	x = 70

y = 20

Scanline c)

Waypoint	E [m]	N [m]	Elev. [m]	SL length [m]	Trend [°]	Plunge [°]	Direction
15C	0312192	5502900	764	7	241	-28	E-W

DATA

Fracture SL Intersection [m]	Dip Dir [°]	Dip [°]	Trace Length strike [m]	Trace Length dip [m]	Upper Termin.	Lower Termin.	Aperture [mm]	Primary roughness	Secondary roughness	Fillings	Movement	Comment
0.15	255	61	1.45		B	B	0	u	s	n	n	
0.33	250	68	1.06		B	T	0	u	s	n	n	
0.63	254	83	0.74		B	T	0	p	s	n	n	
0.92	249	68	0.83		B	T	0	p	s	n	n	
0.95	251	71	1.29		B	T	0	u	s	n	n	
1.17	253	77	0.51		B	B	0	u	s	n	n	
1.46	254	73	0.72		B	B	0	p	s	n	n	
2.15	350	70	2		B	B	0	u	r	n	n	
3.05	265	89	3		U	B	po	u	r	n	n	
3.25	263	86	2.61		U	H	t	p	r	n	n	
4.01	267	88	1.96		T	B	po	u	r	n	n	
4.47	8	74	3.29		A	U	t	u	r	n	n	
6.17	276	86	1.76		A	B	vt	p	r	n	n	
6.3	269	88	3.4		U	T	vt	p	r	n	n	
6.57	271	86	4.03		A	T	vt	u	r	n	n	

Outcrop #	16
General Data	
Date	4-Jun-05
Name Surveyor	HV/JL
Character/dimension of outcrop	A (wall: 3mx8m); B (surface: 5mx4m)
near or away of faulzone?	
Lithology description	
Rocktype	Quartzo feldspat. gneiss
colour fresh/weathered	Fresh: pink to grey, medium grained mostly feldspatic (Na-Al) content, some quartz, some mafics; Weathered: rusty brown, dark to grey lichen and moss
homegeneous vs heterogeneous	heterogeneous
sample taken?	yes
Structures	
Foliation/bedding (Dip Dir./Dip)	very few, not measurable
Liniation (Trend/plunge)	no lineation
folds (amplitude, wavelength, fold axis, fold plane)	
fault (width, trace, gouge, orientation)	
Shear zone (width, trace)	
Rock mass description	
Block shape	i
Block size	ms
weathering class	II
seepage (presence/absence)	absent

Outcrop #: 16

One or more separate scanlines

Photo #:	25b	approximate surface orientation:	Dip Dir. [°]	Dip [°]
			280	70

Outcrop Face Dimensions [m]:

y =8

z = 3

Scanline a)

Waypoint	E [m]	N [m]	Elev. [m]	SL length [m]	Trend [°]	Plunge [°]	Direction
16a	0316069	5489681	722	5.4	201	-18	N-S

DATA

Fracture SL Intersection [m]	Dip Dir [°]	Dip [°]	Trace Length strike [m]	Trace Length dip [m]	Upper Termin.	Lower Termin.	Aperture [mm]	Primary roughness	Secondary roughness	Fillings	Movement	Comment
0.6	15	46		0.48	B	T	t	u	r	n	n	
1.49	23	48		1.12	B	U	t	u	r	n	n	
1.62	20	49		0.96	B	A	vt	u	r	n	n	
2.43	290	14	1.49		A	A	vt	u	r	n	n	weathering z.
2.89	28	55		1.27	B	T	po	u	r	n	n	
3.31	264	11	2.24		B	T	vt	u	r	n	n	weathering z.
3.39	27	56		0.57	B	B	t	u	r	n	n	
3.98	18	61		1.29	B	T	po	u	r	n	n	
4	23	66		0.64	B	B	vt	u	r	n	n	
4.04	21	65		1.69	B	B	t	u	r	n	n	
4.06	276	16	1.6		B	T	po	u	r	n	n	weathering z.
4.57	8	62		1.56	B	B	t	u	r	n	n	

One or more separate scanlines

			Dip Dir. [°]	Dip [°]
Photo #:	26b	approximate surface orientation:	282	21

Outcrop Face Dimensions [m]:
x = 5
y = 4

Scanline b)

Waypoint	E [m]	N [m]	Elev. [m]	SL length [m]	Trend [°]	Plunge [°]	Direction
16b	0316071	5489689	724	4	310	18	W-E

Fracture SL Intersection [m]	Dip Dir [°]	Dip [°]	Trace Length strike [m]	Trace Length dip [m]	Upper Termin.	Lower Termin.	Aperture [mm]	Primary roughness	Secondary roughness	Fillings	Movement	Comment
0.37	129	86	0.45		B	T	vt	u	r	n	n	
0.58	308	78	0.82		B	B	vt	u	r	n	n	
0.67	292	88	0.6		B	T	vt	u	r	n	n	
0.9	2	55	2.86	2.55B	B	U	po	u	r	n	n	
1.39	284	89	0.75		T	B	vt	st	r	n	n	
1.86	282	78	1.74		U	B	po	u	r	n	n	
2.23	117	77	0.82		U	T	t	u	r	n	n	
2.28	115	68	0.77		T	B	t	p	s	n	n	
2.35	115	87	0.37		B	T	t	p	s	n	n	
2.59	117	77	0.46		B	T	t	p	s	n	n	
2.67	26	81	1.76		U	T	t	u	r	n	n	
2.73	111	75	0.87		B	B	t	u	s	n	n	
3.12	108	71	0.58		B	B	vt	u	r	n	n	
3.18	113	74	1		A	B	vt	u	r	n	n	

Outcrop #	17
General Data	
Date	5-Jun-06
Name Surveyor	HV/JL
Character/dimension of outcrop	A (surface: 15mx3m); B (wall: 22mx2m)
near or away of faulzone?	

Lithology description	
Rocktype	amphibolite gneiss
colour fresh/weathered	Fresh: grey, medium to coarse grained, mostly mafic minerals (~60%), about 30% feldspar (up to 2 mm phorphyroblasts and some quartz; Weathered: dark grey to rusty brown with lichen and moss
homegeneous vs heterogeneous	heterogeneous
sample taken?	no
Structures	
Foliation/bedding (Dip Dir./Dip)	195/23
Liniation (Trend/plunge)	not seen!
folds (amplitude, wavelength, fold axis, fold plane)	
fault (width, trace, gouge, orientation)	
Shear zone (width, trace)	
Rock mass description	
Block shape	t
Block size	ms
weathering class	II
seepage (presence/absence)	absent

Outcrop #: 17

One or more separate scanlines

			Dip Dir. [°]	Dip [°]
Photo #:	28b	approximate surface orientation:	205	20

Outcrop Face Dimensions [m]:
x = 15
y = 3

Scanline a)

Waypoint	E [m]	N [m]	Elev. [m]	SL length [m]	Trend [°]	Plunge [°]	Direction
17a	0312188	5499691	535	5	148	-6	N-S

DATA

Fracture SL Intersection [m]	Dip Dir [°]	Dip [°]	Trace Length strike [m]	Trace Length dip [m]	Upper Termin.	Lower Termin.	Aperture [mm]	Primary roughness	Secondary roughness	Fillings	Movement	Comment
0.29	120	89	0.72		B	B	vt	st	s	n	n	
0.51	302	88	3.33		B	B	mw	st	s	n	n	
0.7	295	84	1.7		B	B	po	st	s	n	n	
0.78	296	89	0.18		B	B	vt	p	s	n	n	

Fracture SL Intersection [m]	Dip Dir [°]	Dip [°]	Trace Length strike [m]	Trace Length dip [m]	Upper Termin.	Lower Termin.	Aperture [mm]	Primary roughness	Secondary roughness	Fillings	Movement	Comment
1.12	281	67	4.6		B	B	o	st	s	n	n	
1.44	298	71	0.54		B	B	vt	st	s	n	n	
1.73	288	68	3.82		B	A	po	st	r	n	n	
2.01	288	70	1.14		B	B	t	st	r	n	n	
2.04	290	64	1.5		A	B	vt	st	r	n	n	
2.58	290	70	2.4		B	B	t	st	r	n	n	
2.64	289	70	2.5		B	A	po	st	r	n	n	
3.06	286	70	2.01		B	A	t	st	s	n	n	
3.39	306	73	1.49		B	B	t	u	r	n	n	
3.54	309	80	1.68		B	B	t	u	r	n	n	
3.62	308	72	0.62		B	B	vt	p	r	n	n	
3.66	309	67	0.77		B	B	po	u	r	n	n	
3.67	305	74	1.32		B	H	t	st	r	n		
3.8	305	69	0.52		A	B	t	p	r	n	n	
3.83	306	69	0.77		B	B	t	st	r	n	n	
3.91	304	79	3.03		B	H	po	st	r	n	n	
4.07	294	81	0.34		B	B	vt	st	s	n	n	
4.21	294	80	1.86		B	B	t	st	s	n	n	
4.41	296	80	0.94		B	B	t	st	s	n	n	
4.56	298	80	2.13		B	B	mw	st & u	r	n	n	

One or more separate scanlines

			Dip Dir. [°]	Dip [°]
Photo #:	29b	approximate surface orientation:	103	86

Outcrop Face Dimensions [m]:
y = 22
z = 2

Scanline b)

Waypoint	E [m]	N [m]	Elev. [m]	SL length [m]	Trend [°]	Plunge [°]	Direction
17b	312186	5499689	534	3.1	209	-61	N-S

Fracture SL Intersection [m]	Dip Dir [°]	Dip [°]	Trace Length strike [m]	Trace Length dip [m]	Upper Termin.	Lower Termin.	Aperture [mm]	Primary roughness	Secondary roughness	Fillings	Movement	Comment
0.42	275	62	1.38		T	B	po	u	r	n	n	
1.25	209	20		0.96	B	B	po	u,st	r	n	n	
1.31	212	23		0.49	B	T	vt	u	r	n	n	
1.4	277	62	0.73		B	B	po	u	r	n	n	
1.62	220	22		5.55	B	T	po	p	s	n	n	
2.47	194	31		6.92	U	T	o	st	r	n	n	
2.68	218	24		2.5	U	B	t	u	r	n	n	

Outcrop #	18
General Data	
Date	6-Jun-06
Name Surveyor	HV/JL
Character/dimension of outcrop	A (surface: 10mx 4m); B (wall: 10mx2m)
near or away of faulzone?	
Lithology description	
Rocktype	Ambhibolite gneiss
colour fresh/weathered	Fresh: medium grey, fine to medium grained, mostly amphibolite (~70%) and some feldspar and little quartz; Weathered: rusty brown with dark grey lichen and moss
homegeneous vs heterogeneous	homogeneous
sample taken?	no
Structures	
Foliation/bedding (Dip Dir./Dip)	not measurable, too fine!
Liniation (Trend/plunge)	no lineations
folds (amplitude, wavelength, fold axis, fold plane)	
fault (width, trace, gouge, orientation)	

321

Rock mass description	
Block shape	i
Block size	ms
weathering class	II
seepage (presence/absence)	absent

Outcrop #: 18

One or more separate scanlines

			Dip Dir. [°]	Dip [°]
Photo #:	30b	approximate surface orientation:	222	19

Outcrop Face Dimensions [m]:

x =10

y = 4

Scanline a)

Waypoint	E [m]	N [m]	Elev. [m]	SL length [m]	Trend [°]	Plunge [°]	Direction
18a	0315018	5488915	522	6	169	-11	N-S

DATA

Fracture SL Intersection [m]	Dip Dir [°]	Dip [°]	Trace Length strike [m]	Trace Length dip [m]	Upper Termin.	Lower Termin.	Aperture [mm]	Primary roughness	Secondary roughness	Fillings	Movement	Comment
0	354	85	0.34		T	A	vt	p	r	n	n	
0.01	125	59	0.39		A	B	vt	p	r	n	n	
0.03	120	47	1.84		A	B	po	u	r	n	n	
0.21	167	87	0.56		T	B	vt	u	s	n	n	
0.5	172	88	0.29		A	T	vt	u	r	n	n	
0.55	124	38	0.99		T	T	t	u	s	n	n	
0.66	129	40	0.3		B	B	vt	u	r	n	n	
1.01	170	85	0.51		B	T	vt	p	s	n	n	
1.08	122	42	0.34		B	B	vt	u	r	n	n	

Fracture SL Intersection [m]	Dip Dir [°]	Dip [°]	Trace Length strike [m]	Trace Length dip [m]	Upper Termin.	Lower Termin.	Aperture [mm]	Primary roughness	Secondary roughness	Fillings	Movement	Comment
1.18	171	85	0.24		B	B	vt	st	s	n	n	
1.31	170	83	0.23		B	B	vt	p	s	n	n	
1.54	113	31	1.45		B	B	t	u	r	n	n	
2.06	175	88	0.17		T	T	vt	u	s	n	n	
2.21	163	89	0.27		B	B	vt	u	r	n	n	
2.38	336	75	0.77		T	B	po	u	r	n	n	
2.57	336	68	0.43		T	B	t	st	r	n	n	
2.63	95	52	0.64		T	B	vt	st	r	n	n	
3.37	105	55	1.06		B	B	t	u	s	n	n	
3.86	343	66	1.58		T	T	t	p	r	n	n	
4.01	285	47	1.28		A	A	t	p	s	n	n	
4.81	334	75	0.43		B	A	t	st	r	n	n	
5.07	333	74	0.55		T	T	t	u	r	n	n	
5.17	279	86	4.64		A	T	o	st	s	n	n	
5.45	181	62	0.17		T	T	vt	p	s	n	n	
5.9	94	85	0.97		B	B	t	u	r	n	n	

One or more separate scanlines

				Dip Dir. [°]	Dip [°]	Outcrop Face Dimensions [m]:
Photo #:	31b	approximate surface orientation:		96	65	x =10
						z = 2

Scanline b)

Waypoint	E [m]	N [m]	Elev. [m]	SL length [m]	Trend [°]	Plunge [°]	Direction
18b	0315016	5488910	522	3.3	163	30	S-N

Fracture SL Intersection [m]	Dip Dir [°]	Dip [°]	Trace Length strike [m]	Trace Length dip [m]	Upper Termin.	Lower Termin.	Aperture [mm]	Primary roughness	Secondary roughness	Fillings	Movement	Comment
0.12	85	39	0.4		T	U	o	u	r	n	n	
0.76	97	90	2.67		U	U	u	u	r	n	n	
0.88	269	82	0.44		B	U	vt	u	r	n	n	
1.23	344	64		0.4	B	B	t	u	r	n	n	
1.99	268	86	1.35		B	A	t	u	r	n	n	
2.08	219	24		1.46	T	A	t	p	r	n	n	
3.25	196	20		5.43	T	U	t	u	r	n	n	

Outcrop #	19
General Data	
Date	6-Jun-06
Name Surveyor	HV/JL
Character/dimension of outcrop	A (surface: 8mx12m); B (wall: 1mx8m)
near or away of faulzone?	
Lithology description	
Rocktype	Amphibolite gneiss
colour fresh/weathered	Fresh: dark grey, medium to coarse grained, mostly amphibolite (hornblende ~70%) and feldspar (phorphyroblasts up to 0.5 cm) and little quartz; Weathered: light grey to pinkish with dark grey lichen and moss
homegeneous vs heterogeneous	heterogeneous
sample taken?	no
Structures	
Foliation/bedding (Dip Dir./Dip)	not measurable
Liniation (Trend/plunge)	not measurable
folds (amplitude, wavelength, fold axis, fold plane)	
fault (width, trace, gouge, orientation)	
Shear zone (width, trace)	

Rock mass description	
Block shape	i
Block size	l
weathering class	II
seepage (presence/absence)	absent

Outcrop #: 19

One or more separate scanlines

			Dip Dir. [°]	Dip [°]
Photo #:	32b	approximate surface orientation:	265	20

Outcrop Face Dimensions [m]:
x = 8
y = 12
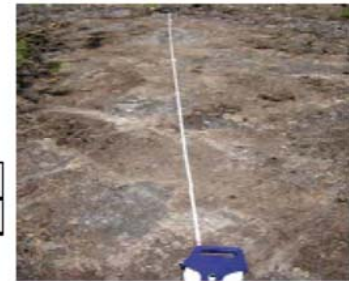
Scanline a)

Waypoint	E [m]	N [m]	Elev. [m]	SL length [m]	Trend [°]	Plunge [°]	Direction
19a	0312904	5501836	861	5	242	-22	E-W

DATA

Fracture SL Intersection [m]	Dip Dir [°]	Dip [°]	Trace Length strike [m]	Trace Length dip [m]	Upper Termin.	Lower Termin.	Aperture [mm]	Primary roughness	Secondary roughness	Fillings	Movement	Comment
0.12	289	89	0.82		B	B	t	st	r	n	n	
0.46	200	87	0.48		T	T	t	u	r	n	n	
0.71	284	51	1.24		A	B	t	st	r	n	n	
0.95	279	79	1.06		B	B	po	st	s	n	n	
1.03	96	78	1.62		B	T	po	st	s	n	n	
1.68	276	79	1.98		T	B	t	st & u	s	n	n	
2	251	83	1.22		B	T	t	u	r	n	n	
2.17	256	86	0.44		T	B	vt	p	r	n	n	
2.31	263	87	1.68		A	B	vt	u	r	n	n	
2.94	306	89	0.78		B	B	vt	st	r	n	n	
3.93	93	73	0.55		B	B	t	u	r	n	n	
4.84	295	82	1.16		B	B	t	u	r	n	n	

One or more separate scanlines

			Dip Dir. [°]	Dip [°]	Outcrop Face Dimensions [m]:
Photo #:	33b	approximate surface orientation:	148	40	y = 8
					z = 1

Scanline b)

Waypoint	E [m]	N [m]	Elev. [m]	SL length [m]	Trend [°]	Plunge [°]	Direction
19b	312907	5501822	860	2.5	50	-6	W-E

DATA

Fracture SL Intersection [m]	Dip Dir [°]	Dip [°]	Trace Length strike [m]	Trace Length dip [m]	Upper Termin.	Lower Termin.	Aperture [mm]	Primary roughness	Secondary roughness	Fillings	Movement	Comment
0.21	356	73		0.29	B	T	t	p	r	n	n	
0.81	245	30		0.89	T	U	po	u	r	n	n	
1.09	290	75	1.3		B	B	t	p	r	n	n	
1.29	295	73	0.94		B	B	t	u	r	n	n	
1.35	105	78		0.95	A	B	t	u	r	n	n	
2.09	285	20		0.69	T	B	vt	u	r	n	n	
2.22	105	72		1.07	U	B	t	u	r	n	n	

Outcrop #	20
General Data	
Date	7-Jun-06
Name Surveyor	HV/JL
Character/dimension of outcrop	A (surface: 40mx10m); B (wall: 30mx1.5m)
near or away of faulzone?	

Lithology description	
Rocktype	Amphibolite gneiss
colour fresh/weathered	Fresh: dark grey, medium grained, mostly amphibolite (~70%) and feldspar (`30%) in form of phorphyroblasts (up to 1cm) and little quartz; Weathered: rusty brown with dak grey lichen and moss
homegeneous vs heterogeneous	heterogeneous
sample taken?	no
Structures	
Foliation/bedding (Dip Dir./Dip)	not measurable
Liniation (Trend/plunge)	294/13
folds (amplitude, wavelength, fold axis, fold plane)	
fault (width, trace, gouge, orientation)	
Shear zone (width, trace)	
Rock mass description	
Block shape	t
Block size	ms
weathering class	II
seepage (presence/absence)	absent

Outcrop #: 20

One or more separate scanlines

			Dip Dir. [°]	Dip [°]
Photo #:	37b, 38b	approximate surface orientation:	245	76
	fracture z.	(38b)		

Outcrop Face Dimensions [m]:
x =40
y = 10

Scanline a)

Waypoint	E [m]	N [m]	Elev. [m]	SL length [m]	Trend [°]	Plunge [°]	Direction
20a	0314533	5493583	633	8	301	-3	E-W

Fracture SL Intersection [m]	Dip Dir [°]	Dip [°]	Trace Length strike [m]	Trace Length dip [m]	Upper Termin.	Lower Termin.	Aperture [mm]	Primary roughness	Secondary roughness	Fillings	Movement	Comment
0	122	85	1.2		B	T	vt	u	r	n	n	
0.03	121	83	0.77		B	U	vt	p	r	n	n	
0.39	291	86	1.65		B	B	t	st	r	n	n	
0.74	119	76	1.31		T	B	vt	st & u	r	n	n	
0.8	110	86	0.73		T	B	vt	u	r	n	n	
0.86	295	87	1.89		B	B	t	st	r	n	n	
0.91	298	89	0.49		B	B	vt	u	r	n	n	
1.02	295	80	0.57		T	B	vt	u	r	n	n	
1.14	287	88	1.53		U	B	t	st & u	r	n	n	
1.26	289	89	1.23		T	B	t	st & u	r	n	n	
1.72	293	89	1.66		B	T	t	st & u	r	n	n	
1.8	288	79	1.38		B	B	po	u	r	n	n	
2.73	280	72	1.39		B	T	t	u	r	n	n	
2.79	280	73	0.58		B	T	t	u	r	n	n	
2.9	276	75	2.84		A	T	po	u	r	n	n	
3.02	278	74	1.88		B	A	po	st & u	r	n	n	
3.07	189	85	0.47		T	T	vt	u	r	n	n	
3.25	280	76	0.6		B	T	vt	p	r	n	n	
3.31	281	73	0.64		N	A	vt	p	s	n	n	
3.48	286	70	1.95		B	B	t	u	s	n	n	
3.62	285	68	1.45		A	T	t	st	s	n	n	
3.82	292	89	1.7		B	A	t	u	r	n	n	
4.18	295	89	3.34		B	B	t	u	r	n	n	start FZ
4.22	103	69	0.45		A	T	vt	p	r	n	n	end FZ
4.31	100	69	0.43		B	B	vt	p	r	n	n	
4.61	102	52	1.98		B	B	t	u	r	n	n	
5.51	285	51	2.16		B	B	t	u	r	n	n	
5.69	188	60	0.46		T	T	vt	st	r	n	n	
5.88	118	75	2.05		T	A	t	st	r	n	n	
5.95	117	84	0.57		B	B	vt	u	r	n	n	
6.68	290	80	1.27		B	B	vt	u	r	n	n	

Fracture SL Intersection [m]	Dip Dir [°]	Dip [°]	Trace Length strike [m]	Trace Length dip [m]	Upper Termin.	Lower Termin.	Aperture [mm]	Primary roughness	Secondary roughness	Fillings	Movement	Comment
6.89	290	88	0.65		B	B	t	p	r	n	n	
7.29	290	86	2.33		A	B	t	u & st	r	n	n	start FZ
7.39	278	84	0.77		B	B	vt	p	r	n	n	
7.45	249	68	0.42		B	B	vt	p	s	n	n	
7.5	254	79	0.64		B	B	vt	p	s	n	n	
7.54	250	68	3.78		B	B	t	u	s	n	n	
7.62	240	63	0.45		B	B	vt	p	s	n	n	
7.64	235	68	2.36		T	B	t	u	s	n	n	
7.68	230	75	1.91		B	B	t	u	s	n	n	
7.79	280	70	2		B	B	t	st & u	s	n	n	

One or more separate scanlines

			Dip Dir. [°]	Dip [°]
Photo #:	39b	approximate surface orientation:		

Outcrop Face Dimensions [m]:
y = 30
z = 1.5

Scanline b)

Waypoint	E [m]	N [m]	Elev. [m]	SL length [m]	Trend [°]	Plunge [°]	Direction
20b	314522	5493586	632	1.5	211	-51	N-S

DATA

Fracture SL Intersection [m]	Dip Dir [°]	Dip [°]	Trace Length strike [m]	Trace Length dip [m]	Upper Termin.	Lower Termin.	Aperture [mm]	Primary roughness	Secondary roughness	Fillings	Movement	Comment
0.48	213	28		0.76	B	B	po	u	r	n	n	
0.55	301	13	1.39		B	A	o	u	r	n	n	
0.71	256	15	0.66		T	B	po	u	r	n	n	
0.72	333	80		0.48	B	T	vt	u	s	n	n	
0.76	182	32		0.36	T	A	vt	p	s	n	n	

Outcrop #	21
General Data	
Date	8-Jun-06
Name Surveyor	HV/JL
Character/dimension of outcrop	A (surface: 5mx5m); B (wall: 10mx2m)
near or away of faulzone?	
Lithology description	
Rocktype	Amphibolite Gneiss
colour fresh/weathered	Fresh: dark grey, medium grained, mostly amphibolite (~70%) with feldspar (phorphyroblasts up to 2 cm) and little quartz; Weathered: rusty brown with dark grey lichen and moss
homegeneous vs heterogeneous	heterogeneous
sample taken?	no
Structures	
Foliation/bedding (Dip Dir./Dip)	315/44
Liniation (Trend/plunge)	not seen
folds (amplitude, wavelength, fold axis, fold plane)	
fault (width, trace, gouge, orientation)	
Shear zone (width, trace)	
Rock mass description	
Block shape	i
Block size	ms
weathering class	II
seepage (presence/absence)	absent

Outcrop #: 21

One or more separate scanlines

			Dip Dir. [°]	Dip [°]	Outcrop Face Dimensions [m]:
Photo #:	40b	approximate surface orientation:	255	10	x =5
					y =5

Scanline a)

Waypoint	E [m]	N [m]	Elev. [m]	SL length [m]	Trend [°]	Plunge [°]	Direction
21a	0311915	5500945	574	4	301	-5	E-W

DATA

Fracture SL Intersection [m]	Dip Dir [°]	Dip [°]	Trace Length strike [m]	Trace Length dip [m]	Upper Termin.	Lower Termin.	Aperture [mm]	Primary roughness	Secondary roughness	Fillings	Movement	Comment
0.03	55	78	0.44		B	B	vt	u	r	n	n	
0.53	314	52	0.5		T	T	vt	u	s	n	n	
0.64	312	57	0.94		T	A	vt	u	s	n	n	
0.65	65	62	0.35		T	B	vt	u	s	n	n	
0.85	312	51	0.68		A	B	vt	p	s	n	n	
0.96	311	81	0.82		T	B	vt	p	s	n	n	
1.21	307	50	0.66		B	U	vt	u	s	n	n	
1.7	255	60	0.28		A	B	vt	u	r	n	n	
1.75	306	49	0.43		B	B	vt	u	s	n	n	
2.09	257	81	0.47		A	A	vt	u	s	n	n	
2.24	206	70	0.76		A	T	vt	u	s	n	n	
2.52	294	70	0.46		B	A	vt	p	r	n	n	
2.57	268	72	0.81		A	T	t	u	s	n	n	
2.83	293	56	0.63		A	A	vt	u	s	n	n	
2.95	347	82	0.28		B	T	vt	u	r	n	n	
3.13	302	60	0.37		B	H	vt	u	s	n	n	
3.29	245	70	1.11		B	T	t	u	r	n	n	
3.6	74	49	1.04		B	A	t	st&u	r	n	n	
3.96	60	55	0.5		B	B	vt	u	r	n	n	

331

One or more separate scanlines

			Dip Dir. [°]	Dip [°]
Photo #:	41b	approximate surface orientation:	265	60

Outcrop Face Dimensions [m]:

y = 10

z = 2

Scanline b)

Waypoint	E [m]	N [m]	Elev. [m]	SL length [m]	Trend [°]	Plunge [°]	Direction
21b	311908	5500951	573	3	306	-41	U-D

DATA

Fracture SL Intersection [m]	Dip Dir [°]	Dip [°]	Trace Length strike [m]	Trace Length dip [m]	Upper Termin.	Lower Termin.	Aperture [mm]	Primary roughness	Secondary roughness	Fillings	Movement	Comment
0.21	239	21		0.74	A	A	vt	u	r	n	n	
0.39	260	82	1.26		B	B	vt	u	r	n	n	
0.5	149	60		1	A	A	o	st	r	n	n	
0.72	254	88	0.69		B	B	vt	u	r	n	n	
0.88	149	61		0.42	T	B	t	u	r	n	n	
0.97	73	83	0.56		B	B	vt	u	r	n	n	
1.11	200	14		1.3	A	B	t	u	r	n	n	
1.3	70	78	0.42		B	A	vt	u	r	n	n	
1.59	115	85	0.69		A	A	vt	u	r	n	n	
1.68	101	85	0.75		U	A	vt	u	s	n	n	
1.87	186	17		1.11	T	B	po	u	r	n	n	
1.97	226	26		1.8	B	A	po	u	r	n	n	
2.44	79	85	0.37		B	B	vt	u	r	n	n	
2.59	81	88	0.51		B	B	vt	u	r	n	n	
2.62	70	83	0.95		B	B	vt	u	r	n	n	
2.75	221	17		0.98	U	A	po	u	r	n	n	

332

Outcrop #	24
General Data	
Date	11-Jun-06
Name Surveyor	HV/JL
Character/dimension of outcrop	A (wall: 4mx12m); B (surface: 2mx4m)
near or away of faulzone?	very close to bigger lineament
Lithology description	
Rocktype	1) Quartzo feldspatic gneiss; 2) Amphibolite gneiss
colour fresh/weathered	1) Fresh: grey, fine to medium grained, mostly quartz (~60%), feldspar (~20%) and mafics (~20%); Weathered: brown with dark grey lichen and moss; 2) Fresh: darl grey, medium grained, mostly mafics (~70%), feldspar (~20%) also as phorphyroblasts up to 2cm and quartz (~10); Weathered: dark brown to black with dark grey lichen and moss
homegeneous vs heterogeneous	1) homegeneous; 2) heterogeneous
sample taken?	1) yes-a; 2) yes-b
Structures	
Foliation/bedding (Dip Dir./Dip)	weakly foliated, hard to measure
Liniation (Trend/plunge)	no
folds (amplitude, wavelength, fold axis, fold plane)	
fault (width, trace, gouge, orientation)	
Shear zone (width, trace)	
Rock mass description	
Block shape	b
Block size	ms
weathering class	II
seepage (presence/absence)	absent

Outcrop #: 24

One or more separate scanlines

Photo #:	59b	approximate surface orientation:	Dip Dir. [°]	Dip [°]	Outcrop Face Dimensions [m]:
			275	75	y =12

Scanline a)   z = 4

Waypoint	E [m]	N [m]	Elev. [m]	SL length [m]	Trend [°]	Plunge [°]	Direction
24a	316647	5492060	923	7	195	-30	N-S

DATA

Fracture SL Intersection [m]	Dip Dir [°]	Dip [°]	Trace Length strike [m]	Trace Length dip [m]	Upper Termin.	Lower Termin.	Aperture [mm]	Primary roughness	Secondary roughness	Fillings	Movement	Comment
0.2	20	83		0.32	B	T	t	p	r	n	n	
0.38	25	56		0.61	B	T	t	u	r	n	n	
0.51	176	76		0.92	T	A	t	u	r	n	n	
0.64	10	86	0.85B	0.65	U	T	o	p	r	n	n	
0.89	185	5		0.77	B	U	t	u	r	n	n	
0.94	14	88		0.54	B	T	t	u	r	n	n	
1.18	223	8	2.67		T	U	t	u	r	n	n	
1.29	21	44		1	A	A	o	u	r	n	n	Est. length
1.57	188	15		1.04	A	A	t	u	r	n	n	
2.35	160	10		2.23	T	T	po	u	r	n	n	
2.5	250	10	0.93		A	B	t	u	r	n	n	
3.11	194	84		0.42	T	A	vt	u	s	n	n	
3.53	241	6	0.76		A	B	vt	u	r	n	n	
3.56	160	34		1.26	B	A	t	u	r	n	n	
3.69	150	14		1.22	A	T	vt	u	s	n	n	
3.86	191	89		0.38	T	T	vt	u	s	n	n	
4.21	254	10	0.95		A	T	vt	u	r	n	n	
4.29	203	82		1.03	T	T	t	u	s	n	n	
4.69	199	85		0.66	B	B	po	u	r	n	n	
4.98	226	10	1.95		B	T	t	u	r	n	n	
5.82	210	6		1.22	U	B	t	u	r	n	n	

One or more separate scanlines

			Dip Dir. [°]	Dip [°]	Outcrop Face Dimensions [m]:
Photo #:	60b	approximate surface orientation:	140	16	x = 2
					y = 4

Scanline b)

Waypoint	E [m]	N [m]	Elev. [m]	SL length [m]	Trend [°]	Plunge [°]	Direction
24b	316654	5492058	924	2.2	153	-4	N-S

DATA

Fracture SL Intersection [m]	Dip Dir [°]	Dip [°]	Trace Length strike [m]	Trace Length dip [m]	Upper Termin.	Lower Termin.	Aperture [mm]	Primary roughness	Secondary roughness	Fillings	Movement	Comment
0.15	280	83	1.17		U	B	po	p	s	n	n	
0.31	189	57	0.34		T	T	t	p	r	n	n	
0.38	283	74	1.38		U	T	t	p	s	n	n	
0.6	194	86	0.87		T	U	t	u	s	n	n	
0.68	98	88	0.7		T	T	t	u	r	n	n	
0.89	283	86	1.28		U	T	vt	p	r	n	n	
0.9	191	72	0.58		B	B	vt	u	r	n	n	
1.26	197	80	1.15		U	B	vt	p	r	n	n	
1.61	288	83	1.69		U	T	po	p	r	n	n	
1.94	108	88	0.58		B	T	vt	u	r	n	n	
2.06	95	89	0.8		T	U	t	u	r	n	n	

Outcrop #	25
General Data	
Date	12-Jun-06
Name Surveyor	HV/JL
Character/dimension of outcrop	A-leg1, C (wall: 5mx10m): B-leg2 (wall: 3mx2m)
near or away of faulzone?	close to fault of penticton creek
Lithology description	
Rocktype	1) Amphibolite gneiss - different stages of weathering/alteration (probably hydrothermal weathering with muscovite as weathering product?); 2) veins of quartz
colour fresh/weathered	1) Fresh: stage a) dark grey, medium grained, mostly mafics (~50%), quartz (~40%) and feldspar (10%); stage b) orange to brown (rusty) with traces of muscovite; stage c) red to orange, rusty brown with greater amounts of muscovite; Weathered colors of all three stages: drak grey with orange lichen and moss; 2) Fresh: grey to white, coarse grained, mostly quartz (~80%), feldspar (~15%) and little mafics (~5%); Weathered: grey brown (light) with dark grey and orange lichen ad moss
homegeneous vs heterogeneous	1) heterogeneous; 2) heterogeneous
sample taken?	1) yes-stage a,b,c; 2) yes
Structures	
Foliation/bedding (Dip Dir./Dip)	weakly in amphibolite gneiss, but hard to measure
Liniation (Trend/plunge)	no
folds (amplitude, wavelength, fold axis, fold plane)	
fault (width, trace, gouge, orientation)	
Shear zone (width, trace)	
Rock mass description	
Block shape	i
Block size	s
weathering class	III
seepage (presence/absence)	Some water seeping dpwn through fractures from moss above…likely just water from rain in last few days percolating through fractures and seeping out (rather than a true spring. seepage along a fracture 285/25, high angle on west side; low angle on east side. Length is 25cm, partly open, does not lie on scanline; also signs of historicially seepage!

Outcrop #: 25

One scanline portioned in different legs

Outcrop Face Dimensions [m]:

x =10 (leg1)   y= 3 (leg2)

Photo #:	62b

z = 5 (leg1)   z= 2 (leg2)

										approximate surface orientation	
Waypoint	E [m]	N [m]	Elev. [m]	SL start point [m]	SL End Point [m]	Leg #	Trend [°]	Plunge [°]	Dip [°]	Dip Dir. [°]	Direction
25a	316483	5485892	506	0	1.7	1	226	22	120	41	W-E
25b	316485	5485887	507	1.7	3.35	2	123	-19	214	80	W-E

DATA

Fracture SL Intersection [m]	Leg #	Dip Dir [°]	Dip [°]	Trace Length strike [m]	Trace Length dip [m]	Upper Termin	Lower Termin	Aperture [mm]	Primary roughness	Secondary roughness	Filling	Movement	Com-ment
0	1	215	72		0.68	T	U	o	u	r	n	n	
0.11	1	214	73		1.05	T	U	mw	u	r	n	n	
0.11	1	114	55		0.6	B	T	t	u	r	n	n	
0.16	1	105	50		0.62	B	T	t	u	r	n	n	
0.2	1	111	52		0.55	A	B	t	u	r	n	n	
0.25	1	110	57		0.7	T	T	t	u	r	n	n	
0.31	1	111	54		0.52	B	T	vt	u	r	n	n	
0.34	1	111	48		0.57	B	T	t	u	r	n	n	
0.39	1	114	48		0.67	B	T	t	u	r	n	n	
0.48	1	115	51		0.73	B	B	t	u	r	n	n	
0.61	1	109	55		0.75	B	B	po	u	r	n	n	
0.68	1	114	58		1.07	B	T	po	u	r	n	n	
0.7	1	116	49		0.85	A	T	po	u	r	n	n	
0.73	1	120	46		0.8	T	U	po	u	r	n	n	
0.82	1	116	47		0.87	T	U	t	u	r	n	n	
0.83	1	111	46		0.75	B	U	t	u	r	n	n	
0.84	1	109	46		0.8	U	U	t	u	r	n	n	
0.86	1	120	46		0.73	B	U	t	u	r	n	n	
0.88	1	111	50		0.75	B	U	t	u	r	n	n	
0.9	1	115	53		0.7	B	U	t	u	r	n	n	
0.91	1	111	55		0.75	B	U	t	u	r	n	n	
0.93	1	114	44		1.33	B	A	t	u	r	n	n	

337

Fracture SL Intersection [m]	Leg #	Dip Dir [°]	Dip [°]	Trace Length strike [m]	Trace Length dip [m]	Upper Termin	Lower Termin	Aperture [mm]	Primary roughness	Secondary roughness	Filling	Movement	Com-ment
0.99	1	110	49		0.47	T	A	t	u	r	n	n	
1.11	1	113	55		0.54	T	B	t	u	r	n	n	
1.26	1	114	48		1.2	T	B	t	u	r	n	n	
1.35	1	109	52		0.75	T	B	t	u	r	n	n	
1.53	1	109	54		1.3	T	B	po	u	r	n	n	
1.63	1	101	55		1.27	B	B	po	u	r	n	n	
1.75	2	101	53		0.71	B	B	po	u	r	n	n	
1.85	2	101	50		1.21	T	B	po	u	r	n	n	
2.05	2	110	59		1.98	T	B	po	u	r	n	n	
2.2	2	235	10	0.45B	0.67	U	B	po	u	r	n	n	
2.21	2	103	60		0.62	B	B	t	u	r	n	n	
2.25	2	104	56		0.8	U	B	t	u	r	n	n	
2.39	2	233	12	0.62U	0.72	B	U	po	p	r	n	n	
2.6	2	116	58		0.83	U	T	o	u	r	n	n	Seep.
2.84	2	304	76		1.8	U	T	o	u	r	n	n	Seep.
2.95	2	103	54		1.07	U	A	o	u	r	n	n	Seep.
3.11	2	104	62		0.99	U	B	po	u	r	n	n	
3.34	2	102	42		0.95	U	U	po	u	r	n	n	

One or more separate scanlines

			Dip Dir. [°]	Dip [°]
Photo #:	63b	approximate surface orientation:	132	71

Outcrop Face Dimensions [m]:
x =10
z = 5

Scanline c)

Waypoint	E [m]	N [m]	Elev. [m]	SL length [m]	Trend [°]	Plunge [°]	Direction
25c	316501	5485887	503	2.7	220	-29	N-S

DATA

Fracture SL Intersection [m]	Dip Dir [°]	Dip [°]	Trace Length strike [m]	Trace Length dip [m]	Upper Termin.	Lower Termin.	Aperture [mm]	Primary roughness	Secondary roughness	Fillings	Movement	Comment
0.02	54	86		1.35	U	U	po	u	r	n	n	
0.02	255	21	0.73	0.13T	U	B	t	u	r	n	n	
0.28	254	22	0.83		T	U	t	u	r	n	n	
0.37	76	75		0.85	U	T	t	u	r	n	n	
0.51	260	14	0.7		T	B	po	u	r	n	n	
0.86	271	15	0.86		B	T	t	u	r	n	n	
1.09	80	71		0.22	T	T	vt	st	r	n	n	
1.28	65	71		0.45	B	B	o	u	r	n	n	
1.3	265	24	1.02		B	T	o	u	r	n	n	
1.74	78	81		0.94	T	T	o	st	r	n	n	
1.75	266	21	0.33		T	T	vt	u	r	n	n	
2.13	76	83		0.83	T	T	o	u	r	n	n	
2.43	60	75		0.56	T	T	o	u	r	n	n	
2.46	258	20	0.86		B	T	o	u	r	n	n	
2.55	79	83		1.21	B	U	o	u	r	n	n	

Outcrop #	27
General Data	
Date	13-Jun-06
Name Surveyor	HV/JL
Character/dimension of outcrop	A,B-leg1,2 (wall: 2mx7m); C (wall: 2mx3m)
near or away of faulzone?	
Lithology description	
Rocktype	Amphibolite Gneiss
colour fresh/weathered	Fresh: dark grey, medium grained mostly mafics (~60%), feldspar (~20%) with phorphyroblasts up to 2 cm and quartz (~20%) - it is banded with portions of lower mafics and more quartz and feldspar; Weathered: rusty brown with dark grey lichen and moss
homegeneous vs heterogeneous	heterogeneous
sample taken?	no

Structures	
Foliation/bedding (Dip Dir./Dip)	22/20
Liniation (Trend/plunge)	no lineation seen
folds (amplitude, wavelength, fold axis, fold plane)	
fault (width, trace, gouge, orientation)	
Shear zone (width, trace)	
Rock mass description	
Block shape	i
Block size	ms
weathering class	II
seepage (presence/absence)	seepage from some fractures through water in moss above

Outcrop #: 27

One scanline portioned in different legs

Outcrop Face Dimensions [m]:
y =7 (leg1,2)
z = 2 (leg1,2)

Photo #:	69b

approximate surface orientation

Waypoint	E [m]	N [m]	Elev. [m]	SL start point [m]	SL End Point [m]	Leg #	Trend [°]	Plunge [°]	Dip [°]	Dip Dir. [°]	Direction
27a	316943	5493377	1009	0	1.55	1	280	74	211	85	D-U
27b	316945	5493379	1010	1.55	5.5	2	114	-18	210	70	W-E

DATA

Fracture SL Intersection [m]	Leg #	Dip Dir [°]	Dip [°]	Trace Length strike [m]	Trace Length dip [m]	Upper Termin	Lower Termin	Aperture [mm]	Primary roughness	Secondary roughness	Filling	Movement	Comment
0.12	1	208	11	0.67		T	T	po	u	s	n	n	
0.49	1	206	15	2.92		T	A	po	u	r	n	n	
0.54	1	236	14	7.65	3.11U	T	U	o	u	r	n	n	
1.13	1	298	24	0.88	0.92	T	B	po	u	r	n	n	Dike
1.26	1	302	21	0.53A	1.13	U	T	o	u	r	n	n	Seep.

Fracture SL Intersection [m]	Leg #	Dip Dir [°]	Dip [°]	Trace Length strike [m]	Trace Length dip [m]	Upper Termin	Lower Termin	Aperture [mm]	Primary roughness	Secondary roughness	Filling	Movement	Com-ment
1.39	1	269	19	0.65U	1.3	U	T	o	u	r	n	n	Seep.
1.56	2	340	82	0.9		B	B	t	u	r	n	n	
1.71	2	230	19	1.22	0.51U	U	T	po	u	r	n	n	
2.01	2	326	83	2.10U	1.68	U	U	t	u	r	n	n	
2.31	2	291	13	1.20U	2.59	T	T	t	u	r	n	n	
2.41	2	334	74	0.5U	1.6	U	U	o	u	r	n	n	Seep.
2.75	2	39	2	1.12		B	T	o	u	r	n	n	
3.28	2	310	69	0.15U	1.14	U	T	t	u	r	n	n	
3.4	2	336	83		0.78	B	T	t	u	r	n	n	
3.73	2	219	11	3.38		B	T	t	u	r	n	n	Seep.
3.98	2	316	72	1.40B	1.68	U	U	po	u	r	n	n	
4.39	2	315	66	1.0U	1.7	T	U	o	u	r	n	n	
4.26	2												
4.62	2	337	64		0.35	T	B	t	u	r	n	n	
4.81	2	339	55		0.61	T	T	t	u	r	n	n	
5.36	2	218	10	1.79		B	T	t	u	r	n	n	

One or more separate scanlines

			Dip Dir. [°]	Dip [°]
Photo #:	70b	approximate surface orientation:	120	75

Outcrop Face Dimensions [m]:

x = 3
z = 2

Scanline c)

Waypoint	E [m]	N [m]	Elev. [m]	SL length [m]	Trend [°]	Plunge [°]	Direction
27c	316949	5493381	1009	4.5	199	40	S-N

DATA

Fracture SL Intersection [m]	Dip Dir [°]	Dip [°]	Trace Length strike [m]	Trace Length dip [m]	Upper Termin.	Lower Termin.	Aperture [mm]	Primary roughness	Secondary roughness	Fillings	Movement	Comment
0.56	240	13	4.85U	2	U	U	o	u	r	n	n	
1.25												leg 1 (0.54cm interestion)
1.27	24	84		0.3	T	T	o	u	r	n	n	
1.78	171	88		0.59	T	T	t	u	r	n	n	
1.94	273	16	1.47	1.68A	U	B	t	u	r	n	n	
2.22	255	28		1.01	A	A	t	u	r	n	n	
2.44	346	6	2.22	.52U	U	B	t	u	r	n	n	
2.56	113	4	.72U	1.41	U	B	vt	u	r	n	n	
2.58	36	65		0.29	T	T	t	u	r	n	n	
2.72	6	8		0.35	B	A	t	u	r	n	n	
2.83	294	38	1.62		A	B	t	u	r	n	n	
3.95	292	17	0.6		B	B	vt	u	r	n	n	
4.38	197	15	3.25U	2.25	U	U						

Outcrop #	28
General Data	
Date	13-Jun-06
Name Surveyor	HV/JL
Character/dimension of outcrop	A (wall: 3mx2m); B (surface: 4.5mx4m)
near or away of faulzone?	
Lithology description	
Rocktype	Amphibolite Gneiss with bands of qfsp gneiss
colour fresh/weathered	Fresh: dark grey, medium grained mostly mafics (~60%), feldspar (~20%) with phorphyroblasts up to 2 cm and quartz (~20%) - it is banded with portions of lower mafics and more quartz and feldspar; Weathered: rusty brown with dark grey lichen and moss
homegeneous vs heterogeneous	heterogeneous
sample taken?	no

Structures	
Foliation/bedding (Dip Dir./Dip)	not measurable, very weakly
Liniation (Trend/plunge)	not seen
folds (amplitude, wavelength, fold axis, fold plane)	
fault (width, trace, gouge, orientation)	
Shear zone (width, trace)	
Rock mass description	
Block shape	t
Block size	ms
weathering class	II
seepage (presence/absence)	absent

Outcrop #: 28

One or more separate scanlines

			Dip Dir. [°]	Dip [°]
Photo #:	71b	approximate surface orientation:	204	8

Outcrop Face Dimensions [m]:
y = 3
z = 2

Scanline a)

Waypoint	E [m]	N [m]	Elev. [m]	SL length [m]	Trend [°]	Plunge [°]	Direction
28a	317295	5493773	1139	2.1	288	-41	E-W

DATA

Fracture SL Intersection [m]	Dip Dir [°]	Dip [°]	Trace Length strike [m]	Trace Length dip [m]	Upper Termin.	Lower Termin.	Aperture [mm]	Primary roughness	Secondary roughness	Fillings	Movement	Comment
0	228	19		0.9	T	T	po	u	r	n	n	
0.34	262	11		0.9	T	T	t	u	r	n	n	
1.02	229	15		2.59	T	T	t	u	r	n	n	
1.18	302	81		1.45	U	U	o	u	r	n	n	
1.23	244	14	0.75B	3.21	U	T	po	u	r	n	n	

343

One or more separate scanlines

		Dip Dir. [°]	Dip [°]	Outcrop Face Dimensions [m]:
Photo #:	72b	approximate surface orientation:	302	12

x =4.5
y = 4

Scanline b)

Waypoint	E [m]	N [m]	Elev. [m]	SL length [m]	Trend [°]	Plunge [°]	Direction
28b	317299	5493783	1139	4.6	338	-5	S-N

DATA

Fracture SL Intersection [m]	Dip Dir [°]	Dip [°]	Trace Length strike [m]	Trace Length dip [m]	Upper Termin.	Lower Termin.	Aperture [mm]	Primary roughness	Secondary roughness	Fillings	Movement	Comment
0.14	291	86	2.2	0.8T	U	T	po	u	r	n	n	
0.52	109	85	0.59		B	T	t	st	r	n	n	
0.58	10	83	0.52		T	T	t	u	r	n	n	
1.17	190	78	0.25		A	B	vt	u	r	n	n	
1.32	301	75	1.22		B	T	t	u	r	n	n	
1.76	294	68	0.9		B	B	vt	u	r	n	n	
2.56	290	77	1.5		B	B	t	u	r	n	n	
3.38	301	66	0.76		B	B	vt	p	r	n	n	
3.43	289	68	1.23		B	B	t	u	r	n	n	
4.16	294	64	2.55		U	B	t	p	r	n	n	
4.26	287	76	1.2		B	U	vt	u	r	n	n	
4.28	289	69	2.97		B	U	vt	u	s	n	n	
4.47	294	67	2.36		B	U	vt	p	r	n	n	

Outcrop #	35
General Data	
Date	15-Aug-06
Name Surveyor	HV
Character/dimension of outcrop	A (Surface: 6mx10m); B (Face: 5mx4m)
near or away of faulzone?	
Lithology description	
Rocktype	Okanagan Batholite - KOL: Granite/Granodiorite
colour fresh/weathered	Fresh: medium grey, pinkish (feldspar), medium to coarse grained, mostly feldspar (~50%), quarzo (~40%) and some amphibole (maybe hornblende ~10%) and traces of biotite; Weathered: medium grey/orange-brown with green and grey lichen and moss
homegeneous vs heterogeneous	homogeneous
sample taken?	yes: 35
Structures	
Foliation/bedding (Dip Dir./Dip)	no foliation
Liniation (Trend/plunge)	no liniation
folds (amplitude, wavelength, fold axis, fold plane)	
fault (width, trace, gouge, orientation)	
Shear zone (width, trace)	
Rock mass description	
Block shape	i
Block size	l
weathering class	II
seepage (presence/absence)	absent

Outcrop #: 35

One or more separate scanlines

Photo #:	96B	approximate surface orientation:	Dip Dir. [°]	Dip [°]	Outcrop Face Dimensions [m]:
			118	19	x =10
					y = 6

Scanline a)

Waypoint	E [m]	N [m]	Elev. [m]	SL length [m]	Trend [°]	Plunge [°]	Direction
35a	329576	5499908	2024	12	68	-15	W-E

DATA

Fracture SL Intersection [m]	Dip Dir [°]	Dip [°]	Trace Length strike [m]	Trace Length dip [m]	Upper Termin.	Lower Termin.	Aperture [mm]	Primary roughness	Secondary roughness	Fillings	Movement	Comment
0.32	6	76	2	.8U	U	B	o	u	r	n	n	
0.67	291	59	2.1		B	T	t	u	r	n	n	
0.93	295	65	2.7		B	T	po	u	r	n	n	
3.31	285	73	4		U	B	o	u	r	n	n	
4.77	275	70	2		U	B	t	u	r	n	n	
6.37	280	50	4		U	T	o	u	r	n	n	
7.81	210	86	7		U	U	o	u	r	n	n	
8.85	283	58	2.3		U	B	t	u	r	n	n	
9.66	300	45	2.5		U	B	t	u	r	n	n	
11.04	299	52	7		U	T	po	u	r	n	n	
11.67	205	84	5		U	U	o	u	r	n	n	

One or more separate scanlines

			Dip Dir. [°]	Dip [°]
Photo #:	97b	approximate surface orientation:	199	68

Outcrop Face Dimensions [m]:

y =5

z = 4

Scanline b)

Waypoint	E [m]	N [m]	Elev. [m]	SL length [m]	Trend [°]	Plunge [°]	Direction
35b	329580	5499893	2021	4.7	190	-66	U-D

Fracture SL Intersection [m]	Dip Dir [°]	Dip [°]	Trace Length strike [m]	Trace Length dip [m]	Upper Termin.	Lower Termin.	Aperture [mm]	Primary roughness	Secondary roughness	Fillings	Movement	Comment
0	132	30	7U	2	U	U	o	u	r	n	n	
0.33	308	68	.6B	0.4	U	B	t	u	r	n	n	
0.49	130	24	7U	2	U	B	o	u	r	n	n	
1.05	128	26	2.5U	1.05	B	U	o	u	r	n	n	
1.34	120	28	7U	4.5	U	B	mw	u	r	n	n	
1.52	125	28	2.5U	2.2	B	U	mw	u	r	n	n	
3.37	129	24		4.4	U	B	o	u	r	n	n	
3.73	130	30	4U	6.4	U	U	mw	u	r	n	n	
3.91	310	70		1.7	B	T	o	u	r	n	n	
4.28	129	29	2.5U	2.06	U	T	o	u	r	n	n	
4.45	131	30		4	U	U	mw	u	r	n	n	
4.59	128	27	2.5U	5	U	U	mw	u	r	n	n	

Outcrop #	36
General Data	
Date	16-Aug-06
Name Surveyor	HV/MAB
Character/dimension of outcrop	A (Surface: 35mx6m); B (Face: 2.5mx9m)
near or away of faulzone?	
Lithology description	
Rocktype	Granodiorite and some more foliated rocks- gneiss
colour fresh/weathered	Fresh: Granodiorite: medium grey, fine to medium grained, mostly quartz (~60%), hornblende and biotite (~20%) and feldspar (~20%) and traces of calcophyrite. In some parts bigger quartz crystals up to 2cm and elongated hornblende crystals up to 1cm (see sample), Gneiss: medium grained with ~33% quartz, ~33% feldspar and ~33% hornblende and biotite; Weathered: dark grey with grey and green lichen and moss. Orange/brown parts from calcophyrite weathering
homegeneous vs heterogeneous	heterogeneous

Structures	
Foliation/bedding (Dip Dir./Dip)	weak, not measurable in gneiss
Liniation (Trend/plunge)	in gneiss: 100/40
folds (amplitude, wavelength, fold axis, fold plane)	
fault (width, trace, gouge, orientation)	
Shear zone (width, trace)	
Rock mass description	
Block shape	i
Block size	l
weathering class	II
seepage (presence/absence)	absent

Outcrop #: 36

One or more separate scanlines

				Dip Dir. [°]	Dip [°]	Outcrop Face Dimensions [m]:
Photo #:	98b	approximate surface orientation:		105	34	x =35
						y = 6

Scanline a)

Waypoint	E [m]	N [m]	Elev. [m]	SL length [m]	Trend [°]	Plunge [°]	Direction
36a	325731	5503981	1760	5.6	98	-35	W-E

DATA

Fracture SL Intersection [m]	Dip Dir [°]	Dip [°]	Trace Length strike [m]	Trace Length dip [m]	Upper Termin.	Lower Termin.	Aperture [mm]	Primary roughness	Secondary roughness	Fillings	Movement	Comment
0.64	297	56	1.47		B	B	t	u	r	n	n	
2.15	265	62	0.27		B	B	vt	u	r	n	n	
2.34	263	61	1		B	B	t	u	r	n	n	

348

Fracture SL Intersection [m]	Dip Dir [°]	Dip [°]	Trace Length strike [m]	Trace Length dip [m]	Upper Termin.	Lower Termin.	Aperture [mm]	Primary roughness	Secondary roughness	Fillings	Movement	Comment
2.73	259	74	1.66		B	B	t	u	r	n	n	
3.46	253	53	2.5		B	B	t	u	r	n	n	
4.11	265	55	2.5		B	B	t	u	r	n	n	
4.56	260	60	0.5		B	B	vt	u	r	n	n	
4.72	270	60	4.1		B	B	t	u	r	n	n	
4.96	269	64	2.2		B	B	t	u	r	n	n	
5.53	268	59	4.1		B	B	t	u	r	n	n	

One or more separate scanlines

		Dip Dir. [°]	Dip [°]
Photo #:	99b	approximate surface orientation:	262	55

Outcrop Face Dimensions [m]:
y = 9
z = 2.5

Scanline b)

Waypoint	E [m]	N [m]	Elev. [m]	SL length [m]	Trend [°]	Plunge [°]	Direction
36b	325741	5503958	1758	2.1	178	-52	N-S

DATA

Fracture SL Intersection [m]	Dip Dir [°]	Dip [°]	Trace Length strike [m]	Trace Length dip [m]	Upper Termin.	Lower Termin.	Aperture [mm]	Primary roughness	Secondary roughness	Fillings	Movement	Comment
0.16	111	35	3.5		B	B	o	u	r	n	n	
0.47	114	39	3.5		B	B	po	u	r	n	n	
0.83	110	36	3.5		U	B	o	u	r	n	n	
1.12	118	30	3		B	U	po	u	r	n	n	
1.45	108	36	4.3		B	U	o	u	r	n	n	
1.61	128	2	1.2		B	B	t	u	r	n	n	
2.04	108	30	3		U	U	po	u	r	n	n	

Outcrop #	37
General Data	
Date	16-Aug-06
Name Surveyor	HV/MAB
Character/dimension of outcrop	A,B-leg1,2 (Face: 9mx2.5m), C (Surface: 8mx1m)
near or away of faultzone?	
Lithology description	
Rocktype	Okanagan Batholite-Granite: KOL
colour fresh/weathered	Fresh: medium grey, medium to coarse grained, mostly quartz (~40%), feldspar (~40%) and ~20% hornblende and traces of biotite; Weathered: medium to dark grey with green and grey lichen and moss
homogeneous vs heterogeneous	
sample taken?	yes: 37
Structures	
Foliation/bedding (Dip Dir./Dip)	no foliation
Liniation (Trend/plunge)	no liniation
folds (amplitude, wavelength, fold axis, fold plane)	
fault (width, trace, gouge, orientation)	
Shear zone (width, trace)	
Rock mass description	
Block shape	i
Block size	l
weathering class	II
seepage (presence/absence)	absent

Outcrop #: 37

One scanline portioned in different legs

Outcrop Face Dimensions [m]:
y =9 (leg1,2)
z = 2 (leg1,2)

Photo #:	102b	103b

approximate surface orientation

Waypoint	E [m]	N [m]	Elev. [m]	SL start point [m]	SL End Point [m]	Leg #	Trend [°]	Plunge [°]	Dip [°]	Dip Dir. [°]	Direction
37a	327269	5503787	1704	0	2.4	1	18	-7	281	61	N-S
37b	327272	5503782	1704	2.4	7	2	218	-35	271	53	N-S

Fracture SL Intersection [m]	Leg #	Dip Dir [°]	Dip [°]	Trace Length strike [m]	Trace Length dip [m]	Upper Termin	Lower Termin	Aperture [mm]	Primary roughness	Secondary roughness	Filling	Movement	Com-ment
0.2	1	161	76		0.97	U	U	vt	u	r	n	n	
0.18	1	148	74		1.24	U	U	po	u	r	n	n	
0.28	1	137	84		0.88	U	A	po	u	r	n	n	
0.37	1	151	76		3.92	U	A	po	u	r	n	n	
0.67	1	146	82		1.38	U	B	t	u	r	n	n	
0.83	1	314	85		1.39	U	B	t	u	r	n	n	
0.92	1	312	84		1.64	U	U	vt	u	r	n	n	
1.44	1	286	49	3.7		T	T	po	u	r	n	n	
1.53	1	163	89		4.25	U	U	po	u	r	n	n	
1.81	1	164	74		0.83	T	B	po	u	r	n	n	
2.05	1	347	69		0.68	U	A	po	u	r	n	n	
2.18	1	188	58		0.6	U	B	vt	u	r	n	n	
3.47	2	91	24	0.92		U	U	t	u	r	n	n	
4.56	2	191	80		1.37	U	B	t	u	r	n	n	
4.96	2	132	31	0.92		T	T	po	u	r	n	n	
6.32	2	254	56	1.42U	1.04	U	U	o	u	r	n	n	
6.6	2	173	71		2.32	U	U	t	u	r	n	n	

One or more separate scanlines			Dip Dir. [°]	Dip [°]	Outcrop Face Dimensions [m]:
Photo #:	104b	approximate surface orientation:	128	44	x =8
					y = 1

Scanline c)

Waypoint	E [m]	N [m]	Elev. [m]	SL length [m]	Trend [°]	Plunge [°]	Direction
37c	327273	5503786	1705	2	251	-1	W-E

DATA

Fracture SL Intersection [m]	Dip Dir [°]	Dip [°]	Trace Length strike [m]	Trace Length dip [m]	Upper Termin.	Lower Termin.	Aperture [mm]	Primary roughness	Secondary roughness	Fillings	Movement	Comment
0.5	273	56	1.01	3.74U	U	U	t	u	r	n	n	
0.78	263	50	5.3		U	B	po	u	r	n	n	
0.99	294	78	1.8		B	A	t	u	r	n	n	
1.3	281	56	0.93		A	B	vt	u	r	n	n	
1.63	279	48	1.72		B	B	t	u	r	n	n	
1.99	292	81	0.84		B	B	vt	u	r	n	n	

Outcrop #	39
General Data	
Date	16-Sep-06
Name Surveyor	HV
Character/dimension of outcrop	B,C-leg1,2 (Face: 9mx2.5m), A (Wall: 5mx2m)
near or away of faulzone?	
Lithology description	
Rocktype	Okanagan Batholite-Granite: KOL
colour fresh/weathered	Fresh: medium grey, medium to coarse grained, mostly quartz (~40%), feldspar (~40%) and ~20% hornblende and traces of biotite; Weathered: medium to dark grey with green and grey lichen and moss
homegeneous vs heterogeneous	
sample taken?	
Structures	
Foliation/bedding (Dip Dir./Dip)	no foliation
Liniation (Trend/plunge)	no liniation

Rock mass description	
Block shape	i
Block size	l
weathering class	II
seepage (presence/absence)	absent

Outcrop #: 39

One or more separate scanlines

			Dip Dir. [°]	Dip [°]
Photo #:	85	approximate surface orientation:	262	60

Outcrop Face Dimensions [m]:

y =5

z = 2
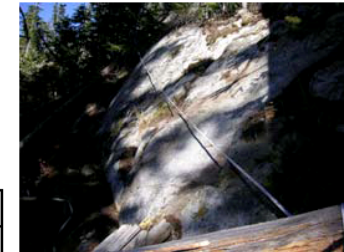
Scanline a)

Waypoint	E [m]	N [m]	Elev. [m]	SL length [m]	Trend [°]	Plunge [°]	Direction
39a	328444	5505080	1906	7	185	-19	N-S

DATA

Fracture SL Intersection [m]	Dip Dir [°]	Dip [°]	Trace Length strike [m]	Trace Length dip [m]	Upper Termin.	Lower Termin.	Aperture [mm]	Primary roughness	Secondary roughness	Fillings	Movement	Comment
0.45	180	89		0.3	T	T	o	u	r	n	n	
0.49	169	72		0.6	A	B	o	u	r	n	n	
0.6	47	26		0.65	T	B	po	p	r	n	n	
0.77	44	59		1.2	B	B	t	u	r	n	n	
0.86	165	78		1.8	U	T	o	u	r	n	n	
0.87	55	60		1	B	B	t	u	r	n	n	
1.14	355	78		0.88	A	T	po	u	r	n	n	

Fracture SL Intersection [m]	Dip Dir [°]	Dip [°]	Trace Length strike [m]	Trace Length dip [m]	Upper Termin.	Lower Termin.	Aperture [mm]	Primary roughness	Secondary roughness	Fillings	Movement	Comment
1.16	171	78		2.8	U	A	t	u	r	n	n	
1.29	154	75		0.65	B	B	vt	u	r	n	n	
1.32	356	74		1	B	B	vt	u	r	n	n	
2.31	161	73		2.57	B	B	o	u	r	n	n	
2.55	177	79		0.9	U	B	t	u	r	n	n	
2.65	7	72		1.5	B	T	po	u	r	n	n	
2.76	95	26		1.77	A	A	o	u	r	n	n	
2.78	170	70		0.7	T	A	po	u	r	n	n	
2.79	10	66		0.95	U	A	t	u	r	n	n	
2.83	65	34		1.02	A	T	po	u	r	n	n	
2.96	60	38		0.97	B	T	t	u	r	n	n	
3.05	170	81		0.5	A	B	t	u	r	n	n	
3.23	2	68		2.1	U	U	o	u	r	n	n	
3.67	176	64		1.37	T	B	t	u	r	n	n	
3.75	69	47		1.57	T	T	po	u	r	n	n	
4.05	181	80		0.8	B	B	t	u	r	n	n	
4.18	55	38		1.95	B	T	po	u	r	n	n	
4.59	352	69		2.8	B	U	po	u	r	n	n	
5.06	180	85		2.05	B	T	t	u	r	n	n	
5.36	185	84		1.15	B	T	vt	u	r	n	n	
6.27	154	77		1.25	B	T	vt	u	r	n	n	
6.3	55	35		0.7	T	B	vt	u	r	n	n	
6.56	60	39		1.15	B	T	vt	u	r	n	n	
6.69	173	87		1.4	B	B	t	u	r	n	n	
6.94	177	86		0.57	B	B	vt	u	r	n	n	

One scanline portioned in different legs

Outcrop Face Dimensions [m]:
y = 11 (leg1,2)
z = 4 (leg1,2)

Photo #:	86, 87

											approximate surface orientation
Waypoint	E [m]	N [m]	Elev. [m]	SL start point [m]	SL End Point [m]	Leg #	Trend [°]	Plunge [°]	Dip [°]	Dip Dir. [°]	Direction
39b	328439	5505055	1907	0	2.5	1	311	-41	254	46	W-E
39c	328450	5505069	1908	2.5	6.8	2	235	-31	80	29	W-E

DATA

Fracture SL Intersection [m]	Leg #	Dip Dir [°]	Dip [°]	Trace Length strike [m]	Trace Length dip [m]	Upper Termin	Lower Termin	Aperture [mm]	Primary roughness	Secondary roughness	Filling	Movement	Com-ment
0.38	1	138	65		0.8	U	U	vt	u	r	n	n	
0.52	1	122	60		0.9	U	U	t	u	r	n	n	
0.69	1	135	50		1.2	U	U	t	u	r	n	n	
1.34	1	129	60		0.82	U	U	o	u	r	n	n	
1.62	1	140	45		1.8	B	B	t	u	r	n	n	
1.75	1	156	83		0.75	B	B	vt	u	r	n	n	
1.91	1	50	34		1.8	T	U	o	u	r	n	n	
1.96	1	149	64		2	U	B	po	u	r	n	n	
2.13	1	139	69		1.44	U	B	t	u	r	n	n	
2.51	2	261	65	2		U	U	o	u	r	n	n	
5.56	2	261	63	2.2		U	U	o	u	r	n	n	
6.57	2	271	75	1.5		U	B	po	u	r	n	n	

355

A.2. Processed outcrop scale data – separated stereonets

Parameters	Set 1_1	Set 1_2		Set 1_4
Trend/Plunge [°], Dispersion	85/4, k= 35	321/9, k= 20		77/58, k= 25
Mean Persistence [m], Std. Dev.	1.60, 0.94	2.40, 0.47		4.40, 2.60
P10 Intensity measured	2.00	1.33		4.08
P32 Intensity upscaled	1.94	0.31		1.29

Parameters	Set 2_1	Set 2_2	Set 2_3	Set 2_4
Trend/Plunge [°], Dispersion	116/04, k= 30	256/12, k= 70	217/27, k= 80	16/68, k= 80
Mean Persistence [m], Std. Dev.	0.82, 0.62	1.41, 1.04	0.50, 0.18	2.97, 0.74
P10 Intensity measured	4.54	4.08	1.33	2.26
P32 Intensity upscaled	0.82	1.02	0.21	0.43
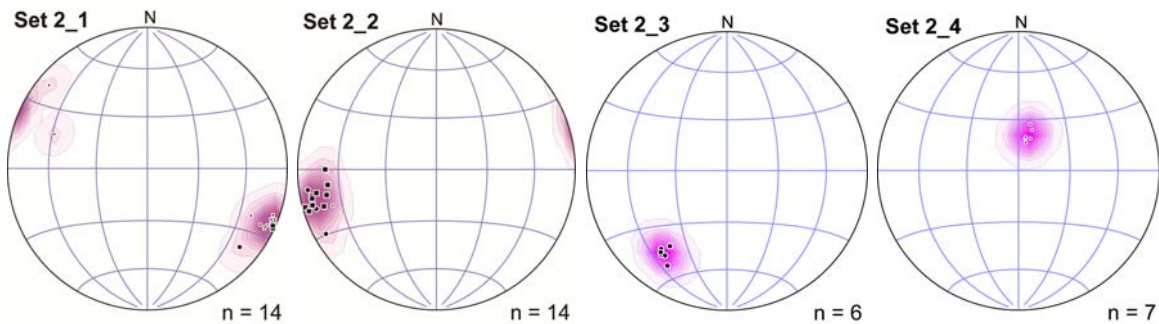
Parameters	Set 3_1	Set 3_2	Set 3_3	Set 3_4
Trend/Plunge [°], Dispersion	117/09, k= 25	298/20, k= 30	200/02, k= 30	148/78, k= 70
Mean Persistence [m], Std. Dev.	2.31, 2.02	2.77, 2.30	3.62, 3.30	1.03, 0.86
P10 Intensity measured	2.18	2.87	0.91	2.94
P32 Intensity upscaled	0.33	1.03	0.15	1.35
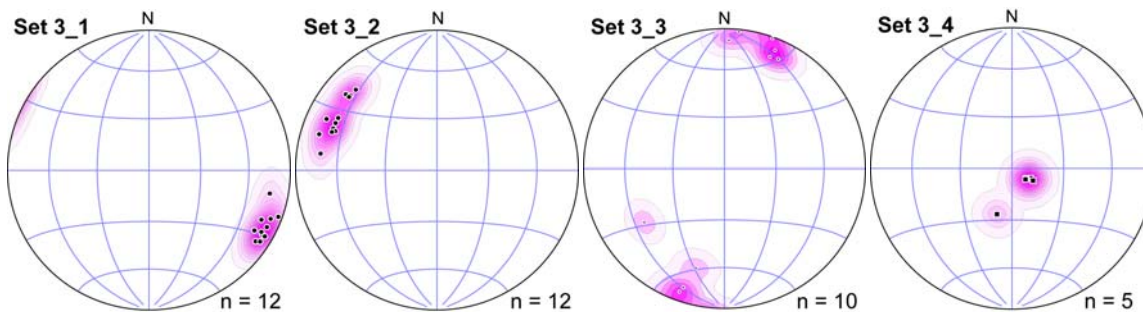
Parameters	Set 4_1		Set 4_3	Set 4_4
Trend/Plunge [°], Dispersion	129/04, k= 30		35/02, k= 100	178/82, k= 80
Mean Persistence [m], Std. Dev.	0.73, 0.24		1.70, 1.14	1.58, 0.69
P10 Intensity measured	4.50		3.30	9.40
P32 Intensity upscaled	0.83		0.53	1.69
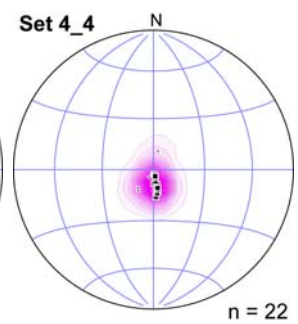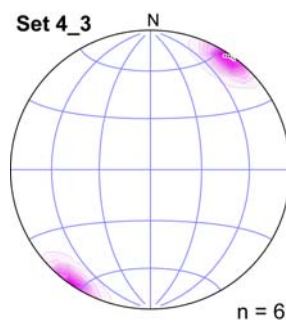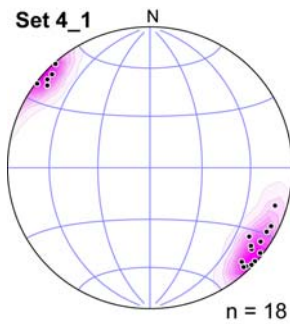
Parameters	Set 5_1	Set 5_2		Set 5_4
Trend/Plunge [°], Dispersion	282/15, k= 25	320/16, k= 60		45/73, k= 56
Mean Persistence [m], Std. Dev.	1.01, 0.65	1.22, 0.74		1.77, 0.84
P10 Intensity measured	3.14	3.43		1.67
P32 Intensity upscaled	1.54	0.71		0.75
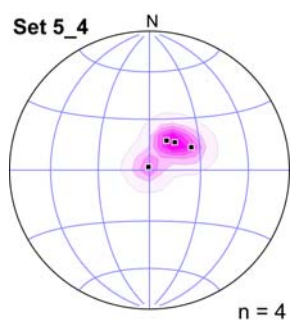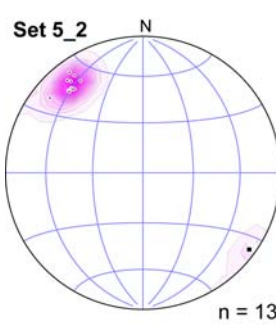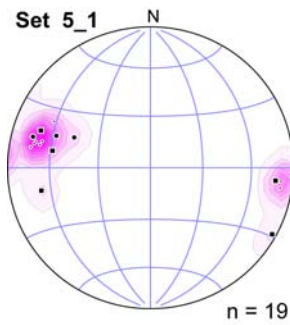
Parameters	Set 6_1		Set 6_3	Set 6_4
Trend/Plunge [°], Dispersion	95/10, k= 40		177/01, k= 25	266/77, k= 30
Mean Persistence [m], Std. Dev.	3.58, 3.01		1.19, 0.57	0.95, 0.30
P10 Intensity measured	2.24		2.43	1.88
P32 Intensity upscaled	0.32		0.59	0.84
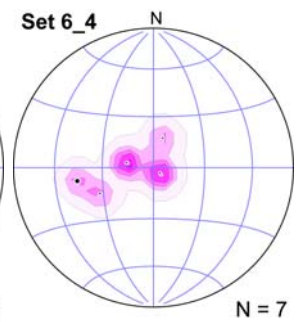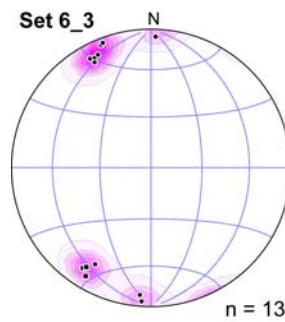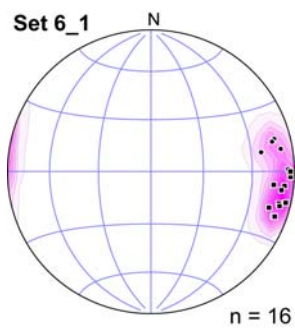
Parameters		Set 7_2		Set 7_4
Trend/Plunge [°], Dispersion		288/29, k= 61		46/79, k= 50
Mean Persistence [m], Std. Dev.		0.96, 0.33		1.63, 0.86
P10 Intensity measured		6.55		1.50
P32 Intensity upscaled		2.78		1.47

358
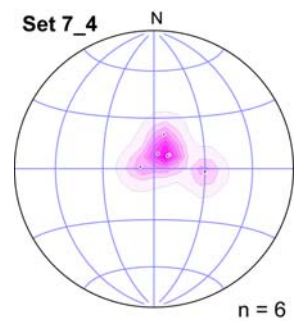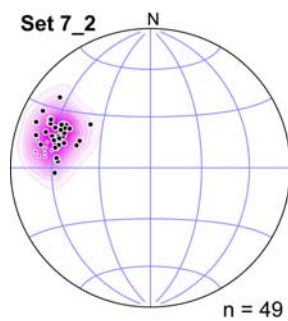
Parameters	Set 8_1		Set 8_3	Set 8_4
Trend/Plunge [°], Dispersion	116/07, k= 150		193/35, k= 45	76/81, k= 130
Mean Persistence [m], Std. Dev.	0.70, 0.43		0.77, 0.72	1.55, 0.83
P10 Intensity measured	9.2		3.0	3.18
P32 Intensity upscaled	1.3		0.71	0.28
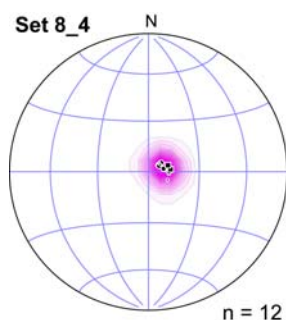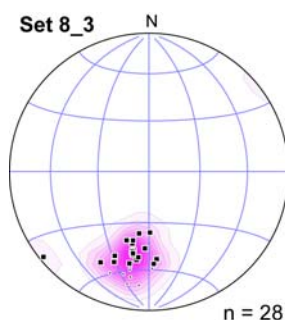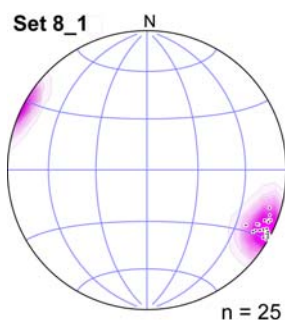
Parameters	Set 9_1		Set 9_3	Set 9_4
Trend/Plunge [°], Dispersion	82/07, k= 30		145/13, k= 35	200/73, k= 20
Mean Persistence [m], Std. Dev.	2.09, 1.42		3.25, 1.14	2.19, 1.26
P10 Intensity measured	1.90		1.52	1.43
P32 Intensity upscaled	0.23		0.27	0.12
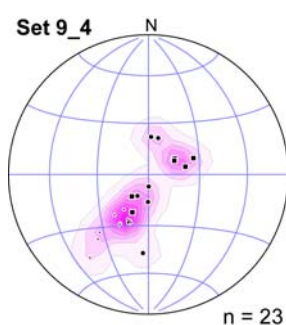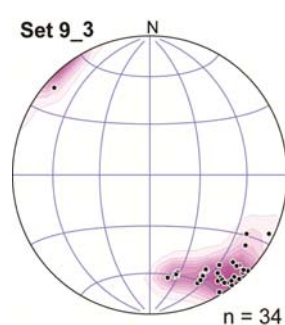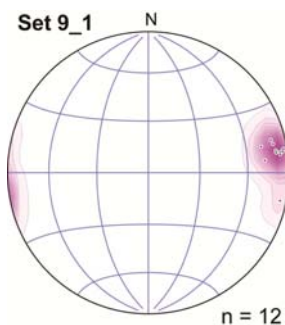
Parameters	Set 10_1	Set 10_2	Set 10_3	
Trend/Plunge [°], Dispersion	278/02, k= 50	326/44, k= 60	173/20, k= 35	
Mean Persistence [m], Std. Dev.	1.52, 0.82	1.78, 0.80	1.99, 1.09	
P10 Intensity measured	3.20	0.70	3.10	
P32 Intensity upscaled	0.69	0.06	0.42	
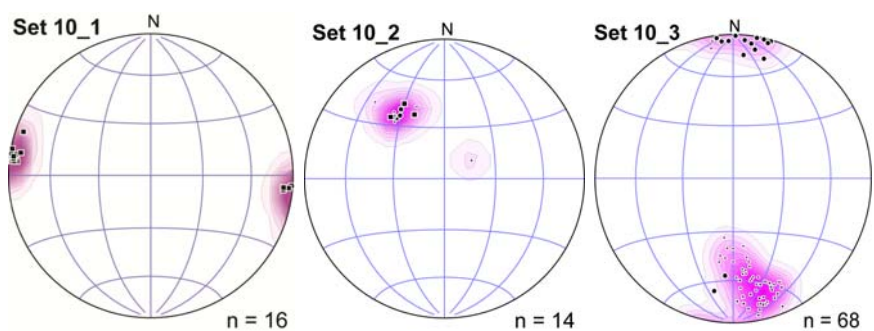
Parameters	Set 11_1			Set 11_4
Trend/Plunge [°], Dispersion	74/6, k= 60			90/72, k= 80
Mean Persistence [m], Std. Dev.	2.76, 1.05			2.51, 1.40
P10 Intensity measured	2.55			1.40
P32 Intensity upscaled	0.29			0.26

Parameters	Set 12_1		Set 12_3	Set 12_4
Trend/Plunge [°], Dispersion	85/03, k= 15		135/11, k= 20	257/56, k= 35
Mean Persistence [m], Std. Dev.	1.19, 0.79		1.00, 0.39	1.10, 0.40
P10 Intensity measured	7.21		1.92	7.37
P32 Intensity upscaled	1.93		0.40	1.90
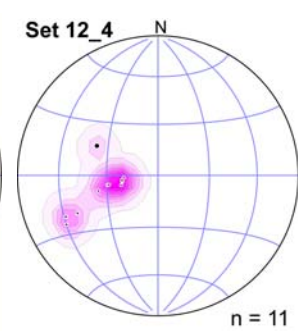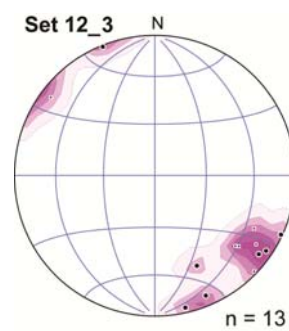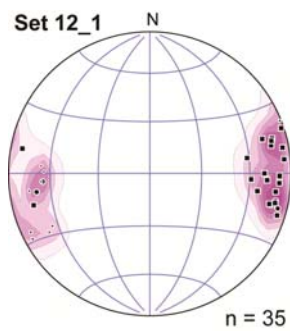
Parameters	Set 13_1		Set 13_3	Set 13_4
Trend/Plunge [°], Dispersion	87/08, k= 20		28/05, k= 30	62/76, k= 123
Mean Persistence [m], Std. Dev.	0.77, 0.73		1.24, 0.63	2.78, 2.10
P10 Intensity measured	2.90		0.73	1.85
P32 Intensity upscaled	0.62		0.07	0.39
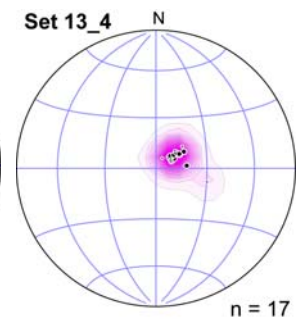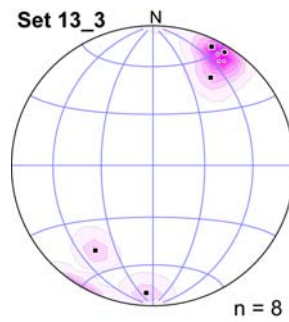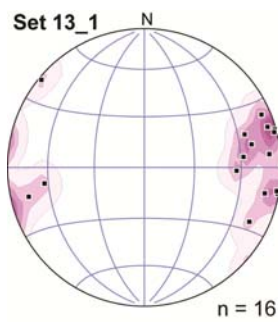
Parameters		Set 14_2	Set 14_3	Set 14_4
Trend/Plunge [°], Dispersion		293/33, k= 50	28/21, k= 25	60/87, k= 50
Mean Persistence [m], Std. Dev.		1.10, 1.10	0.81, 0.41	0.70, 0.14
P10 Intensity measured		9.29	2.86	0.24
P32 Intensity upscaled		3.92	1.05	0.20
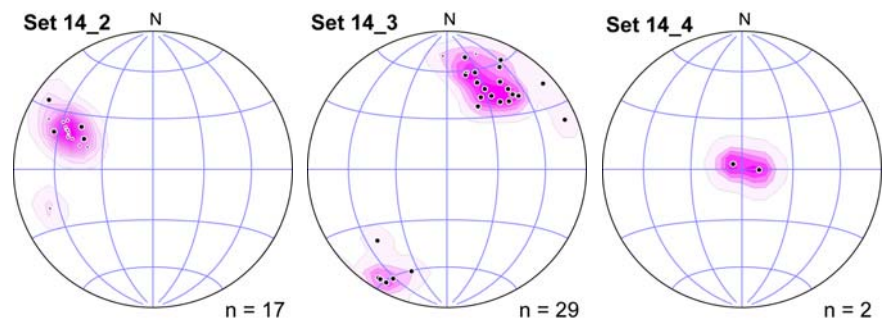
Parameters	Set 15_1	Set 15_2	Set 15_3	
Trend/Plunge [°], Dispersion	80/11, k= 42	315/62, k= 45	353/01, k= 35	
Mean Persistence [m], Std. Dev.	1.80, 1.14	2.04, 2.92	1.20, 0.93	
P10 Intensity measured	1.86	2.22	2.53	
P32 Intensity upscaled	0.49	0.64	0.56	
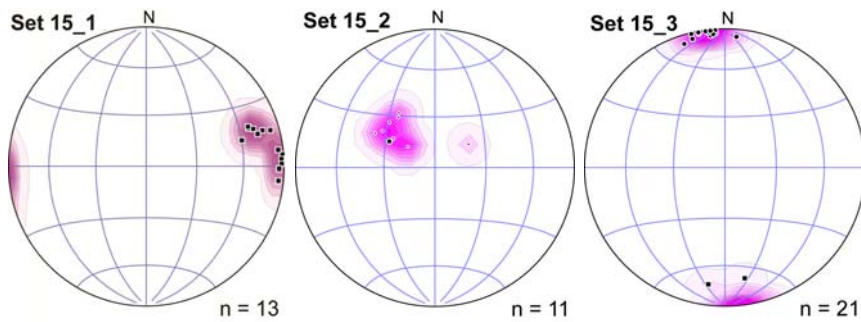
Parameters	Set 16_1		Set 16_3	Set 16_4
Trend/Plunge [°], Dispersion	294/07, k= 35		199/32, k= 49	98/77, k= 70
Mean Persistence [m], Std. Dev.	0.77, 0.36		1.40, 0.75	1.78, 0.41
P10 Intensity measured	3.00		1.67	1.50
P32 Intensity upscaled	1.64		0.66	1.18
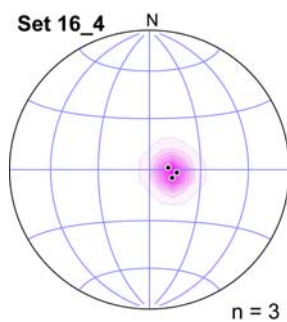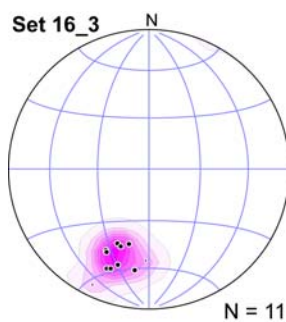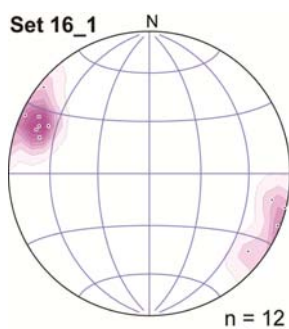
Parameters	Set 17_1			Set 17_4
Trend/Plunge [°], Dispersion	116/16, k= 30			30/66, k= 40
Mean Persistence [m], Std. Dev.	1.62, 1.12			3.28, 2.84
P10 Intensity measured	4.60			6.20
P32 Intensity upscaled	2.05			3.12
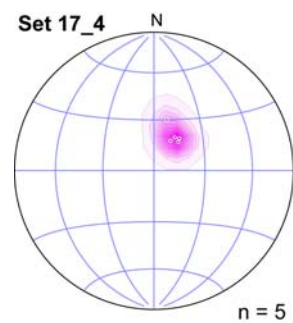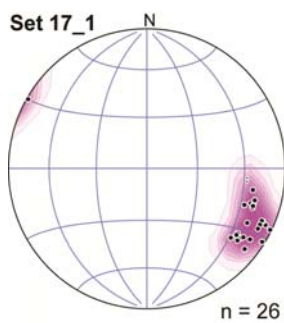
Parameters	Set 18_1	Set 18_2	Set 18_3	Set 18_4
Trend/Plunge [°], Dispersion	95/08, k= 45	293/46, k= 40	166/05, k= 35	29/68, k= 70
Mean Persistence [m], Std. Dev.	1.90, 1.53	0.82, 0.50	0.46, 0.35	3.45, 2.80
P10 Intensity measured	0.90	1.30	2.30	0.6
P32 Intensity upscaled	0.57	0.98	1.25	0.57
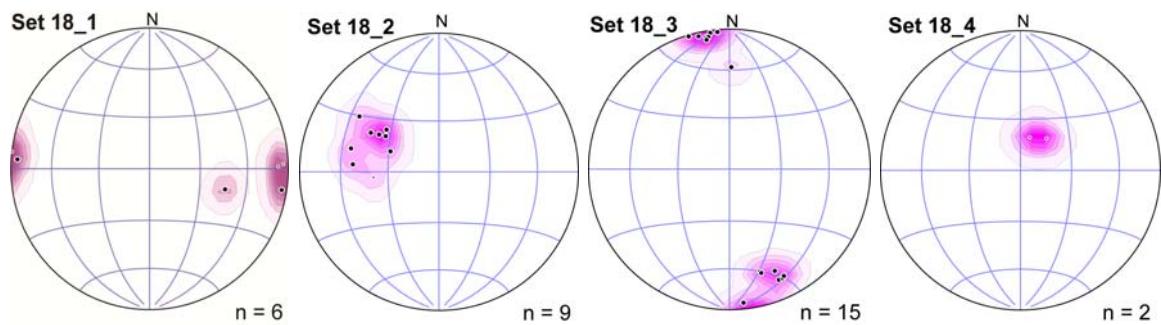
Parameters	Set 19_1		Set 19_3	Set 19_4
Trend/Plunge [°], Dispersion	100/01, k= 20		188/07, k= 30	92/58, k= 25
Mean Persistence [m], Std. Dev.	1.11, 0.43		1.00, 0.50	0.94, 0.28
P10 Intensity measured	2.60		1.20	1.60
P32 Intensity upscaled	1.36		1.14	1.00
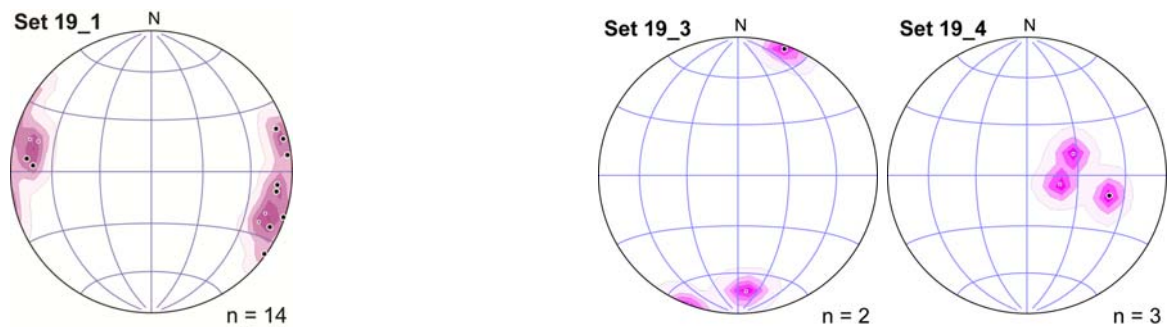
Parameters	Set 20_1		Set 20_3	Set 20_4
Trend/Plunge [°], Dispersion	110/04, k= 30		53/21, k= 30	53/75, k= 40
Mean Persistence [m], Std. Dev.	1.35, 0.74		1.31, 1.25	0.85, 0.35
P10 Intensity measured	4.13		1.00	4.00
P32 Intensity upscaled	2.10		1.10	2.90
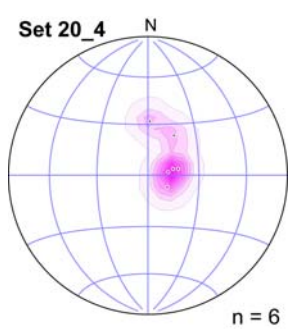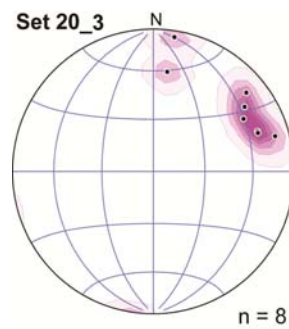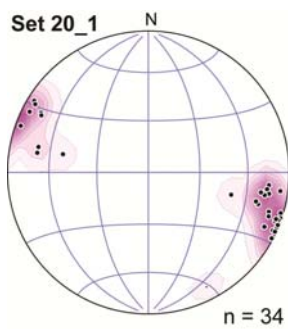
Parameters	Set 21_1		Set 21_3	Set 21_4
Trend/Plunge [°], Dispersion	255/04, k= 25		128/28, k= 30	10/62, k= 35
Mean Persistence [m], Std. Dev.	0.66, 0.30		0.59, 0.20	1.01, 0.41
P10 Intensity measured	2.00		2.50	2.30
P32 Intensity upscaled	1.00		0.46	1.08
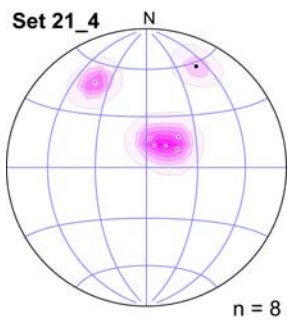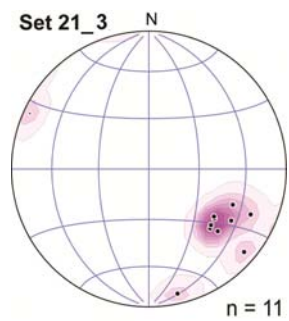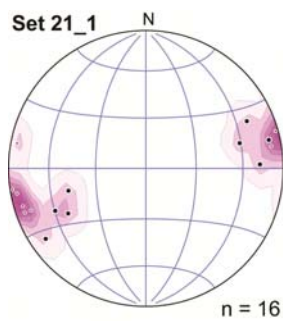
Parameters	Set 24_1		Set 24_3	Set 24_4
Trend/Plunge [°], Dispersion	102/04, k= 40		14/05, k= 30	15/83, k= 60
Mean Persistence [m], Std. Dev.	1.09, 0.40		0.67, 0.26	1.19, 0.56
P10 Intensity measured	3.18		1.29	2.00
P32 Intensity upscaled	2.13		1.10	1.65

Set 24_1 N n = 7

Set 24_3 N n = 13

Set 24_4 N n = 14
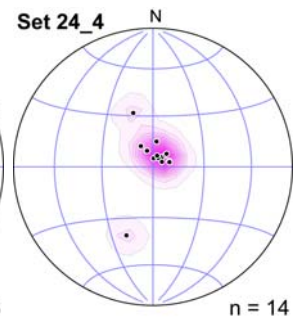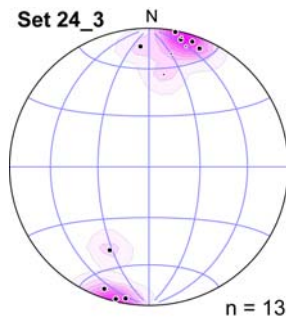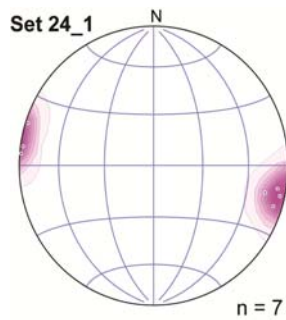
Parameters	Set 25_1	Set 25_2		Set 25_4
Trend/Plunge [°], Dispersion	245/07, k= 30	290/37, k= 90		77/73, k= 80
Mean Persistence [m], Std. Dev.	0.81, 0.35	0.88, 0.34		0.71, 0.19
P10 Intensity measured	3.00	15.3		2.60
P32 Intensity upscaled	1.66	8.12		2.41

Set 25_1 N N = 10

Set 25_2 N n = 36

Set 25_4 N n = 9
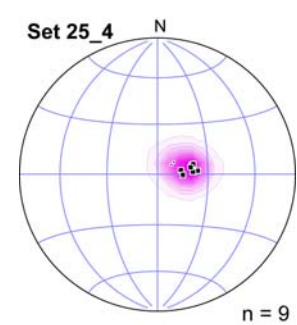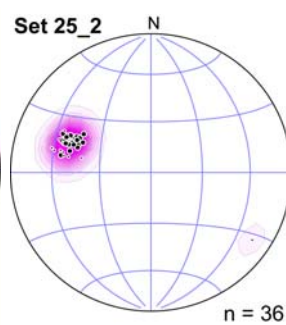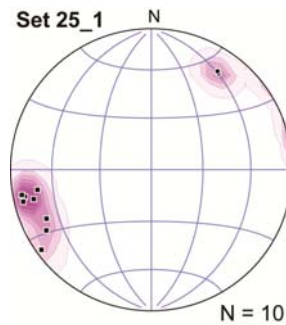
Parameters			Set 27_3	Set 27_4
Trend/Plunge [°], Dispersion			80/79, k= 50	157/17, k= 25
Mean Persistence [m], Std. Dev.			2.20, 1.99	0.99, 0.61
P10 Intensity measured			2.22	2.28
P32 Intensity upscaled			1.55	1.41
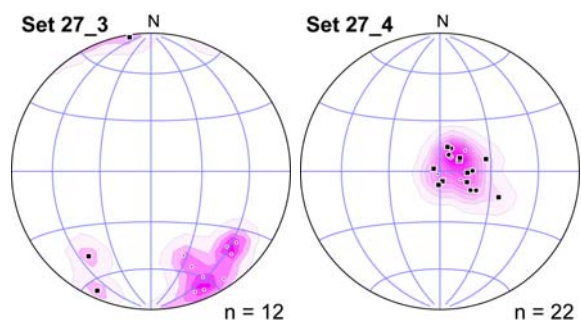
Parameters	Set 28_1		Set 28_3	Set 28_4
Trend/Plunge [°], Dispersion	113/16, k= 25		10/03, k= 35	57/78, k= 80
Mean Persistence [m], Std. Dev.	1.58, 0.76		0.39, 0.19	1.88, 1.02
P10 Intensity measured	2.39		0.43	2.86
P32 Intensity upscaled	1.17		0.24	1.48
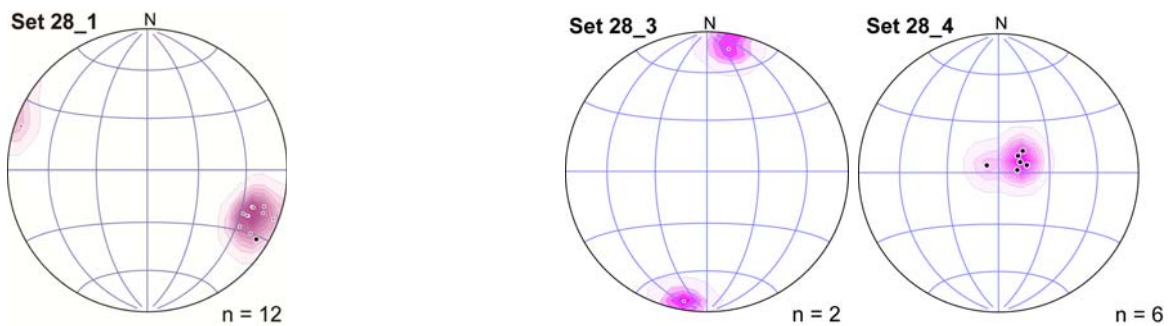
Parameters	Set 35_1	Set 35_2	Set 35_3	
Trend/Plunge [°], Dispersion	112/30, k= 36	308/62, k= 70	201/01, k= 30	
Mean Persistence [m], Std. Dev.	2.66, 1.83	3.80, 1.97	3.70, 2.82	
P10 Intensity measured	0.67	2.13	0.25	
P32 Intensity upscaled	0.46	0.95	0.11	
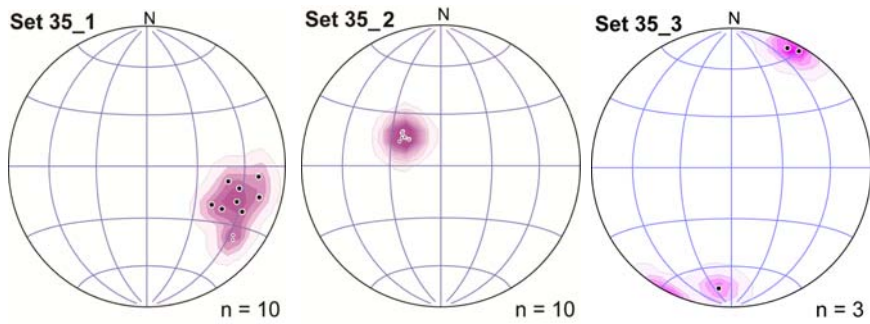
Parameters	Set 36_1	Set 36_2		
Trend/Plunge [°], Dispersion	87/30, k= 65	292/60, k= 60		
Mean Persistence [m], Std. Dev.	2.03, 1.33	3.14, 0.96		
P10 Intensity measured	1.79	2.80		
P32 Intensity upscaled	0.34	1.23		
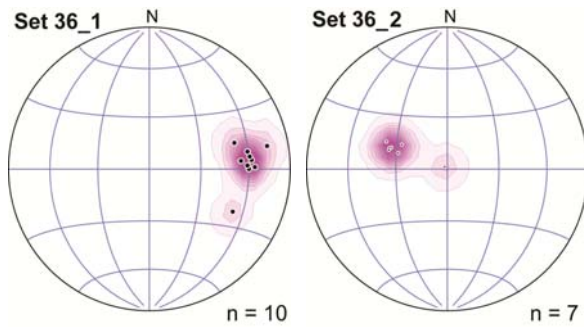
Parameters	Set 37_1	Set 37_2	Set 37_3	
Trend/Plunge [°], Dispersion	98/32, k= 30	294/68, k= 50	337/09, k= 30	
Mean Persistence [m], Std. Dev.	2.14, 1.54	0.92, 0.30	1.65, 1.17	
P10 Intensity measured	3.00	4.60	0.43	
P32 Intensity upscaled	1.60	0.20	1.60	
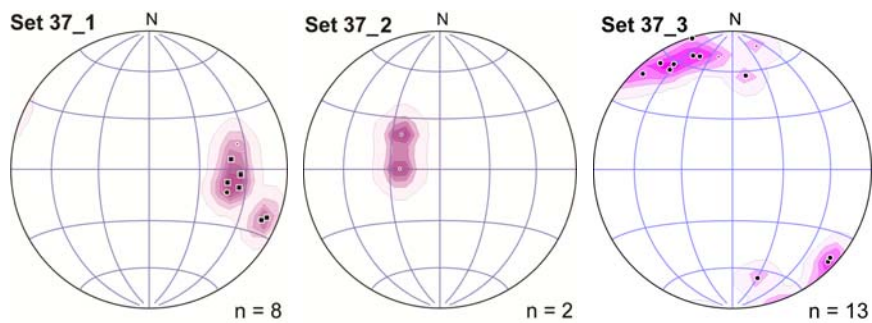
Parameters	Set 39_1		Set 39_3	Set 39_4
Trend/Plunge [°], Dispersion	85/22, k= 35		346/10, k= 25	238/51, k= 38
Mean Persistence [m], Std. Dev.	1.90, 0.36		1.28, 0.68	1.25, 0.45
P10 Intensity measured	0.70		3.14	1.43
P32 Intensity upscaled	0.27		0.68	0.82
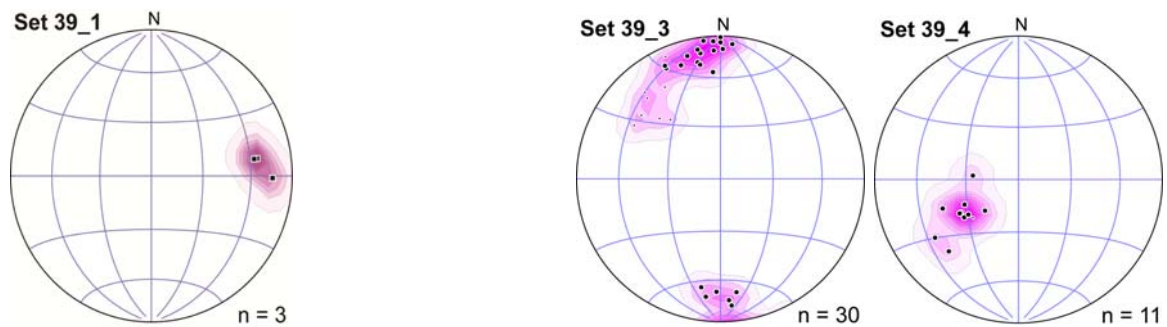
A.3. Climate data
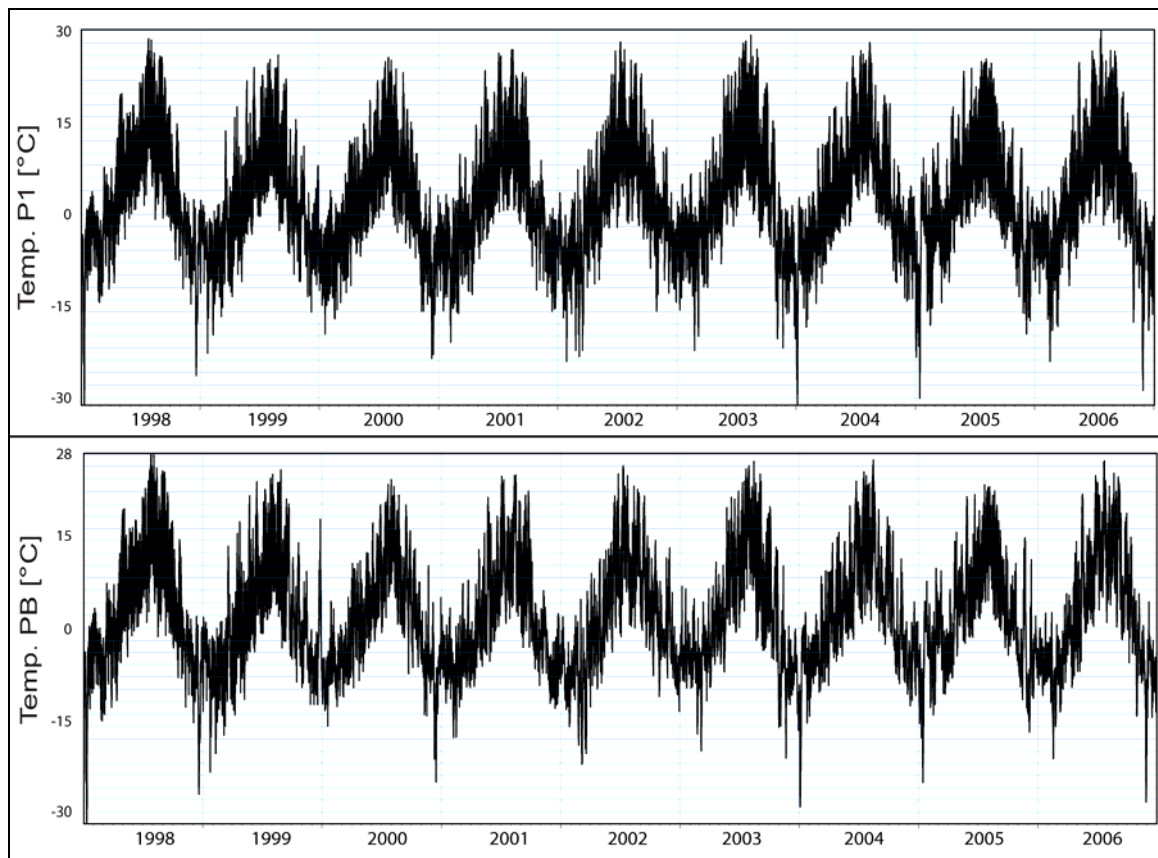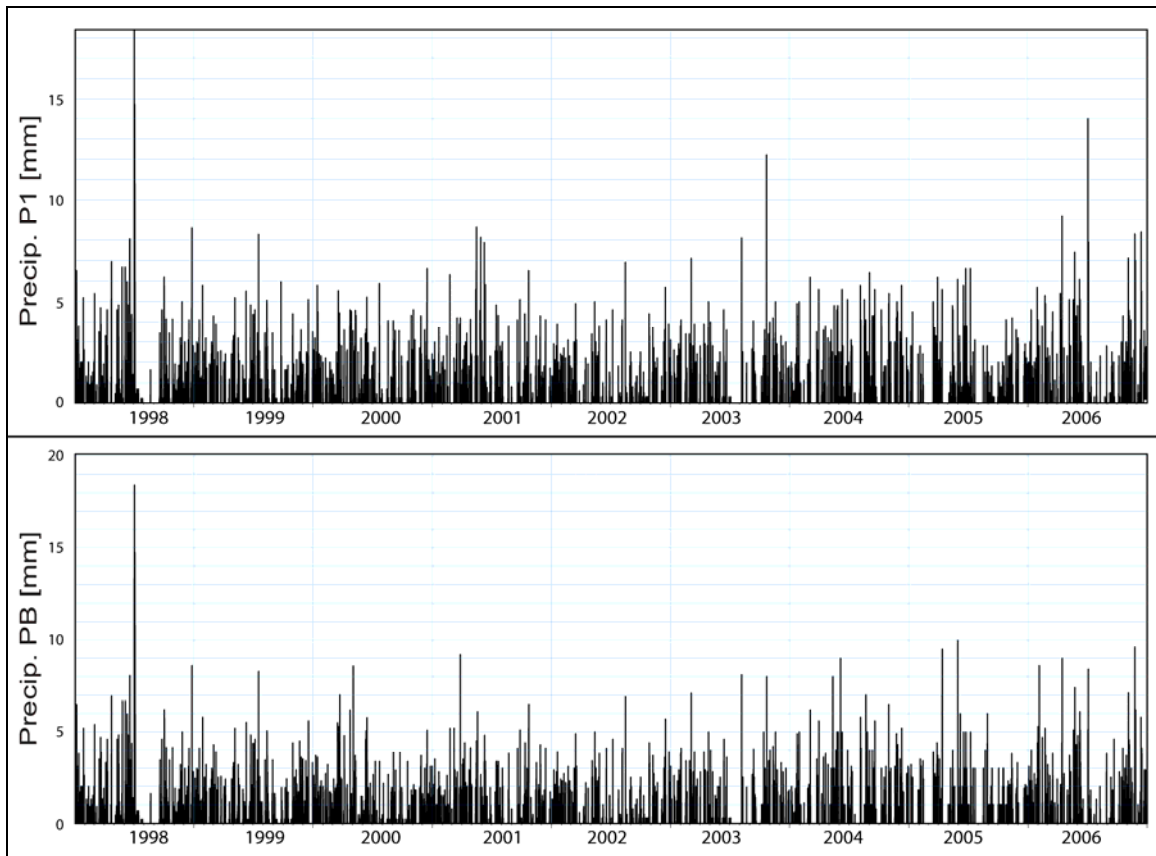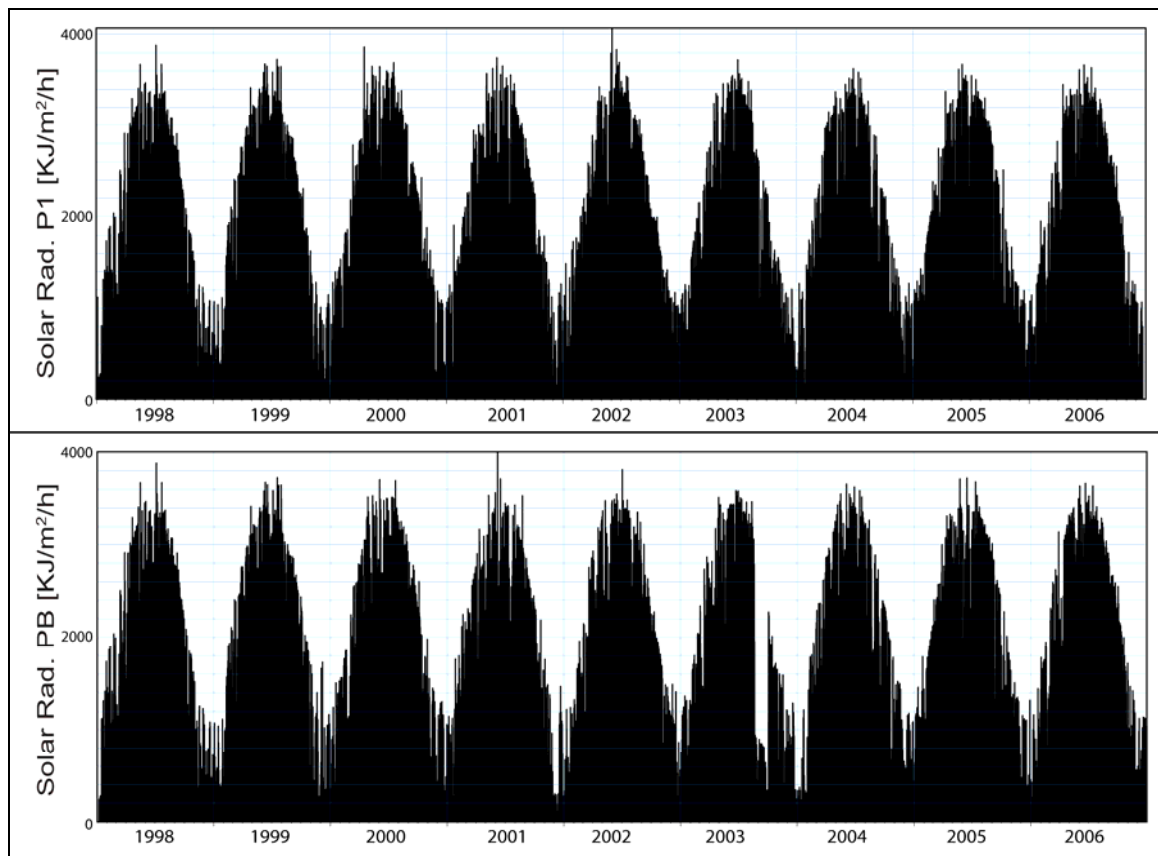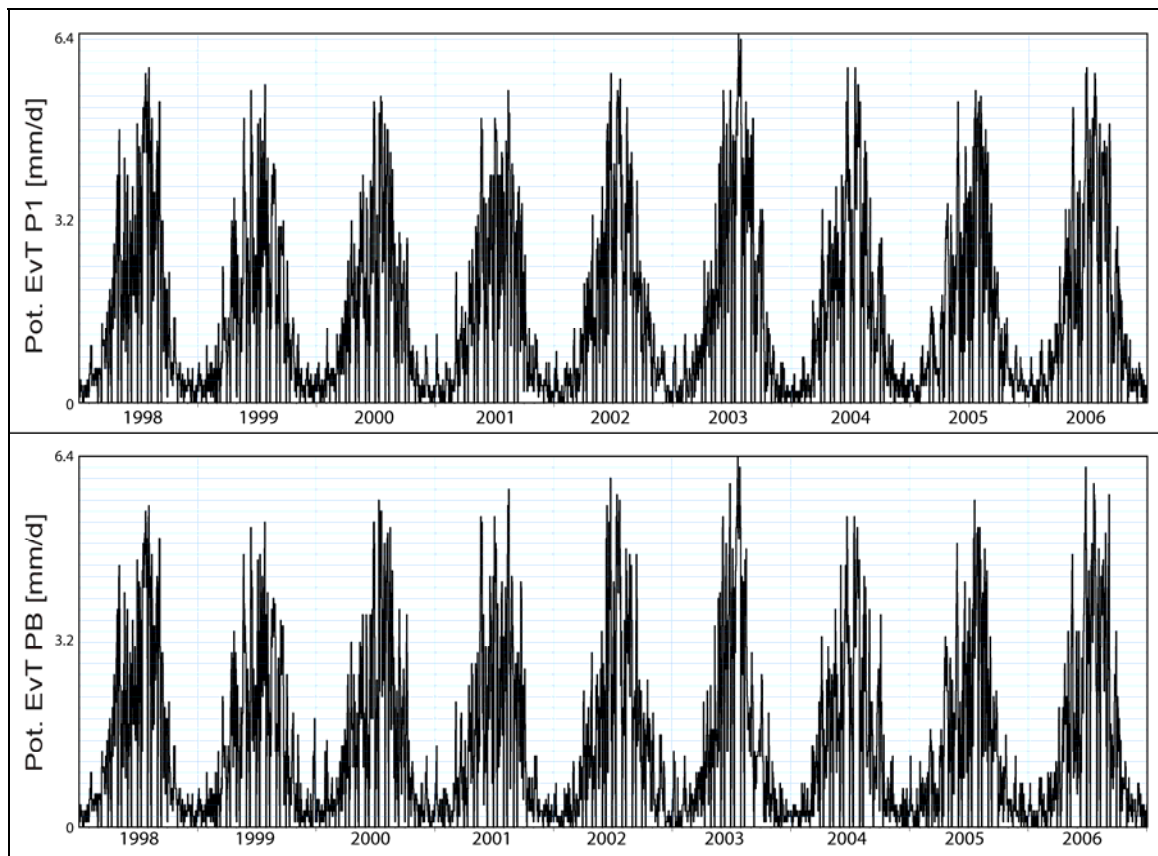
A.4. Streamflow data

A.5. Soil water data

P3 - 21152 Soil WT

missing data

P4 - 32001 Soil WT

P5 - 23387 Soil WT

P6 - 21155 Soil WT

P7 - 23391 Soil WT

P8 - 23388 Soil WT

P9 - 23392 Soil WT

P10 - 23390 Soil WT

P13 - 20073 Soil WT

P15 - 33000 Soil WT
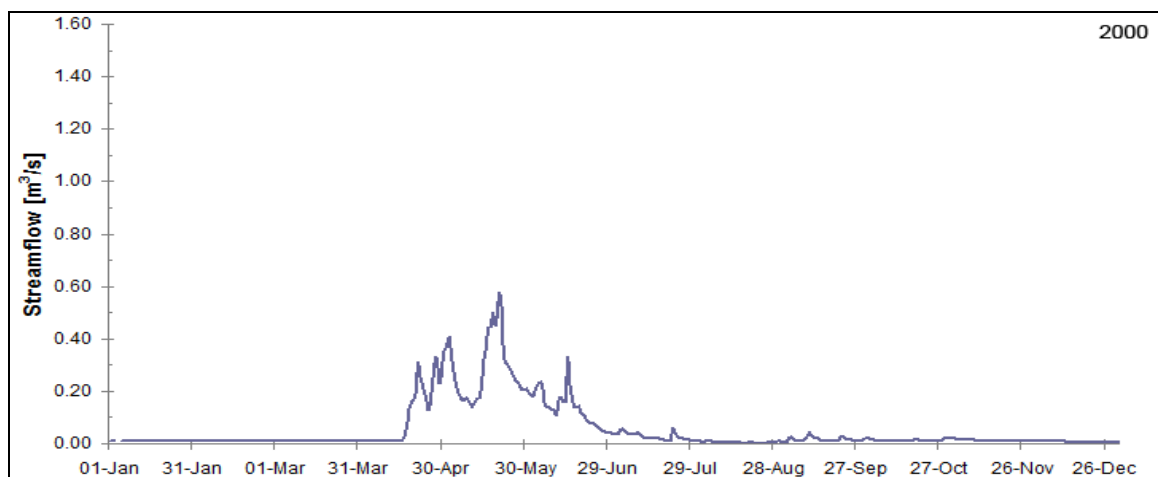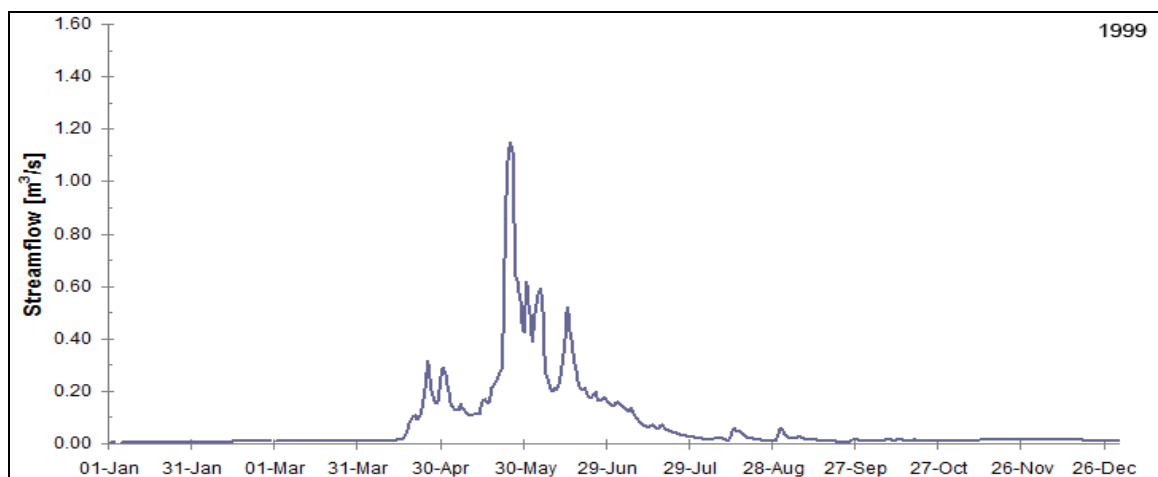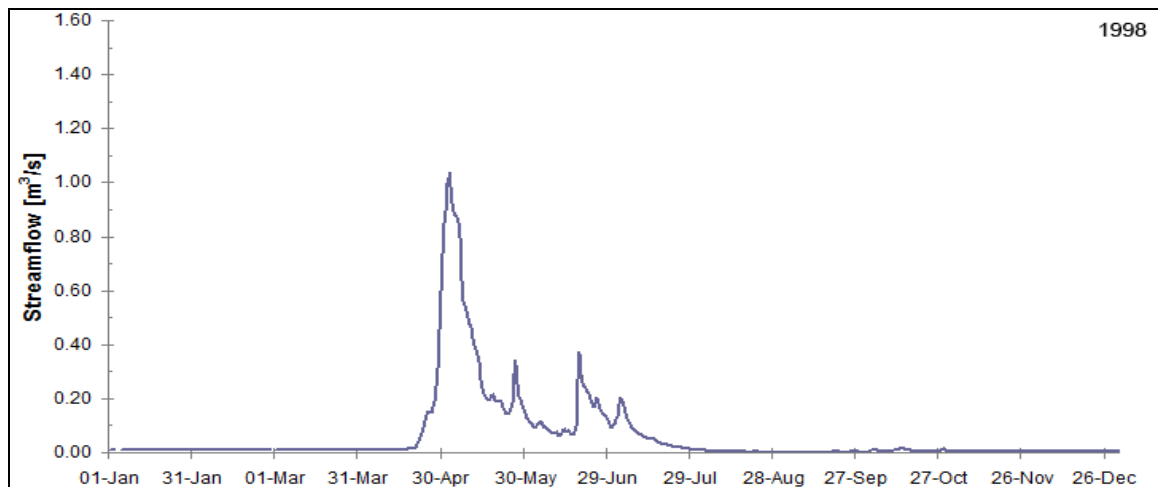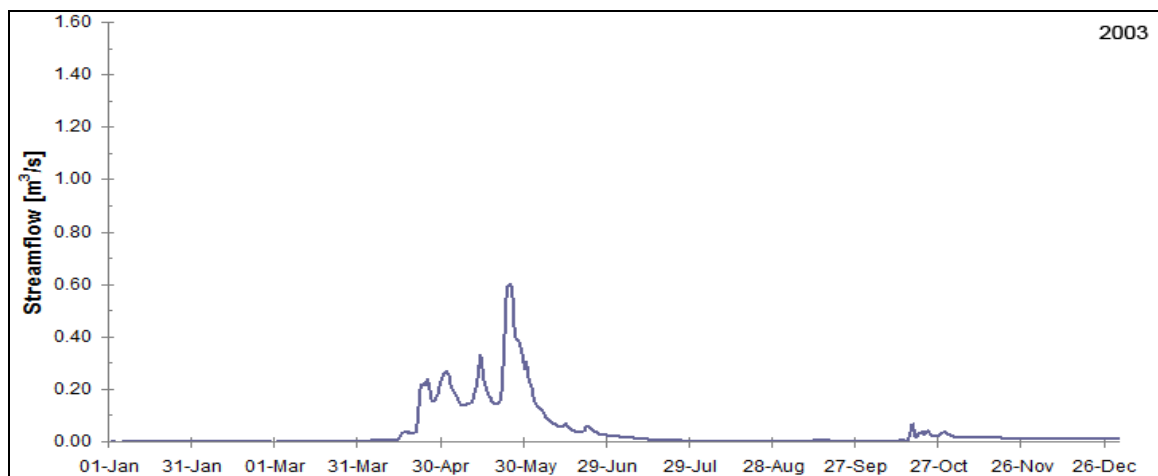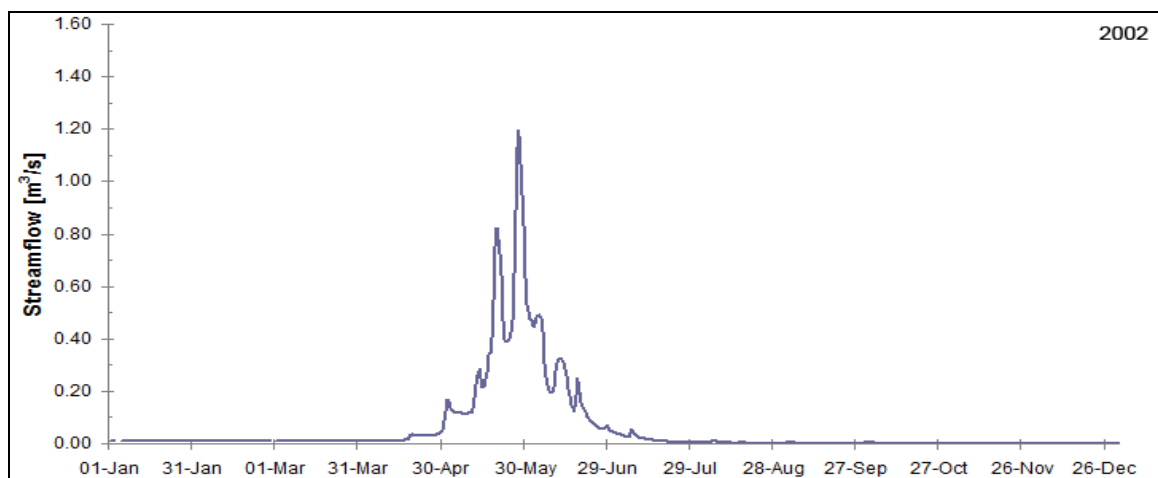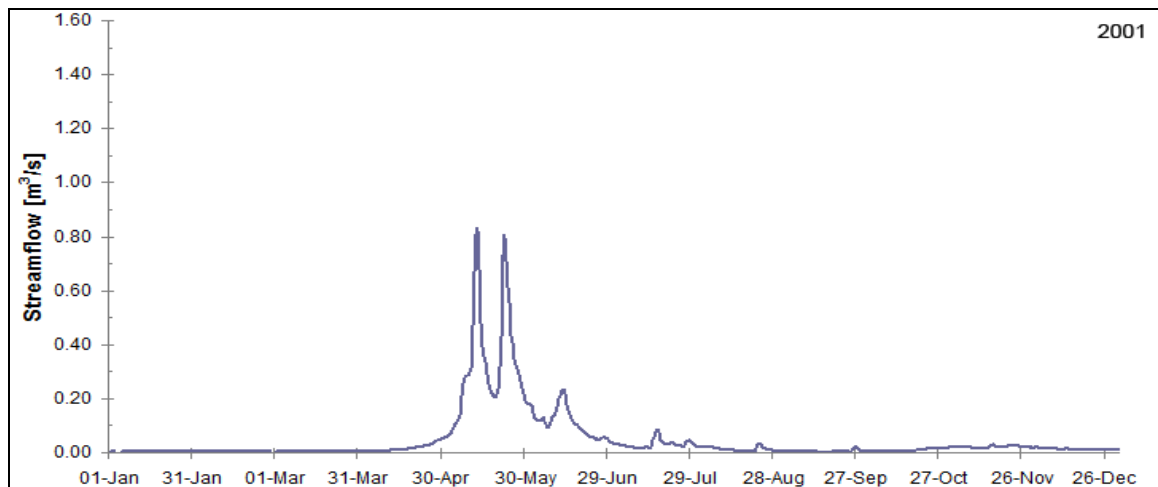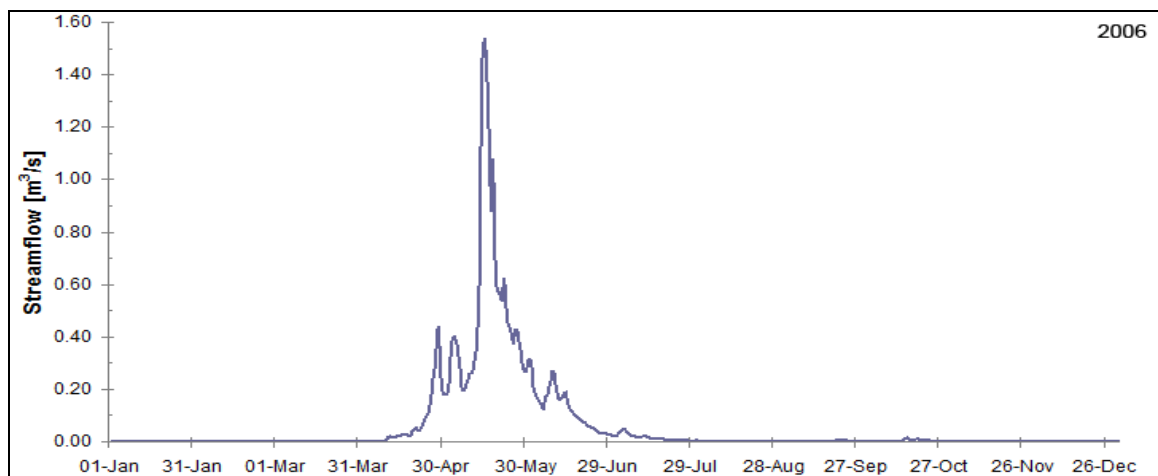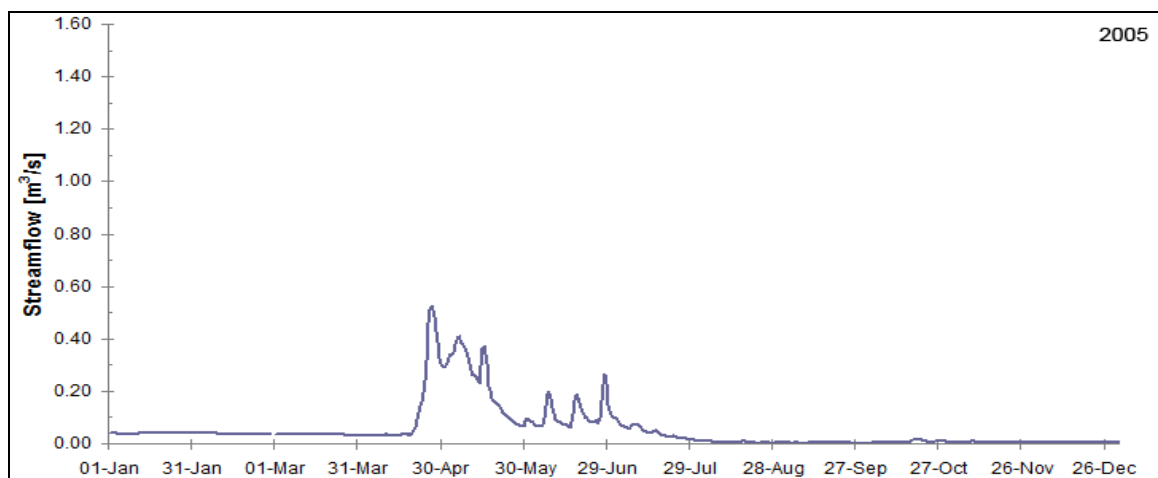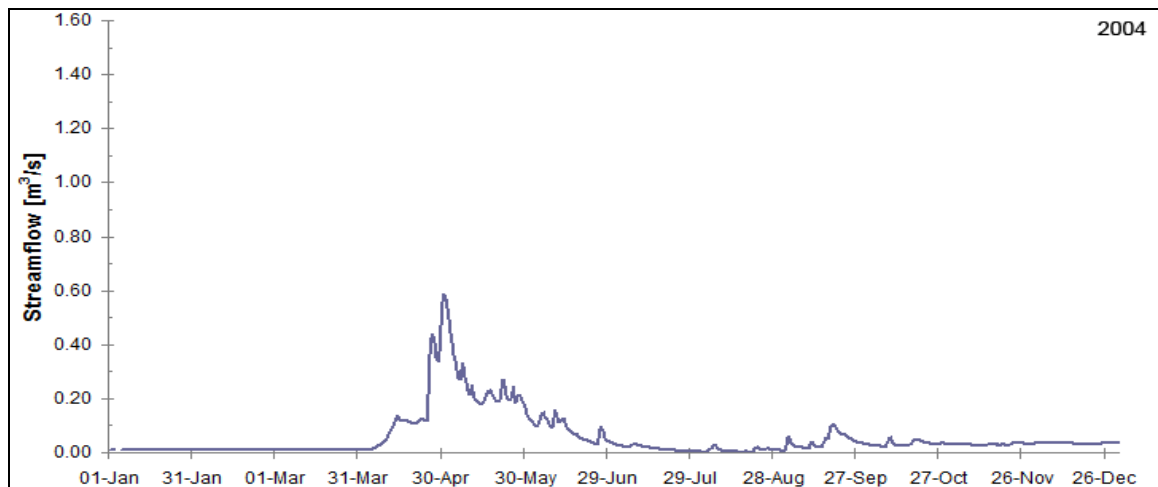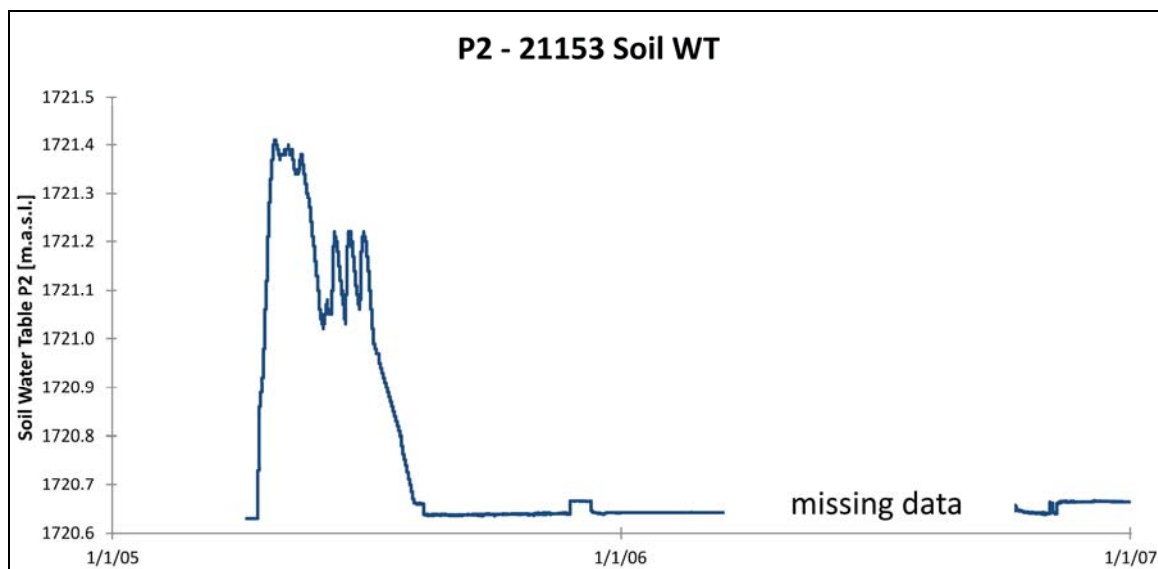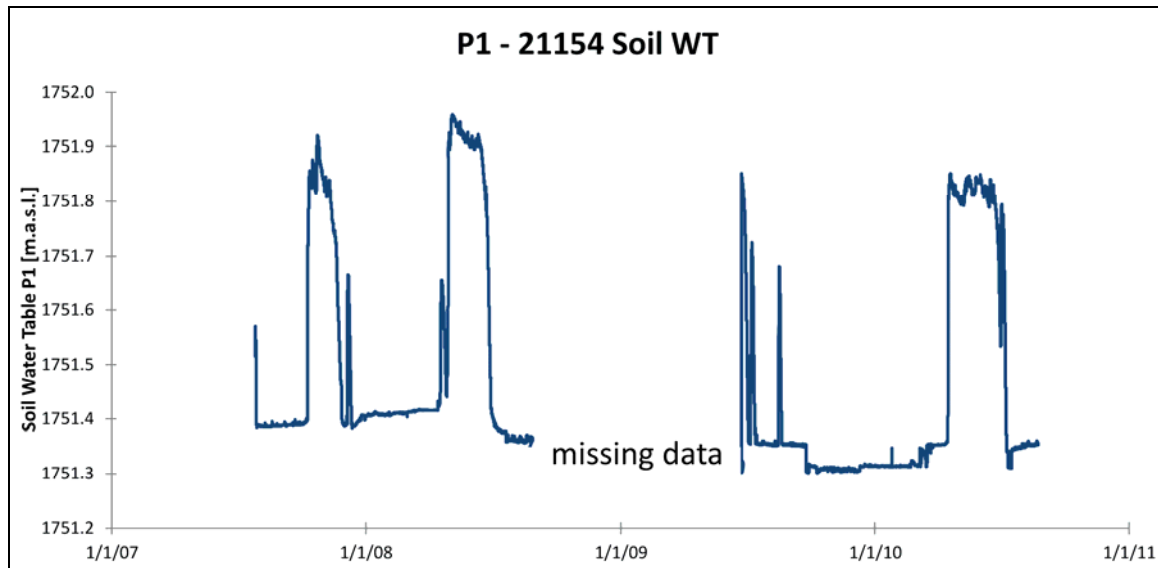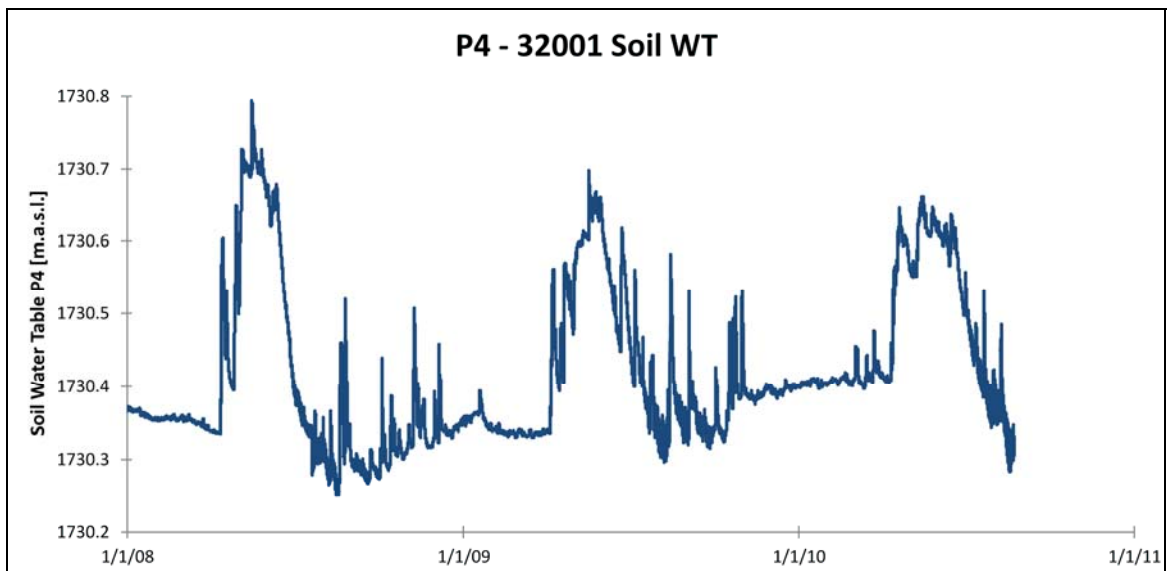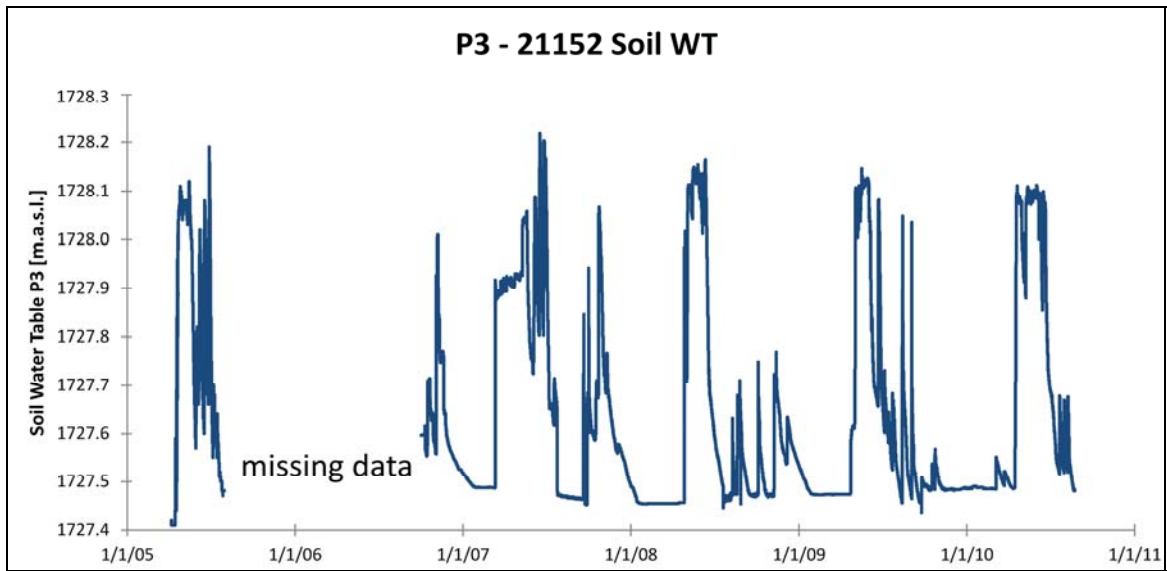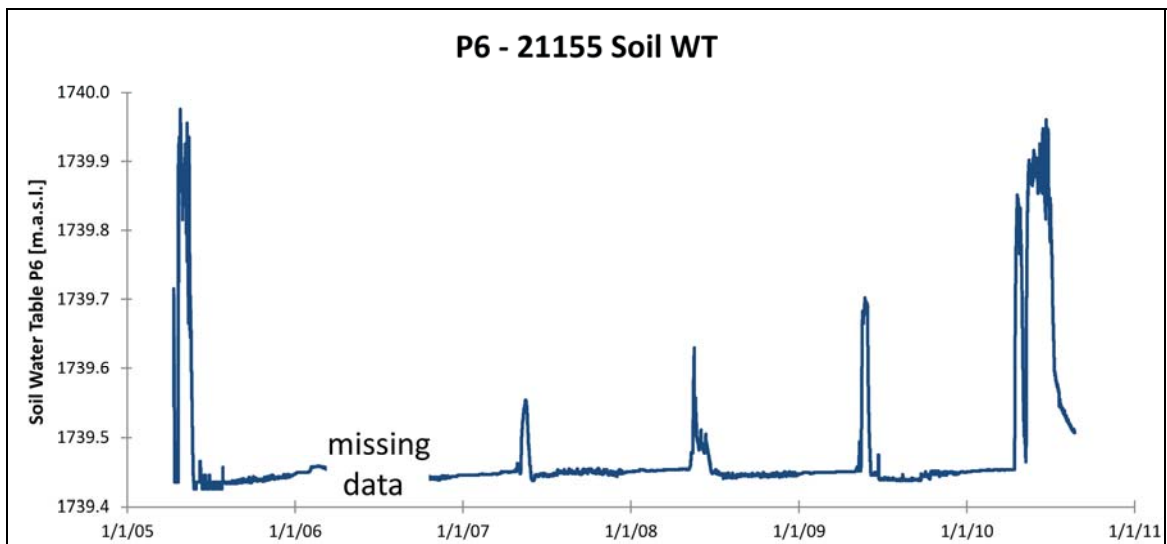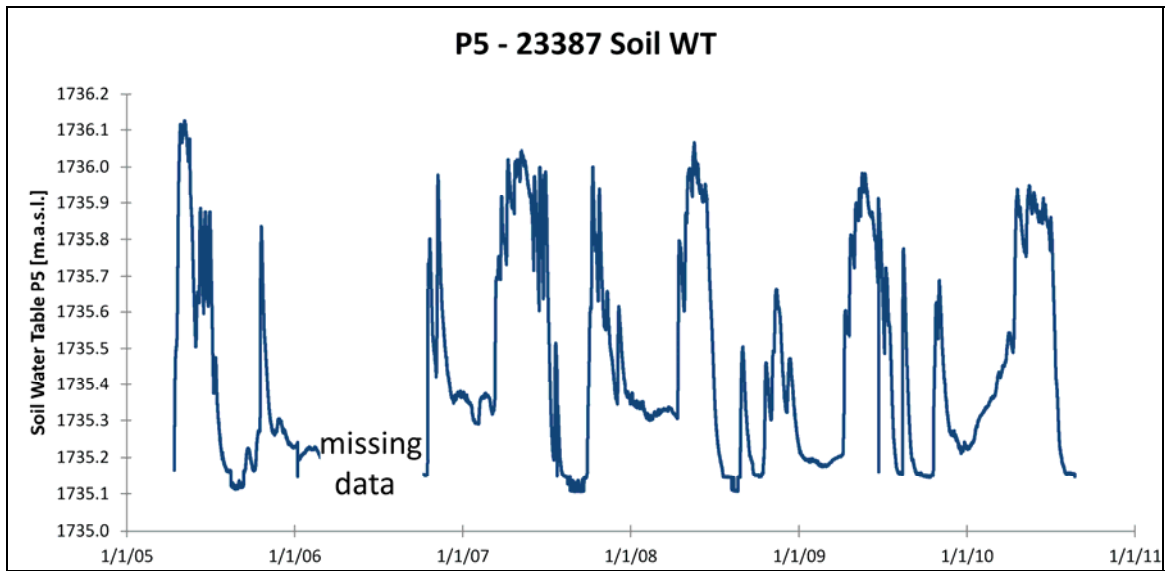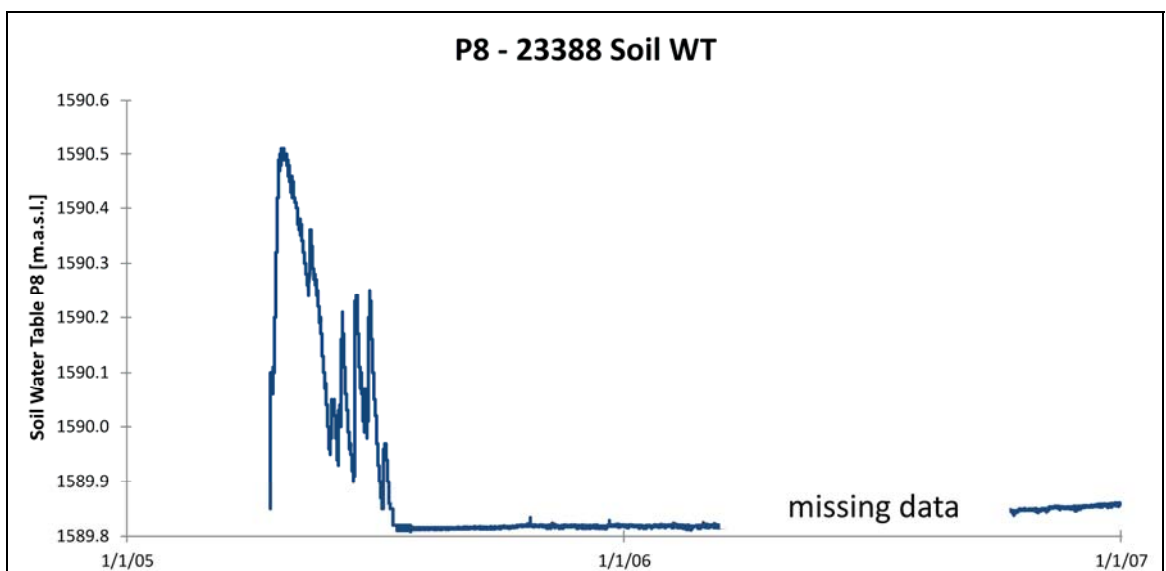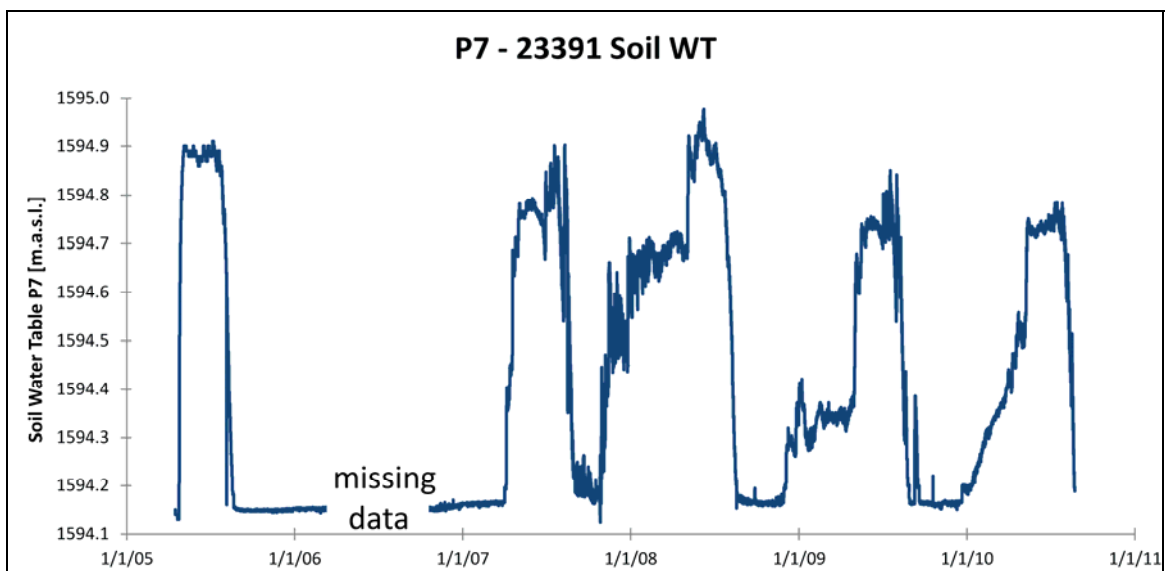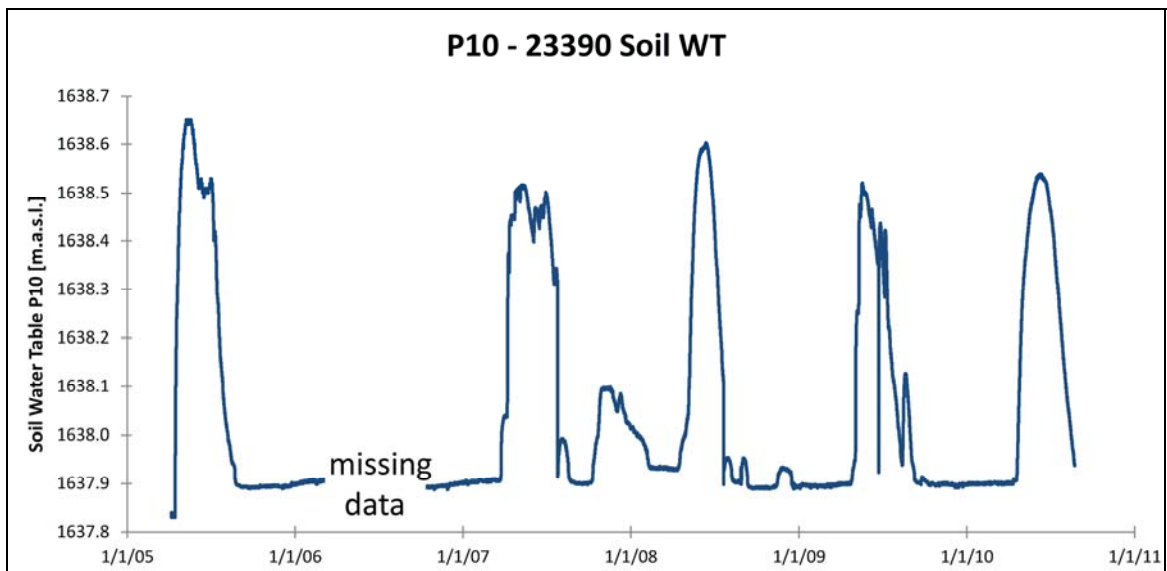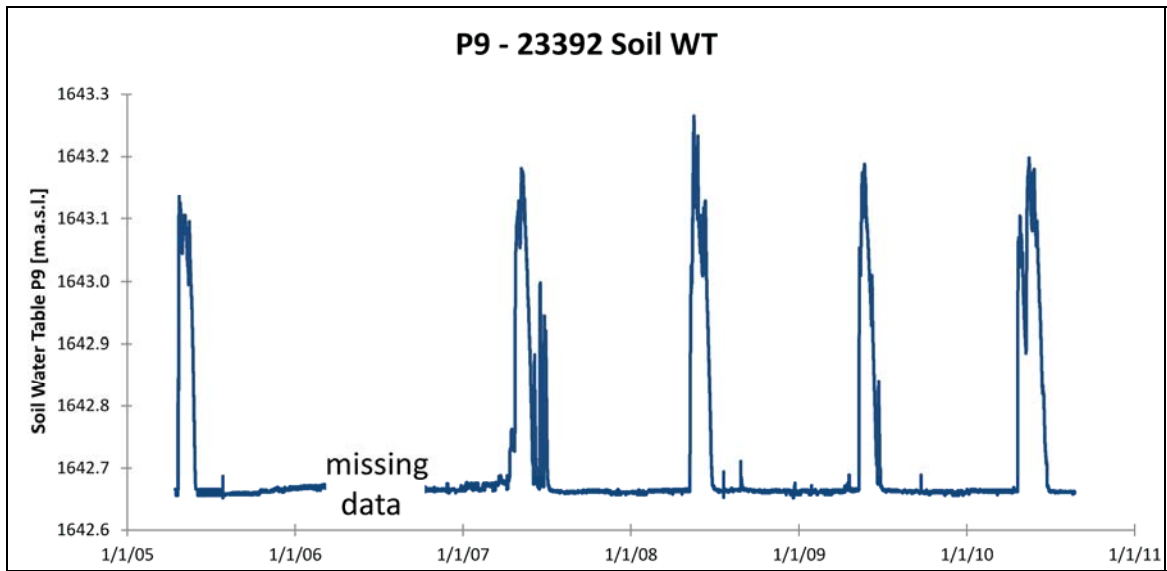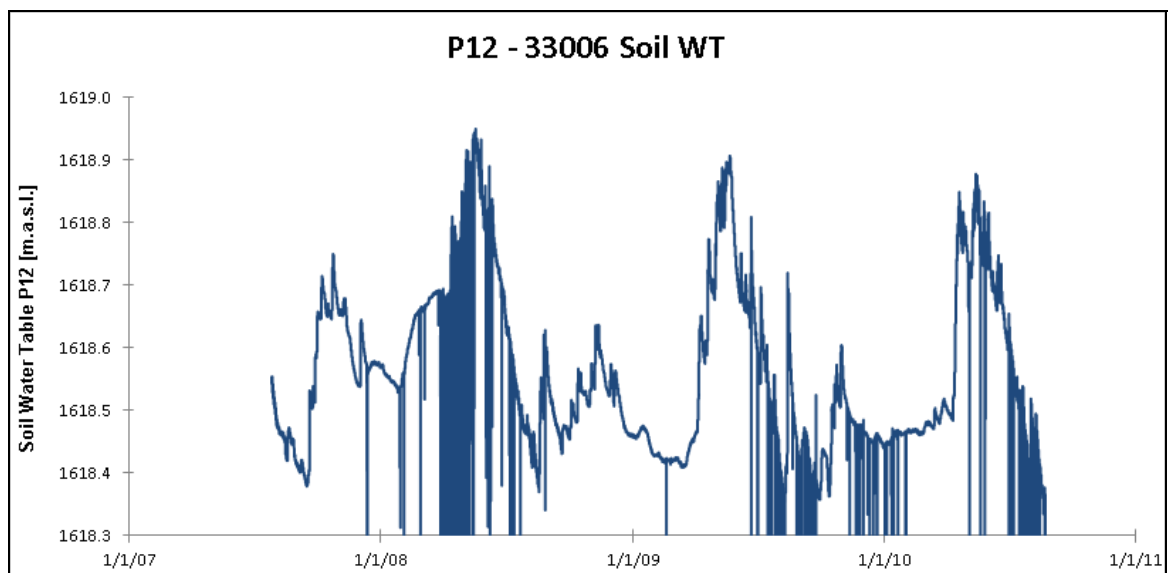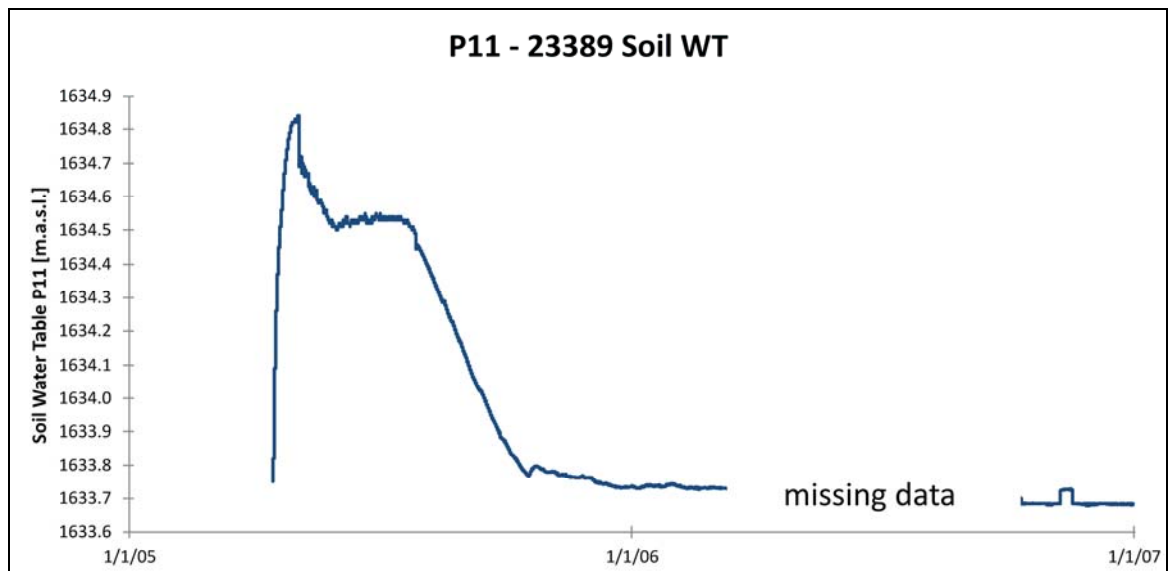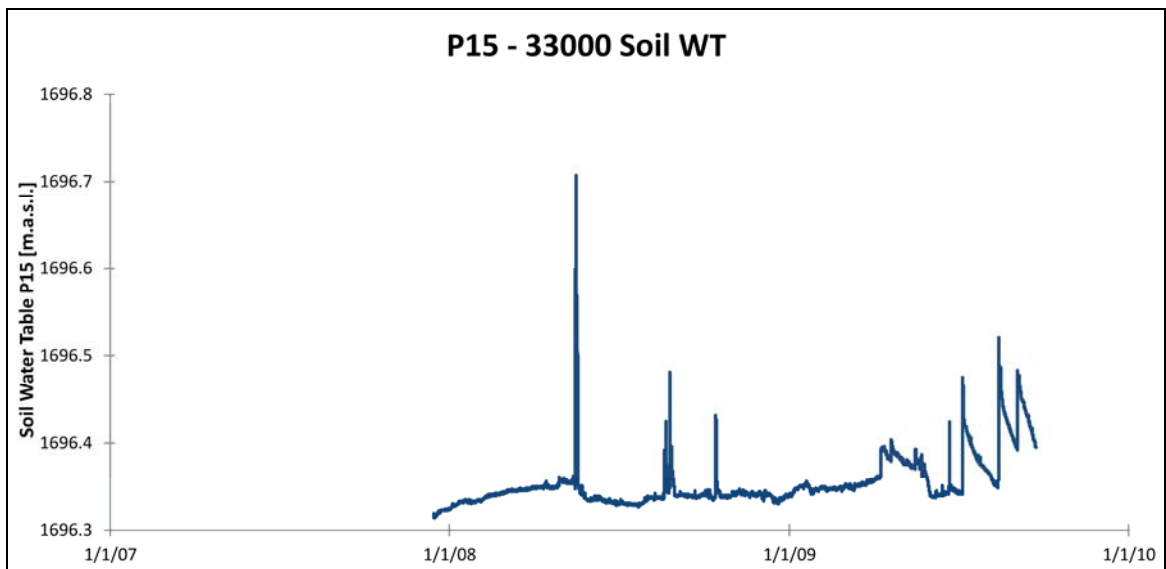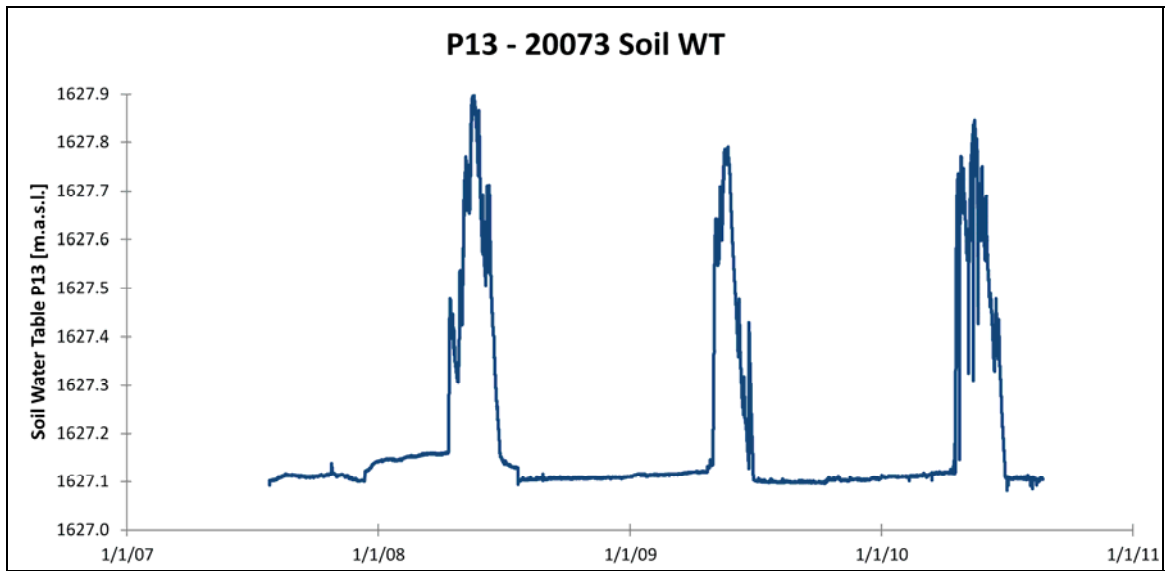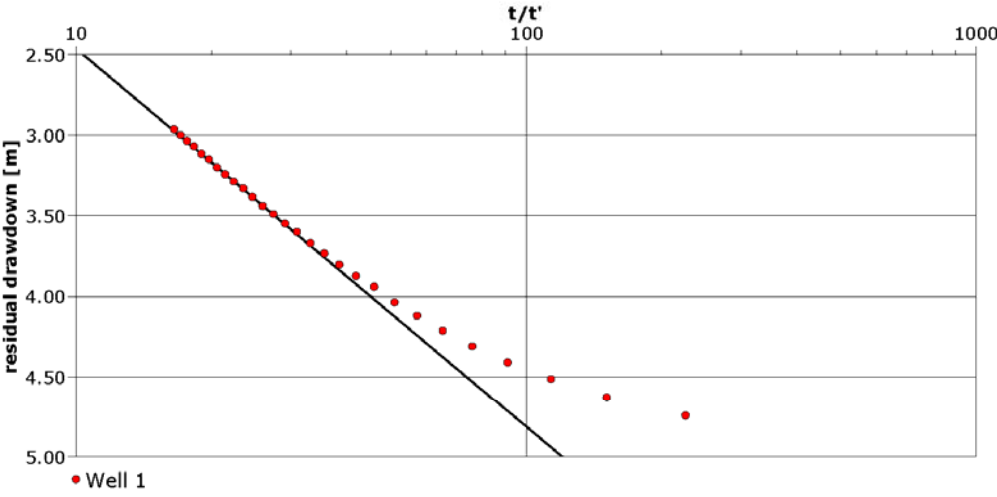
A.6. Bedrock well data
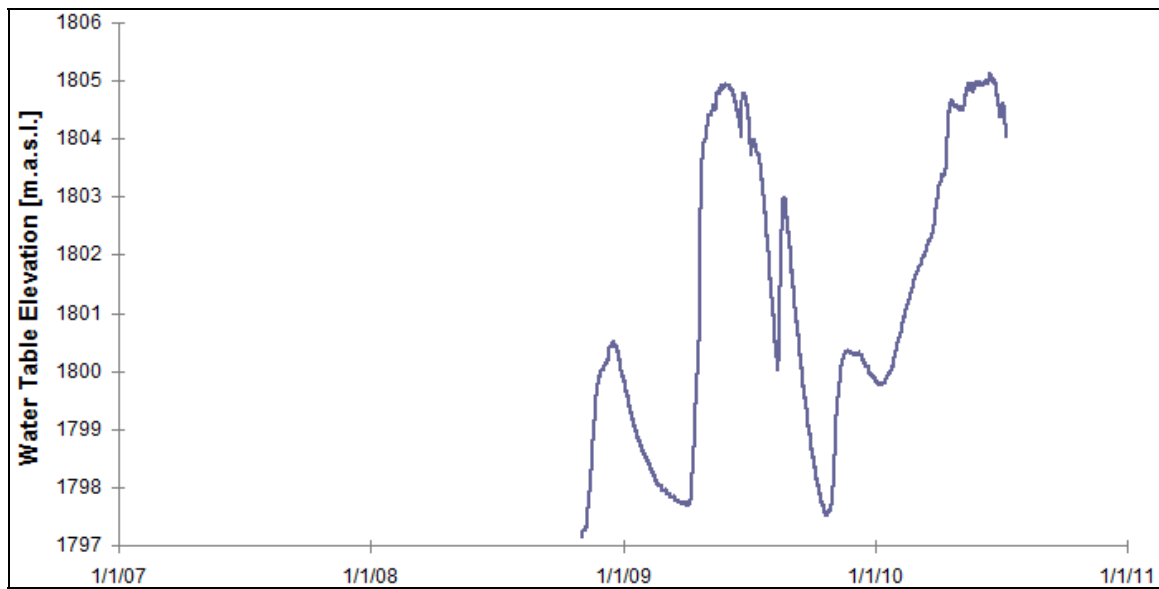
A.7. Bedrock well pumping test data and analyses

Company Name Contact Info Address City, State/Province	Pumping Test Analysis Report	
	Project: Hendrik - Pumping Tests; Slug & Bail Tests	
	Number:	
	Client:	

Location: UPC 241	Pumping Test: Pumping Test 1	Pumping Well: Well 1
Test Conducted by: H. Voeckler, D. Allen		Test Date: 7/27/2008
Analysis Performed by: John Mayer	Well 1 - Cooper Jacob 1	Analysis Date: 6/8/2010
Aquifer Thickness: 38.00 m	Discharge: variable, average rate 0.06 [l/s]	

Calculation after Cooper & Jacob

Observation Well	Transmissivity [m²/s]	Hydraulic Conductivity [m/s]	Storage coefficient	Radial Distance to PW [m]	
Well 1	4.44×10^{-6}	1.17×10^{-7}	2.89×10^{-1}	0.08	

Company Name **Contact Info** **Address** **City, State/Province**	**Pumping Test Analysis Report**
	Project: Hendrik - Pumping Tests; Slug & Bail Tests
	Number:
	Client:

Location: UPC 241	Pumping Test: Pumping Test 1	Pumping Well: Well 1
Test Conducted by: H. Voeckler, D. Allen		Test Date: 7/27/2008
Analysis Performed by: John Mayer	Well 1 - Recovery	Analysis Date: 6/9/2010
Aquifer Thickness: 38.00 m	Discharge: variable, average rate 0.06 [l/s]	

Calculation after Theis & Jacob

Observation Well	Transmissivity [m²/s]	Hydraulic Conductivity [m/s]	Radial Distance to PW [m]	
Well 1	4.68×10^{-6}	1.23×10^{-7}	0.08	

386

	Company Name Contact Info Address City, State/Province	Pumping Test Analysis Report	
		Project: Hendrik - Pumping Tests; Slug & Bail Tests	
		Number:	
		Client:	

Location: UPC 241	Pumping Test: Pumping Test 1	Pumping Well: Well 1
Test Conducted by: H. Voeckler, D. Allen		Test Date: 7/27/2008
Analysis Performed by: John Mayer	Well 2 - Cooper Jacob 1	Analysis Date: 6/8/2010
Aquifer Thickness: 38.00 m	Discharge: variable, average rate 0.06 [l/s]	

Calculation after Cooper & Jacob

Observation Well	Transmissivity [m²/s]	Hydraulic Conductivity [m/s]	Storage coefficient	Radial Distance to PW [m]	
Well 2	5.50×10^{-6}	1.45×10^{-7}	6.24×10^{-4}	3.3	

387

Company Name **Contact Info** **Address** **City, State/Province**		**Pumping Test Analysis Report**	
		Project: Hendrik - Pumping Tests; Slug & Bail Tests	
		Number:	
		Client:	

Location: UPC 241	Pumping Test: Pumping Test 2	Pumping Well: Well 3
Test Conducted by: H. Voeckler, D. Allen		Test Date: 7/28/2008
Analysis Performed by: John Mayer	Well 3 - Cooper Jacob 1	Analysis Date: 6/9/2010
Aquifer Thickness: 30.30 m	Discharge: variable, average rate 0.08 [l/s]	

▲ Well 3

Calculation after Cooper & Jacob

Observation Well	Transmissivity [m²/s]	Hydraulic Conductivity [m/s]	Storage coefficient	Radial Distance to PW [m]	
Well 3	6.66×10^{-5}	2.20×10^{-6}	3.05×10^{-1}	0.08	

I'm not very confident in my analysis because I'm not really sure what is going on here

The time interval 0.2 to 1 min was used for the analysis due to the derivative method indicating that radial flow was occurring during this time interval

A.8. Bedrock well slug and bail test data and analyses

Well 2: Slug Test, Hvorslev Method

K = 4.02e-7 m/s

Well 2: Bail Test, Hvorslev Method

K = 3.44e-7 m/s

Well 2: Slug Test, Bouwer & Rice Method

K = 2.96e-7 m/s

Well 2: Bail Test, Bouwer & Rice Method

K = 2.54e-7 m/s

Well 3: Bail 1 Test, Hvorslev Method

K = 3.49e-6 m/s

Well 3: Bail 2 Test, Hvorslev Method

K = 8.25e-6 m/s

Well 3: Bail 1 Test, Bouwer & Rice Method

K = 2.79e-6 m/s

Well 3: Bail 2 Test, Bouwer & Rice Method

K = 6.60e-6 m/s
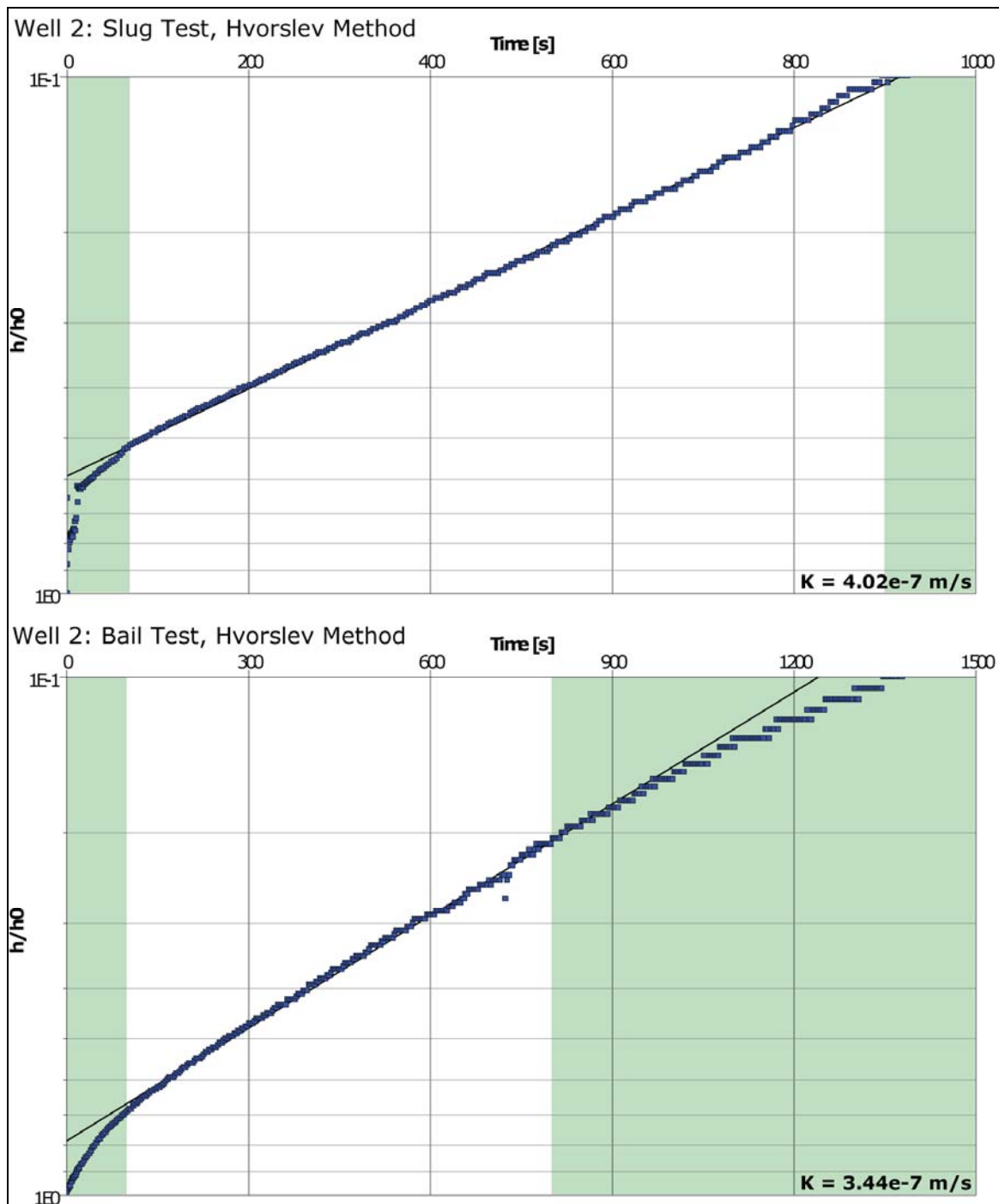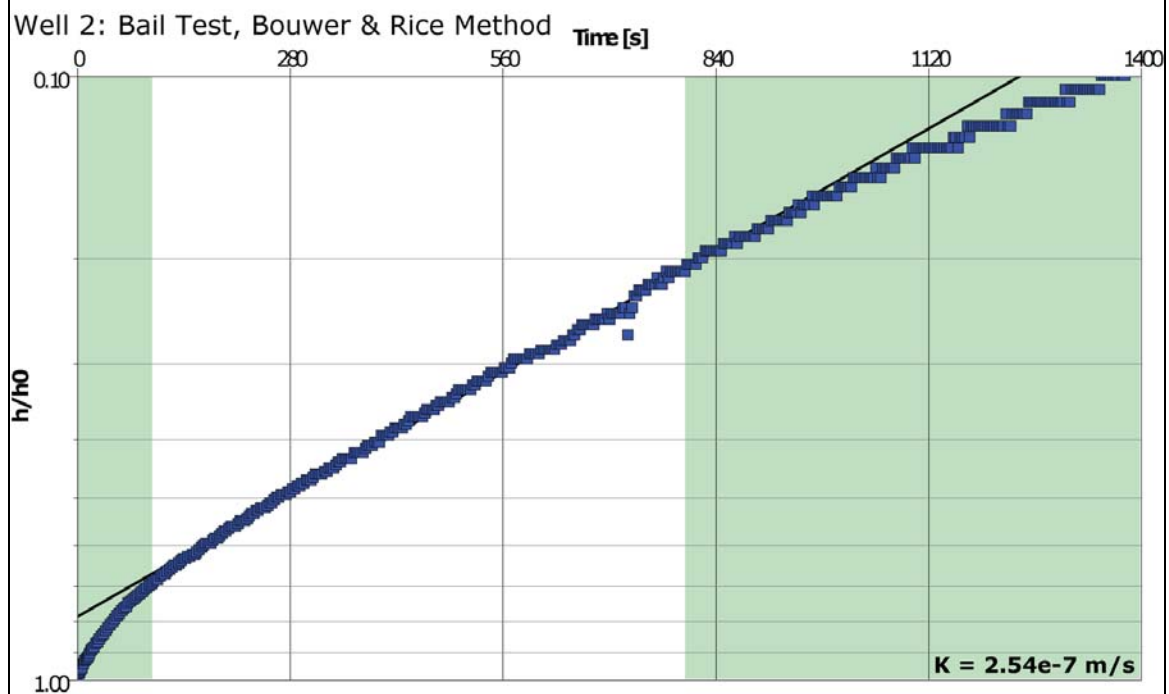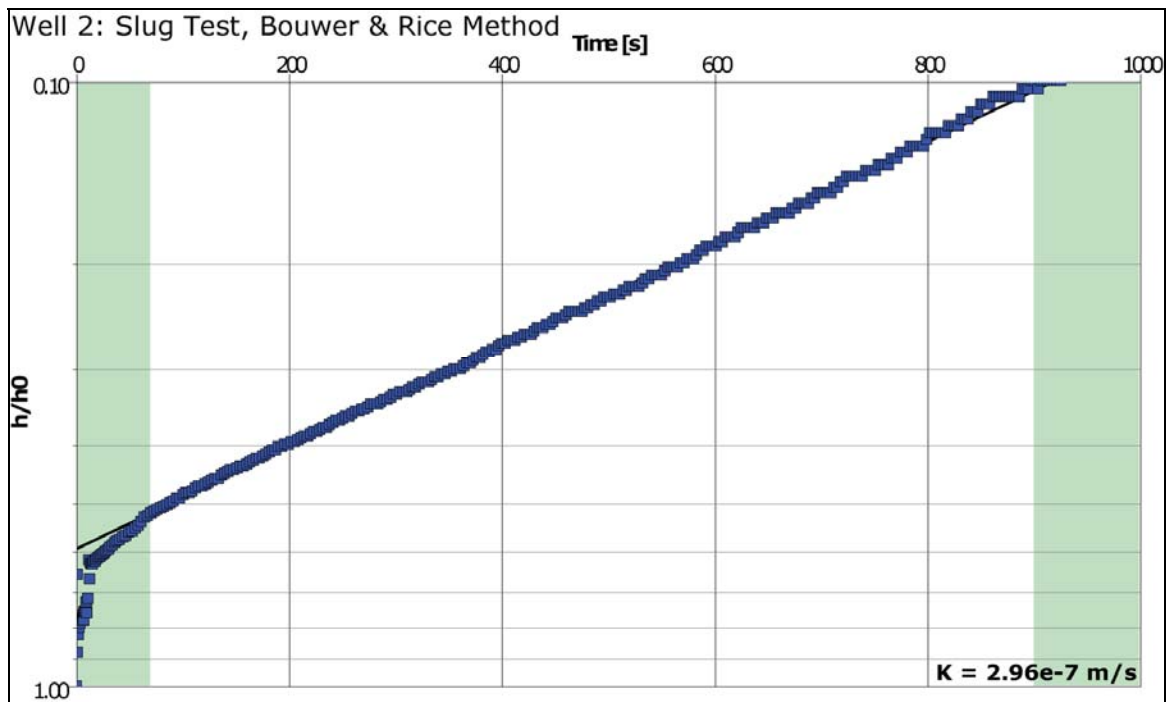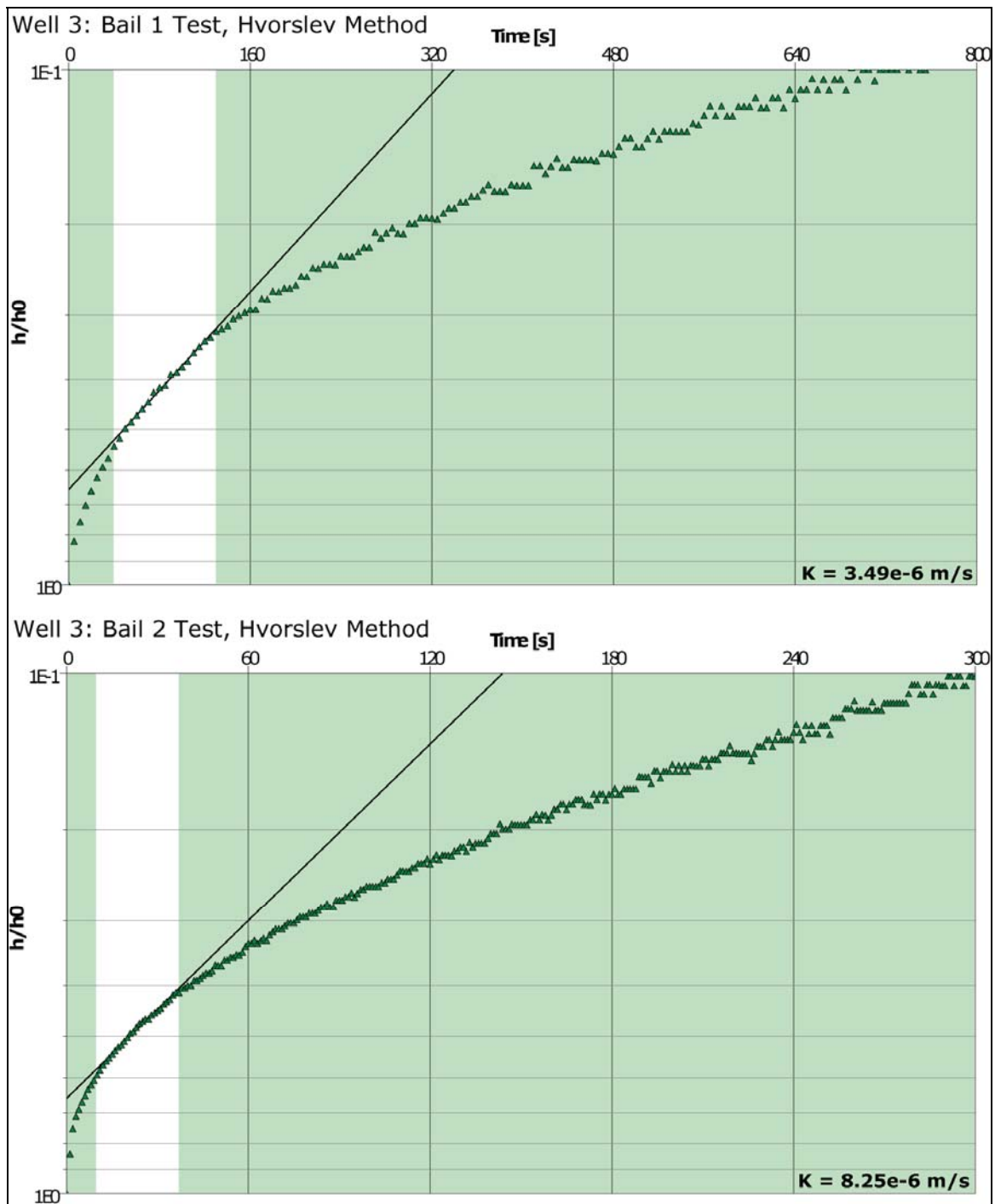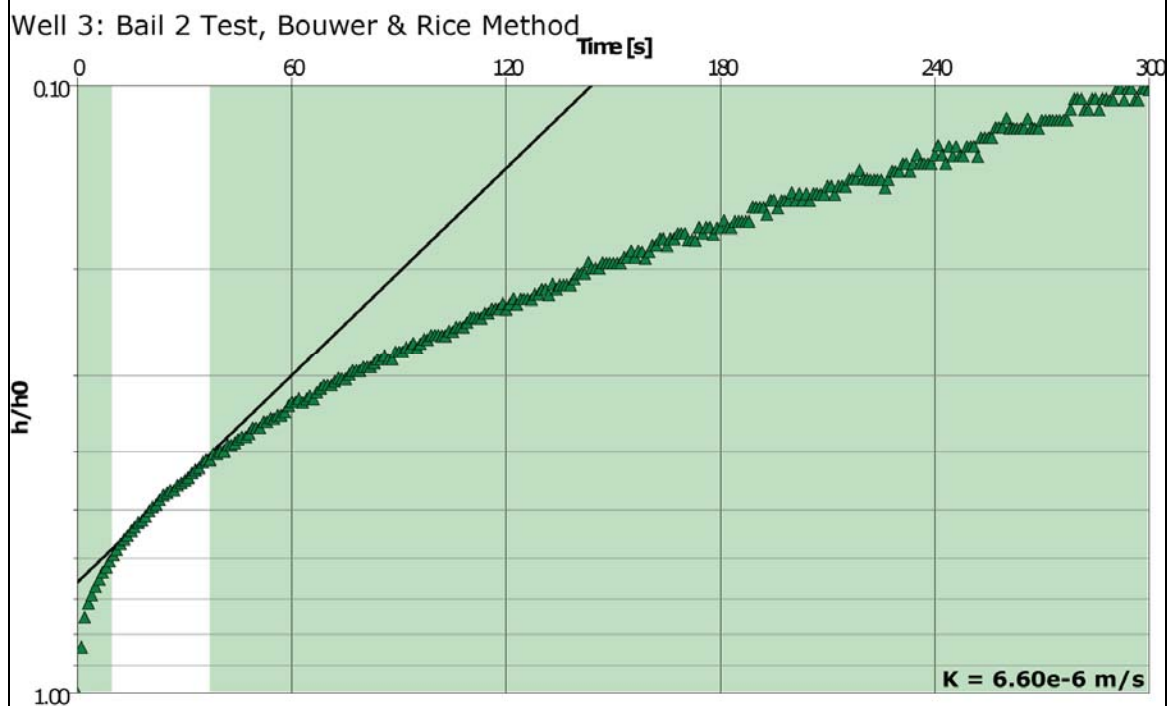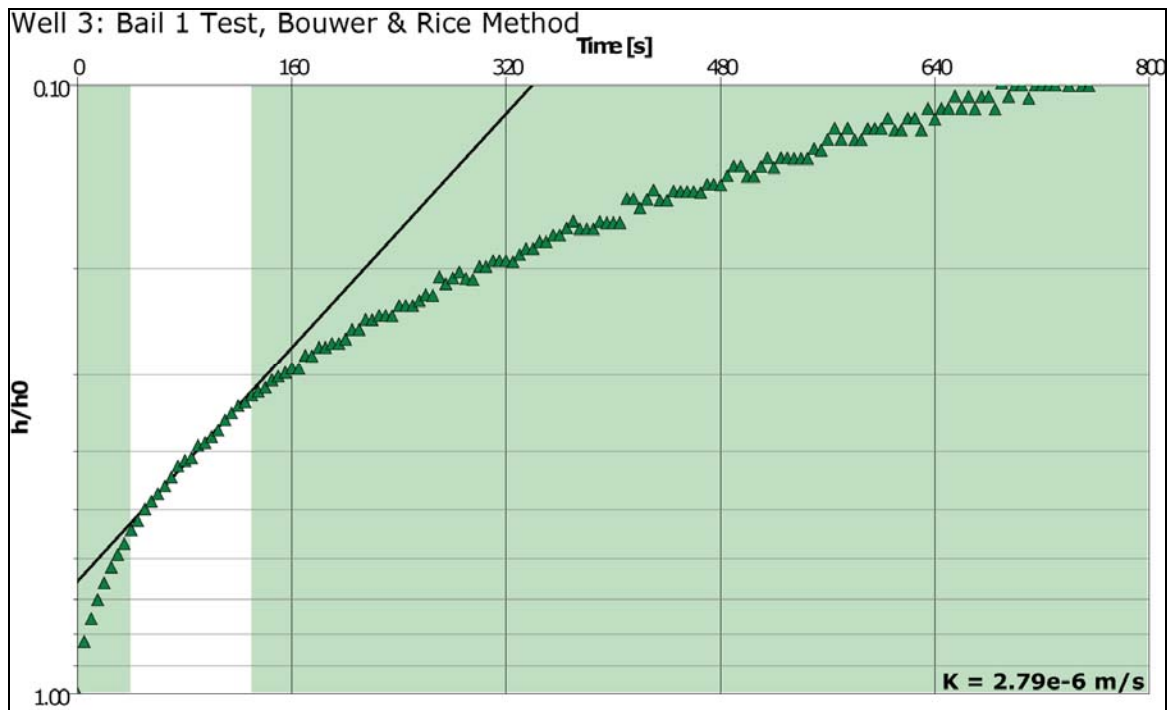
Appendix B: DFN Modeling Results

B.1. Directional hydraulic conductivity K_m and specific storage

Low Density Zone								
Outcrop #	**Kx[m/s]** E-W	Log Kx	**Ky[m/s]** N-S	Log Ky	**Kz[m/s]** T-B	Log Kz	**Ss$_m$ [m^{-1}]**	Log Ss
35	7.10E-08	-7.15E+00	8.40E-08	-7.08E+00	4.50E-08	-7.35E+00	1.70E-04	-3.77E+00
37	1.30E-07	-6.89E+00	1.40E-07	-6.85E+00	1.80E-07	-6.74E+00	3.90E-04	-3.41E+00
36	7.00E-08	-7.15E+00	9.80E-08	-7.01E+00	3.80E-08	-7.42E+00	1.80E-04	-3.74E+00
39	1.00E-07	-7.08E+00	1.00E-07	-7.15E+00	1.20E-07	-7.10E+00	2.00E-04	-3.70E+00
		-7.07E+00		-7.02E+00		-7.15E+00		-3.66E+00
Geometric Mean of K$_m$ [m/s]& Ss$_m$ [m^{-1}]	**8.56E-08**		**9.51E-08**		**7.02E-08**			**2.21E-04**

Medium Density Zone								
Outcrop #	**Kx[m/s]** E-W	Log Kx	**Ky[m/s]** N-S	Log Ky	**Kz[m/s]** T-B	Log Kz	**Ss$_m$ [m^{-1}]**	Log Ss
4	1.60E-07	-6.80E+00	1.50E-07	-6.82E+00	9.20E-08	-7.04E+00	3.50E-04	-346E+00
2	5.90E-08	-7.23E+00	1.30E-07	-6.89E+00	1.30E-07	-6.89E+00	2.80E-04	-3.55E+00
8	8.00E-08	-7.10E+00	1.00E-07	-7.00E+00	1.10E-07	-6.96E+00	2.60E-04	-3.59E+00
24	1.20E-07	-6.92E+00	2.30E-07	-6.64E+00	1.40E-07	-6.85E+00	5.50E-04	-3.26E+00
28	1.30E-07	-6.89E+00	1.60E-07	-6.80E+00	9.00E-08	-7.05E+00	3.30E-04	-3.48E+00
		-6.99E+00		-6.83E+00		-6.96E+00		-3.47E+00
Geometric Mean of K$_m$ [m/s]& Ss$_m$ [m^{-1}]	**1.03E-07**		**1.48E-07**		**1.11E-07**			**3.41E-04**

High Density Zone

Outcrop #	Kx[m/s] E-W	Log Kx	Ky[m/s] N-S	Log Ky	Kz[m/s] T-B	Log Kz	Ss_m [m^{-1}]	Log Ss
15	7.50E-08	-7.12E+00	7.00E-08	-7.15E+00	7.50E-08	-7.12E+00	1.90E-04	-3.72E+00
9	2.10E-08	-7.68E+00	2.90E-08	-7.54E+00	3.30E-08	-7.48E+00	7.20E-14	-4.14E+00
13	3.30E-08	-7.48E+00	6.50E-08	-7.19E+00	4.40E-08	-7.36E+00	1.30E-04	-3.89E+00
19	1.30E-07	-6.89E+00	1.50E-07	-6.82E+00	1.80E-07	-6.74E+00	4.00E-04	-3.40E+00
21	9.40E-08	-7.03E+00	1.40E-07	-6.85E+00	1.10E-07	-6.96E+00	2.90E-04	-3.54E+00
5	9.40E-08	-7.03E+00	1.60E-07	-6.80E+00	1.40E-07	-6.85E+00	3.50E-04	-3.46E+00
17	1.00E-07	-7.00E+00	1.70E-07	-6.77E+00	1.30E-07	-6.89E+00	3.50E-04	-3.46E+00
7	1.50E-07	-6.82E+00	2.60E-07	-6.59E+00	1.50E-07	-6.82E+00	4.90E-04	-3.31E+00
6	9.00E-08	-7.05E+00	7.80E-08	-7.11E+00	6.40E-08	-7.19E+00	2.00E-04	-3.70E+00
12	1.20E-07	-6.92E+00	2.50E-07	-6.60E+00	1.90E-07	-6.72E+00	4.80E-04	-3.32E+00
1	3.10E-08	-7.51E+00	1.40E-07	-6.85E+00	1.30E-07	-6.89E+00	2.70E-04	-3.57E+00
11	2.70E-08	-7.57E+00	6.40E-08	-7.19E+00	5.20E-08	-7.28E+00	1.30E-04	-3.89E+00
20	2.30E-07	-6.64E+00	3.50E-07	-6.46E+00	2.30E-07	-6.64E+00	7.00E-04	-3.15E+00
27	1.70E-07	-6.77E+00	1.30E-07	-6.89E+00	9.00E-08	-7.05E+00	3.40E-04	-3.47E+00
10	4.50E-08	-7.35E+00	5.40E-08	-7.27E+00	8.00E-08	-7.10E+00	1.60E-04	-3.80E+00
16	1.30E-07	-6.89E+00	1.80E-07	-6.74E+00	1.40E-07	-6.85E+00	4.00E-04	-3.40E+00
18	1.50E-07	-6.82E+00	1.40E-07	-6.85E+00	1.50E-07	-6.82E+00	3.90E-04	-3.41E+00
14	1.70E-07	-6.77E+00	2.70E-07	-6.57E+00	2.40E-07	-6.62E+00	6.00E-04	-3.22E+00
25	4.10E-07	-6.39E+00	7.30E-07	-6.14E+00	4.60E-07	-6.34E+00	1.40E-03	-2.85E+00
3	1.00E-07	-7.00E+00	1.10E-07	-6.96E+00	3.70E-08	-7.43E+00	2.10E-04	-3.68E+00
		-7.04E+00		-6.87E+00		-6.96E+00		-3.52E+00
Geometric Mean of K_m [m/s]& Ss_m [m^{-1}]	**9.21E-08**		**1.36E-07**		**1.10E-07**		**3.03E-04**	

Appendix C: MIKE SHE Modeling Results

C.1. Bedrock wells

C.2. Soil Piezometers

399

400

401

404

405